Contribution to 3D modelling of the human thorax in breathing movement : in vivo analysis of thorax joint kinematics

Benoit Beyer

Contribution to 3D modelling of the human thorax in breathing movement: In vivo analysis of thorax joint kinematics

Contribution à la modélisation 3D du thorax humain durant le mouvement respiratoire: Analyse in vivo de la cinématique des articulations du thorax

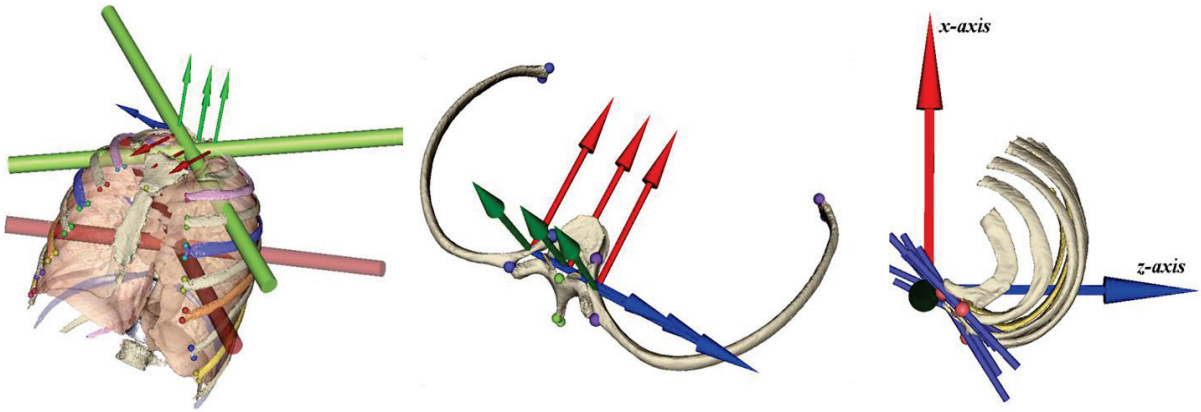

UNIVERSITÉ LIBRE DE BRUXELLES
Faculté de Médecine : Laboratoire d'Anatomie, Biomécanique et Organogenèse (LABO)
Faculté des Sciences de la Motricité : Laboratoire d'Anatomie Fonctionnelle (LAF)
Brussels, Belgium

UNIVERSITÉ CLAUDE BERNARD LYON1
Laboratoire de Biomécanique et Mécanique des Chocs (LBMC), Ecole doctorale MEGA, UMR_T9406, F69622 Lyon, France

Benoit BEYER

Doctoral thesis in Biomedical and Pharmaceutical Sciences, Brussels, Belgium, 2016
Doctoral thesis in Biomechanics, Lyon, France, 2016

Promoters:

Pr. Serge VAN SINT JAN	Université Libre de Bruxelles, *Laboratory of Anatomy, Biomechanics and Organogenesis (L.A.B.O),* Faculty of Medicine (ULB, Brussels, Belgium)
Pr. Laurence CHÈZE	Université Claude Bernard - Lyon1 ; *Biomechanics and Impact Mechanics Laboratory* (LBMC UMR_T9406) (UCBL, Lyon, France)

Co-promoter:

Pr. Véronique FEIPEL	Université Libre de Bruxelles, *Laboratory of Functional Anatomy (L.A.F)*, Faculty of Motor Sciences (ULB, Brussels, Belgium)

Jury composition:

Université Libre de Bruxelles

Prof. Serge VAN SINT JAN	(Faculty of Medicine, ULB, Brussels, Belgium)
Prof. Christian MELOT	(Faculty of Medicine, ULB, Brussels, Belgium)
Prof. Vincent NINANE	(Faculty of Medicine, ULB, Brussels, Belgium)

Université Claude Bernard Lyon1

Prof. Laurence CHÈZE	(Univ_Lyon1, LBMC UMR_T9406, Lyon, France)
Dr. Bertrand FRECHEDE	(Univ_Lyon1, LBMC UMR_T9406, Lyon, France)
Prof. SHARIAT-TORBAGHAN Behzad	(LIRIS, UMR 5205 CNRS, Lyon, France)

External examiners

Prof. Andrea ALIVERTI
(Department of Electronic, Information and Biomedical Engineering-Politecnico di Milano, Italy)

Prof. Damien SUBIT
(Institut de Biomécanique Humaine Georges Charpak, Arts et Métiers, ParisTech, France)

Acknowledgments

Firstly, I would like to express my sincere gratitude to my advisors Serge VAN SINT JAN, Véronique FEIPEL and Laurence CHÈZE. It has been an honor and pleasure to embark with them on this scientific journey.

I am very grateful to Laurence CHÈZE and her team, in particular, Pr. Raphael DUMAS, Pr. Bertrand FRECHEDE, Dr. Yoann LAFON and Dr.Laure-Lise GRAS, for accepting this "joint PhD" as well as for our challenging and prolific discussions! They forced me to consider my topic from a different angle, leading me on parallel roads towards the same scientific goal. I will always remember the course on "Mécanique des systèmes de solide et de points materiels". I learned so much in a field and language that initially rather seemed like "chaos" before slowly becoming more or less manageable…. Thank you Laurence for your availability, your advice, patience, and for your ability to transmit your knowledge. Working with you and your team demonstrated the need to develop interdisciplinary approaches to solve scientific questions or just to think!

Thank you Véronique for introducing me to the scientific and pedagogical world. I remember my first master thesis with you in anatomy (2005), my first post as "assistant chargé d'éxercice" in 2006...Yes, it has already been ±10 years… The list of things I learned from you is long…. But I would say I mostly benefitted from - and admire greatly - your receptiveness, determination and efficiency.

Thank you Serge for your determined collaboration. Thank you for all the work you put into building your "baby" the lhpFusionBox without which this doctoral thesis could not have been written.

Again, thanks to all my advisors, this PhD was an extremely rewarding experience, from both a human and scientific point of view.

A very special thanks goes to Pr. Victor SHOLUKHA who took the time to understand my scientific problem. We finally found a way to build the tool which enabled writing this thesis in five years rather than five decades! Your contribution as regards computation and programming was really substantial. All our discussions about underlying mathematics were a perfect continuity and complementary to the approach I learned in Lyon with Laurence's team. Спасибо !

Another special thanks to Dr. Patrick SALVIA for his patience, creativity and receptiveness. Thank you for the endless discussions concerning fundamentals of "screw axis" theory and philosophy! Thank you for all you taught me as regards motion analysis from both a technical/practical and scientific aspect. Thank you also for introducing me to anatomy "in the arts".

I would especially like to thank Pr. Marcel ROOZE and Pr. Stéphane LOURYAN, respectively past and present director of the LABO, for allowing me to integrate the "Anatomy and biomechanics" team. I thank them for their ample reflections, suggestions and knowledge in the fields of anatomy and scientific methodology.

In addition, my thanks go to Dr. Olivier SNOECK for the time spent during in vitro experiments on "soft tissues". Our discussions led to scientific methodological reflections and constructive ideas. They also allowed me to step back from my specific field of research, and added a new methodological approach of some of our common topics related to biomechanics.

I also want to thank Dr. Jérome COUPIER for all these moments in the dissection room and during in vitro experimentations…and for your ability to focus on a specific target. I'll remember "one thing at a time!" Thank you also for your availability and simplicity.

I thank Pr. Pierre-Michel DUGAILLY for his expertise and our endless discussions about biomechanics and applications to manual approaches.

Thanks to all other colleagues from the L.A.B.O, Clara LEYH, Céline MAHIEU, Bruno BONNECHERE and the entire technical department, especially, Jean Louis STERCKS (my "roommate"), Hakim BAJOU, Sonia Telese IZZI, Paul SANDERS and Leslie VANDER MARKEN.

I thank also all students that had to elaborate a master thesis with me…The list is long so I will not mention all of you but you should know that all your contributions were significant.

Thanks to all other people that I could have forgotten….

I would also like to thank my committee members.

Je remercie aussi ma famille, ma sœur Flora, mes parents - Alain et Kiki - qui ont permis de tracer cette route biscornue qui devait finalement avoir un certain sens... Si je devais résumer….Je retiens de tout cela la cohésion au sein de la dispersion, et je vous le dois. Merci !

And finally, I would especially like to thank my partner, Elisabeth SCHOEFFMANN, mother of our beloved children, for supporting me in everything and encouraging me throughout this long, time and brain consuming scientific journey. Our family journey remains the "one" in which science is included.With all my love.

A mes enfants Béla, Camille et Theo

"Le commencement de toutes les sciences, c'est l'étonnement de ce que les choses sont ce qu'elles sont"

Aristote, Métaphysique (- IV^{e} s. av. J.C)

"L'ignorant affirme, le savant doute, le sage réfléchit."

"The ignorant assert, the experts doubt, the wise reflect"

Aristote, Discours de morale (- IV^{e} s. av. J.C)

" La science ne souscrit à une loi ou une théorie qu'à l'essai, ce qui signifie que toutes les lois et les théories sont des conjectures ou des hypothèses provisoires."

"...our knowledge can be only finite, while our ignorance must necessarily be infinite."

Karl Popper, Conjectures and refutations: The Growth of Scientific Knowledge, 1963.

RÉSUMÉ SUBSTANTIEL

La respiration constitue un mécanisme vital qui implique la mise en jeux de diverses structures anatomiques qui constituent le thorax. La physiologie respiratoire a été largement étudiée ; cependant la physiologie articulaire impliquée dans la mécanique respiratoire reste peu étudiée chez l'humain. Diverses pathologies peuvent avoir un impact sur les articulations costo-vertébrales ou sternocostales et par conséquent sur la mécanique respiratoire.

L'objet de ce travail doctoral fut donc de développer une méthodologie complète permettant la modélisation tridimensionnelle, la visualisation et la quantification de la cinématique des articulations constitutives du thorax humain lors du mouvement respiratoire. Pour réaliser cette étude, une base de données rétrospective d'imageries tomodensitométriques obtenues à trois volumes pulmonaires autour de la capacité inspiratoire a été récoltée. Les volumes pulmonaires d'intérêt étaient : la capacité pulmonaire totale (CPT), la capacité résiduelle fonctionnelle (CRF) et la moitié de la capacité inspiratoire moyenne (CIM correspondant à la CRF +50% de la capacité inspiratoire). Deux échantillons de sujets adultes ont pu être obtenus : un groupe de 12 sujets asymptomatiques ainsi qu'un échantillon de 12 patients atteints de mucoviscidose. Dans un premier temps les travaux ont visé à établir la faisabilité de la méthodologie. Celle-ci combine : segmentation d'imagerie tomodensitométrique aux trois volumes pulmonaire afin d'obtenir les reconstructions 3D de chaque structure osseuse d'intérêt (les vertèbres thoraciques et les côtes) ; définition de repères anatomiques d'intérêt, création de référentiels anatomiques locaux ; quantification des paramètres cinématiques (axes de mouvement et amplitudes de déplacements angulaires).

La première partie de ce travail s'est concentrée sur les côtes dites sternales ou « vraies », les 7 premières paires. Le logiciel lhpFusionBox, développé au sein Laboratoire d'Anatomie Biomécanique et Organogenèse, a permis de placer virtuellement des marqueurs anatomiques sur chaque modèle osseux afin de créer des référentiels anatomiques locaux. Les transformations spatiales des référentiels des côtes par rapport aux vertèbres associées ont été calculées. Au niveau costo-vertébral, les résultats montraient que les déplacements angulaires se réalisaient dans deux plans principaux correspondant aux mouvements en « bras de pompe » (dans le plan sagittal) et en « anse de seau » (dans le plan frontal). L'orientation des axes hélicoïdaux moyens était similaire aux sept premiers étages costo-vertébraux. Cependant ces orientations étaient sujettes à une variabilité individuelle importante.

Dans un deuxième temps, afin d'améliorer la fiabilité de la méthode, l'effet de l'erreur sur la détermination des marqueurs anatomiques sur les résultats cinématiques a été évalué. De plus, la méthode a été automatisée afin de pouvoir rendre le temps de traitement des données plus compatible avec de possibles applications cliniques. Une simulation de Monte-Carlo a permis de réitérer la modification du positionnement des différents marqueurs anatomiques à partir de valeurs de dispersions pertinentes, obtenues suite à une analyse de la reproductibilité du placement des marqueurs. Une interpolation entre les positions discrètes a été utilisée afin d'augmenter le nombre de

positions des référentiels anatomiques permettant de définir la position et l'orientation des axes hélicoïdaux caractérisant la cinématique des articulations CV. Finalement, la dispersion moyenne de l'orientation des axes hélicoïdaux moyens obtenus entre diverses simulations a pu être évaluée. Les déplacements angulaires autour de l'axe hélicoïdal moyen ont ainsi été utilisés.

Troisièmement, une fois la méthodologie élaborée, celle-ci a été appliquée à l'ensemble des côtes dites respiratoires (les 10 premières paires). Les déplacements angulaires des articulations costo-vertébrales ont été exprimés cette fois en fonction des volumes pulmonaires d'intérêt. Les résultats ont montré que le déplacement angulaire des côtes se réalise principalement en dessous de la capacité inspiratoire moyenne. L'amplitude des mouvements costaux diminue graduellement dans les étages inférieurs. Au-dessus de la capacité inspiratoire moyenne, les amplitudes de mouvements costaux ne diffèrent pas entre les étages. L'orientation des axes hélicoïdaux moyens n'est pas influencée significativement par le niveau costal. Aucune corrélation n'a été mise en évidence entre les amplitudes de mouvements costaux et les paramètres pulmonaires ou anthropométriques. A ce stade, l'objectif de l'analyse détaillée de la cinématique des articulations costo-vertébrales, autant d'un point de vue qualitatif que quantitatif, était atteint. L'influence d'une condition pathologique sur les paramètres cinématiques a donc été évaluée. La même méthode a été appliquée sur l'échantillon de sujets atteints de mucoviscidose. L'objectif était de comparer les résultats obtenus avec ceux obtenus lors des études précédentes sur les sujets asymptomatiques. Les résultats montrent que la pathologie influence les amplitudes de mouvements costaux, principalement pour les côtes supérieures (5 premières paires). En revanche, la pathologie n'a aucune influence sur l'orientation des axes hélicoïdaux moyens. Une nuance doit être apportée, l'explication des diminutions d'amplitude de mouvements costaux devrait être attribuée plutôt au symptôme d'hyperinflation chronique fréquent chez les patients atteints de mucoviscidose, plutôt qu'à la mucoviscidose elle-même.

Enfin, la dernière partie de ce travail s'est orientée vers l'analyse des articulations antérieures du thorax, au niveau des articulations sternocostales des côtes dites « sternales » ou « vraies » (les 7 premières paires). En complément, le déplacement du sternum et les variations de l'angle sternal (ou angle manubrio-sternal) lors du mouvement respiratoire ont été analysés en suivant la méthodologie développée au cours de ce travail doctoral. Les résultats ont montré que l'angle sternal se modifie durant le mouvement respiratoire. Les amplitudes des mouvements costaux par rapport au sternum diminuent graduellement dans les étages inférieurs. La position et l'orientation des axes hélicoïdaux fini et moyen a été détaillée. Cette dernière étude est la première présentant une analyse quantifiée in vivo des cinématiques articulaires sternocostales durant le mouvement respiratoire chez l'humain.

En conclusion, ce travail doctoral a permis de développer une méthode d'analyse détaillée des cinématiques articulaires du thorax in vivo lors du mouvement respiratoire. Les résultats obtenus ouvrent des perspectives autant en modélisation que pour des applications cliniques diverses.

ABSTRACT

Breathing is a vital phenomenon that implies synergy of various anatomical structures that constitute the thorax. Joint physiology remains a relatively poorly-known component of the overall thorax physiology. Quantitative literature related to in vivo thorax kinematics during breathing is scarce. The present work focuses specifically on developing and applying a methodology to reach this goal. The developed method combined processing of CT data obtained at different lung volumes and infographic techniques. Detailed ranges of motion (ROMs) and axes of movement (mean helical axes, MHAs) were obtained at costovertebral joints in 12 asymptomatic subjects; rib ROMs gradually decrease with increasing rib number; lung volume and rib level have a significant influence on rib ROM; MHAs did not differ between rib levels. In addition, the method was applied on a sample of 10 patients with cystic fibrosis. The pathological condition significantly influenced CVJ ROMs while the orientation of the MHAs did not differ. Finally, the sternal displacement, sternal angle variations and sternocostal joints (SCJ at rib1 to 7) kinematics during breathing motion were analyzed. Rib ranges of motion relative to sternum decreased with increasing rib number similarly to CVJ. Orientation of the MHAs did not differ between SCJ levels. A significant linear correlation was demonstrated between sternum vertical displacement and rib ranges of motion at both CVJ and SCJ. The present work substantially contributes to 3D modelling of human thorax in breathing at a joint level both qualitatively and quantitatively.

RÉSUMÉ

La respiration est un phénomène vital qui implique une synergie entre diverses structures anatomiques qui constituent le thorax. La physiologie articulaire reste un parent pauvre de la physiologie et la littérature concernant la quantification de la cinématique 3D des articulations du thorax durant le mouvement respiratoire est rare. Ce travail se concentre sur le développement et l'application d'une méthodologie permettant de répondre à cet objectif. La méthode développée combine le traitement de données tomodensitométriques réalisées à trois volumes pulmonaires différents et des techniques d'infographies. Les amplitudes (ROMs) et axes de mouvements (axe hélicoïdaux moyen, AHMs) ont été obtenus au niveau des articulations costo-vertébrales de 12 sujets asymptomatiques. En résumé, les amplitudes diminuent graduellement dans les étages inférieurs ; le volume pulmonaire et l'étage costal influencent significativement les amplitudes costales ; l'orientation des AHMs ne diffère pas entre les étages costaux. En complément, la méthode a été appliquée pour un échantillon de 10 patients atteints de mucoviscidose. La condition pathologique influençait significativement les amplitudes de mouvements mais pas l'orientation des AHMs. Enfin, le déplacement sternal, les variations de l'angle sternal et la cinématique des articulations sternocostales a été analysée. Les déplacements angulaires des côtes par rapport au sternum diminuaient dans les étages inférieurs comme au niveau des articulations costo-vertébrales. L'orientation des AHMs des articulations sternocostales ne différait pas entre les étages. Une corrélation linéaire a été mise en évidence entre les déplacements verticaux du sternum et les amplitudes de mouvement costales au niveau costo-vertébral et sternocostal. Ce travail contribue de façon substantielle à la modélisation 3D du thorax humain durant le mouvement respiratoire d'un point de vue qualitatif et quantitatif.

List of abbreviations

AF	Anatomical frame
AL	Anatomical landmark
ANOVA	Analysis of variance
AS	Asymptomatic subjects
BMI	Body mass index
CF	Cystic fibrosis
COPD	chronic obstructive pulmonary disease
CT	computed tomography
CVJ	costovertebral joint
FHA	finite helical axis
FRC	functional residual capacity
IC	Inspiratory capacity
JPP	Joint pivot point
MHA	mean helical axis
MIC	middle of the inspiratory capacity
MPP	mean pivot point
MSJ	Manubriosternal joint
ROM	range of motion
RV	Residual volume
SCJ	sternocostal joint
TLC	total lung capacity
VC	Vital capacity
VRML	Virtual Reality Modelling Language

Contents

Chapter 1:

General Introduction

The word "thorax" has a long history starting approximately in 8th century B.C. with Homer's poems in which he referred to the protection of the chest of soldiers. During centuries of Greek history, the thorax referred to protective fortified wall over the body or building. The entrance in medicine came with Hippocrates, and was defined later by Galen who explained "all that cavity bounded by the ribs on both sides, extending to the sternum and diaphragm in front and curving down to the spine in the rear is customarily called Thorax by the physicians" (cited by French, 1978; Roussos, 1995). An ancient representation of the thorax is presented in figure 1.

Figure 1: From French R.K., The thorax in history, Thorax, 33, 1978

Today, the definition from medical sciences is not far from previous historic anatomic descriptions. Considering anatomical structures, the thorax is formed by 12 thoracic vertebrae and intervertebral discs (i.e. the thoracic spine), 12 pairs of ribs and costal cartilages, the sternum (see figure 2A) and the muscles and fasciae attached to these; below; it is separated from the abdomen by the diaphragm (see figure2B from Graeber & Nazim, 2007); it contains the chief organs of the circulatory and respiratory systems, respectively heart and lungs.

Considering functional aspect, the thorax is a fundamental anatomical entity that provides vital organs protection and structural support for both respiratory function (Cappello and De Troyer, 2002) and spinal stiffness (Oda et al., 1996, 2002; Takeuchi et al., 1999).

The present work will focus on the respiratory function and more specifically on the thorax joints physiology and biomechanics during breathing.

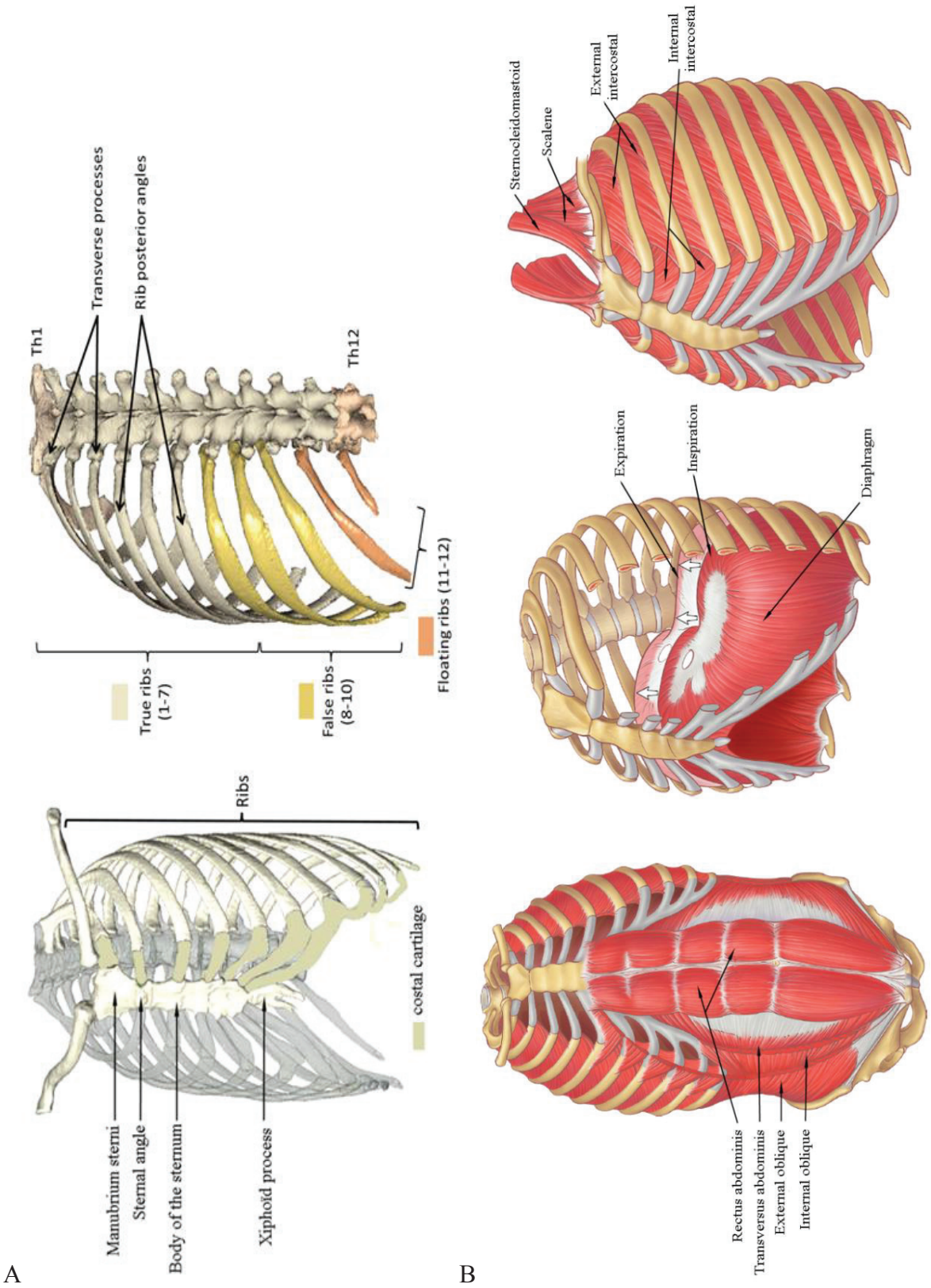

Figure 2: A: Bones and cartilages of the thorax (modified from Van Sint Jan, 2007); B: Chest wall and muscles implicated in breathing function (Modified from Graeber & Nazim, 2007). Left: Muscles of the abdomen; Middle: Diaphragm muscle in inhalation (or inspiration) and exhalation (or expiration); Right: intercostal, scalene and sternocleidomastoid muscles.

1. Anatomy of the thorax

Since the present thesis will concentrate on joint kinematics, the following anatomic description will mainly focus on bones and joints of the thorax. The descriptions refer to figure 2 and 3.

1.1. Thoracic vertebrae

The thoracic spine consists in a series of 12 thoracic vertebrae (Th) that articulates through thoracic intervertebral discs. Th2 to Th9 are typical vertebrae while Th1, Th10, Th11 and Th12 are considered as transition vertebrae. Semifacets for the heads of the ribs are found superiorly and inferiorly at the junction between the body and the pedicles. The transverse processes of Th1 to Th10 have costal facets that articulate with the tubercles of the ribs. The transverse processes are oriented laterally and increasingly backward from Th1 to Th12.

1.2. Ribs, costal cartilages and sternum

The 12 pairs of ribs can be divided in sub-groups (see figure 2A); the seven first pairs are attached posteriorly to the vertebra and anteriorly to the sternum through the costal cartilage. Therefore, these ribs are denominated as “true” or vertebrosternal ribs (Drake et al., 2010) and constitute the vertebrosternal costal arches (Osmond, 1995). The five rib pairs underneath are “false” ribs, the 8^{th}, 9^{th} and 10^{th} have their cartilage attached to the one of the rib above forming vertebrochondral costal arches. The two last ribs 11^{th} and 12^{th} terminate freely in a small cartilaginous tip, constituting the “floating” ribs.

The sternum can be divided in three parts, the manubrium (upper part), the body of the sternum and the xyphoid process. The entire sternum embryologically derived from the combination of five sternebrae that are laterally attached to costal cartilages. The angle between manubrium and sternum body forms the so-called “sternal angle” in sagittal plane (Osmond, 1995).

1.3. Joints of the thorax

The articulations of the thoracic spine encompass several amphiarthrodial joints between vertebral bodies through the intervertebral discs, and several diarthrodial joints between vertebral arches through the zygapopghyseal facets.

At the posterior part of the thorax, the ribs articulate with thoracic vertebra through synovial costovertebral joint complexes. Typically, at each costal level, the rib head articulates with the bodies' of two adjacent vertebrae (see figure 3B). This architecture differs for rib1, 10, 11 and 12 where the ribs articulate with a single vertebra through a single facet. The articular facets for rib on the vertebral bodies and transverse processes are shown in figure 3A.

At the anterior extremity of each rib, direct continuity of the costal cartilages forms a series of costochondral joints. All chondrosternal joints are of synovial type, but the first chondrosternal joint that shows continuity between bone and cartilage as for all costochondral junctions (see figure 4) is of synchondrosis.

Note that a series of well-developed ligaments are increasing the stability of each joint, however we will not describe these ligaments in further details.

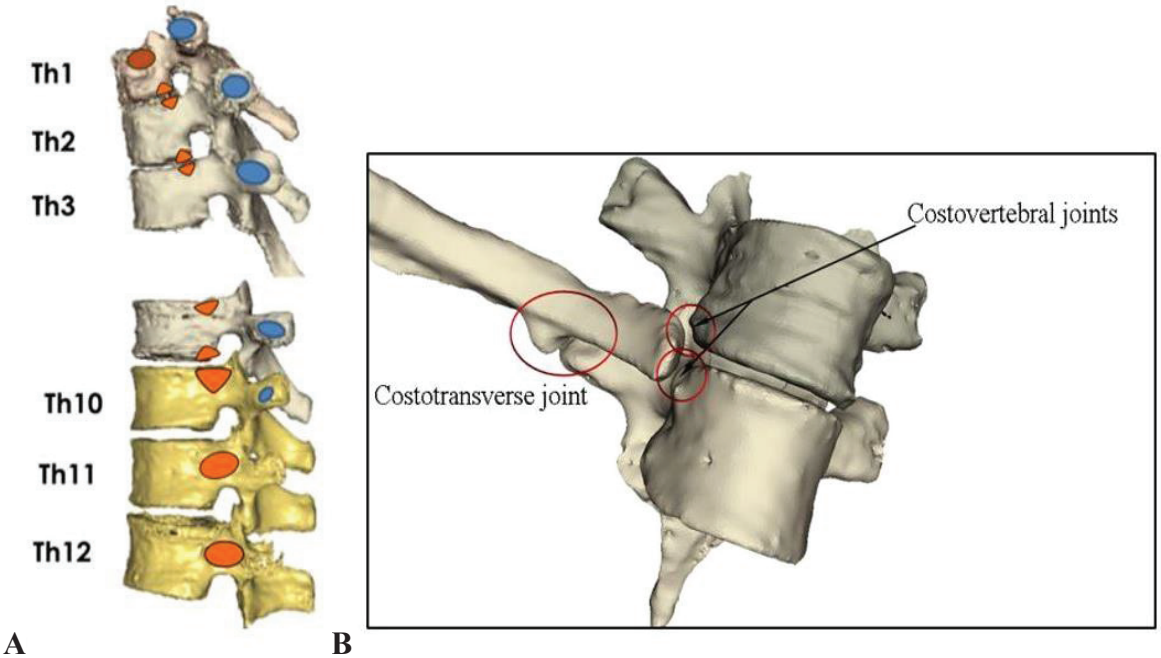

Figure 3: A: representation of thoracic vertebrae and costal surfaces. B: Typical costovertebral joint complex organisation.

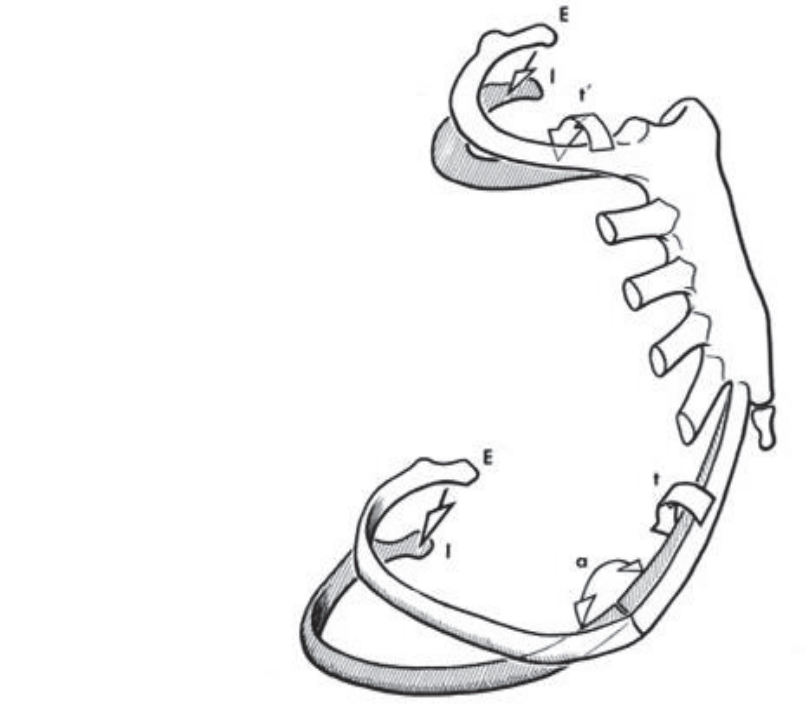

A

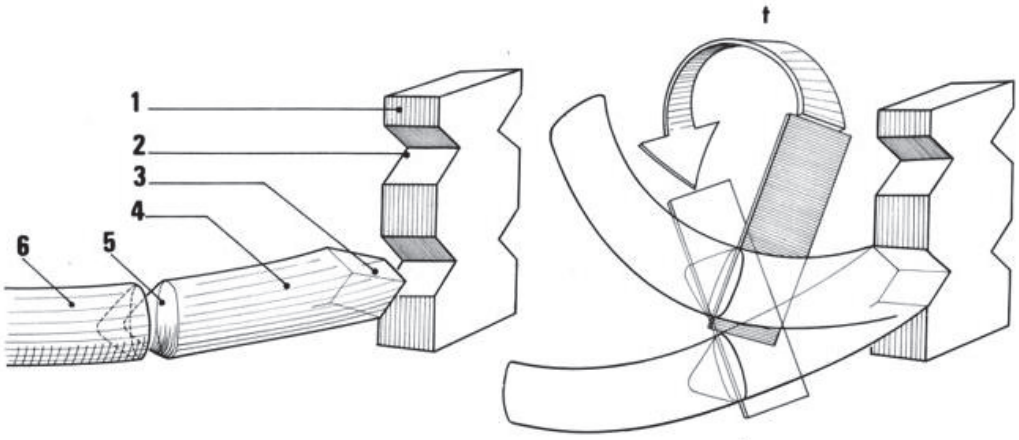

B

Figure 4: Sternocostal joints (from Kapandji, 1964). A: E = expiration, I = Inspiration; during inspiration, a rotation (t and t') occurred around costal cartilages.
B: Representation of the anterior end (6) of the true ribs link to the sternum border (1) through costal cartilage (4) at costochondral and chondrosternal joints. Right: cone shaped lateral extremity of the costal cartilage (5); dihedral shape of the medial part of the costal cartilage (3) that fit the dihedral angle of the sternal border (2). Note that these descriptions are not based on measurements.

2. Mechanics of breathing

The act of breathing constitutes a vital phenomenon that allows oxygen transfer from air to blood while carbon dioxide is removed. Two main successive mechanisms are adapted to work in parallel, the ventilation and the diffusion. The ventilation allows displacement of air from the surrounding environment to lungs through the rhythmic inspiration and expiration processes, while gas-exchange occurs in the lungs within the alveoli during diffusion mechanism through the alveolar-capillary membrane. This ventilation is organized from two rhythmic successive events, inspiration (inhalation) and expiration (exhalation), while the ventilation rate is defined by the frequency of these combined events.

During the inspiratory phase, the rib cage and abdomen expand due to the activation of several respiratory muscles that act in synchrony with chest wall as a thoracic pump. During expansion of the chest wall, the system store energy through the elastic properties of the lungs (pulmonary alveoli), the joints and costal cartilages in combination with respiratory muscles activation. During quiet expiration, this energy is restored explaining how unforced expiration is a passive mechanism. Note that the elastic recoil of the chest wall seems to assist the return of the chest wall to the neutral position mainly above +-75% of the total lung capacity (Agostoni et al., 1965; Agostoni and Hyatt, 2011).

Note that breathing rate is about 12-20 cycles per minute in human adults at rest, that represents around 17000 to 29000 cycles a day and some billions of cycles during lifetime. The chest wall expansion that occurs during inspiration is determined by the articulations between ribs and vertebrae at the costovertebral joint (CVJ) and sternocostal joints (SCJ) complexes at the anterior extremity of the ribs, connecting the ribs to the sternum through the costal cartilages. Considering the joint structures, it is worth noting that no other articulation except the temporomandibular joint is supporting such a permanent cyclic and rhythmic activity.

2.1. Clinical implications

In manual therapies, such as osteopathy, physiotherapy or physical therapy, it has been recognized for a long time that breathing could have an influence on the global body function. It has been demonstrated that breathing function can be altered due to several different factors. Thoracic shape can be altered in various congenital diseases such as idiopathic scoliosis in which the severity of pulmonary impairments has been correlated to the degree of spinal deformity (Weber et al., 1975).

In lung pathology, the modification of lung volumes, such as in patients with chronic hyperinflation, can be responsible for breathing dysfunctions. In chronic obstructive pulmonary disease (COPD), asthma, modifications of neural drive of the respiratory muscles can lead to a decrease of the efficiency of the respiratory mechanics (Dassios et al., 2013). Furthermore, the configuration and dimension of the thorax can be altered in patient with lung hyperinflation (Cassart et

al., 1996; Laghi and Tobin, 2003; Sharp et al., 1986; Walsh et al., 1992). Stress or diseases are both able to modify respiratory drive. The latter modification was demonstrated to possibly alter tonicity of the respiratory muscles (Konno and Mead, 1967; Meessen et al., 1993; Muller et al., 1981), especially when these factors are repeated and become chronic.

Back pain in the thoracic region is recognized to be related to joint facets in 10-15% of the spinal pain (Manchikanti et al., 2004). Pain is also commonly related to both musculoskeletal and emotional conditions (Arroyo et al., 1992; Sales et al., 2007). Recent clinical studies have shown that costovertebral joint dysfunction can be a cause of misdiagnose atypical chest pain (Arroyo et al., 1992). At the anterior part of the chest wall, costochondritis is also described in literature as an anxiogenic pain (Proulx and Zryd, 2009). Numbers of structural modifications of the structures surrounding the joints are also able to cause pain. These modifications such as exostosis, erosion, sclerosis at a bone/cartilage level; calcification, fibrosis at a ligament level are often demonstrated in normal aging, or during rheumatologic conditions such as Rheumatoid arthritis (Cohen et al., 1978) or ankylosing spondylitis (Pascual et al., 1992). Finally, the relation between back pain, motor control and breathing dysfunction has been revealed in few studies (Hodges and Gandevia, 2000; Lee et al., 2010).

In such conditions, the goal of manual approaches (i.e. physical therapy, manual therapy, osteopathy…) is to restore "normal" physiology of the target structures (e.g. lungs, joints, muscles…) using exercises, manipulation/mobilization of soft tissues and joints.

Therefore, estimating the "normal" behavior of the joints in both qualitative and quantitative way is an issue.

2.2. Chest wall kinematics in breathing

Breathing physiology analysed respiratory function from gas exchanges, focusing on pressure/volume and global shape variations along the breathing cycle (Cala et al., 1996, Bellemare et al., 2001b, Bellemare et al., 2001a, Kenyon et al., 1997, Hostettler et al., 2011). Chest wall motion expansion was quantified in several studies using various instrumentations such as medical imaging (Cassart et al., 1996; Sharp et al., 1986; Walsh et al., 1992; Wilson et al., 1987, 2001) or optoelectronic stereophotogrametry (Bruni et al., 2011; Cala et al., 1996; Parreira et al., 2012). However, literature concerning breathing kinematic quantification at a segmental joint level is scarce.
As mentioned previously (Ward and Macklem, 1995), the "understanding of the kinematics of the chest wall and the mechanisms responsible for its efficient functioning has evolved slowly. This has largely been due to the difficulty in making direct measurement in human subjects." This is especially true for determining segmental joint kinematics which is still not achieved to date.

2.2.1. Rib and chest wall motion

Typical motion at costovertebral joint is described as following (see figure 5):

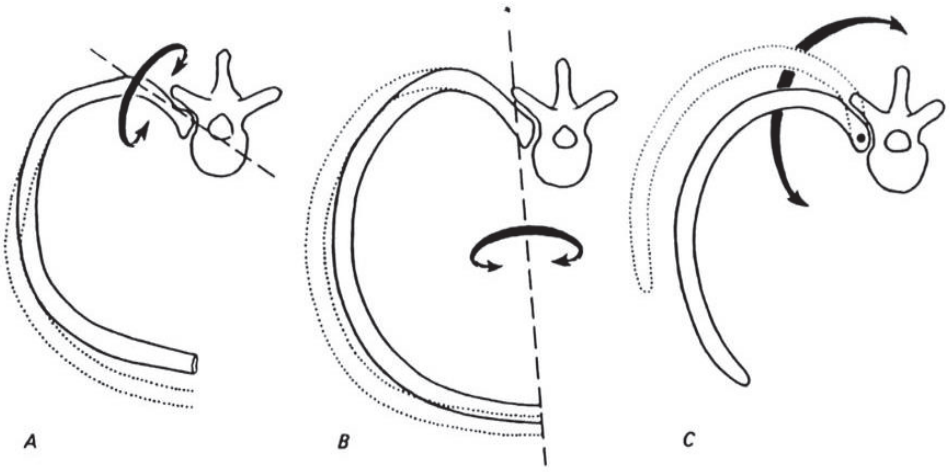

Figure 5: Schematic representation presented by Osmond (1995) of axes and direction of movement of (A) upper ribs ("pump handle" movement), (B) lower ribs ("bucket handle" movement), and (C) lowest ribs ("caliper" movement). Inspiratory positions are indicated by broken lines.

Literature usually describes a change in orientation of the axis of rib rotation as shown in figure 6. At upper rib levels, the axis is supposed to follow the orientation of the transverse process, i.e. close to a frontal plane, while at lower levels, orientation gradually points obliquely between dorsoventral and mediolateral axes.

Since the ribs rotate mainly around an oblique axis, chest wall diameters are altered in both frontal and sagittal plane according to "bucket-handle" and "pump handle" motion respectively (see figure 6).

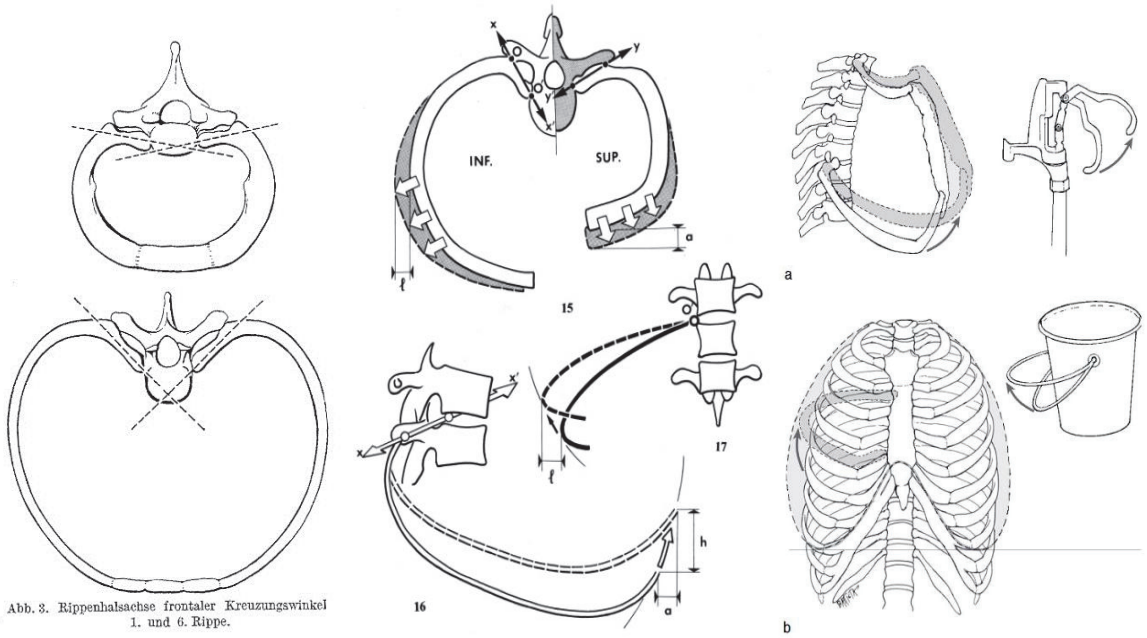

Figure 6: Change in orientation of the costovertebral joint axis of rotation between upper and lower rib level. Left: in (Von Hayek, 1970) ; Center: in (Kapandji, 1964); Right: in (DeStefano, 2011).

2.2.2. Modelling of the thorax

Various models are presented in literature depending on which parameter is analyzed. For example, chest wall response to dynamic impact or quasi static/dynamic loading was studied, using in vitro methods and finite element modeling (Bir et al., 2004; Chen, 1978; Closkey et al., 1992; Eckert et al., 2000; Eckert, 2001; Vezin and Berthet, 2009; Vezin and Verriest, 2005; Viano, 1978). These studies are mainly used in the field of accidentology in order to develop injury criterions as a function of several mechanical parameters (a representation of such a model is given in figure 7B). Other applications were develop for surgical approaches such as in scoliosis (Andriacchi et al., 1974; Closkey et al., 1992; Kenyon et al., 1991) in which the rib are constructed as a series of articulated portions in order to determine rib deformations associated to the disease (see figure 7A). Several necessary parameters are of importance to introduce in finite element modelling is the mechanical properties of each component of the thorax (i.e. bones, joints, soft tissues…). Thorax joints mechanical properties were analyzed using various *in vitro* methodologies (Duprey et al., 2010; Eckert et al., 2000; Oda et al., 1996; Schultz et al., 1974a; Takeuchi et al., 1999). Rib mechanical properties were studied in various analysis during loading (Roberts and Chen, 1970, 1972; Schultz et al., 1974b) or from medical imaging techniques (Perz et al., 2015; Zhu et al., 2013) and were demonstrated to be flexible (Schultz et al., 1974b). However, further specific analysis on respiratory movement of the chest wall mentioned that "forces required to bend a human rib or costal cartilage are very much greater than those required to move a rib around its joints" and therefore, kinematic analysis of the rib during breathing motion could be assessed considering the ribs as rigid bodies (Saumarez, 1986).

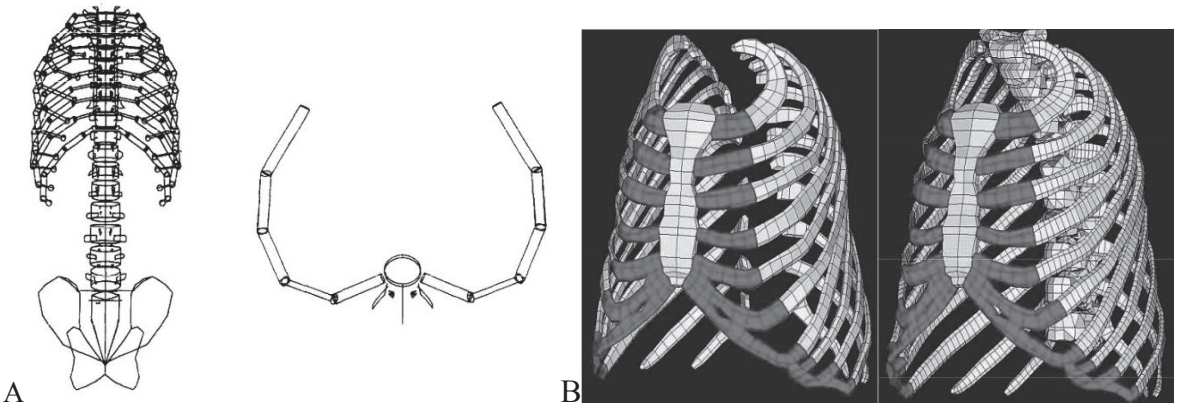

A B

Figure 7: 3D models of the thorax. A: from (Closkey et al., 1992); B: Chest wall model from (Vezin and Verriest, 2005).

Concerning respiratory mechanics, mechanical models were found in the early literature (see figure 8A,B) focusing on thorax shape variations (Fick, 1911; Hayek, 1960). Later, a two compartment model of the chest wall was described (combining rib cage and abdomen) to estimate chest wall change as a function of lung volume using one degree of freedom (Konno and Mead, 1967). Adaptations were then made to include respiratory muscles contributions (Loring, 1986; Macklem et al., 1983; Mead and Loring, 1982). More recently, the development of technologies enables to build

very sophisticated models (Aliverti and Pedotti, 2014; Kenyon et al., 1991; Pelosi et al., 1998; Ward et al., 1992) that combine chest wall compartment, lung (see figure 8C) .

A B

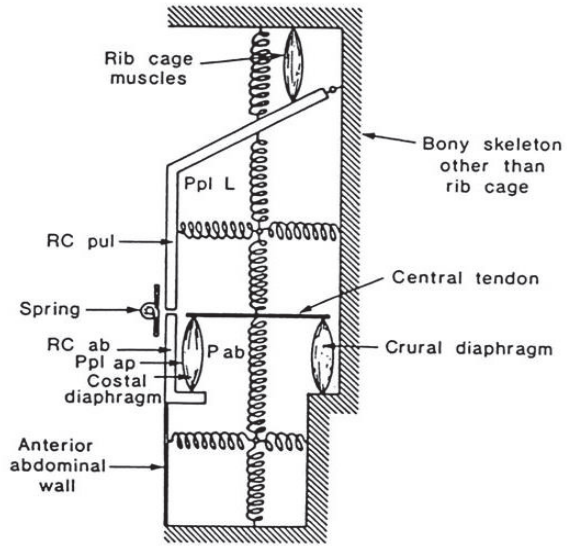

C

Figure 8: A: Thorax model from (Fick, 1911); B: Model proposed by (Kapandji, 1964) C: Modern model from (Ward et al., 1992) combining, chest wall motion, muscles properties, lung elastic properties.

While a relatively significant number of models concerning the entire chest wall are described in literature, only few studies have detailed in vivo kinematics of the joints of the thorax in breathing conditions in a quantitative manner. Most of previous results related to costovertebral joints were obtained from geometrical extrapolations (see figure 9) combined with in vivo measurements (Jordanoglou, 1970; Saumarez, 1986).

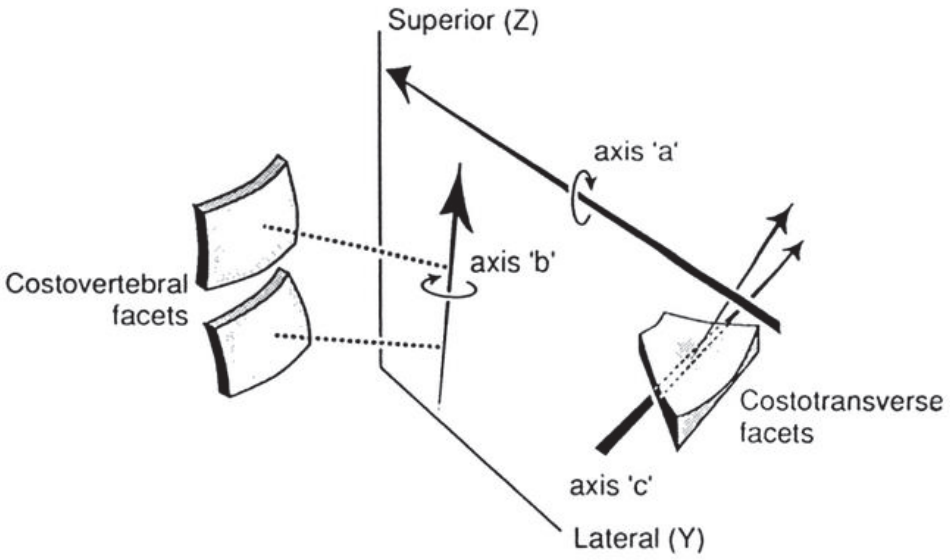

Figure 9: Schematic explanation of costovertebral joint complex geometry and probable axes of rotations (Saumarez, 1986).

In humans, the only studies that measured segmental 3D kinematics of rib motion in breathing from medical images are those from Wilson et al. (Wilson et al., 1987, 2001) on samples of 2 (at rib 3 to 7) and 5 subjects (at rib 2 to 9). In these studies, cartesian coordinate system was oriented as follow: x-axis, caudal to cephalic, y-axis, right to left z-axis adjusted so that it layed "in the sagittal midplane behind the spine", with an "arbitrary origin of the coordinate system" (Figure 10A). Then, they fitted a plane passing through a set of landmarks (70-80 points) along the ribs reconstruction to define rib coordinate system (ξ ; η ; ζ) (Figure 10B) with vertical axis (ζ-axis) normal to the "best fitting" plane (ξ ; η) (pointing cephalically), and therefore not passing through the rib neck (Figure 10B).

Finally the orientation of the "rib plane" relative to the global coordinate system was expressed using α (between x-axis and ξ-axis) and β (between y-axis and η-axis) angles for "pump handle" and "bucket handle" respectively (see Figure 10C and D).

The transformation between the two poses was computed relative to the fixed global coordinate system, therefore the spine was considered fixed (see Figure 10). In addition, data of different subjects were shifted so that the spine and rib positions matched "as well as possible", probably introducing some unquantified artefacts in the final results.

Note that the later studies from Wilson et al, 1997 and 2001 formed the basis for reflection of the present doctoral thesis.

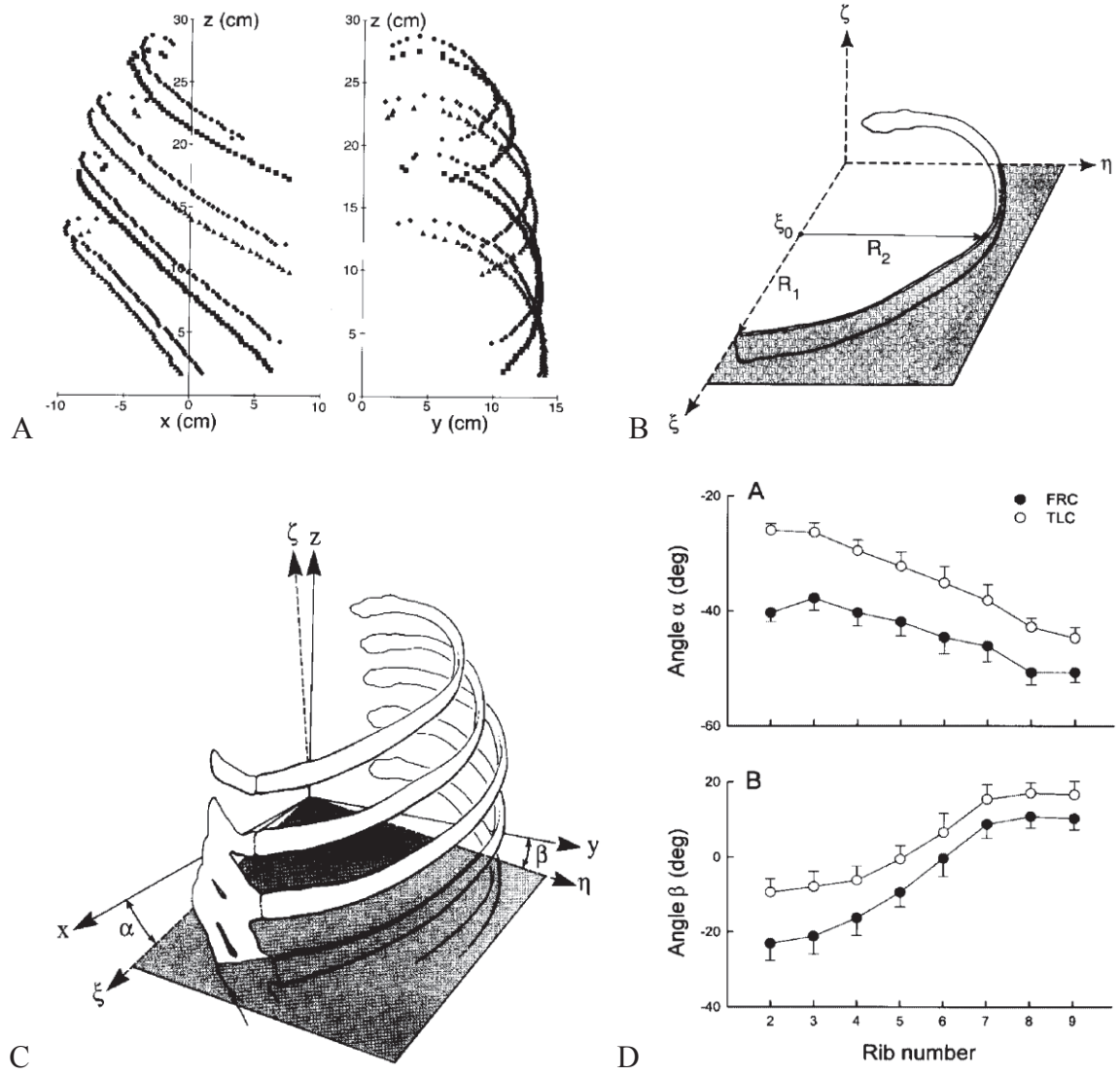

Figure 10: Methods used by Wilson et al, 1987, 2001. Details are presented in the text.

The later studies do not describe a method especially dedicated for the computation of the axes of movement of the ribs during respiratory movement. The 3D representation with integration of the both kinematic parameters and geometry of the bones of interests was also not available.

A method often use in joint kinematics is the finite helical axis (FHA) that allows describing movement of rigid bodies through a rotation around and translation along one single axis (Woltring et al., 1985). This method have been previously used for various joints of the human body such as the cervical spine (Cattrysse et al., 2013; Cescon et al., 2014; Dugailly et al., 2010), the wrist (Salvia et al., 2000) or also for the rib displacements for applications in radiation oncology (Didier et al., 2007; Ladjal et al., 2013; Marshall et al., 2015). This method (see figure 11 from Marshall et al, 2015) was used for computation of respiratory movement at tidal volume directly from extraction of computed tomography (CT) scan images (Ladjal et al., 2013; Marshall et al., 2015), without describing the

influence of rib level or in relation to lung volumes. Note that this method was combined with 3D representation of the kinematic parameters and 3D bones geometry for the cervical spine (Dugailly et al., 2010, 2013, 2014).

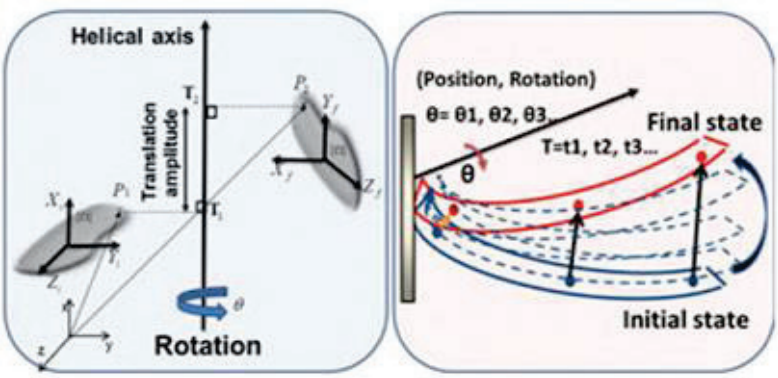

Figure 11: Representation of the finite helical axis method and application on a rib at two successive position. This figure was adapted from Marshall et al, 2015.

3. Overall methodology

Use of CT-scan data at various lung volumes

The above description of the methods used to estimate chest wall kinematics has underlined that the only in vivo methodology that enables segmental quantification at a joint level remains the use of medical imaging. The use of radiography has shown several limitations, especially due to planar approach while the use of CT data at various lung volumes seemed to be the most accurate and relevant tool to obtain reproducible measurements (Mueller et al., 2012), accurate bone geometry and to compute discrete kinematics (Wilson et al., 1987, 2001). However, some concerns related to recent radiation recommendations (Van Sint Jan et al., 2006) were raised.

Therefore, we explored the availability of retrospective data in the Erasme academic hospital of the Université Libre de Bruxelles. Studies were found that used spiral CT-scan at three different lung volumes in order to estimate effect of lung volumes on diaphragm and chest wall parameters in hyperinflated patients and normal volunteers (Cassart et al., 1996, 1997). Further studies were performed in a cohort of patients with cystic fibrosis (Dufresne et al., 2009). The CT data obtained during these previous studies were used to constitute the basis of the present research. In total, data were obtained in a sample of 12 asymptomatic subjects and 12 stable patients with cystic fibrosis.

Details of the breathing manoeuver performed during CT acquisition

During these studies, the CT data acquisition procedure was performed by senior pneumologist and radiologist. The method they developed for the respiratory manoeuver was organized as follows: the subjects were asked to perform few practice trials of the entire breathing manoeuver to familiarize themselves with the procedures and with the sensation of respiratory muscle relaxation. While wearing a nose-clip and lying supine with their upper limbs

raised above the head, the patients were asked to breathe to total lung capacity (TLC), functional residual capacity (FRC), and FRC plus one-half inspiratory capacity (MIC), where the acquisitions were performed. To attain this last volume, the subjects were connected to a spirometer and instructed to breathe in to TLC and slowly expire until MIC was reached. At each volume, the subjects were asked to hold their breath and relax against a closed airway. During the acquisitions, one of the investigators encouraged the subjects to appropriately relax the respiratory muscles.

Kinematics computation and 3D representation

While the finite helical axis method was used to compute rib displacement, no consensus exists concerning the use of a series of anatomical landmarks to define vertebra, rib and sternum coordinate system. Based on a previous description, the rib will be considered as rigid bodies (Saumarez, 1986).The present research first focus on the development of the entire methodology to describe rib kinematics and to allow 3D representation of kinematic parameters with respect to bone geometry.

4. Aims of the doctoral thesis

Firstly, the aim is to develop a method that allows robust computation and 3D representation of thorax joints kinematics from the use of CT data obtained at three different lung volumes.

Secondly, as described by Wilson et al. (1987, 2001), rib displacement seemed to be dependent on the rib level but literature focused only on ribs 2 to 9 and no further analysis was performed to estimate the influence of lung volumes on rib kinematics. In addition rib displacement is supposed to be dependent on the orientation of the transverse process of the thoracic vertebra, and as a consequence the orientation of the rib axis of motion is supposed to follow the orientation of the transverse processes. Therefore, in asymptomatic subjects, we hypothesized that the rib angular displacement could be modified by rib level, lung volume and laterality. As a consequence, the same hypothesis related to the axes of rib rotation will be assessed.

Thirdly, studies have demonstrated that thoracic kyphoscoliosis and ankylosing spondylitis may alter rib motion (Jordanoglou, 1969; Jordanoglou et al., 1972), however the assessment of rib motion in respiratory disease such as chronic obstructive pulmonary disease (COPD) is poorly described and is mainly based on planar estimations (Cassart et al., 1996; Sharp et al., 1986, 1986). The latter researches have shown that the change in rib angle (from lateral radiograph) between lung volumes can be reduced due to lung hyperinflation. Therefore, we hypothesized that a pathology that could alter both lung volume and/or chest wall geometry should lead to a decrease in amplitude of ribs rotation without any change in the orientation of the rib axes of rotation. This hypothesis is tested from the analysis of a sample of patients with cystic fibrosis.

Finally, the above hypotheses focus on costovertebral joints while respiratory kinematics involves the anterior joints of the thorax as well. The relation between rib and sternum kinematics was

previously assessed in only two studies in dogs (De Troyer and Decramer, 1985; De Troyer and Wilson, 1993) while description in humans is lacking. The objective was therefore to investigate and compute a detailed analysis of the SCJ kinematics. The hypothesis is that rib level and lung volume could influence SCJ kinematics similarly to CVJ.

Dissertation outline

The present doctoral work will focus on the skeletal and joint components of the thorax, and will be especially dedicated to analyse joint physiology during breathing motion using 3D modelling infographic technics.

The first five chapters are presented following the format of published articles or articles in submission (see figure 12 for a schematic overview of the relation between these five chapters). Finally, these chapters will be discussed in the last section of the present dissertation.

In the first chapter (Chapter 2), the methodology aiming to quantify costovertebral joint (CVJ) 3D kinematics from medical imaging (computed tomodensitometry or CT) data obtained at three different lung volumes is developed. The kinematic analysis concerned only the 7 first ribs, anatomically described as “true” ribs according to their direct relation with the sternum. The main objectives were to develop a methodology usable for the remaining of the thesis and to obtain a combination of joint kinematics quantification and representation through 3D subject specific modelling of the bones of interests over the breathing manoeuver.

The second chapter (Chapter 3) focuses on the effect of anatomical landmarks (ALs) definitions on the computation of the axes of motion. The use of interpolation and the propagation of ALs errors on the position and orientation of the mean helical axes of CVJ were analyzed. The goal was to estimate the accuracy of the entire methodology, and to propose the use of mean helical axes to align proximal/distal anatomical frames of the joint coordinate system. In the same time, the position of the pivot points relative to the joints of interest is reported.

In the third chapter (Chapter 4), the full methodology was extended on lower rib levels 8 to 10 on a larger sample. An analysis of respiratory ribs (i.e. functional aspect considering rib 1 to 10) is reported. The aims were to test the hypothesis that rib level and lung volume may alter kinematic parameters. The influence of the side on kinematic parameters was also tested. Further estimation of the correlation between rib kinematics and lung volumes was analyzed.

The fourth chapter (Chapter 5) presents the comparison of costovertebral joints kinematics obtained in asymptomatic subjects with those of a sample of patients with cystic fibrosis. The

influence of a pathological condition on the costovertebral joint kinematics was tested following above mentioned methodology.

In the fifth part (Chapter 6), kinematic analysis of the anterior joints of the thorax is presented. The developed method was used to compute the kinematics of the ribs ("true ribs") relative to the sternum. In addition, the sternum displacement relative to the thoracic spine was also considered as well as the correlation between sternum and rib displacements.

Finally, the last chapter (Chapter 7) is dedicated to the discussion and conclusion of the present doctoral thesis. Various aspects, such as methodological considerations, clinical implications and research perspectives will be described.

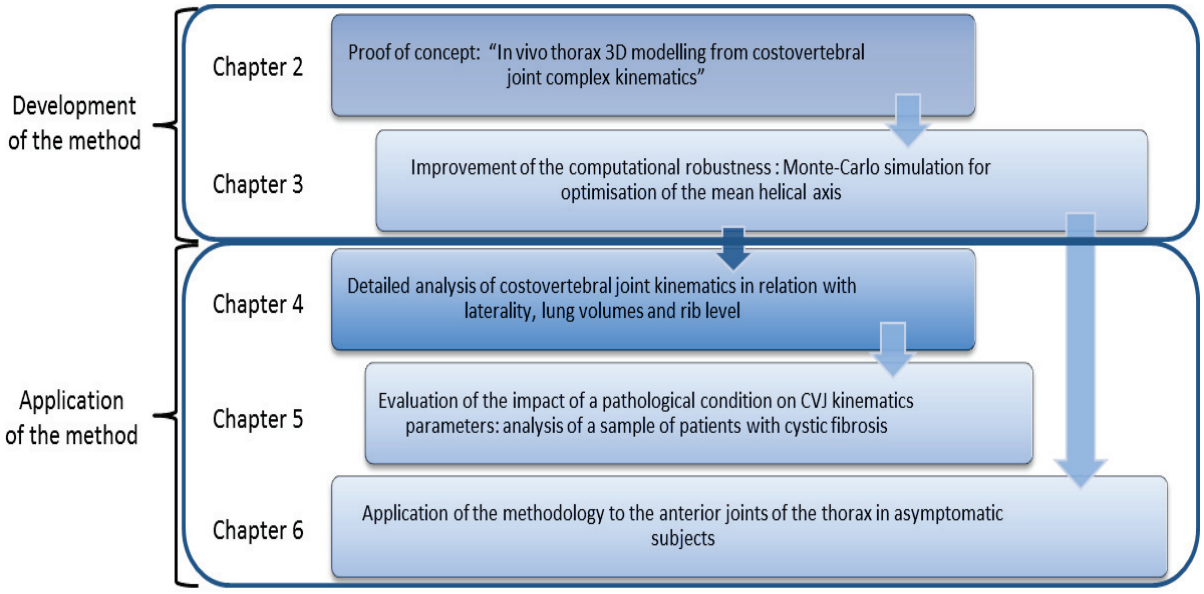

Figure 12: Schematic overview of the organization of the different sections and studies of the doctoral thesis.

References

Agostoni, E., Hyatt, R.E., 2011. Static Behavior of the Respiratory System, in: Comprehensive Physiology. John Wiley & Sons, Inc.

Agostoni, E., Mognoni, P., Torri, G., Agostoni, A.F., 1965. Static features of the passive rib cage and abdomen-diaphragm. J. Appl. Physiol. 20, 1187–1193.

Aliverti, A., Pedotti, A. (Eds.), 2014. Mechanics of Breathing. Springer Milan, Milano.

Andriacchi, T., Schultz, A., Belytschko, T., Galante, J., 1974. A model for studies of mechanical interactions between the human spine and rib cage. J. Biomech. 7, 497–507.

Arroyo, J.F., Jolliet, P., Junod, A.F., 1992. Costovertebral joint dysfunction: another misdiagnosed cause of atypical chest pain. Postgrad. Med. J. 68, 655–659.

Bir, C., Viano, D., King, A., 2004. Development of biomechanical response corridors of the thorax to blunt ballistic impacts. J. Biomech. 37, 73–79.

Bruni, G.I., Gigliotti, F., Scano, G., 2011. Optoelectronic Plethysmography for Measuring Rib Cage Distortion. INTECH Open Access Publisher.

Cala, S.J., Kenyon, C.M., Ferrigno, G., Carnevali, P., Aliverti, A., Pedotti, A., Macklem, P.T., Rochester, D.F., 1996. Chest wall and lung volume estimation by optical reflectance motion analysis. J. Appl. Physiol. Bethesda Md 1985 81, 2680–2689.

Cappello, M., De Troyer, A., 2002. On the respiratory function of the ribs. J. Appl. Physiol. 92, 1642–1646. doi:10.1152/japplphysiol.01053.2001

Cassart, M., Gevenois, P.A., Estenne, M., 1996. Rib cage dimensions in hyperinflated patients with severe chronic obstructive pulmonary disease. Am. J. Respir. Crit. Care Med. 154, 800–805. doi:10.1164/ajrccm.154.3.8810622

Cassart, M., Pettiaux, N., Gevenois, P.A., Paiva, M., Estenne, M., 1997. Effect of chronic hyperinflation on diaphragm length and surface area. Am. J. Respir. Crit. Care Med. 156, 504–508.

Cattrysse, E., Cescon, C., Clijsen, R., Barbero, M., 2013. Finite Helical Axis Behavior In Cervical Kinematics. Presented at the XXIV Congress of the International Society of Biomechanics, Natal, Rio Grande do Norte - Brazil.

Cescon, C., Cattrysse, E., Barbero, M., 2014. Methodological analysis of finite helical axis behavior in cervical kinematics. J. Electromyogr. Kinesiol. Off. J. Int. Soc. Electrophysiol. Kinesiol. 24, 628–635. doi:10.1016/j.jelekin.2014.05.004

Chen, P.H., 1978. Finite element dynamic structural model of the human thorax for chest impact response and injury studies. Aviat. Space Environ. Med. 49, 143–149.

Closkey, R.F., Schultz, A.B., Luchies, C.W., 1992. A model for studies of the deformable rib cage. J. Biomech. 25, 529–539.

Cohen, M.J., Ezekiel, J., Persellin, R.H., 1978. Costovertebral and costotransverse joint involvement in rheumatoid arthritis. Ann. Rheum. Dis. 37, 473–475.

Dassios, T., Katelari, A., Doudounakis, S., Mantagos, S., Dimitriou, G., 2013. Respiratory muscle function in patients with cystic fibrosis. Pediatr. Pulmonol. 48, 865–873. doi:10.1002/ppul.22709

De Troyer, A., Decramer, M., 1985. Mechanical coupling between the ribs and sternum in the dog. Respir. Physiol. 59, 27–34. doi:doi/10.1016/0034-5687(85)90015-5

De Troyer, A., Wilson, T.A., 1993. Sternum dependence of rib displacement during breathing. J. Appl. Physiol. 75, 334–340.

DeStefano, L.A., 2011. Greenman's Principles of Manual Medicine. Lippincott Williams & Wilkins.

Didier, A.-L., Villard, P., Bayle, J.-Y., Beuve, M., Shariat, B., 2007. Breathing Thorax Simulation based on Pleura Physiology and Rib Kinematics, in: International Conference on Medical Information Visualisation - BioMedical Visualisation, 2007. MediVis 2007. Presented at the International Conference on Medical Information Visualisation - BioMedical Visualisation, 2007. MediVis 2007, pp. 35–42. doi:10.1109/MEDIVIS.2007.8

Drake, R.L., Vogl, W., Mitchell, A.W.M., Gray, H., Gray, H., 2010. Gray's anatomy for students. Churchill Livingstone/Elsevier, Philadelphia, PA.

Dufresne, V., Knoop, C., Van Muylem, A., Malfroot, A., Lamotte, M., Opdekamp, C., Deboeck, G., Cassart, M., Stallenberg, B., Casimir, G., Duchateau, J., Estenne, M., 2009. Effect of Systemic Inflammation on Inspiratory and Limb Muscle Strength and Bulk in Cystic Fibrosis. Am. J. Respir. Crit. Care Med. 180, 153–158. doi:10.1164/rccm.200802-232OC

Dugailly, P.-M., Beyer, B., Sobczak, S., Salvia, P., Rooze, M., Feipel, V., 2014. Kinematics of the upper cervical spine during high velocity-low amplitude manipulation. Analysis of intra- and inter-

operator reliability for pre-manipulation positioning and impulse displacements. J. Electromyogr. Kinesiol. 24, 621–627. doi:10.1016/j.jelekin.2014.05.001

Dugailly, P.-M., Sobczak, S., Lubansu, A., Rooze, M., Jan, S.S., Feipel, V., 2013. Validation protocol for assessing the upper cervical spine kinematics and helical axis: An in vivo preliminary analysis for axial rotation, modeling, and motion representation. J. Craniovertebral Junction Spine 4, 10–15. doi:10.4103/0974-8237.121617

Dugailly, P.-M., Sobczak, S., Sholukha, V., Jan, S.V.S., Salvia, P., Feipel, V., Rooze, M., 2010. In vitro 3D-kinematics of the upper cervical spine: helical axis and simulation for axial rotation and flexion extension. Surg. Radiol. Anat. 32, 141–151. doi:10.1007/s00276-009-0556-1

Duprey, S., Subit, D., Guillemot, H., Kent, R.W., 2010. Biomechanical properties of the costovertebral joint. Med. Eng. Phys. 32, 222–227. doi:10.1016/j.medengphy.2009.12.001

Eckert, M., 2001. Comportement des articulations costo-vertébrales lors du chargement frontal quasi-statique de la cage thoraxique.

Eckert, M., Fayet, M., Cheze, L., Bouquet, R., Voiglio, E., Verriest, J.P., 2000. Costovertebral joint behaviour during frontal loading of the thoracic cage. Presented at the Proceedings of the 2000 International IRCOBI conference on the biomechanics of impact , September 20-22, 2000, Montpelier, France.

Fick, R., 1911. Handbuch der Anatomie und Mechanik der Gelenke T. 3. T. 3. Fischer, Jena.

French, R.K., 1978. The thorax in history 1. From ancient times to Aristotle. Thorax 33, 10–18.

Graeber, G.M., Nazim, M., 2007. The anatomy of the ribs and the sternum and their relationship to chest wall structure and function. Thorac. Surg. Clin. 17, 473–489, vi. doi:10.1016/j.thorsurg.2006.12.010

Hayek, H. von, 1960. The human lung. Hafner Pub. Co.

Hodges, P.W., Gandevia, S.C., 2000. Activation of the human diaphragm during a repetitive postural task. J. Physiol. 522, 165–175. doi:10.1111/j.1469-7793.2000.t01-1-00165.xm

Jordanoglou, J., 1970. Vector analysis of rib movement. Respir. Physiol. 10, 109–120.

Jordanoglou, J., 1969. Rib movement in health, kyphoscoliosis, and ankylosing spondylitis. Thorax 24, 407–414.

Jordanoglou, J., Kontos, J., Gardikas, C., 1972. Relative position of the rib within the chest and its determination on living subjects with the aid of a computer program. Respir. Physiol. 16, 41–50.

Kapandji, I.A., 1964. Illustrated physiology of joints. Med. Biol. Illus. 14, 72–81.

Kenyon, C.M., Pedley, T.J., Higenbottam, T.W., 1991. Adaptive modeling of the human rib cage in median sternotomy. J. Appl. Physiol. 70, 2287–2302.

Konno, K., Mead, J., 1967. Measurement of the separate volume changes of rib cage and abdomen during breathing. J. Appl. Physiol. 22, 407–422.

Ladjal, H., Shariat, B., Azencot, J., Beuve, M., 2013. Appropriate biomechanics and kinematics modeling of the respiratory system: Human diaphragm and thorax, in: 2013 IEEE/RSJ International Conference on Intelligent Robots and Systems. Presented at the 2013 IEEE/RSJ International Conference on Intelligent Robots and Systems, pp. 2004–2009. doi:10.1109/IROS.2013.6696623

Laghi, F., Tobin, M.J., 2003. Disorders of the Respiratory Muscles. Am. J. Respir. Crit. Care Med. 168, 10–48. doi:10.1164/rccm.2206020

Lee, L.-J., Chang, A.T., Coppieters, M.W., Hodges, P.W., 2010. Changes in sitting posture induce multiplanar changes in chest wall shape and motion with breathing. Respir. Physiol. Neurobiol. 170, 236–245. doi:10.1016/j.resp.2010.01.001

Loring, S.H., 1986. Structural model of thorax and abdomen for respiratory mechanics. Math. Model. 7, 1083–1098. doi:10.1016/0270-0255(86)90150-8

Macklem, P.T., Macklem, D.M., De Troyer, A., 1983. A model of inspiratory muscle mechanics. J. Appl. Physiol. 55, 547–557.

Manchikanti, L., Boswell, M.V., Singh, V., Pampati, V., Damron, K.S., Beyer, C.D., 2004. Prevalence of facet joint pain in chronic spinal pain of cervical, thoracic, and lumbar regions. BMC Musculoskelet. Disord. 5, 15. doi:10.1186/1471-2474-5-15

Marshall, B., Miller, K., Wittek, A., Nielsen, P.M.F., 2015. Computational Biomechanics for Medicine: New Approaches and New Applications. Springer.

Mead, J., Loring, S.H., 1982. Analysis of volume displacement and length changes of the diaphragm during breathing. J. Appl. Physiol. 53, 750–755.

Meessen, N.E.L., van der Grinten, C.P.M., Folgering, H.T.M., Luijendijk, S.C.M., 1993. Tonic activity in inspiratory muscles during continuous negative airway pressure. Respir. Physiol. 92, 151–166. doi:10.1016/0034-5687(93)90035-9

Mueller, G., Perret, C., Michel, F., Berger, M., Hopman, M.T.E., 2012. Reproducibility of assessing rib cage mobility from computed tomography images. Clin. Physiol. Funct. Imaging 32, 282–287. doi:10.1111/j.1475-097X.2012.01123.x

Muller, N., Bryan, A.C., Zamel, N., 1981. Tonic inspiratory muscle activity as a cause of hyperinflation in asthma. J. Appl. Physiol. 50, 279–282.

Oda, I., Abumi, K., Cunningham, B.W., Kaneda, K., McAfee, P.C., 2002. An in vitro human cadaveric study investigating the biomechanical properties of the thoracic spine. Spine 27, E64-70.

Oda, I., Abumi, K., Lü, D., Shono, Y., Kaneda, K., 1996. Biomechanical role of the posterior elements, costovertebral joints, and rib cage in the stability of the thoracic spine. Spine 21, 1423–1429.

Osmond, D.G., 1995. Functionnal anatomy of the chest wall, in: The Thorax: Part A, 2nd Ed. Roussos C., New York, pp. 413–444.

Parreira, V.F., Vieira, D.S.R., Myrrha, M.A.C., Pessoa, I.M.B.S., Lage, S.M., Britto, R.R., 2012. Optoelectronic plethysmography: a review of the literature. Rev. Bras. Fisioter. São Carlos São Paulo Braz. 16, 439–453.

Pascual, E., Castellano, J.A., López, E., 1992. Costovertebral joint changes in ankylosing spondylitis with thoracic pain. Br. J. Rheumatol. 31, 413–415.

Pelosi, P., Aliverti, A., Dellaca, R., 1998. Chest Wall Mechanics: Methods of Measurement and Physiopathologic Insights, in: Vincent, P.J.-L. (Ed.), Yearbook of Intensive Care and Emergency Medicine 1998, Yearbook of Intensive Care and Emergency Medicine. Springer Berlin Heidelberg, pp. 361–376. doi:10.1007/978-3-642-72038-3_32

Perz, R., Toczyski, J., Subit, D., 2015. Variation in the human ribs geometrical properties and mechanical response based on X-ray computed tomography images resolution. J. Mech. Behav. Biomed. Mater. 41, 292–301. doi:10.1016/j.jmbbm.2014.07.036

Proulx, A.M., Zryd, T.W., 2009. Costochondritis: diagnosis and treatment. Am. Fam. Physician 80, 617–620.

Roberts, S.B., Chen, P.H., 1972. Global geometric characteristics of typical human ribs. J. Biomech. 5, 191–201. doi:10.1016/0021-9290(72)90055-3

Roberts, S.B., Chen, P.H., 1970. Elastostatic analysis of the human thoracic skeleton. J. Biomech. 3, 527–545. doi:10.1016/0021-9290(70)90037-0

Roussos, C., 1995. The Thorax -- Part A: Physiology (In Three Parts), Second Edition. CRC Press.

Sales, J.R., Beals, R.K., Hart, R.A., 2007. Osteoarthritis of the costovertebral joints: The results of resection arthroplasty. J. Bone Joint Surg. Br. 89–B, 1336–1339. doi:10.1302/0301-620X.89B10.19721

Salvia, P., Woestyn, L., David, J.H., Feipel, V., Van, S., Jan, S., Klein, P., Rooze, M., 2000. Analysis of helical axes, pivot and envelope in active wrist circumduction. Clin. Biomech. Bristol Avon 15, 103–111.

Saumarez, R.C., 1986. An analysis of possible movements of human upper rib cage. J. Appl. Physiol. 60, 678–689.

Schultz, A.B., Benson, D.R., Hirsch, C., 1974a. Force-deformation properties of human costo-sternal and costo-vertebral articulations. J. Biomech. 7, 311–318.

Schultz, A.B., Benson, D.R., Hirsch, C., 1974b. Force-deformation properties of human ribs. J. Biomech. 7, 303–309.

Sharp, J.T., Beard, G.A., Sunga, M., Kim, T.W., Modh, A., Lind, J., Walsh, J., 1986. The rib cage in normal and emphysematous subjects: a roentgenographic approach. J. Appl. Physiol. Bethesda Md 1985 61, 2050–2059.

Takeuchi, T., Abumi, K., Shono, Y., Oda, I., Kaneda, K., 1999. Biomechanical role of the intervertebral disc and costovertebral joint in stability of the thoracic spine. A canine model study. Spine 24, 1414–1420.

Van Sint Jan, 2007. Color atlas of skeletal landmark definitions: guidelines for reproducible manual and virtual palpations. Churchill Livingstone/Elsevier, Edinburgh ; New York.

Van Sint Jan, S., Sobzack, S., Dugailly, P.-M., Feipel, V., Lefèvre, P., Lufimpadio, J.-L., Salvia, P., Viceconti, M., Rooze, M., 2006. Low-dose computed tomography: A solution for in vivo medical imaging and accurate patient-specific 3D bone modeling? Clin. Biomech. 21, 992–998. doi:10.1016/j.clinbiomech.2006.05.007

Vezin, P., Berthet, F., 2009. Structural characterization of human rib cage behavior under dynamic loading. Stapp Car Crash J. 53, 93–125.

Vezin, P., Verriest, J.P., 2005. Development of a Set of Numerical Human Models for Safety. Presented at the 19th International Technical Conference on the Enhanced Safety of Vehicles (ESV).

Viano, D.C., 1978. Evaluation of biomechanical response and potential injury from thoracic impact. Aviat. Space Environ. Med. 49, 125–135.

Von Hayek, H., 1970. Die Menschliche Lunge. Springer.

Walsh, J.M., Webber, C.L., Fahey, P.J., Sharp, J.T., 1992. Structural change of the thorax in chronic obstructive pulmonary disease. J. Appl. Physiol. Bethesda Md 1985 72, 1270–1278.

Ward, M.E., Macklem, P.T., 1995. Kinematics of the chest wall, in: The Thorax: Part A, 2nd Ed. Roussos C., New York, pp. 515–533.

Ward, M.E., Ward, J.W., Macklem, P.T., 1992. Analysis of human chest wall motion using a two-compartment rib cage model. J. Appl. Physiol. Bethesda Md 1985 72, 1338–1347.

Weber, B., Smith, J.P., Briscoe, W.A., Friedman, S.A., King, T.K., 1975. Pulmonary function in asymptomatic adolescents with idiopathic scoliosis. Am. Rev. Respir. Dis. 111, 389–397. doi:10.1164/arrd.1975.111.4.389

Wilson, T.A., Legrand, A., Gevenois, P.A., De Troyer, A., 2001. Respiratory effects of the external and internal intercostal muscles in humans. J. Physiol. 530, 319–330.

Wilson, T.A., Rehder, K., Krayer, S., Hoffman, E.A., Whitney, C.G., Rodarte, J.R., 1987. Geometry and respiratory displacement of human ribs. J. Appl. Physiol. Bethesda Md 1985 62, 1872–1877.

Woltring, H.J., Huiskes, R., de Lange, A., Veldpaus, F.E., 1985. Finite centroid and helical axis estimation from noisy landmark measurements in the study of human joint kinematics. J. Biomech. 18, 379–389.

Zhu, Y., Fang, Y., Bermond, F., Bruyère-Garnier, K., Ellouz, R., Rongieras, F., Mitton, D., 2013. Relationship between human rib mechanical properties and cortical bone density measured by high-resolution quantitative computed tomography. Comput. Methods Biomech. Biomed. Engin. 16 Suppl 1, 191–192. doi:10.1080/10255842.2013.815888

Chapter 2:

In vivo thorax 3D modelling from costovertebral joint complex kinematics

Published as:

Benoît Beyer[1,*], Victor Sholuka[1,4], Pierre Michel Dugailly[2,3], Marcel Rooze[1,2], Fedor Moiseev[1], Véronique Feipel[2] , Serge Van Sint Jan[1];

Clinical Biomechanics (Bristol, Avon) 2014 April; 29(4): 434-438.

1: Laboratory of Anatomy, Biomechanics and Organogenesis, Université Libre de Bruxelles, Bruxelles, Belgium.
2: Laboratory of Functional Anatomy, Université Libre de Bruxelles, Bruxelles, Belgium.
3: Laboratory of Manual Therapy, Université Libre de Bruxelles, Bruxelles, Belgium.
4: Department of Applied Mathematics, State Polytechnical University (SPbSPU), Saint Petersburg, Russia

ABSTRACT

Background: The costovertebral joint complex is mechanically involved in both respiratory function and thoracic spine stability. The thorax has been studied for a long time to understand its involvement in the physiological mechanism leading to specific gas exchange. Few studies have focused on costovertebral joint complex kinematics, and most of them focused on experimental *in vitro* analysis related to loading tests or global thorax and/or lung volume change analysis. There is however a clinical need for new methods allowing to process *in vivo* clinical data. This paper presents results from *in vivo* analysis of the costovertebral joint complex kinematics from clinically-available retrospective data.

Methods: In this study, *in vivo* spiral computed tomography imaging data were obtained from 8 asymptomatic subjects at three different lung volumes (from total lung capacity to functional residual capacity) calibrated using a classical spirometer. Fusion methods including 3D modelling and kinematic analysis were used to provide 3D costovertebral joint complex visualisation for the true ribs (i.e., first seven pairs of ribs).

Findings: The 3D models of the first seven pairs of costovertebral joint complexes were obtained. A continuous kinematics simulation was interpolated from the three discrete CT positions. Helical axis representation was also achieved.

Interpretation: Preliminary results show that the method leads to meaningful and relevant results for clinical and pedagogical applications. Research in progress compares data from a sample of healthy volunteers with data collected from patients with cystic fibrosis to obtain new insights about the costovertebral joint complex range of motion and helical axis assessment in different pathological conditions.

Keywords: *costovertebral kinematics, rib cage mechanics, respiratory mechanics, thorax modelling, helical axis*

1. Introduction

The rib cage is regarded as an anatomical structure organized for both protection of vital organs, and mechanical support for respiratory function and spinal stiffness. Rib cage mobility function was previously demonstrated to support breathing (Cappello and De Troyer, 2002). The relationships between the costovertebral joints (CVJs) and the thoracic spine were also described (Oda et al., 2002, 1996; Takeuchi et al., 1999). Functional impairments of the respiratory function and the thoracic spine has been related to show important kinematic and compliance consequences (De Troyer et al., 1986a; M Estenne et al., 1985; Gilmartin and Gibson, 1986). Quantification of rib cage mobility from computerized tomography (CT) images is a reproducible method (Mueller et al., 2012). Clinical perspectives of this method are promising in order to describe normal and pathological patterns of both respiratory and postural thorax mechanics (e.g., neuromuscular or musculo-skeletal diseases, etc...). Also, as no evidence is currently available on manual therapy techniques for improving rib mobility or alveolar gas exchange, methods should be developed to evaluate validity and kinematics impact of such therapeutic approaches. According to the literature (Dugailly et al., 2010; Salvia et al., 2000), the 3D orientation of motion axis was reported to provide qualitative description of motion.

The aim of the present study was to develop a methodological protocol allowing *in vivo* quantification and representation of CVJs 3D kinematic behaviour with an emphasis on using motion representation that would respect the physiological CVJ behaviour (Beyer et al, 2011; Beyer et al, 2013). Another aim of the study was to develop the protocol from data that are ethically acceptable in clinical practise; therefore use of invasive methods was avoided.

2. Method

2.1. Subjects

This study is based on a previously-described method used for CVJ motion representation (Beyer et al, 2011; Beyer et al., 2013). This study relied on the latter method to collect data related to *in vivo* CVJ behaviour during breathing. Retrospective codified medical imaging datasets were obtained from the Department of Radiology of the Erasme Academic Hospital for 8 asymptomatic volunteers (mean age 30.4 (5.5) years old; mean body mass index 21.1 (2.2) kg/cm²). The protocol was approved by the local ethical committee (P2005/021).

2.2. Medical imaging and 3D bone model reconstruction

Spiral Computed Tomography (Siemens SOMATOM, helical mode, slice thickness = 0.5 mm, inter-slice spacing = 1 mm, image data format: DICOM 3.0) was performed at three different lung volumes: Total lung capacity (TLC); Middle Inspiratory Capacity (MIC); and Functional Residual Capacity (FRC) (Cassart et al., 1997; Gauthier et al., 1994a; Pettiaux et al., 1997). TLC and FRC respectively ranged from 4.86 L to 7.33 L and from 2.75 L to 4.04 L). Lung function was tested before

imaging was realized on the complete thorax from the 1st to the 12th thoracic level. Each lung volume corresponded to one particular thorax attitude; therefore three discrete positions of the thorax were available for further CVJ kinematic analysis.

A data segmentation software interface (Amira 4.0, San Diego, CA, USA) was used to obtain 3D models of all bony thorax structures from the three available CT datasets (Fig. 1). Both manual and semi-automated procedures were used during the segmentation process. All bone models were stored in Virtual Reality Modelling Language (VRML) prior to further processing.

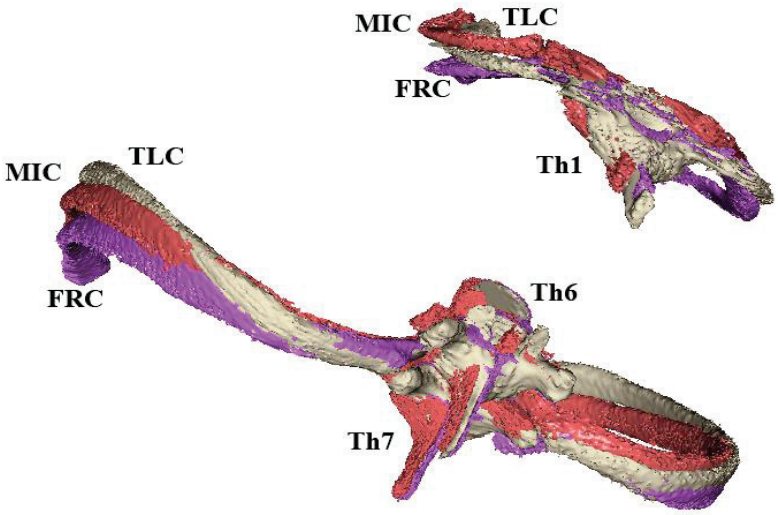

Figure 1: First and seventh CVJ complex (involving respectively 1st thoracic vertebra (Th1); the 7th rib and the 6th and 7th vertebrae (Th6 and Th7)) in the three available discrete positions (TLC in white, MIC in red and FRC in purple). Posterior view.

2.3. Kinematics computing and analysis

A custom-made software (called lhpFusionBox) was used to process the obtained 3D models. This software was developed from the open-source MAF library (Viceconti et al., 2007) and allowed virtual palpation of anatomical landmarks (ALs) observed at the surface of the bone models (Van Sint Jan et al., 2006; Van Sint Jan, 2007) (Fig. 2A, B). All AL coordinates were defined in the technical frame of the original CT dataset. Strict palpation definitions were adopted to increase palpation reproducibility (Van Sint Jan and Della Croce, 2005). Five ALs were palpated on each rib and each vertebra model. The palpation protocol reproducibility (3 repetitions performed by 2 operators during two sessions with a 24-hour interval) was assessed and showed an inter-session maximal standard deviation (SD) of 1.4 mm on AL location, and an intra-examiner variation inferior to 1 mm (Table 1). The discrete spatial location of the palpated ALs was further processed to determine each bone spatial displacements defined in the CT global coordinate system and obtain helical axis data (such as mean helical axis (MHA) and pivot point) related to each CVJ joint component (Van Sint Jan, 1997; Beyer et al., 2013).

	INTER Examiner					
	Day 1			**Day 2**		
	x	y	z	x	y	z
RMS	0,6	0,8	0,7	0,7	0,9	0,9
	INTRA Examiner					
	Exam 1			**Exam 2**		
	x	y	z	x	y	z
RMS	0,4	0,4	0,2	0,2	0,3	0,3
	INTRA SESSION					
	Exam 1			**Exam 2**		
	x	y	z	x	y	z
MSD Day 1	0,3	0,3	0,3	0,2	0,2	0,3
MSD Day2	0,3	0,4	0,5	0,2	0,2	0,1

Table 1: RMS for intra/inter examiner palpation reliability; RMS = root mean square error. MSD = mean of standard deviation. All results are presented in millimeter (mm).

2.4. CVJ local coordinate system definition and HA representation

In order to represent CVJ kinematics, two supplementary ALs were added at the centre of upper and lower endplates of each vertebra (Fig. 2) to create vertebral and costal anatomical coordinate systems, or anatomical frames (AFs), corresponding to each CVJ segment. Rib and vertebra specific coordinate systems were used to express rigid body kinematics, according to previously-proposed orientation recommendations (Beyer et al., 2011, Beyer et al., 2013; Wu and Cavanagh, 1995; Wu et al., 2002) (Fig 2C) . The X-axis was oriented forward, the Y-axis upward and the Z-axis to the right. Rib AFs were manually oriented so they were collinear to vertebra AF for each true rib level with the origin at mid-distance between R1 and R2 (Fig 2C). The mean pivot closest to all available finite helical axes (FHA) in a least squared sense was calculated to define the optimal position vector. Then the optimal direction vector (i.e., mean helical axis or MHA) was calculated as the vector with the smallest angle between axes (Stokdijk et al., 1999; Woltring et al., 1990). Two points located along the MHA at equal distance from the MHA pivot point (Van Sint Jan et al., 1997) were computed to express the orientation of local rib MHA relative to the vertebrae over the complete range of motion. Motion around the X-axis, Y-axis and Z-axis were defined as upward (+) / downward (-) bending, right (+) / left (-) rotation and flexion (+) / extension (-), respectively.

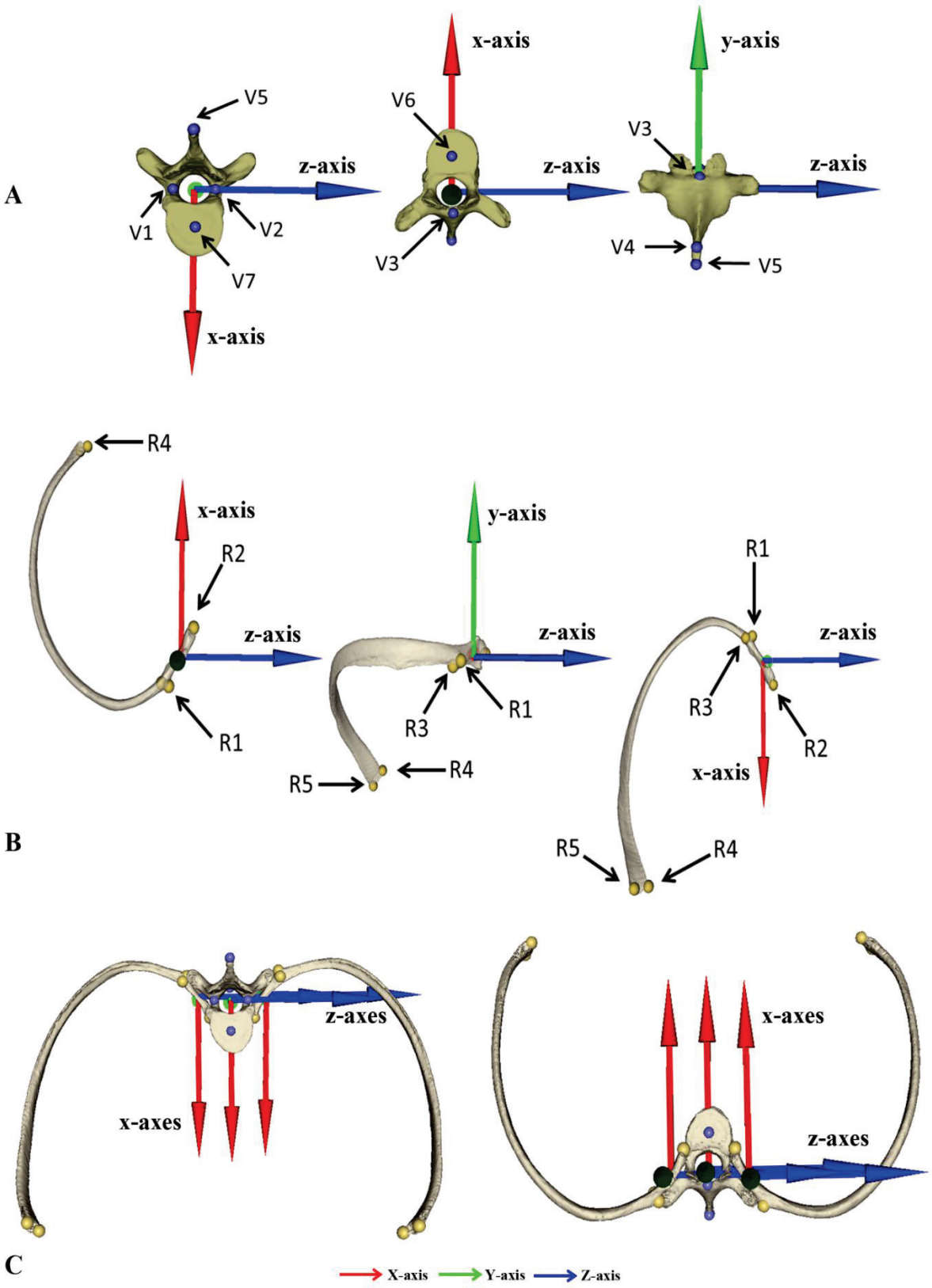

Figure 2: A: Anatomical landmarks (ALs) and Anatomical coordinate systems used for vertebra (from left to right: inferior, superior and posterior view); B: ALs and coordinate frames used for ribs (from left to right: superior, posterior and inferior view); C: AFs alignment at TLC position as referential position (left: inferior view, right: superior view).

Vertebra Landmarks: (Fig. 2A)	
V1	Centre of inferior border of left pedicle
V2	Centre of inferior border of right pedicle
V3	Superior junction of lamina
V4	Posterior and superior apex of spinous process
V5	Posterior and inferior apex of spinous process
V6	Center of upper endplate
V7	Center of lower endplate
Rib Landmarks: (Fig. 2B)	
R1	Posterior apex of tuberosity
R2	Anterior apex of inter-articular crest of costo-corporeal joint
R3	Inferior point of tuberosity
R4	Superior apex of costo-chondral surface
R5	Inferior apex of costo-chondral surface

3. Results

3.1. Local coordinate systems and absolute range of motion

CVJ motion representations and absolute ranges of motion were obtained (Table 2, figures 3 and supplementary material) for all true ribs. CVJ behaviour computed showed that the motion components around the X- and Z-axes were similar for each pair of homologue (i.e. left-right ribs: mean X-range between 4.6° ((7th rib) and 8.9° (2nd rib), Z-range between 5.7° (7th rib) and 12.2° (1st rib)). Mean displacements around the Y-axis showed smaller ranges (between 2.4° (5th rib) and 4.8° (1st rib)). Mean standard deviation concerning all degrees-of-freedom of all rib ranges of motion was 2.8°.

Intervertebral motion displayed a similar range around all axes, between 1.0° and 2.8° with a mean standard deviation of 1.0°. Supplementary material (in annex) gives the opportunity to visualize continuous motion simulation.

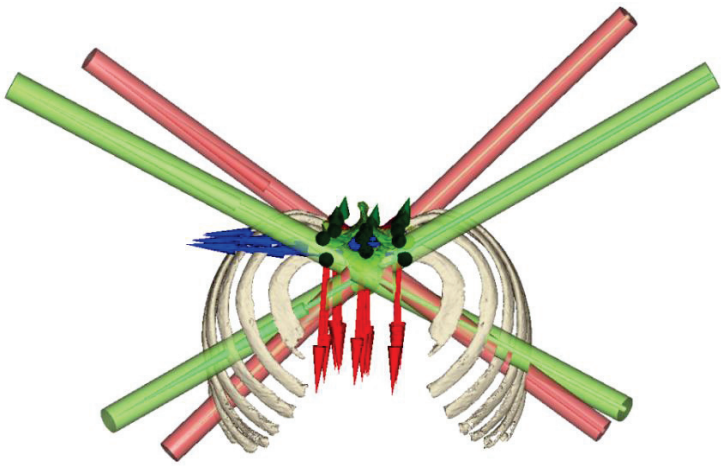

Figure 3: Superior view of CVJ Complex with specific costal and vertebral AFs and example of MHA visualisation for first (green) and seventh (red) thoracic level for both right and left side.

	Θx		Θy		Θz			Θx	Θy	Θz
	Left	Right	Left	Right	Left	Right				
Rib1	7,0	8,1	4,3	4,8	11,2	12,2	**Th1/Th2**	1,7	1,4	1,9
	(4,5)	(3,9)	(2,4)	(1,7)	(2,7)	(2,3)		(1,4)	(0,8)	(0,9)
Rib2	8,9	6,7	3,2	4,3	10,1	10,7	**Th2/Th3**	1,3	1,2	2,8
	(3,3)	(3,7)	(0,9)	(1,8)	(2,8)	(2,6)		(1,1)	(0,8)	(1,7)
Rib3	8,6	7,8	3,7	3,8	7,1	9,4	**Th3/Th4**	1,9	1,9	2,1
	(3,9)	(2,2)	(0,9)	(0,9)	2,2)	(2,2)		(1,5)	(1,2)	(1,3)
Rib4	8,2	5,9	3,7	3,3	7,5	9,4	**Th4/Th5**	2,2	1,4	1,6
	(2,9)	(2,5)	(1,4)	(1,8)	(1,7)	(1,8)		(0,7)	(1,2)	(1,0)
Rib5	7,0	6,2	2,8	2,4	6,8µ	7,8	**Th5/Th6**	1,0	1,4	2,3
	(2,6)	(2,3)	(1,2)	(1,1)	(2,3)	(2,1)		(0,6)	(0,6)	(1,0)
Rib6	6,6	5,5	3,2	3,9	6,6	7,2	**Th6/Th7**	1,6	1,5	1,8
	(2,3)	(2,3)	(0,8)	(2,7)	(1,8)	(2,2)		(0,8)	(0,7)	(0,9)
Rib7	5,1	4,6	2,8	3,1	5,7	7,1				
	(2,7)	(2,0)	(1,9)	(1,2)	(2,3)	(2,2)				

Table 2: Mean ranges of motion (in degrees). Results are defined in terms of rotation around the x-, y- and z-axes as θx; θy and θz. Maximum are displayed in red and minimum underlined.

3.2.HA orientation and location

MHA data were determined for both sides and all levels for the global motion (from TLC to FRC). Visualisation of MHA results for the 1st and 7th CVJ levels is provided in Fig. 3 for one subject. HA location and orientation with respect to each local vertebral AF are given in Table 3 for the same subject. Results show that, for example, the 1st rib HA is obliquely oriented in similar way caudally, laterally and anteriorly for both sides. HA for the 7th rib level is oriented more laterally and caudally, closer to the frontal plane for the 7th level.

Mean orientation (average direction cosines with respect to each x, y and z axis) of MHA is given in Table 4 for the 1st and 7th CVJ levels. It is presented as an average of direction cosines for the 8 subjects studied in this study. Both x and z direction cosines were similar for 1st to 7th level. Inter-subject variability in direction cosines range between 0.09663 and 0.73673 with maximal value for 7th CVJ (Table 4).

	Direction cosines						**Pivot Point coordinates in Vertebra AF (in mm)**					
	Left			**Right**			**Left**			**Right**		
	x	**y**	**z**	**x**	**y**	**z**	**X**	**y**	**z**	**x**	**y**	**z**
Rib1	0,5334	-0,6396	0,5535	-0,6604	0,2337	0,7136	9,50	-9,84	4,73	14,45	-0,49	1,23
Rib2	0,5317	-0,0344	0,8461	-0,5334	0,2880	0,7952	-0,11	0,86	-24,43	1,26	5,16	23,42
Rib3	0,9546	-0,0340	0,2960	-0,6447	0,2286	0,7294	6,20	5,56	-22,34	5,64	1,97	5,01
Rib4	0,6893	-0,1369	0,7114	-0,8831	0,1216	0,4530	17,40	1,29	-13,38	-6,81	0,15	21,81
Rib5	0,5674	-0,1174	0,8151	-0,6549	0,2123	0,7252	-12,38	-0,83	-27,65	-0,26	-6,52	21,11
Rib6	0,8817	-0,2656	0,3899	-0,6798	0,5024	0,5342	9,02	4,27	-19,24	-1,43	8,63	25,59
Rib7	0,1782	-0,2379	0,9548	-0,4312	-0,1507	0,8896	-8,97	28,89	-55,39	-25,36	14,72	35,29

Table 3: Mean Helical Axis orientation (direction cosines) and position (spatial coordinates of MHA pivot point) with respect to x, y and z axes for one subject,

Direction cosines					
x		**y**		**z**	
Left					
0,54396	(0,13478)	-0,15226	(0,23993)	0,77629	(0,11726)
0,50372	(0,33989)	-0,07369	(0,16722)	0,76985	(0,16065)
0,66837	(0,20538)	-0,20363	(0,13932)	0,65151	(0,19558)
0,60517	(0,12506)	-0,16206	(0,13389)	0,75496	(0,09663)
0,63948	(0,12951)	-0,19411	(0,23511)	0,68284	(0,16577)
0,61650	(0,18367)	-0,20050	(0,21067)	0,69995	(0,13021)
0,47978	(0,25306)	-0,01524	(0,44636)	0,67098	(0,31892)
Right					
-0,60801	(0,10793)	0,28983	(0,15123)	0,70542	(0,14539)
-0,52112	(0,14716)	0,15264	(0,18089)	0,80580	(0,09688)
-0,31298	(0,64515)	0,17000	(0,15245)	0,35266	(0,64519)
-0,46966	(0,26509)	0,16469	(0,15929)	0,80129	(0,17414)
0,00274	(0,73673)	0,09587	(0,27405)	0,33883	(0,61907)
-0,37289	(0,53352)	0,20977	(0,18846)	0,60096	(0,44803)
-0,21007	(0,55932)	0,11308	(0,30929)	0,40251	(0,69582)

Table 4: Average (n=8) of mean helical axis direction cosines and standard deviations for both sides with respect to x-, y- and z- axes, Minimal and maximal SD is respectively underlined and written in red.

4. Discussion

4.1.CVJ local coordinate system

In this study, kinematics results are expressed according to a previous proposal of specific CVJ anatomical frames (Beyer et al., 2011, Beyer et al., 2013). Motion representation was realized using conventional anatomical planes to describe rib displacements to improve our understanding of thorax deformation during breathing and to develop novel visualization tools understandable for clinicians. As presented previously, it is possible to characterize CVJ kinematics in both mechanical and clinical representation (Beyer et al, 2011, Beyer et al., 2013). The method presented in this paper allows motion representation of the CVJ behaviour during breathing. Previous work (Wilson et al., 1987; Wilson et al., 2001) reported a different method to quantify rib motions using for example the best fit plane passing through the anterior body of the rib, and relative to global sagittal and frontal midplane. Despite its usefulness, such global representation does not allow local CVJ joint representation. Our method proposes local CVJ coordinate system built from anatomical landmarks, allowing anatomically-meaningful representation for clinician, especially when the rib local coordinate system is localised within the rib neck. Results are however describing similar CVJ behaviour. As such, the main rib displacement is often referred as a so-called "bucket handle" (corresponding to the rotation about the x-axis in our study) and "pump handle" (rotation about the z-axis in this paper) between two extreme positions (maximal inhalation and exhalation) (Wilson et al.,

1987; Wilson et al., 2001). Results from our paper indicate that the largest amplitudes are found around the X- and Z-axes (see Table 2).

4.2.Global range of motion and HA

The ranges-of-motion measured in this study seem to be in agreement with previous reports related to "bucket" (sagittal axis) and "pump" (frontal axis) handle angle variations (Wilson et al., 1987; Wilson et al., 2001) stating that both decrease with the rib number. In this study, the MHA were not strictly oriented along the rib neck axis as approximated in most previous theoretical papers (Hayek, 1960; Kapandji, 1964). However, a previous experimental study (Wilson et al., 2001) already discussed the possibility that during passive inflation, with gliding movement of costotransverse joint, the axis of rib rotation and rib neck would not coincide. Our results enhance that first rib motion for example was shown to occur almost equally around Z-axis and X-axis instead of the classical frontal "pump handle" axis description. Also average MHA orientation between 1st and 7th rib showed similar orientation with respect to the X-axis and Z-axis. This similar orientation of MHA for each level correspond to what was proposed in previous experimental work that estimates around 45° the angle between axis of rib rotation and transverse midplane (Wilson et al., 2001). In this study we obtained complete 3D parameters of effective rib rotation axis along each plane.

Inter-individual variations of MHA seemed to be more important at lower levels. The impact of different diseases (i.e. pulmonary; neuro-musculo-skeletal, etc…) on kinematics parameters should be evaluated.

The authors acknowledge that the data used in this study were obtained from discrete positions. Continuous motion would probably be more representative of actual joint kinematics. However, techniques based on continuous tracking of external landmarks (i.e., reflective markers) are difficult to implement for CVJ motion *in vivo*, due to the problems related to marker positioning and skin motion artifacts. The main advantage of the presented method is that it can be used within existing clinical imaging protocols like in this study, and could be therefore useful to understand thorax biomechanics in different pathological conditions.

4.3.Perspectives: correlation with anthropometrical measurements and functional pulmonary test

A study is currently running to quantify the links between ribs/vertebrae kinematics determined in this study and other clinically-relevant information such as anthropometrical measurements and functional pulmonary tests. The long-term objective is to create a larger database including the same kind of data. Few studies have already tested such an influence of anthropometrical parameters on thoracic cage dimensions (Bellemare et al., 2003; F. Bellemare et al., 2001; J. F. Bellemare et al., 2001; Gayzik et al., 2008; Laurin et al., 2012). Our study offers the perspective to complement these previous results and provide kinematics parameters for clinical applications. It is

also expected that results will allow improving our general understanding of the relationships between clinical measurements of physiological signals (e.g., FPT), thorax behavior obtained from clinical medical imaging and the underlying disorders (e.g., cystic fibrosis, asthma, etc...). Note that this study was limited to analysing the behavior from ribs 1 to 7 because of the constraints of the underlying clinical medical imaging protocol (see method section). The remaining ribs (from 8 to 12) could be studied by extending the imaging protocol to the entire thorax and applying the data processing method described in this study.

5. Conclusion

This paper presents a novel methodology related to CVJ kinematics. It has been applied on 8 asymptomatic subjects to describe normal CVJ behaviour. Classical description of "bucket handle" and "pump handle" component of rib motion seemed to occur similarly for each level. The method seems promising in order to link particular thorax disorders with CVJ behaviour. Running work on patient data should determine if results can be clinically-linked to other available clinical parameters.

6. Conflict of interest

No authors have any conflict of interest to report.

7. Acknowledgments

The authors are grateful to the Radiological Department of Erasme Academic Hospital for contributing to this research.

References

Bellemare, F., Couture, J., Cordeau, M.P., Leblanc, P., Lafontaine, E., 2001. Anatomic landmarks to estimate the length of the diaphragm from chest radiographs: effects of emphysema and lung volume reduction surgery. Chest 120, 444–452.

Bellemare, F., Jeanneret, A., Couture, J., 2003. Sex differences in thoracic dimensions and configuration. Am. J. Respir. Crit. Care Med. 168, 305–312.

Bellemare, J.F., Cordeau, M.P., Leblanc, P., Bellemare, F., 2001. Thoracic dimensions at maximum lung inflation in normal subjects and in patients with obstructive and restrictive lung diseases. Chest 119, 376–386.

Beyer, B., Dugailly, P.M., Moiseev, F., Van Sint Jan, S., Sobczak, S., Feipel, V., Salvia, P., Rooze, M., 2011. Kinematics analysis of the costovertebral joint complex. Proceedings at the XXIIIrd congress of the International Society of Biomechanics, Bruxelles, p. 119.

Beyer, B., Feipel, V. Coupier, J., Snoek, O., Dugailly, P.M., Van Sint Jan, S., Rooze, M., 2013. Thorax 3D modelling from costovertebral joint complex kinematics: preliminary results. Proceedings of the XXIVth congress of the International Society of Biomechanics, Natal, p. 185.

Cappello, M., De Troyer, A., 2002. On the respiratory function of the ribs. J Appl Physiol 92, 1642–1646.

Cassart, M., Pettiaux, N., Gevenois, P.A., Paiva, M., Estenne, M., 1997. Effect of chronic hyperinflation on diaphragm length and surface area. Am. J. Respir. Crit. Care Med. 156, 504–508.

De Troyer, A., Estenne, M., Vincken, W., 1986. Rib cage motion and muscle use in high tetraplegics. Am. Rev. Respir. Dis. 133, 1115–1119.

Dugailly, P.-M., Sobczak, S., Sholukha, V., Jan, S.V.S., Salvia, P., Feipel, V., Rooze, M., 2010. In vitro 3D-kinematics of the upper cervical spine: helical axis and simulation for axial rotation and flexion extension. Surg Radiol Anat 32, 141–151.

Estenne, M., Yernault, J.C., De Troyer, A., 1985. Rib cage and diaphragm-abdomen compliance in humans: effects of age and posture. J. Appl. Physiol. 59, 1842–1848.

Gauthier, A.P., Verbanck, S., Estenne, M., Segebarth, C., Macklem, P.T., Paiva, M., 1994. Three-dimensional reconstruction of the in vivo human diaphragm shape at different lung volumes. J. Appl. Physiol. 76, 495–506.

Gayzik, F.S., Yu, M.M., Danelson, K.A., Slice, D.E., Stitzel, J.D., 2008. Quantification of age-related shape change of the human rib cage through geometric morphometrics. Journal of Biomechanics 41, 1545–1554.

Gilmartin, J.J., Gibson, G.J., 1986. Mechanisms of paradoxical rib cage motion in patients with chronic obstructive pulmonary disease. Am. Rev. Respir. Dis. 134, 683–687.

Hayek, H. von, 1960. The human lung. Hafner Pub. Co.

Kapandji, I.A., 1964. Illustrated physiology of joints. Med Biol Illus 14, 72–81.

Laurin, L.-P., Jobin, V., Bellemare, F., 2012. Sternum length and rib cage dimensions compared with bodily proportions in adults with cystic fibrosis. Can. Respir. J. 19, 196–200.

Mueller, G., Perret, C., Michel, F., Berger, M., Hopman, M.T.E., 2012. Reproducibility of assessing rib cage mobility from computed tomography images. Clin Physiol Funct Imaging 32, 282–287.

Oda, I., Abumi, K., Cunningham, B.W., Kaneda, K., McAfee, P.C., 2002. An in vitro human cadaveric study investigating the biomechanical properties of the thoracic spine. Spine 27, E64–70.

Oda, I., Abumi, K., Lü, D., Shono, Y., Kaneda, K., 1996. Biomechanical role of the posterior elements, costovertebral joints, and rib cage in the stability of the thoracic spine. Spine 21, 1423–1429.

Pettiaux, N., Cassart, M., Paiva, M., Estenne, M., 1997. Three-dimensional reconstruction of human diaphragm with the use of spiral computed tomography. J. Appl. Physiol. 82, 998–1002.

Salvia, P., Woestyn, L., David, J.H., Feipel, V., Van, S., Jan, S., Klein, P., Rooze, M., 2000. Analysis of helical axes, pivot and envelope in active wrist circumduction. Clin Biomech (Bristol, Avon) 15, 103–111.

Stokdijk, M., Meskers, C.G., Veeger, H.E., de Boer, Y.A., Rozing, P.M., 1999. Determination of the optimal elbow axis for evaluation of placement of prostheses. Clin Biomech (Bristol, Avon) 14, 177–184.

Takeuchi, T., Abumi, K., Shono, Y., Oda, I., Kaneda, K., 1999. Biomechanical role of the intervertebral disc and costovertebral joint in stability of the thoracic spine. A canine model study. Spine 24, 1414–1420.

Van Sint Jan, 2007. Color atlas of skeletal landmark definitions: guidelines for reproducible manual and virtual palpations. Churchill Livingstone/Elsevier, Edinburgh ; New York.

Van Sint Jan, S., Della Croce, U., 2005. Accurate palpation of skeletal landmark locations: Why standardized definitions are necessary. A proposal. Clinical biomechanics 20, 659–660.

Van Sint Jan, S., Giurintano, D.J., Thompson, D.E., Rooze, M., 1997. Joint kinematics simulation from medical imaging data. IEEE Trans Biomed Eng 44, 1175–1184.

Van Sint Jan, S., Salvia, P., Feipel, V., Sobzack, S., Rooze, M., Sholukha, V., 2006. In vivo registration of both electrogoniometry and medical imaging: development and application on the ankle joint complex. IEEE Trans Biomed Eng 53, 759–762.

Viceconti, M., Zannoni, C., Testi, D., Petrone, M., Perticoni, S., Quadrani, P., Taddei, F., Imboden, S., Clapworthy, G., 2007. The multimod application framework: a rapid application development tool for computer aided medicine. Comput Methods Programs Biomed 85, 138–151.

Wilson, T.A., Legrand, A., Gevenois, P.A., De Troyer, A., 2001. Respiratory effects of the external and internal intercostal muscles in humans. J. Physiol. (Lond.) 530, 319–330.

Wilson, T.A., Rehder, K., Krayer, S., Hoffman, E.A., Whitney, C.G., Rodarte, J.R., 1987. Geometry and respiratory displacement of human ribs. J. Appl. Physiol. 62, 1872–1877.

Woltring H.J., 1990. Data processing and error analysis. In: Biomechanics of human movement: Applications in Rehabilitation, Sport and Ergonomics. (Edited by Capozzo, A and Berme P.) 10.1, 203-237.

Wu, G., Cavanagh, P.R., 1995. ISB recommendations for standardization in the reporting of kinematic data. J Biomech 28, 1257–1261.

Wu, G., Siegler, S., Allard, P., Kirtley, C., Leardini, A., Rosenbaum, D., Whittle, M., D'Lima, D.D., Cristofolini, L., Witte, H., Schmid, O., Stokes, I., 2002. ISB recommendation on definitions of joint coordinate system of various joints for the reporting of human joint motion--part I: ankle, hip, and spine. International Society of Biomechanics. J Biomech 35, 543–548.

Next steps

The previous chapter focused in designing methodology to obtain 3D representation of CVJ joints 1 to 7 from CT data. Further work was needed to improve the processing of the kinematic data obtained, especially concerning the orientation of the helical axes. Therefore the next chapter will focus on improving the above-developed computational method and will estimate the error propagation of AL location on motion representation.

Chapter 3:

Effect of anatomical landmark perturbation on mean helical axis parameters of in vivo upper costovertebral joints

Published as:

Benoît Beyer[1,2,*], Victor Sholukha[1,3], Patrick Salvia1[1], Marcel Rooze[1,2], Véronique Feipel[1,2], Serge Van Sint Jan[1];

Journal of Biomechanics 2015; 48(3): 534-538.

1: Laboratory of Anatomy, Biomechanics and Organogenesis, Université Libre de Bruxelles, Brussels, Belgium.
2: Laboratory of Functional Anatomy, Université Libre de Bruxelles, Brussels, Belgium.
3: Department of Applied Mathematics, State Polytechnical University (SPbSPU), Saint Petersburg, Russia.

ABSTRACT

Literature concerning quantification of costovertebral joint (CVJ) motion under *in vivo* conditions is scarce. Most papers concerning this topic are related to *ex vivo* loading conditions. *In vivo* protocols are available from the literature to determine rib and vertebra kinematics but new developments are needed to improve data processing concerning CVJ behaviour obtained from discrete breathing positions showing limiting ranges-of-motion and sensitive to noise. Data from previous work were used to implement a method analysing mean helical axis (MHA) and pivot point parameters of the CVJ complexes. Several levels of noises were estimated within Monte-Carlo simulations to optimize MHA results. MHA parameters were then used to transform and define a CVJ-specific local coordinate system. This study proposes an improvement for CVJ kinematics processing and description from *in vivo* data obtained from computed tomography. This methodology emphasizes the possibility to work with variability of MHA parameters using Monte-Carlo procedures on anatomical landmark coordinates and to define a local coordinate system from this particular joint behaviour. Results from the CVJ joint model are closer to a hinge joint (secondary motions inferior to 3°) when anatomical frames are expressed from MHA orientation. MHA orientation and position data obtained from the proposed method are relevant according to angular dispersion obtained (from 7.5° to 13.9°) and therefore relevant to define behaviour of CVJ.

Keywords: Mean helical axis, Monte-Carlo procedure, costovertebral joint, rib kinematics, pivot point, breathing thorax

1. Introduction

The rib cage is a multiple joint complex organisation implicated in respiratory function and spine stability (Cappello and De Troyer, 2002; Oda et al., 1996; Takeuchi et al., 1999). Due to the number of degrees of freedoms (DoFs) of the thorax that includes many joints, costovertebral joint (CVJ) kinematic analysis at a specific level is difficult. Previous *in vivo* CVJ kinematic analysis proposed a method based on medical imaging (i.e., 3D modelling) and mean helical axis (MHA) computation (Beyer et al., 2014a, 2013b). Thorax medical imaging in 3 different positions (Cassart et al., 1997; Gauthier et al., 1994a; Pettiaux et al., 1997) previously allowed estimation of local kinematic impairments of CVJ complexes (Beyer et al., 2014a); this previous work recognised to be limited by the influence of small range-of-motions (RoM) on the helical axis determination (de Lange et al., 1990) and by the reduced amount of available discrete positions (i.e., 3). In a previous study (Beyer et al., 2014), the authors acknowledged that discrete data are probably less representative than continuous motions obtained from external landmarks tracking; unfortunately the latter method is difficult to implement for accurate *in-vivo* CVJ motion analysis due to small rib displacements and skin motion artifacts. Therefore, a more complete description of RoM effect on finite helical axis (FHA) and MHA parameters related to CVJ behaviour is needed to extend this previous work and obtain better interpretation of the available raw data. Another issue is to determine the influence of virtual palpation performed on medical imaging data on CVJ mechanical parameters for clinical applications.

The purpose of this paper was therefore to investigate CVJ helical parameters from the effect of Monte-Carlo random noise simulation using spatial locations of anatomical landmarks (ALs) obtained from *in vivo* medical imaging. The influence of interpolation between discrete positions on MHA parameters and ranges-of-motions analysis using two different coordinate systems was also tested.

2. Method

2.1. Data acquisition and organisation

CT-scan data acquisition procedure (including three respiratory poses, or frames, for each subject) and AL virtual palpation methodology were described in previous work (Beyer et al., 2014a). . Six subjects were analyzed. On each subject, the 7 first left and right ribs, and corresponding vertebrae were virtually palpated to locate 5 ALs on each available bone (Fig. 1). Then, 3D locations of the left ALs were mirrored (Meskers et al.,1998) to the right side to avoid sign errors from left/right anatomical coordinate systems and to increase representativeness of the data.

For 3 subjects, the entire palpation procedure was repeated twice after 24 hours for reproducibility purposes. (Max SD = 2.1 mm; Mean SD= 1.4 mm). Note inter-observer repeatability

of this palpation procedure was previously assessed and showed an RMS error close to 1mm on AL location (Beyer et al., 2014).

In summary, a pool of 9 (6+3) subjects (18 half-thoraxes) was analysed. Due to too large error on further transformation residual, 3 sides were removed from the study leading to 15 available half thoraxes.

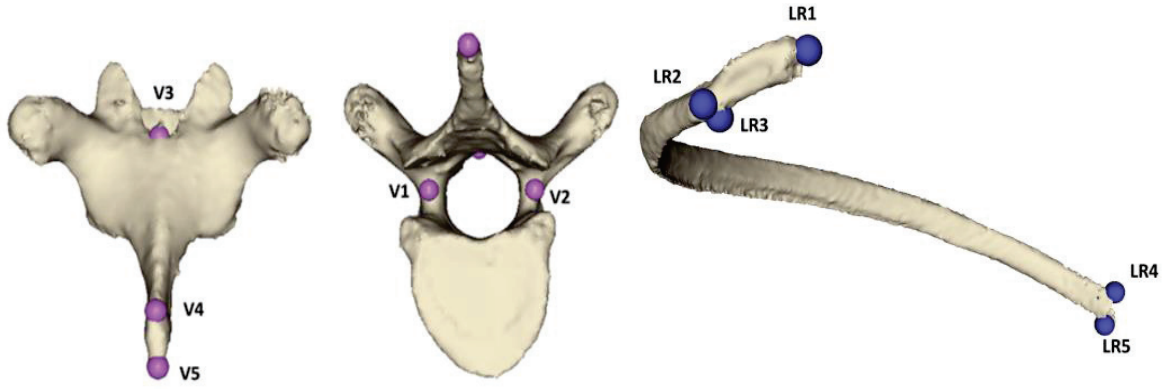

A **B**

Figure 1. ALs used in this study. In this figure and in figure 2, rib laterality is indicated with the prefix R or L for right and left, respectively.

Vertebra Landmarks: (Fig. A)	
V1	Centre of inferior border of left pedicle
V2	Centre of inferior border of right pedicle
V3	Superior junction of lamina
V4	Posterior and superior apex of spinous process
V5	Posterior and inferior apex of spinous process
Rib Landmarks: (Fig. B)	
R1	Posterior apex of tuberosity
R2	Anterior apex of inter-articular crest of costo-corporeal joint
R3	Inferior point of tuberosity
R4	Superior apex of costo-chondral surface
R5	Inferior apex of costo-chondral surface

Four ALs (from the first CT-scan frame) were used to convert 3D data from CT coordinate system to a unified coordinate system (UCS) using right hand rule as following. Let us define four (3×1) column P matrix: $P_i=(V1_i+V2_i)/2$, $i=1,7$; $P_2=LR4_5$; $P_3=RR4_5$ from ALs palpated at CVJ levels 1, 5 and 7, where V_i , LR_i and RR_i are vertebrae, left ribs, and right ribs respectively (see Figure1 and Figure 2B). Then, by defining the Euclidian matrix norm $\|...\|$, we obtained $Y=(P_1-P_7)/\|P_1-P_7\|$; $X_t=(Y\times(P_3-P_2))$; $X=X_t/\|X_t\|$; $Z=X\times Y$. Finally, point $\boldsymbol{U}$ in UCS could be obtained from point P in CT as $U=T\left[P^T,1\right]^T$, where is $T=\left[X,Y,Z,P_7\right]$ is the (3×4) transformation matrix required to transform data from the CT reference frame to the UCS frame.

For each bone AL cloud solidification (Chèze et al., 1995) was applied using the 3 available poses and rigid cloud transformation (Söderkvist and Wedin, 1993). Analysis of the transformation residuals allows estimating the range of palpation error for vertebrae and ribs. This error was further used to estimate the range of random noise introduced in further Monte-Carlo simulation.

2.2. Monte-Carlo simulation and kinematics parameters

Due to discrete nature of the raw data (i.e., obtained from medical imaging) and the small ranges of motion of the costovertebral joints (Beyer et al., 2014a), it has been supposed in this paper that MHA orientation and position could have been ill-determined as described in a previous paper (de Lange et al., 1990).

After processing original CT-scan data obtained in 3 positions only 2 finite helical axis (FHA) (de Lange et al., 1990) could have been evaluated to estimate MHA. However, the availability of 2 FHA only makes results sensitive to errors from AL palpation. In order to decrease the amplitude of this noise issue, and before running further random variations of palpated AL location as explained in the next alinea, an interpolation was applied in order to increase the amount of available positions and to smooth the data. Spatial coordinates of ALs associated to each available bone pose were then first stored using the so-called “pre-processed gait data” (or PGD) convention (the PDG convention has been previously recommended for motion data storage, see Cappozzo et al., 1995). Then, a parabolic interpolation was performed on each PGD DOF independently and between each bone pose. At last, interpolated intermediate data were solidified (Chèze et al., 1995). This artificial data creation procedure allowed to estimate the optimal amount of intermediate data (or artificial time-like step) required to minimize differences in MHA orientation between the intermediate poses. (See Annex A for MHA parameters estimation).

In order to perform the final interpolation step (for MHA evaluation) and the filtering of rotational angle values, a Monte-Carlo method was applied to imitate the influence on MHA orientation evaluation using the error magnitude of the reproducibility analysis related to AL palpation errors. Intra-observer distribution of error on ALs location was similar at all levels therefore 3 different amplitudes of noise with common mean standard deviation of the reproducibility were used as input for Monte-Carlo procedure (0.7; 1.4 and 2.1 mm) in each direction. Three levels of simulation noise were adopted to reflect the reproducibility issue between different research sites reported in the literature (Van Sint Jan and Della Croce, 2005). The procedure was applied in loop for each selected half-thorax. Four hundreds iterations were adopted after convergence analysis ensured results stabilization. All seven available CVJ levels were processed to estimate mean and standard deviation (mean, SD) from all trials for each individual level and subject. Then, similar estimation was performed to estimate mean values for the entire sample to obtain the dominant direction of CVJ MHA from breathing positions.

2.3. CVJ local coordinate system definition and comparison

Results obtained in previous work (Beyer et al., 2014a) proposed rib and vertebra local coordinates built following ISB recommendations (Wu and Cavanagh, 1995; Wu et al., 2002). The X-axis was oriented forward, the Y-axis upward and the Z-axis to the right. In this paper, first angular displacements were obtained from "ISB-like" coordinate orientations (UCS, Figure 3). A reorientation is then proposed to define a MHA oriented (MHAO) reference frame constructed from MHA parameters (i.e. orientation and position) obtained after Monte-Carlo iterations. The Z-axis was oriented along the MHA (with positive projection on UCS Z-axis) with its origin located at the mean pivot point.

3. Results

Raw AL data, previously captured in three positions, were solidified (Chèze et al., 1995) and each bone anatomical frame (AF) global transformations were interpolated and finally reframed to obtain 41 poses (following analysis of MHA orientation convergence vs. reframing). Then, for the MHA orientation evaluation, each level data were filtered by selecting frames of the CVJ angular rotation (between frames) larger than 0.5°. The amount of selected frames was between 15 and 40, depending on the subject and CVJ level range-of-motion.

3.1. Local coordinate systems and range-of-motion

From both AF representations (i.e., UCS and MHAO), CVJ motion parameterization was obtained and compared. The two AF parameterizations lead to different out-of-plane or secondary

motion representations (Figure 3); this discrepancy in the motion representation is well-known for specific joints moving around one principal axis (Piazza and Cavanagh, 2000). CVJ behaviour computed using UCS AF was not comparable to a hinge joint (the amplitudes of rotations along the X-axis and Z-axis were similar). For MHAO, angular components demonstrated a behaviour closer to a hinge-like joint mechanism (i.e., the primary displacement took place around the Z-axis). A complete description of the MHAO results is given in Table 1.

	1	2	3	4	5	6	7	8	9	10	11	12
	RoM X[°]				RoM Y[°]				RoM Z[°]			
level	min	max	mean	SD	min	max	mean	SD	min	max	mean	SD
1	0.2	4.4	1.4	1.1	0.1	3.3	1.5	1	9.6	34.4	17.7	7.5
2	0.2	6.1	2.2	1.6	0.2	3.9	1.4	0.9	10.7	30	16.3	5.8
3	0.1	4.4	1.9	1.4	0.3	2.9	1.5	0.8	9.8	27.2	15.2	4.7
4	0.1	4.3	2.1	1.3	0.2	3	1.1	0.7	11.9	21.9	14.3	3.1
5	0.1	4.4	1.6	1.3	0.1	2	0.8	0.6	8.5	18.5	12.2	2.7
6	0.1	3.9	1.3	0.9	0.2	2.6	1.2	0.7	7.7	15.8	12	2.3
7	0.6	3.1	1.7	0.8	0.2	3.1	1.1	0.9	8.8	15.1	11.3	1.8
mean	0.2	4.4	1.7	1.2	0.2	3	1.2	0.8	9.6	23.3	14.2	4
SD	0.2	0.8	0.3	0.3	0.1	0.5	0.2	0.1	1.3	6.9	2.2	1.9

Table 1: Amplitudes of CVJ angular rotation defined in the MHAO proposed in this paper.

Amplitudes of CVJ angular rotation for each level were estimated relative to the joint coordinate system constructed from MHA orientation (Z-axis) and two axes (X- and Y-axes) orthogonal to Z. Results are presented in the column 1-12 (Table 1). As expected, the major rotation occurred around the Z-axis (mean (SD) value 14.2° (4°) in columns 11, 12). Amplitude of rotation around secondary axes [mean (SD): X=1.7° (1.2°); Y=1.2° (0.8°)] were almost within expected accuracy of measurements. Maximum values for the X- and Y-axes (X=4.4°; Y=3°) were expected due to the use of averaged MHA orientation in total from 6000 (400 iterations *15 sets of ribs) trials for each of seven CVJ levels. For angular displacements obtained from each AF orientation an example is given (Figure 3) for one subject showing obvious decreases of secondary motion (around X- and Y-axes) at 4 different CVJ levels.

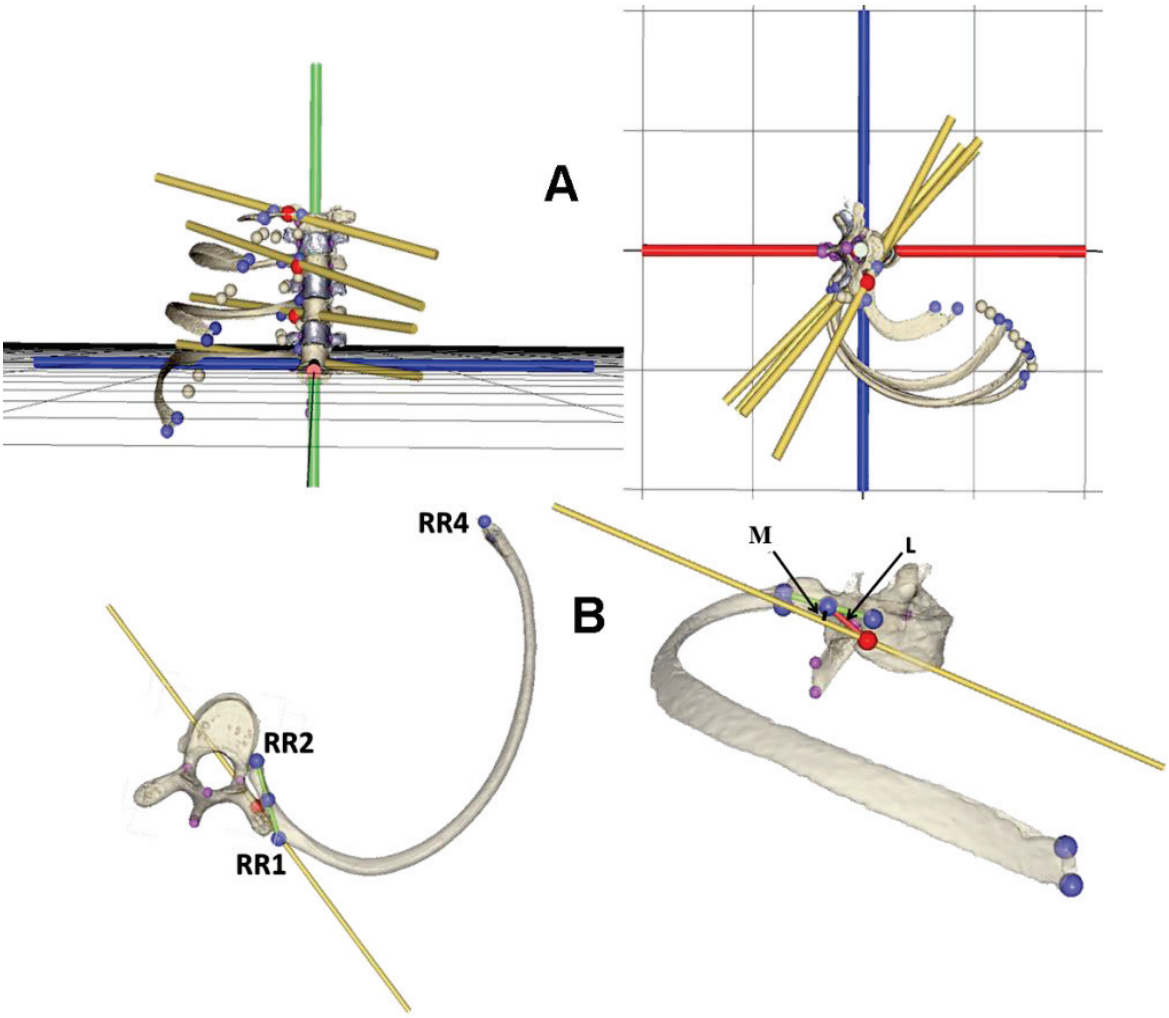

Figue 3: A: Frontal (Left) and superior view (right) of MHA orientation (yellow lines). Pivot points are displayed as red balls. Unified coordinate system (UCS) following ISB convention is displayed in Red, Green, Blue corresponding to X, Y and Z-axes. Blue balls correspond to AL of levels1, 3, 5 and 7. Gray balls correspond to AL from levels 2, 4 and 6. B: Superior view (Left) of AL used to calculate distances; Antero-lateral visualization (Right) of distance (L) between midpoint of RR1 and RR2 and CVJ mean pivot point; and shortest distance (M) between this midpoint and the MHA.

3.2. MHA and mean pivot point parameters

Table 2 contains a summary of results for the 6000 trials for one selected subject CT-scan data. For each level and each side, MHA orientation was first estimated by averaging the results of 400 random trials of the AL locations. Then, for each level MHA orientation was estimated as the mean of 15 right sides. Results are presented as direction cosines in UCS with XYZ oriented anteriorly, vertically and right laterally respectively.

0	1	2	3	4	5	6	7	8	9
	L [mm]	M [mm]	Pivot [mm]			D [°]	MHA direction cosines		
level	mean(SD)	mean(SD)	X	Y	Z		X	Y	Z
1	14.8 (10.4)	5.4 (4.2)	6.9	137.0	18.6	11.1	-0.54981	0.19732	0.81165
2	13.5 (9.7)	4.6 (3.6)	1.0	118.6	25.5	13.9	-0.67907	0.1712	0.71383
3	15.1 (10.7)	6.0 (3)	-4.7	93.8	21.3	11.2	-0.68252	0.19524	0.70431
4	17.2 (9.8)	7.7 (3)	-2.1	69.3	18.5	13.6	-0.63826	0.18387	0.74754
5	18.8 (11.3)	8.3 (4.4)	-9.9	50.3	23.3	13.4	-0.66891	0.09902	0.73672
6	20.9 (10.7)	8.6 (3.5)	-1.6	22.6	16.1	7.5	-0.62952	0.08359	0.77247
7	18.4 (9.8)	9.0 (3.8)	-1.2	1.7	19.6	13.9	-0.62393	0.02526	0.78107
mean	17.0 (10.3)	7.1 (3.7)	-1.7	70.5	20.4	12.1	-0.64109	0.13698	0.75514

Table 2: Results of pivot point position (columns 3-5) and MHA orientation (columns 7-9, direction cosines around X, Y and Z-axis) evaluation presented in the first frame of the UCS for 7 levels obtained from Monte-Carlo procedure and averaged for 15 right sides of the selected subject CT-scan data. Column 1 contains mean distances L from midpoint of the CVJ to mean pivot point. Column 2 contains mean shortest distances M from midpoint of the CVJ to the MHA line. Column 6 contains mean angular dispersion D [°] values. All data were estimated for each level from 15 right sides and 400 trials each.

The mean angular dispersion (see Annex A) of the seven CVJ levels was calculated as 12.1 (2.3)°. Results showed that the dominant MHA orientation is postero-lateral. In Table 2, column 1 contains mean distances L (also illustrated in Figure 1B) from midpoint of CVJ to the mean pivot point (MPP). Column 2 contains mean shortest distances M from midpoint of CVJ to MHA. Column 6 contains mean angular dispersion D[°] values. Visualisation (see supplementary materials) of results concerning MHA and pivot point during full range was obtained after fusion of kinematics and 3D bone models using a custom made software (i.e., lhpFusionBox, (Van Sint Jan et al., 2013)), giving the opportunity to visualise the proximity of MPP to the real anatomical CVJ complexes i.e. between two ALs in costovertebral and costotransverse joints (see Figure. 2B).

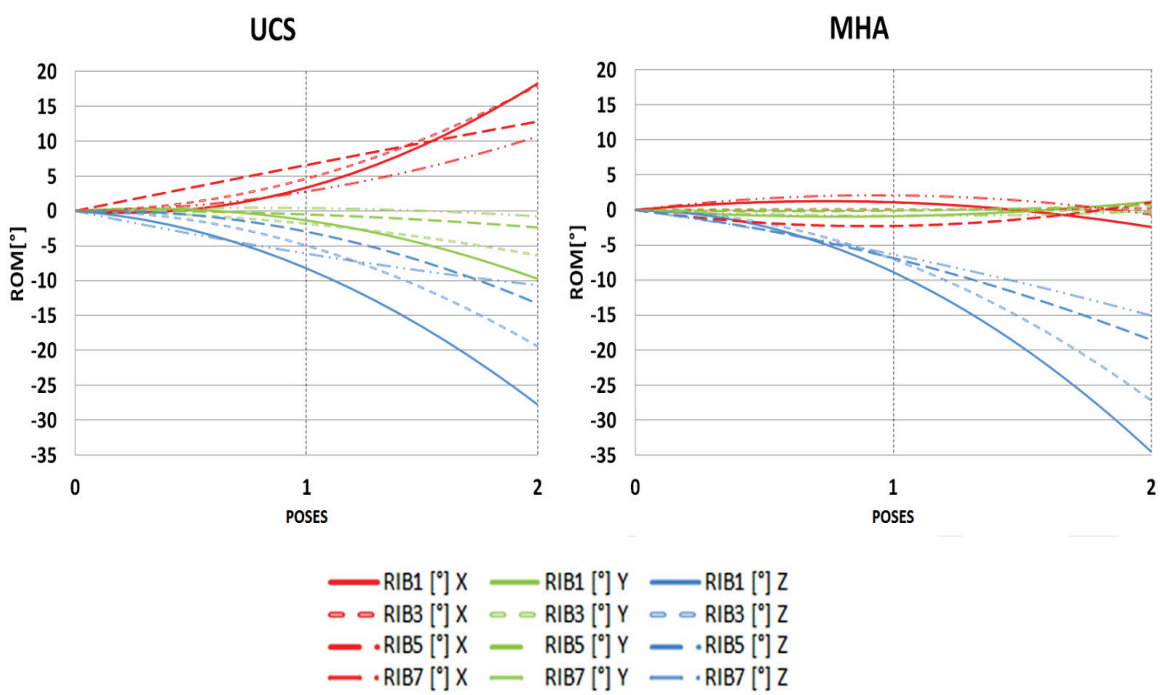

Figure 3. Graphic presentation of ranges of motion (vs. interpolated poses 0, 1, 2) relative to respectively X (Red), Y (Green) and Z-axis (Blue) in both AF representation (UCS on the left; MHA on the right) for one subject. Results are given for right CVJ levels 1, 3, 5 and 7.

4. Discussion

4.1. Local coordinate systems and range of motion

A previous paper proposed rib and vertebra-specific AFs to express CVJ kinematics (Beyer et al., 2013, 2014) organised following anatomical conventions but the functional method (Besier et al., 2003; Mannel et al., 2004) was not used to express kinematics. In addition to previous work we attempted to use this method on CVJ mechanism considered to be close to a hinge joint and not aligned with conventional anatomical planes (Saumarez, 1986; Wilson et al., 1987). The method (MHA orientation) proposed in this paper to orient the AF Z-axis along the average of MHA obtained from iterations allow minimizing the result cross-talk obtained using UCS from ISB conventions. Ranges of motion are decreasing with rib level as previously described (Beyer et al., 2014a; Sharp et al., 1986; Wilson et al., 1987). One subject in this sample showed very high ranges of motion at upper levels (presented in Figure 3). Inter-individual variations could explain higher SD observed at upper level compared to smaller ranges and SD at lower levels. This observation could be explained by so-called various breathing patterns (Tobin et al., 1983) and should be analysed on larger sample.

4.2. MHA and mean pivot point parameters

MHA parameters could be ill-determined (de Lange et al., 1990) especially for small ranges of motion joints (Ehrig et al., 2007). This procedure, combined with a large number of iterations (400 in

this study), allows noise reduction of MHA parameters and provided a mechanism closer to a hinge joint with respect to the real anatomical joint organization (Kapandji, 1964). The distance L between MPP and anatomical CVJ (Figure 1B) could be increased in a real hinge, but the results obtained concerning shortest distance M from CVJ to MHA lead to relevant joint mechanism considering that MPP should be located next to the area of the anatomical joints.

This paper presents results from Monte Carlo simulation performed with 3 levels of noise. A 95% confidence interval could have been adopted from the reproducibility study performed but it must be stressed that it is acknowledged in the literature that AL location shows important discrepancies between individuals from various groups (Van Sint Jan and Della Croce, 2005). The use of 3 levels of noise aims to consider 3 scenarios ranging from most the optimal to the worst case of AL location and to therefore better reflect discrepancies of AL location performed at different sites.

The authors recognize that the obtained results are processed from the discrete position interpolation, but the presented method allows reduction of noise on MHA parameters. Results for each level show few disparities concerning secondary motions for some levels that could be attributed to subject-specific mechanism or error of AL virtual palpation. Nevertheless inter-individual variations in shape and orientation of different articular surfaces involved in the mechanism, and also "misfit" during motion (Saumarez, 1986; Wilson et al., 1987) at each costotransverse and costovertebral joints could explain the mean angular dispersion of MHA (from 7.5° to 13.6°). Error filtering could be proposed using transformation residual for inexperienced users who would produce little accurate virtual palpation. To the best of the author's knowledge no procedure is available today to collect continuous motion of each rib and vertebra in *in vivo* conditions. Neither external (e.g. external landmark recording) nor internal measurement (e.g. dynamic magnetic resonance) tools are currently available to sample continuous motion of each a specific CVJ level that could more accurately describe this particular joint complex mechanism during full breathing.

5. Conclusion

This paper presents an improvement to a previous analysis (Beyer et al., 2014a) of CVJ-related kinematic data characterized by small spatial displacements. Data processing was oriented to obtain motion representation respecting the underlying hinge-joint like behaviour of the CVJ joints. Results obtained from random noise simulation and filtering proposed in this study indicate that the method is robust and leads to a relevant joint mechanism and better understanding of the CVJ complex which is poorly explored. Compared to the previously published paper, results show the robustness of the method and support the use of interpolation for stabilisation of MHA parameters. This could allow a better understanding of breathing patterns in normal and pathological conditions. Current work focuses on applying the procedures on a larger set of normal subjects and cystic fibrosis patients.

6. Conflict of interest

No authors have any conflict of interest to report.

7. Acknowledgments

The authors are grateful to the Radiological Department of Erasme Academic Hospital for contributing to this research.

8. References

Besier, T.F., Sturnieks, D.L., Alderson, J.A., Lloyd, D.G., 2003. Repeatability of gait data using a functional hip joint centre and a mean helical knee axis. J Biomech 36, 1159–1168.

Beyer, B., Feipel, V., Rooze, M., Van Sint Jan, S., Dugailly, P.-M., 2013. In Vivo spinal and costo-spinal kinematics in the respiratory mechanism: A preliminary study on Helical Axis and dynamic 3D anatomical Model. La Revue de l'ostéopathie 10, 29–35.

Beyer, B., Sholukha, V., Dugailly, P.M., Rooze, M., Moiseev, F., Feipel, V., Van Sint Jan, S., 2014. In vivo thorax 3D modelling from costovertebral joint complex kinematics. Clin Biomech (Bristol, Avon). doi:10.1016/j.clinbiomech.2014.01.007

Cappello, M., De Troyer, A., 2002. On the respiratory function of the ribs. J Appl Physiol 92, 1642–1646. doi:10.1152/japplphysiol.01053.2001

Cappozzo, A., Catani, F., Croce, U.D., Leardini, A., 1995. Position and orientation in space of bones during movement: anatomical frame definition and determination. Clin Biomech (Bristol, Avon) 10, 171–178.

Cassart, M., Pettiaux, N., Gevenois, P.A., Paiva, M., Estenne, M., 1997. Effect of chronic hyperinflation on diaphragm length and surface area. Am. J. Respir. Crit. Care Med. 156, 504–508.

Chèze, L., Fregly, B.J., Dimnet, J., 1995. A solidification procedure to facilitate kinematic analyses based on video system data. J Biomech 28, 879–884.

De Lange, A., Huiskes, R., Kauer, J.M., 1990. Effects of data smoothing on the reconstruction of helical axis parameters in human joint kinematics. J Biomech Eng 112, 107–113.

Ehrig, R.M., Taylor, W.R., Duda, G.N., Heller, M.O., 2007. A survey of formal methods for determining functional joint axes. J Biomech 40, 2150–2157. doi:10.1016/j.jbiomech.2006.10.026

Gauthier, A.P., Verbanck, S., Estenne, M., Segebarth, C., Macklem, P.T., Paiva, M., 1994. Three-dimensional reconstruction of the in vivo human diaphragm shape at different lung volumes. J. Appl. Physiol. 76, 495–506.

Kapandji, I.A., 1964. Illustrated physiology of joints. Med Biol Illus 14, 72–81.

Mannel, H., Marin, F., Claes, L., Dürselen, L., 2004. Establishment of a knee-joint coordinate system from helical axes analysis--a kinematic approach without anatomical referencing. IEEE Trans Biomed Eng 51, 1341–1347. doi:10.1109/TBME.2004.828051

Meskers, C.G., van der Helm, F.C., Rozendaal, L.A., Rozing, P.M., 1998. In vivo estimation of the glenohumeral joint rotation center from scapular bony landmarks by linear regression. J Biomech 31, 93–96.

Oda, I., Abumi, K., Lü, D., Shono, Y., Kaneda, K., 1996. Biomechanical role of the posterior elements, costovertebral joints, and rib cage in the stability of the thoracic spine. Spine 21, 1423–1429.

Pettiaux, N., Cassart, M., Paiva, M., Estenne, M., 1997. Three-dimensional reconstruction of human diaphragm with the use of spiral computed tomography. J. Appl. Physiol. 82, 998–1002.

Piazza, S.J., Cavanagh, P.R., 2000. Measurement of the screw-home motion of the knee is sensitive to errors in axis alignment. J Biomech 33, 1029–1034.

Saumarez, R.C., 1986. An analysis of possible movements of human upper rib cage. J Appl Physiol 60, 678–689.

Sharp, J.T., Beard, G.A., Sunga, M., Kim, T.W., Modh, A., Lind, J., Walsh, J., 1986. The rib cage in normal and emphysematous subjects: a roentgenographic approach. J. Appl. Physiol. 61, 2050–2059.

Söderkvist, I., Wedin, P.A., 1993. Determining the movements of the skeleton using well-configured markers. J Biomech 26, 1473–1477.

Takeuchi, T., Abumi, K., Shono, Y., Oda, I., Kaneda, K., 1999. Biomechanical role of the intervertebral disc and costovertebral joint in stability of the thoracic spine. A canine model study. Spine 24, 1414–1420.

Tobin, M.J., Chadha, T.S., Jenouri, G., Birch, S.J., Gazeroglu, H.B., Sackner, M.A., 1983. Breathing patterns. 1. Normal subjects. Chest 84, 202–205.

Van Sint Jan, S., Della Croce, U., 2005. Accurate palpation of skeletal landmark locations: why standardized definitions are necessary. A proposal. Clin. Biomech. 20, 659–660.

Van Sint Jan, S., Wermenbol, V., Van Bogaert, P., Desloovere, K., Degelaen, M., Dan, B., Salvia, P., Ortibus, E., Bonnechère, B., Le Borgne, Y.-A., Bontempi, G., Vansummeren, S., Sholukha, V., Moiseev, F., Rooze, M., 2013. A technological platform for cerebral palsy - The ICT4Rehab project. Médecine/Sciences 29, 529–536. doi:10.1051/medsci/2013295017

Wilson, T.A., Rehder, K., Krayer, S., Hoffman, E.A., Whitney, C.G., Rodarte, J.R., 1987. Geometry and respiratory displacement of human ribs. J. Appl. Physiol. 62, 1872–1877.

Annex A. Mean helical evaluation algorithm.

"To provide an indication of the precision of the FHA estimation procedure, the dispersion of the FHA's was calculated, with respect to a Mean Helical Axis (MHA). First, a mean rotation "pivot" of all FHA's, defined as the point with the smallest rms distance D_s to the FHA's was calculated. The D_s-value was taken as a measure for the error in the helical position estimation. Subsequently, the optimal direction vector of the MHA was defined through this pivot by minimizing the rms values of the sines of the angles between the MHA and the FHA's. Herewith, the angular dispersion x_n is defined as the arcsine of this rms value. Its value was taken as a measure for the error in the helical direction estimation." (de Lange et al., 1990).

Mean helical axis (MHA) unit vector $\underline{u}_0$ ($|\underline{u}_0| = 1$) estimation is based on a set (size n) of finite helical axis (FHA) $\underline{u}_i, i = 1,...,n$ unit vectors. Let us define $\hat{u}_i = (u_{ix}, u_{iy}, u_{iz})^T, (3\times 1)$ vector column of $\underline{u}_i$projections. Also let us define $\tilde{u}_i = \begin{bmatrix} 0 & -u_{iz} & u_{iy} \\ u_{iz} & 0 & -u_{ix} \\ -u_{iy} & u_{ix} & 0 \end{bmatrix}, (3\times 3)$ a skew symmetric matrix. Then $\tilde{u}_i^T = -\tilde{u}_i,\ \tilde{u}_i^2 = \tilde{u}_i\tilde{u}_i = \hat{u}_i\hat{u}_i^T - E$, where E is (3×3) identity matrix. Let $s_i = \sin^2(\varphi_i) = (\underline{u}_i \times \underline{u}_0)\cdot(\underline{u}_i \times \underline{u}_0), i = 1,...,n$, where φ_i is angle between two directions then is $s_i = (\tilde{u}_i\hat{u}_0)^T(\tilde{u}_i\hat{u}_0) = \hat{u}_0^T(-\tilde{u}_i^2)\hat{u}_0 = \hat{u}_0^T(E - \hat{u}_i\hat{u}_i^T)\hat{u}_0$. Then mean s_i characterizes MHA dispersion and is calculated as $S = \frac{1}{n}\sum_{i=1}^{n} s_i = \frac{1}{n}\hat{u}_0^T A\hat{u}_0$, where $A = \sum_{i=1}^{n}(E - \hat{u}_i\hat{u}_i^T)$ is a (3×3) symmetric matrix. Minimal value of S corresponds to the minimal eigenvector $u_{\min}$ of the matrix A with eigenvalue $\lambda_{\min}$. Finally, $\hat{u}_0 = u_{\min}$ and angular dispersion is evaluated as $d = arc\sin\sqrt{\lambda_{\min}/n}$.

Next steps

Chapters 2 and 3 aimed to develop an entire methodology enabling 3D modelling of costovertebral joint kinematics from CT scan data. The accuracy and reproducibility were estimated and results obtained are therefore considered relevant and applicable to any rib level. However, the previous results were not linked to pulmonary function. Therefore, the next chapter aims to evaluate the influence of laterality, lung volume and rib level on kinematic parameters of the respiratory ribs 1 to 10.

Chapter 4:

Relationship between costovertebral joint kinematics and lung volume in supine humans

Published as:

Benoît Beyer[1,2,4,*], Serge Van Sint Jan[1], Laurence Chèze[4], Victor Sholukha[1,3], Véronique Feipel[2]

Respiratory physiology and neurobiology, 2016 Volume 232: 57-65

1: Laboratory of Anatomy, Biomechanics and Organogenesis (L.A.B.O), Université Libre de Bruxelles, Brussels, Belgium.
2: Laboratory of Functional Anatomy, Université Libre de Bruxelles, Brussels, Belgium.
3: Department of Applied Mathematics, St. Petersburg Polytechnic University (SPbPU), Russia.
4: Université de Lyon, F-69622, Lyon, France; Université Claude Bernard Lyon 1, F- 69 622, Villeurbanne ; IFSTTAR, UMR_T9406, LBMC Laboratoire de Biomécanique et Mécanique des Chocs, F-69675, Bron
***: Corresponding author. bbeyer@ulb.ac.be; L.A.B.O, Lennik Street 808; CP 619; 1070 Brussel; Belgium**

List of abbreviations:

BMI	Body mass index
CVJi	costovertebral joint (i = joint level (from 1 to 10))
TLC	total lung capacity
MIC	middle of inspiratory capacity
FRC	Functional residual capacity
IC	Inspiratory capacity
VC	Vital capacity
RV	Residual volume
MHA	Mean helical axis
FHA	Finite helical axis
ALs	Anatomical landmarks

1. Introduction

Since the descriptions of Von Hayek (Hayek, 1953) and Felix (Felix, 1928), ribs have been demonstrated to be involved in both respiratory function (Cappello and De Troyer, 2002) and thoracic spine stability (Oda et al., 1996; Takeuchi et al., 1999). Literature concerning *in vivo* segmental costovertebral (CVJ) kinematics during breathing is scarce. Planar radiographic techniques were previously used to quantify 2D rib angle variations (i.e., the "pump handle") at various lung volumes over the vital capacity (VC) (Sharp et al., 1986). Three-dimensional (3D) kinematics of the upper ribs were quantified at specific costal level according to vector displacement analysis from external measurements (Jordanoglou, 1970, 1969; Jordanoglou et al., 1972) and joint surface geometry (Saumarez, 1986). 3D rib displacements between total lung capacity (TLC) and functional residual capacity (FRC) were also obtained from medical images on small samples (Wilson et al., 2001, 1987). Recently, a method was developed using computed tomography (CT) data (obtained at three different lung volumes (Cassart et al., 1997; Pettiaux et al., 1997)) and virtual palpation of few anatomical landmarks (ALs) on the 3D bone models reconstructed from the available CT data (Beyer et al., 2014b). Sensitivity analysis was used to quantify the influence of AL palpation errors on the determination of the axis of motion at each specific CVJ level (Beyer et al., 2015b). These previous works focused on the CVJ ranges-of-motion (ROMs) of the seven first pairs of ribs only and did not attempt to quantify the relations between CVJ ROMs and lung volumes. A non-uniform coupling between the ribs and the lungs was also previously demonstrated in dogs; no conclusive explanation was however given to explain the underlying coupling mechanism (De Troyer and Leduc, 2004; De Troyer and Wilson, 2002). The influence of both rib level and lung volume above FRC was demonstrated to alter rib compliance in caudal-cephalic direction (De Troyer et al., 2005b; Wilson and De Troyer, 2004). Further, force transmission during diaphragmatic contraction has been previously demonstrated to create a mechanical linkage between the ribs in the lower rib cage and those in the upper rib cage (De Troyer, 2012). From these studies, one may expect that the behaviours described will be reflected in the kinematics of the CVJ, but detailed quantified relationships between rib 3D kinematics at a specific CVJ level and lung volumes are yet to be described in humans.

In this paper, a previously-published method (Beyer et al., 2015b; Beyer et al., 2014b) was used to analyse the 3D angular displacements and axes of rotation of the ten first rib pairs relative to the vertebrae in 12 humans in supine position. The main objectives of this study were: 1) to quantify CVJ 3D kinematics at CVJ 1 to 10 as function of lung volume; 2) to test the correlation with functional respiratory measurements and anthropometrical characteristics; 3) to test the influence of laterality, CVJ level and lung volume on CVJ 3D kinematics parameters.

2. Methods

2.1. Computed tomography data

Retrospective codified CT datasets were obtained from the Department of Radiology of the Erasme Academic Hospital. Spiral computed tomography (Siemens SOMATOM, helical mode, slice thickness = 0.5 mm, inter-slice spacing = 1 mm, image data format: DICOM 3.0) was performed in asymptomatic volunteers at three different lung volumes. Lung volumes were previously obtained during pulmonary functional tests and available for this study. CT images were sequentially performed at total lung capacity (i.e, TLC pose), middle inspiratory capacity (MIC pose) corresponding to FRC+50% of inspiratory capacity (IC) and functional residual capacity (FRC pose), (Cassart et al., 1997; Gauthier et al., 1994a; Pettiaux et al., 1997). In order to control the lung capacity adopted during the CT sequences, patients were connected to a spirometer and instructed to hold their breath against a closed airway at each expected lung volume. The protocol was approved by the Erasme Hospital Ethics Committee (P2005/021). Just prior to CT data collection, subjects were allowed to perform a few rehearsal trials to get acquainted with the breathing procedure (Cassart et al., 1997; Pettiaux et al., 1997). A sample of 12 datasets from asymptomatic adults (mean age 31± 6 years old) was obtained. Details of anthropometric and pulmonary characteristics of the subjects are given in Table 1.

Age, yr	30	±	6
Sex, M/F	6/6		
Height, cm	171	±	8
Weight, kg	63	±	13
TLC, l	6,25	±	1,1
MIC, l	4,86	±	0,7
FRC, l	3,44	±	0,43
RV, l	1,67	±	0,37
IC, l	2,82	±	0,87

Table 1: Anthropometric and functional characteristics of the subjects. Values are means ± SD. All lung volumes were measured seated during functional pulmonary tests.

2.2. 3D-data extraction and kinematics computation

The entire procedure allowing to obtain 3D models and to compute costovertebral joint (CVJ) kinematics for the true ribs (n°1 to 7) has been previously described (Beyer et al., 2015b; Beyer et al., 2014b). In the present study, this procedure was used and extended to lower CVJ levels (n°8 to 10) to describe the individual behaviour of all ribs involved in breathing (i.e., CVJ1 to 10) and to perform a comparison with the related lung volume quantified by the spirometer. A custom made software (Van Sint Jan et al., 2013) (called lhpFusionBox) was used to locate the spatial coordinates of 5 well-defined ALs on the reconstructed 3D model of each rib and vertebra (Beyer et al., 2015b) (Figure). Rigid transformation parameters of ALs clouds between poses (Söderkvist and Wedin, 1993) were

obtained from the available AL coordinates using so-called "pre-processed gait data" (or PGD) convention (Cappozzo et al., 1995) for each rib relative to vertebra of same level (Beyer et al., 2015b).

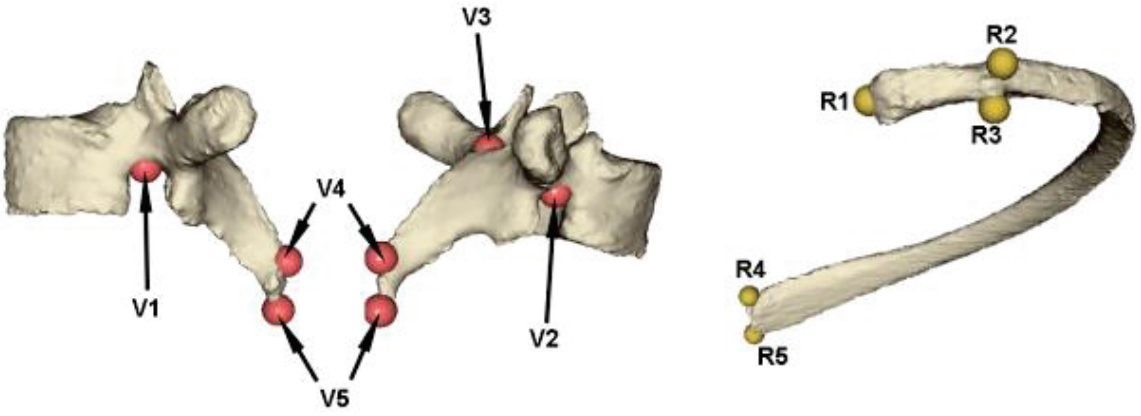

Figure 1: Definition of anatomical landmarks (ALs) which spatial coordinates were used to compute transformation matrices between breathing poses. Vertebra ALs: V1**, Centre of inferior border of left pedicle;** V2**, Centre of inferior border of right pedicle;** V3**, Superior junction of lamina;** V4**, Posterior and superior apex of spinous process;** V5**, Posterior and inferior apex of spinous process. Rib ALs:** R1**, Posterior apex of tuberosity;** R2**, Anterior apex of inter-articular crest of costo-corporeal joint;** R3**, Inferior point of tuberosity;** R4**, Superior apex of costo-chondral surface;** R5**, Inferior apex of costo-chondral surface.**

ALs cartesian coordinates were converted from the CT coordinate system to a global thorax coordinate system oriented following conventional anatomical planes obtained from recommendations of the International Society of Biomechanics (Beyer et al., 2015b; Beyer et al., 2014b; Wu et al., 2002; Wu and Cavanagh, 1995): x-axis pointing anteriorly, y-axis point upwards and z-axis pointing laterally to the right as shown in Figure .

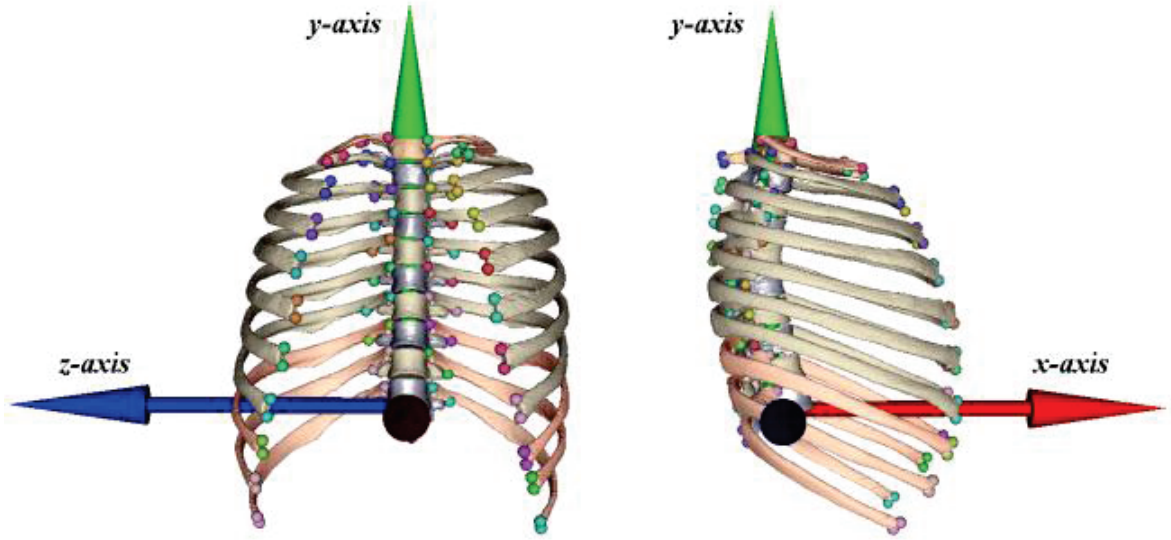

Figure 2: Global thorax coordinate system used to express kinematic parameters at each costovertebral joint level.

The CVJ axes of motion were then computed using finite helical axes (FHA) description (de Lange et al., 1990) which consists in the determination of the axis around which a solid rotates and translates during one single spatial displacement between two successive poses. Then the mean helical axes (MHA), defined as the mean of the finite helical axes (FHA) (de Lange et al., 1990) were computed (see appendix A for details).

At each CVJ level, MHAs orientation was represented in the local vertebra coordinate system which axes were collinear to the thorax coordinate system (Beyer et al., 2015b) at TLC pose. MHA were then used to create joint coordinate systems (Beyer et al., 2015b; Wu et al., 2002) between each rib and the physiologically-related vertebra (see Figure) at each CVJ level. This local CVJ coordinate system was created with a new Z-axis oriented along MHA and the x- and y-axes pointing anteriorly and upwards, respectively. By convention, rotations around the *Z-axis,* i.e. rib lowering, were given negative values. TLC position was chosen as reference (i.e., baseline) position for the registration procedure. Angular displacements were then calculated and the average of dispersion angle (see appendix A for details) (Beyer et al., 2015b) of MHA between subjects was obtained for each CVJ level.

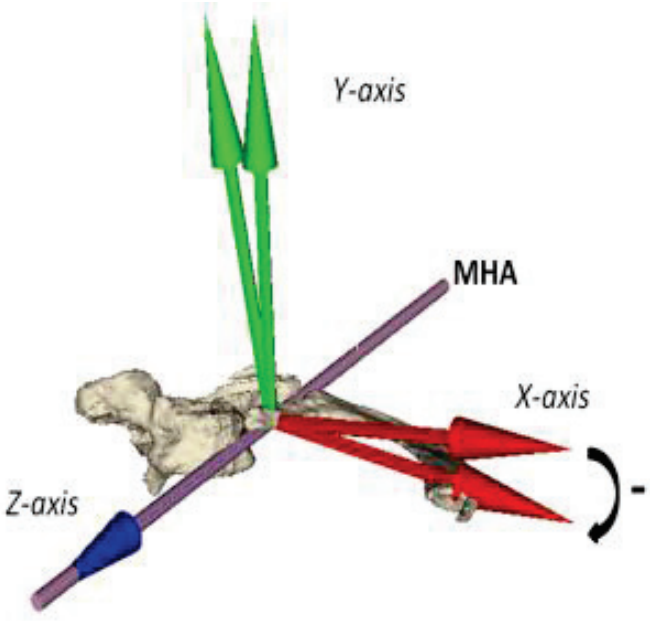

Figure 3: CVJ coordinate system constructed from MHA. Negative value was assigned for caudal direction.

2.3. Statistical analysis

In order to test the relation between anthropometric and kinematic parameters, parametric correlation coefficients (Pearson's coefficients r) were estimated and considered significant if $p<0.05$ and $r\geq0.70$ (Portney and Watkins, 2015). Analysis of variance (ANOVA) for repeated measurements

was used to evaluate the influence of the following factors: respiratory position (at MIC and FRC compared to the TLC reference position), laterality (left and right), CVJ level of rib pairs (n°1 to 10), and motion component (X-axis, Y-axis and Z-axis component). A total of 120 kinematic parameters (2 volumes *10 CVJ levels * 3 components = 60 parameters per side) was tested. Values of $p<0.05$ were considered statistically significant. When ANOVA indicated significant difference for specific factor, a supplementary Bonferroni post-hoc test was used to determine the significant factors at $p<0.05$.
Statistical analysis was performed using Statistica software (Statistica 8.0© StatSoft. Inc., Tulsa, USA).

3. Results

3.1. Rib angular displacements

Mean angular displacements (and standard deviations) at each CVJ level and for each component are given in Table 2 at MIC and at FRC relative to TLC. Both X- and Y-axes variations were small, ranging from -1.3° to 1.1° (mean standard deviation = 1.1°) at any lung volume (MIC and FRC). The principal motion component (i.e., around Z-axis in this study) ranged from -2.7° to -5.8° and from -5.8° to -18.2° at MIC and FRC respectively.

At middle of inspiratory capacity MIC

	LEFT						***RIGHT***					
Rib Level	X		Y		Z		X		Y		Z	
L1	-0.7	(1.6)	-1.3	(1.1)	-3.7	(3.6)	-0.1	(1.6)	-0.9	(1.5)	-4.3	(3.6)
L2	-0.8	(1.3)	0.2	(0.9)	-4.6	(3.4)	1.1	(2.2)	-0.4	(1.1)	-4.7	(2.9)
L3	-0.8	(1.8)	-0.3	(1.0)	-5.8	(3.2)	0.2	(1.8)	-0.2	(1.2)	-4.7	(2.9)
L4	-0.1	(2.1)	-0.1	(1.0)	-5.0	(2.7)	0.0	(1.7)	0.0	(0.8)	-5.0	(3.1)
L5	-0.4	(1.4)	0.3	(0.8)	-5.1	(2.6)	0.3	(1.6)	0.1	(1.2)	-4.9	(3.2)
L6	0.2	(1.7)	0.1	(0.7)	-4.7	(2.4)	0.2	(1.5)	0.4	(1.0)	-5.1	(3.3)
L7	0.3	(1.2)	0.0	(0.5)	-4.5	(2.2)	-0.1	(0.9)	0.0	(1.4)	-5.0	(2.8)
L8	0.3	(1.2)	-0.3	(1.4)	-3.8	(2.0)	-0.2	(1.3)	0.4	(1.4)	-4.4	(2.6)
L9	0.7	(1.0)	0.2	(1.7)	-3.3	(2.4)	0.1	(0.6)	-0.3	(1.0)	-4.3	(3.1)
L10	0.0	(1.3)	-0.2	(1.5)	-3.4	(1.6)	0.3	(1.4)	-0.3	(1.7)	-2.7	(2.5)

At functional residual capacity FRC

	LEFT						***RIGHT***					
Rib Level	X		Y		Z		X		Y		Z	
L1	-0.1	(1.4)	0.1	(1.2)	-16.7	(7.4)	-0.1	(1.0)	-0.2	(1.3)	-18.2	(7.3)
L2	0.0	(0.6)	0.3	(0.4)	-15.6	(5.9)	-0.3	(0.8)	-0.2	(0.4)	-15.9	(5.7)
L3	-0.4	(1.0)	0.2	(0.5)	-14.5	(4.6)	0.3	(0.8)	0.1	(0.5)	-14.3	(4.8)
L4	0.2	(1.2)	-0.1	(0.7)	-13.7	(3.5)	-0.4	(1.0)	-0.2	(0.4)	-13.4	(3.8)
L5	0.1	(0.4)	0.1	(0.3)	-11.8	(2.9)	-0.5	(1.0)	0.0	(0.4)	-11.5	(3.0)
L6	-0.1	(0.8)	-0.1	(0.4)	-10.2	(2.3)	0.1	(1.1)	0.1	(0.5)	-10.6	(2.7)
L7	0.1	(0.5)	0.1	(0.6)	-9.5	(2.5)	0.2	(0.5)	-0.2	(1.0)	-9.9	(2.5)
L8	0.0	(0.4)	-0.2	(0.8)	-9.1	(2.8)	0.2	(0.6)	0.1	(1.2)	-9.6	(2.8)
L9	0.2	(0.6)	-0.1	(0.8)	-8.1	(1.9)	0.2	(1.0)	0.0	(1.0)	-7.7	(3.0)
L10	0.0	(0.9)	0.2	(0.8)	-5.8	(2.3)	0.8	(1.5)	0.0	(1.8)	-6.2	(1.7)

Table 2: Mean (SD) angular displacements in degree around CVJ coordinate system for left and right sides. Results are given at MIC and FRC relative to TLC reference position. *Z*-axis was directed according to MHA orientation. *X*-axis and *Y*-axis variations are secondary components.

Results of principal component are summarized in Figure at MIC and FRC. In addition, data were normalized by dividing the angular displacement variations by the inspiratory capacity (IC). The average ROMs per liter of IC ranged from -2.1°/l to -1.3°/l and from -2.4°/l to 7.0°/l at MIC and FRC respectively. No effect of side (p=0.942) on kinematic parameters was found; this indicates the symmetry of motion within each rib pair. This symmetry was altered neither by the lung volume (p=0.565) nor by motion component (p= 0.358). Therefore, further results will be considered regardless of the rib laterality.

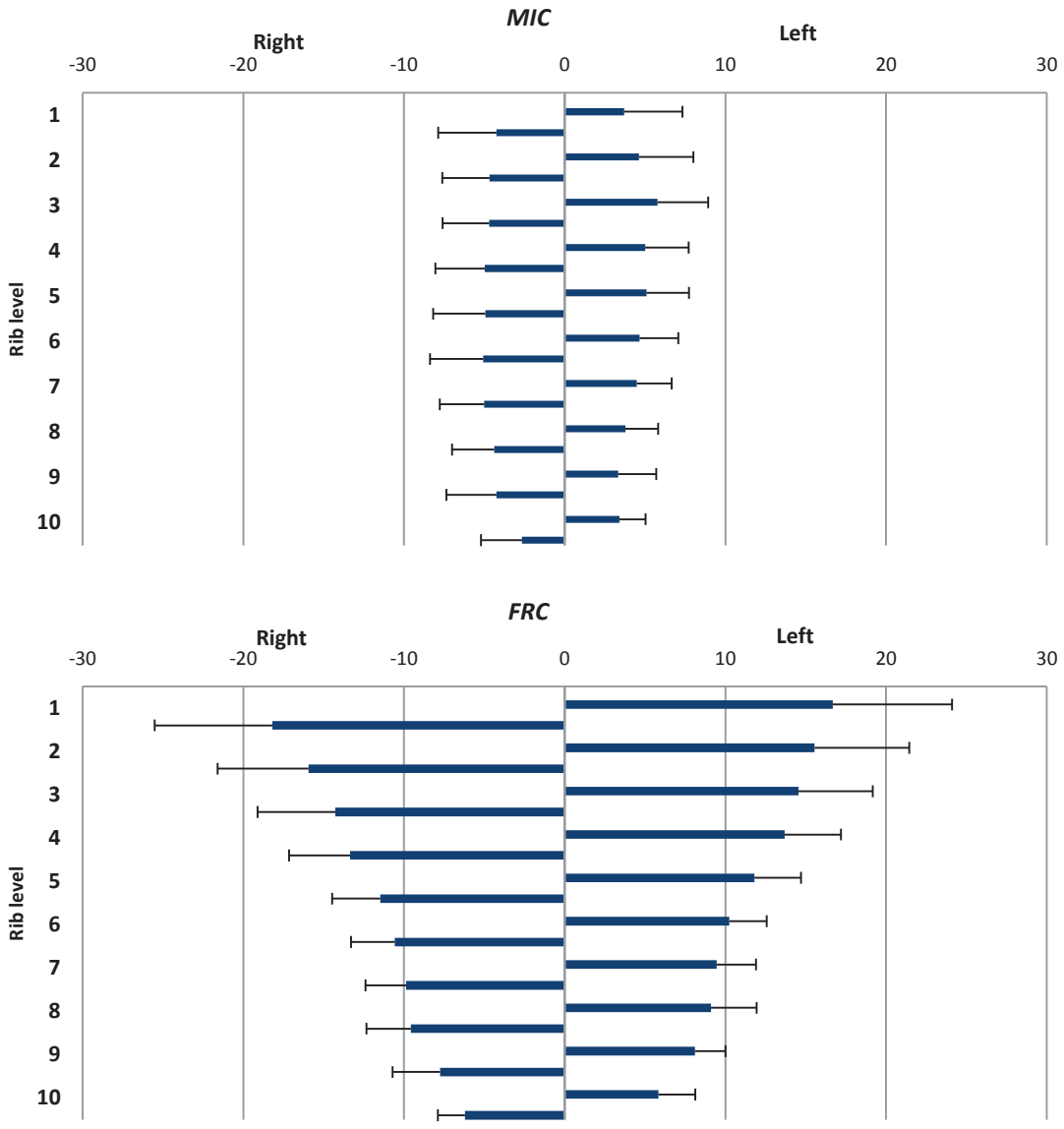

Figure 4: Angular displacements around mean helical axis of motion in degree (°). Results are presented for right and left sides at each costovertebral joint level to look like a patient seen from the front: left and right CVJ levels are presented respectively on right (positive values) and left (negative values) side of abscissa.

3.2. Axes of rotation

Results related to the MHA orientation are given in Figure A using direction cosines. These results indicate that the MHA axes were symmetric and similarly oriented (i.e., ventrally, medially and caudally) at all CVJ levels. MHA at all CVJ levels mainly projected on the x- and z-axes (direction cosines of 0.58 and 0.74 respectively) of the global anatomical thorax frame. (See Figure 6) allows visualizing this similarity). In other words, considering anatomical planes, the MHA orientation was intermediate between the frontal and sagittal planes at all CVJ level. An example of the 3D model obtained at CVJ1 for the subject with the maximal ROMs (34.5°) is given in supplementary material. The direction cosine on the y-axis direction was also variable, reflecting a small component of axial rotation in the transverse plane. This component decreased, i.e. the axis got closer to horizontal, in the lower CVJ levels (especially for CVJ 8 to 10). Inter-subject dispersion angle D of MHA (Figure 5B) ranged from 8.3° to 25.5°. This dispersion increased at CVJ 8 to 10. The mean dispersion for all levels and sides was 14.9° (±5.0°).

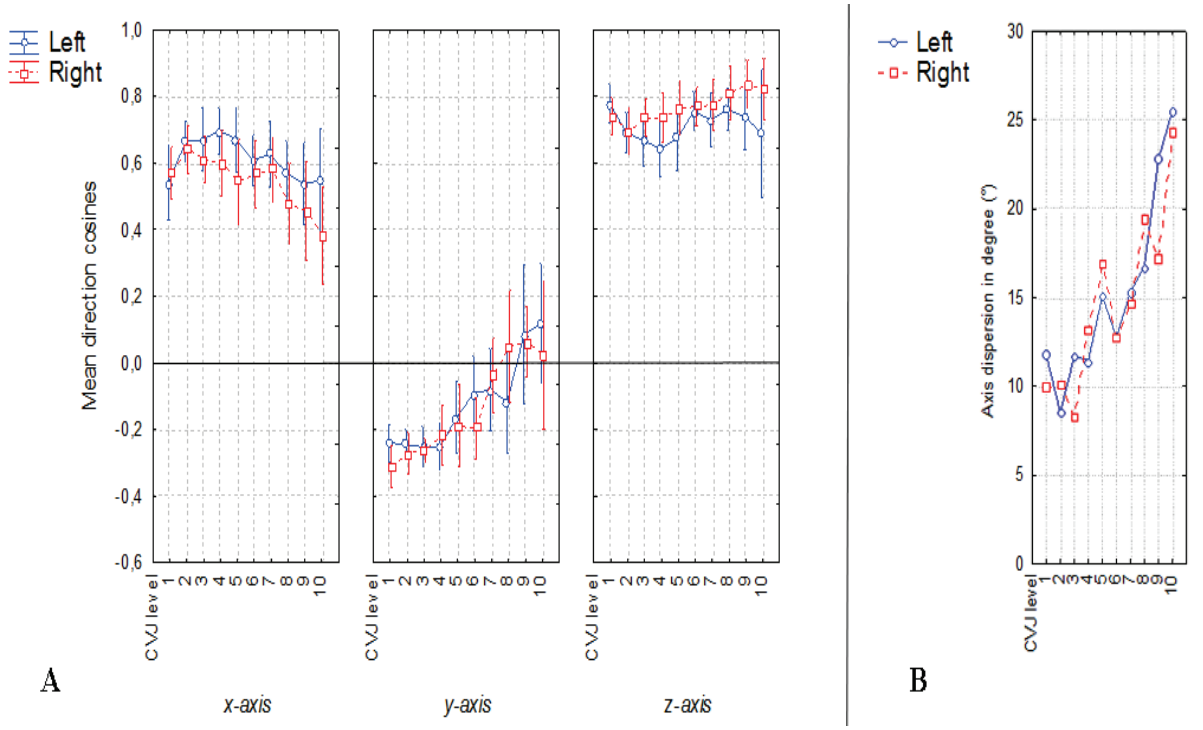

Figure 5: A: MHA direction cosines according to axis components, CVJ levels and sides. Results show for each CVJ level the MHA orientation expressed as percentage of MHA unit vector projection on each axis of the thorax coordinate system (See figure 6). See text for further comments. B: MHA dispersion angle (in degree) at each CVJ level for both left and right side.

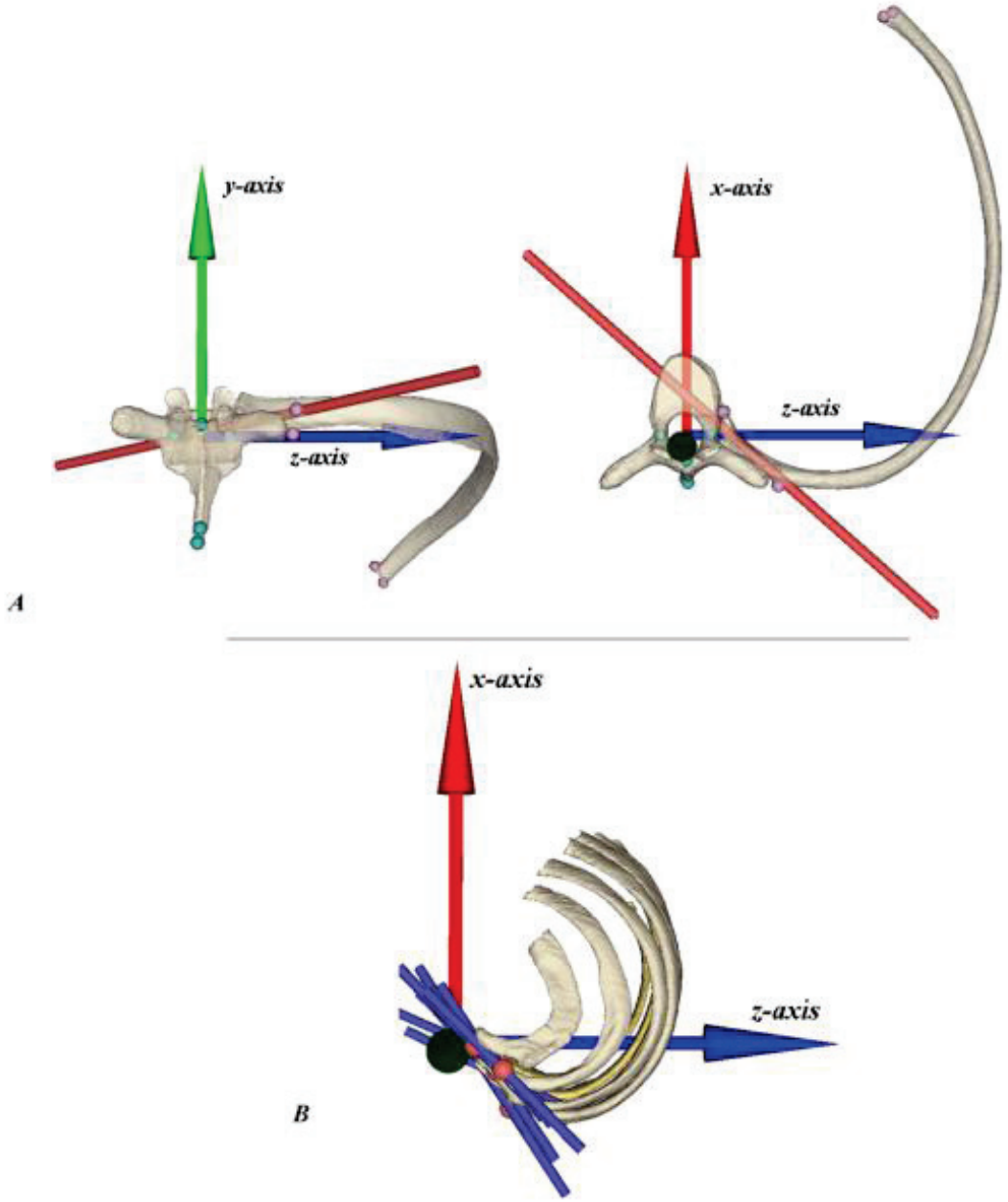

Figure 6: A: Representation of MHA at CVJ level 3 of a single subject in frontal (left) and transversal (right) planes (x-, y- and z-axes related to these planes are indicated). For a given side, MHA is oriented ventrally, medially and caudally (MHA is displayed as a cylinder in this figure). B: Example of representation of MHA of a single subject at all CVJ levels displayed in the transverse plane of the thorax coordinate system. The similar rough orientation of the MHAs at all CVJ levels is clearly observable. Such illustration shows the relevancy of using 3D representation of experimental measurements to visualize relevant anatomical and physiological results obtained from a specific subject. The other processed subjects showed similar MHA alignment.

3.3. Correlation between anthropometric and kinematic parameters

No significant linear correlation was demonstrated between any of the anthropometric/pulmonary variable and kinematics parameter ($p>0.05$ and $r<0.70$).

3.4. Effects of lung volume and CVJ level on angular displacements

Due to the absence of linear correlations between kinematic parameters and anthropologic measurements, no covariate was introduced in the statistical model. ANOVA results are given below:

- *Lung volume:* (see Figure and Table 2) CVJ kinematics parameters were significantly different between volume changes ($p=2.2\ 10^{-12}$). This difference occurred at MIC ($p=1.6\ 10^{-5}$) and FRC ($p=1.35\ 10^{-12}$) compared to TLC (i.e., the reference pose). Also a significant difference was demonstrated between MIC and FRC ($p=1.8\ 10^{-8}$).

- *CVJ level:* The ranges of rib motion were significantly influenced by CVJ level ($p=1.8\ 10^{-14}$). Post hoc analysis showed the following differences between analysed CVJ level (see Figure 7): - CVJ 1 differed from CVJ 5 to 10; - CVJ 2 and 3 differed from CVJ 7 to 10; - CVJ 5 and 6 differed from CVJ 1 and 10; - CVJ 7 and 8 differed from CVJ 1 to 3; - CVJ 9 differed from CVJ 1 to 4; - and CVJ 10 differed from CVJ 1 to 6. Note that ROMs did not differ between 2 to 4 adjacent ribs and that ROMs were always significantly larger in upper ribs.

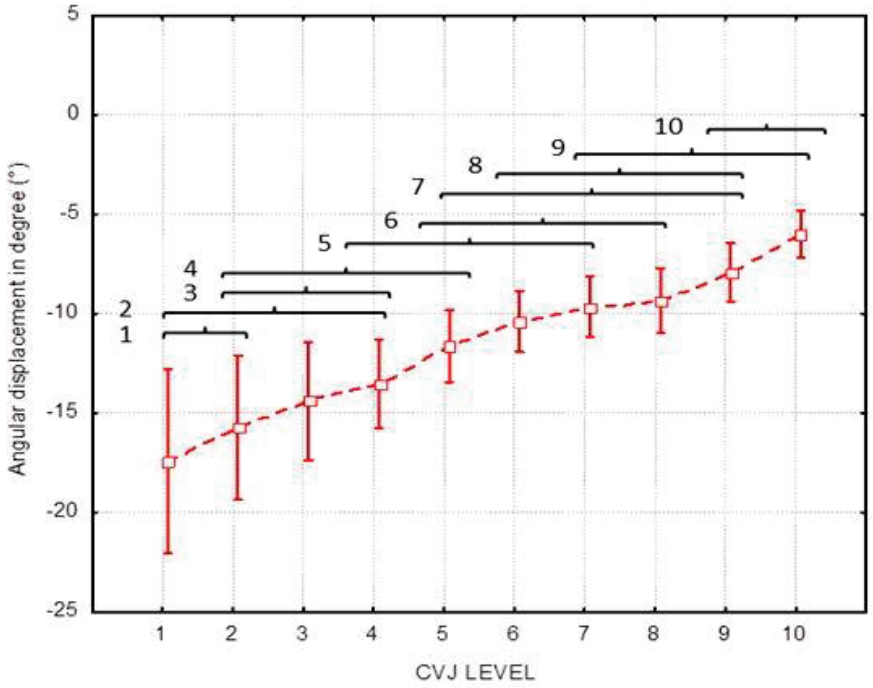

Figure 7: CVJ ROMs over the inspiratory capacity per CVJ level with 0.95 confidence interval (vertical bars). The brackets show groupings of CVJ levels with similar behaviour compared to the level tested given on the left of the bracket). See text for explanations

The interactions between CVJ level and specific volume change had a significant influence on angular displacements ($p=4.8\ 10^{-7}$). Above MIC, ROMs did not differ ($p>0.05$) between CVJ levels (see Figure and Table 2). Below MIC, however, similar ROM differences ($p<0.05$) to the ones described

above for total rib excursion were found. Note that the results of the above statistical comparisons were not altered when performed on data normalized with the inspiratory capacity.

3.5. Effect of CVJ level and component on MHA orientation

CVJ levels and motion components (x-, y- and z-components) had a significant influence on MHA parameters ($p<0.001$). Bonferroni post-hoc tests showed that MHA orientation did not differ ($p>0.05$) for group of adjacent ribs (see Figure A). MHA orientations at CVJ 1 differed from those at CVJ 7 to CVJ 10 ($p<0.001$). Regardless of the CVJ level, mean orientation occurred preferentially on z-axis ($p=0.00014$). Considering interaction with CVJ level, orientation was similar on x-axis and z-axis from levels 2 to 7 but greater on z-axis (closer to frontal plane) at CVJ 1 and CVJ 8 to 10. Orientation on cephalo-caudal direction (*y-axis* component) was similar ($p>0.05$) at CVJ 1 to 6 and differed from CVJ 7 to 10 ($p<0.05$). MHA was pointing caudally at upper CVJ levels and changed gradually at each CVJ level pointing progressively closer to transverse plane.

4. Discussion

The present study describes for the first time a detailed analysis of segmental CVJ kinematics for all respiratory ribs (i.e., all first ten pairs of ribs were processed) and their relation with lung volume changes above the FRC. The results support the hypothesis that for a same lung volume variation (i.e. 50% of the IC), the CVJ ROMs are significantly reduced above MIC. In addition, this decrease is also dependant on the CVJ level.

Considering joint physiology, the first main result is the gradual decrease of rib ROMs between TLC and FRC with increasing rib number (i.e., the higher the rib number, the smaller the related ROMs). This confirms previous studies in which samples were relatively small (Wilson et al., 2001, 1987) and did not consider all respiratory ribs simultaneously (Beyer et al., 2015b; Beyer et al., 2014b; Sharp et al., 1986; Wilson et al., 1987). Our results showed that adjacent ribs did not differ in terms of kinematics. The groups of adjacent ribs shown in Figure 7 largely overlapped, suggesting a continuum in CVJ behavior. From a purely kinematics point of view, these considerations do not support the subdivision of the rib cage in upper and lower regions (e.g. ribs 1-5 and 6-10). Nevertheless, the influence of lung volume and costal geometry on such a kinematic pattern was not determined.

A second important finding of this study is the critical influence of lung volume on the ROMs. Above MIC, the CVJ level has no significant effect on ROMs. ROMs above MIC correspond to approximately 35% of the total ROMs at upper CVJ levels (CVJ 1 to 4) and to 50% at lower CVJ levels (CVJ $\leq$ 5). Note that a larger variability in FRC/MIC ratio observed at upper CVJ levels suggests individual behaviour in this region.

Concerning the larger ROMs found below MIC, to the authors' knowledge, this study is the first to report quantified analysis of the previously-formulated assumption that segmental rib rotations are altered by lung volume level. However, this finding is consistent with the decrease in chest wall compliance with increasing lung volume (Agostoni and Hyatt, 2011; De Troyer et al., 2005b; West, 2012; Wilson and De Troyer, 2004) especially above ±75% of TLC (corresponding approximately to MIC). Moreover, this result is in agreement with previous studies on dogs that have demonstrated that for a given rib rotation, the associated changes in lung volume is lower at high volumes than at FRC (De Troyer and Leduc, 2004; De Troyer and Wilson, 2002).

The lack of correlation between kinematics and lung volumes can be related to the substantial role of the diaphragm muscle during breathing ; indeed, previous reports concluded that 50 to 60% of the vital capacity is attributed to diaphragm displacement (Cluzel et al., 2000a; Finucane and Singh, 2009; Singh et al., 2003). These results are in agreement with the conclusions of previous work in dogs concerning the role of diaphragmatic and rib cage compliance in the coupling between rib movements and lung volumes (De Troyer and Leduc, 2004; De Troyer and Wilson, 2002). Thus, although the inspiratory volume attributable to the diaphragm will tend to obscure the relationship between lung volume changes and rib kinematics, any relationship should be studied more appropriately by relating regional kinematics and regional rib cage variations. This lack of a relationship also raises the possibility that an important additional function of the ribs and their motion with intercostal muscles activity is to stabilize the rib cage during inspiration (De Troyer et al., 2005b; Wilson et al., 2001; Wilson and De Troyer, 2004).

Finally, this study also shows that MHA spatial orientation within the usual clinical planes was similar at all processed CVJ levels. This is in agreement with previous work (Beyer et al., 2014b; Wilson et al., 2001) reporting similar orientation of the rotation axes for ribs at all levels (i.e., according to these authors, these axes to lie close to 45° from the sagittal midplane). As previously mentioned (Beyer et al., 2015b; Beyer et al., 2014b; Wilson et al., 2001), this axis similarity differs from conventional descriptions used in earlier anatomy textbooks (Kapandji, 1964; Von Hayek, 1970). Few individual variations were observed at CVJ 1, and CVJ 8 to 10 that could reflect regional variations of joint geometry (Drake et al., 2010). The orientation of MHA was occasionally found to be oriented more frontally at lower CVJ levels as confirmed in previous reports (Beyer et al., 2015b; Beyer et al., 2014b). A rotation axis oriented closer to the frontal plane would induce chest wall diameters variations in both sagittal and frontal planes with a preference for anteroposterior variations. This supports previous descriptions of diameter variations during tidal breathing (Groote et al., 1997) or over vital capacity (Cassart et al., 1996).

Rib kinematics description according to MHA orientation (Beyer et al., 2015b) allows quantification of rib rotation as a single component. The secondary motion components allow to understand the variation of MHA orientation during motion reflecting the fact that rib rotation does not occur around single "fixed" axis (Saumarez, 1986; Wilson et al., 1987). This single-axis

representation often leads to difficulty for clinicians to visualise motion along conventional anatomical planes; results in this paper were therefore also represented using anatomical representation in Figure. This representation is closer to the previous description (Beyer et al., 2014b; Wilson et al., 2001, 1987) of “pump” and “bucket” handle variations. Nevertheless, the present description following the MHA orientation still gives opportunity to represent the “bucket handle” , “pump handle” and “caliper” rib behaviour (Osmond, 1995; Wilson et al., 2001) if those would have been observable. The slight cephalo-caudal MHA orientation (and the θy rotation in Figure A) found in this paper for all CVJ levels confirms a "caliper like" motion at all CVJ levels, although previously-published literature attributed this phenomenon to floating ribs only (Osmond, 1995). As explained in previous publications (Saumarez, 1986; Wilson et al., 1987), MHA orientation of a specific CVJ level is running along the exact orientation neither of the local transverse process nor of the costal neck.

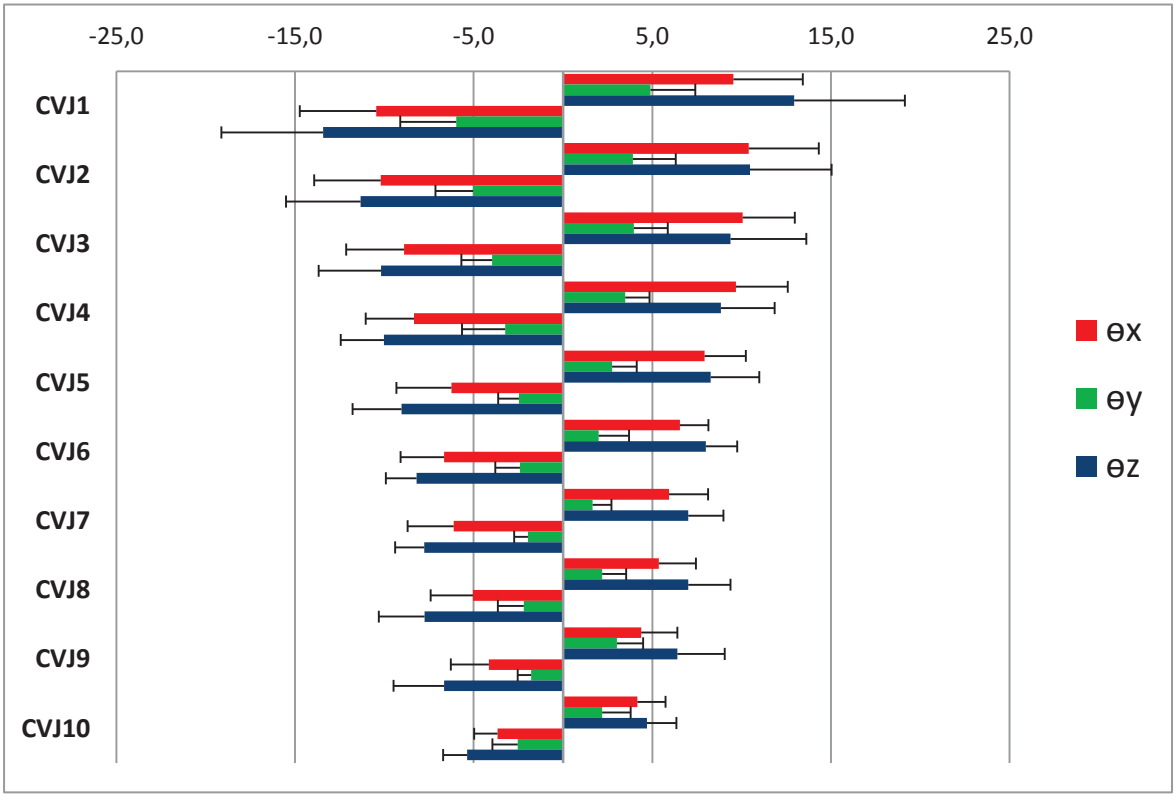

Figure 8: Maximal ranges of motion expressed according to anatomical planes in thorax coordinate system (see Figure 2) for CVJ levels 1 to 10. At each CVJ level, x, y and z component are presented successively from top to bottom. Values are mean (bars are standard deviations) ranges of rotation obtained around each anatomical axis for left (positive values on the right) and right sides (negative values on the left).

4.1. Limitations to the study

Note that the computational robustness of the method used in the present paper was previously validated through reproducibility and reliability determination for both CVJ ROM and MHA orientation (Beyer et al., 2015b; Beyer et al., 2014b).

Nevertheless, there are several limitations to the present study. Firstly, the supine position adopted by the subjects during medical imaging is a factor that does not allow generalisation of results to normal breathing behaviour in standing and sitting position. Indeed, posture has been demonstrated to alter chest wall kinematics (Lee et al., 2010; Romei et al., 2010; Sharp et al., 1975) as in the same time compliance of both rib cage and diaphragm-abdomen are sensitive to posture (M Estenne et al., 1985; Lee et al., 2010).

In our study the subject kept their upper limbs raised above the head ; this pose proves to raise ribs closer to the body transverse plane (Sharp et al., 1986; Wilson et al., 1987) and could consequently alter the rib ROMs. The latter could be slightly overestimated in our study compared to in subjects lying supine with their arms alongside. Secondly, interpretation of results should not be generalized to younger and elderly populations in which growth and aging could alter rib motion since chest wall compliance was demonstrated to be age-related (M Estenne et al., 1985; Sharma and Goodwin, 2006).

5. Conclusion

The present study provides a comprehensive and detailed 3D analysis of costovertebral joints kinematics in breathing motion. The results demonstrate quantitatively that rib behaviour depends on both rib level and lung volume and therefore highlight the regional specificity of rib kinematics in respiratory mechanics. The findings provide a basis for costovertebral joint analysis and could be useful to determine the influence of various pathological conditions affecting the relation between respiratory parameters and rib displacements. Further research is required to determine the regional change in lung volume associated with segmental CVJ kinematics.

6. Acknowledgements

The authors thank the Radiology department of Erasme Academic Hospital. The authors are most grateful to A. De Troyer for helpful discussions.

Appendix A. Mean helical evaluation algorithm.

"To provide an indication of the precision of the FHA estimation procedure, the dispersion of the FHA's was calculated, with respect to a Mean Helical Axis (MHA). First, a mean rotation "pivot" of all FHA's, defined as the point with the smallest rms distance D_s to the FHA's was calculated. The D_s-value was taken as a measure for the error in the helical position estimation. Subsequently, the optimal direction vector of the MHA was defined through this pivot by minimizing the rms values of the sines of the angles between the MHA and the FHA's. Herewith, the angular dispersion x_n is defined as the arcsine of this rms value. Its value was taken as a measure for the error in the helical direction estimation." (de Lange et al., 1990).

Mean helical axis (MHA) unit vector $\underline{u}_0\,(|\underline{u}_0|=1)$ estimation is based on a set (size n) of finite helical axis (FHA) $\underline{u}_i, i=1,...,n$ unit vectors. Let us define $\hat{u}_i=(u_{ix},u_{iy},u_{iz})^T,(3\times1)$ vector column of $\underline{u}_i$projections. Also let us define $\tilde{u}_i=\begin{bmatrix}0 & -u_{iz} & u_{iy}\\ u_{iz} & 0 & -u_{ix}\\ -u_{iy} & u_{ix} & 0\end{bmatrix},(3\times3)$ a skew symmetric matrix. Then $\tilde{u}_i^T=-\tilde{u}_i,\ \tilde{u}_i^2=\tilde{u}_i\tilde{u}_i=\hat{u}_i\hat{u}_i^T-E$, where E is (3×3) identity matrix. Let $s_i=\sin^2(\varphi_i)=(\underline{u}_i\times\underline{u}_0)\cdot(\underline{u}_i\times\underline{u}_0), i=1,...,n$, where φ_i is angle between two directions then is $s_i=(\tilde{u}_i\hat{u}_0)^T(\tilde{u}_i\hat{u}_0)=\hat{u}_0^T(-\tilde{u}_i^2)\hat{u}_0=\hat{u}_0^T(E-\hat{u}_i\hat{u}_i^T)\hat{u}_0$. Then mean s_i characterizes MHA dispersion and is calculated as $S=\frac{1}{n}\sum_{i=1}^{n}s_i=\frac{1}{n}\hat{u}_0^TA\hat{u}_0$, where $A=\sum_{i=1}^{n}(E-\hat{u}_i\hat{u}_i^T)$ is a (3×3) symmetric matrix. Minimal value of S corresponds to the minimal eigenvector $u_{\min}$ of the matrix A with eigenvalue $\lambda_{\min}$. Finally, $\hat{u}_0=u_{\min}$ and angular dispersion is evaluated as $d=arc\sin\sqrt{\lambda_{\min}/n}$.

7. Bibliography

Agostoni, E., Hyatt, R.E., 2011. Static Behavior of the Respiratory System, in: Comprehensive Physiology. John Wiley & Sons, Inc.

Beyer, B., Sholukha, V., Dugailly, P.M., Rooze, M., Moiseev, F., Feipel, V., Van Sint Jan, S., 2014. In vivo thorax 3D modelling from costovertebral joint complex kinematics. Clin Biomech (Bristol, Avon) 29, 434–438. doi:10.1016/j.clinbiomech.2014.01.007

Beyer, B., Sholukha, V., Salvia, P., Rooze, M., Feipel, V., Van Sint Jan, S., 2015. Effect of anatomical landmark perturbation on mean helical axis parameters of in vivo upper costovertebral joints. J Biomech 48, 534–538. doi:10.1016/j.jbiomech.2014.12.035

Cappello, M., De Troyer, A., 2002. On the respiratory function of the ribs. J Appl Physiol 92, 1642–1646. doi:10.1152/japplphysiol.01053.2001

Cappozzo, A., Catani, F., Croce, U.D., Leardini, A., 1995. Position and orientation in space of bones during movement: anatomical frame definition and determination. Clin Biomech (Bristol, Avon) 10, 171–178.

Cassart, M., Gevenois, P.A., Estenne, M., 1996. Rib cage dimensions in hyperinflated patients with severe chronic obstructive pulmonary disease. Am. J. Respir. Crit. Care Med. 154, 800–805. doi:10.1164/ajrccm.154.3.8810622

Cassart, M., Pettiaux, N., Gevenois, P.A., Paiva, M., Estenne, M., 1997. Effect of chronic hyperinflation on diaphragm length and surface area. Am. J. Respir. Crit. Care Med. 156, 504–508.

Cluzel, P., Similowski, T., Chartrand-Lefebvre, C., Zelter, M., Derenne, J.-P., Grenier, P.A., 2000. Diaphragm and Chest Wall: Assessment of the Inspiratory Pump with MR Imaging—Preliminary Observations1. Radiology 215, 574–583.

de Lange, A., Huiskes, R., Kauer, J.M., 1990. Effects of data smoothing on the reconstruction of helical axis parameters in human joint kinematics. J Biomech Eng 112, 107–113.

De Troyer, A., 2012. Respiratory effect of the lower rib displacement produced by the diaphragm. J. Appl. Physiol. 112, 529–534. doi:10.1152/japplphysiol.01067.2011

De Troyer, A., Kirkwood, P.A., Wilson, T.A., 2005. Respiratory Action of the Intercostal Muscles. Physiological Reviews 85, 717–756. doi:10.1152/physrev.00007.2004

De Troyer, A., Leduc, D., 2004. Effects of inflation on the coupling between the ribs and the lung in dogs. J. Physiol. (Lond.) 555, 481–488. doi:10.1113/jphysiol.2003.057026

De Troyer, A., Wilson, T.A., 2002. Coupling between the ribs and the lung in dogs. The Journal of Physiology 540, 231–236. doi:10.1113/jphysiol.2001.013319

Drake, R.L., Vogl, W., Mitchell, A.W.M., Gray, H., Gray, H., 2010. Gray's anatomy for students. Churchill Livingstone/Elsevier, Philadelphia, PA.

Estenne, M., Yernault, J.C., De Troyer, A., 1985. Rib cage and diaphragm-abdomen compliance in humans: effects of age and posture. J. Appl. Physiol. 59, 1842–1848.

Felix, W., 1928. Topographische Anatomie des Brustkorbes der Lungen und der Lungenfelle. [S.l.].

Finucane, K.E., Singh, B., 2009. Human diaphragm efficiency estimated as power output relative to activation increases with hypercapnic hyperpnea. J. Appl. Physiol. 107, 1397–1405. doi:10.1152/japplphysiol.91465.2008

Gauthier, A.P., Verbanck, S., Estenne, M., Segebarth, C., Macklem, P.T., Paiva, M., 1994. Three-dimensional reconstruction of the in vivo human diaphragm shape at different lung volumes. J. Appl. Physiol. 76, 495–506.

Groote, A.D., Wantier, M., Cheron, G., Estenne, M., Paiva, M., 1997. Chest wall motion during tidal breathing. Journal of Applied Physiology 83, 1531–1537.

Hayek, H. von, 1953. Die menschliche Lunge. Springer, Berlin; Göttingen; Heidelberg.

Jordanoglou, J., 1970. Vector analysis of rib movement. Respir Physiol 10, 109–120.

Jordanoglou, J., 1969. Rib movement in health, kyphoscoliosis, and ankylosing spondylitis. Thorax 24, 407–414.

Jordanoglou, J., Kontos, J., Gardikas, C., 1972. Relative position of the rib within the chest and its determination on living subjects with the aid of a computer program. Respir Physiol 16, 41–50.

Kapandji, I.A., 1964. Illustrated physiology of joints. Med Biol Illus 14, 72–81.

Lee, L.-J., Chang, A.T., Coppieters, M.W., Hodges, P.W., 2010. Changes in sitting posture induce multiplanar changes in chest wall shape and motion with breathing. Respiratory Physiology & Neurobiology 170, 236–245. doi:10.1016/j.resp.2010.01.001

Oda, I., Abumi, K., Lü, D., Shono, Y., Kaneda, K., 1996. Biomechanical role of the posterior elements, costovertebral joints, and rib cage in the stability of the thoracic spine. Spine 21, 1423–1429.

Osmond, D.G., 1995. Functionnal anatomy of the chest wall, in: The Thorax: Part A, 2nd Ed. Roussos C., New York, pp. 413–444.

Pettiaux, N., Cassart, M., Paiva, M., Estenne, M., 1997. Three-dimensional reconstruction of human diaphragm with the use of spiral computed tomography. J. Appl. Physiol. 82, 998–1002.

Portney, L.G., Watkins, M.P., 2015. Foundations of clinical research: applications to practice.

Romei, M., Mauro, A.L., D'Angelo, M.G., Turconi, A.C., Bresolin, N., Pedotti, A., Aliverti, A., 2010. Effects of gender and posture on thoraco-abdominal kinematics during quiet breathing in healthy adults. Respiratory Physiology & Neurobiology 172, 184–191. doi:10.1016/j.resp.2010.05.018

Saumarez, R.C., 1986. An analysis of possible movements of human upper rib cage. J Appl Physiol 60, 678–689.

Sharma, G., Goodwin, J., 2006. Effect of aging on respiratory system physiology and immunology. Clin Interv Aging 1, 253–260.

Sharp, J.T., Beard, G.A., Sunga, M., Kim, T.W., Modh, A., Lind, J., Walsh, J., 1986. The rib cage in normal and emphysematous subjects: a roentgenographic approach. J. Appl. Physiol. 61, 2050–2059.

Sharp, J.T., Goldberg, N.B., Druz, W.S., Danon, J., 1975. Relative contributions of rib cage and abdomen to breathing in normal subjects. J Appl Physiol 39, 608–618.

Singh, B., Panizza, J.A., Finucane, K.E., 2003. Breath-by-breath measurement of the volume displaced by diaphragm motion. J. Appl. Physiol. 94, 1084–1091. doi:10.1152/japplphysiol.00256.2002

Söderkvist, I., Wedin, P.A., 1993. Determining the movements of the skeleton using well-configured markers. J Biomech 26, 1473–1477.

Takeuchi, T., Abumi, K., Shono, Y., Oda, I., Kaneda, K., 1999. Biomechanical role of the intervertebral disc and costovertebral joint in stability of the thoracic spine. A canine model study. Spine 24, 1414–1420.

Van Sint Jan, S., Wermenbol, V., Van Bogaert, P., Desloovere, K., Degelaen, M., Dan, B., Salvia, P., Ortibus, E., Bonnechère, B., Le Borgne, Y.-A., Bontempi, G., Vansummeren, S., Sholukha, V., Moiseev, F., Rooze, M., 2013. A technological platform for cerebral palsy - The ICT4Rehab project. Médecine/Sciences 29, 529–536. doi:10.1051/medsci/2013295017

Von Hayek, H., 1970. Die Menschliche Lunge. Springer.

West, J.B., 2012. Respiratory Physiology: The Essentials. Lippincott Williams & Wilkins.

Wilson, T.A., De Troyer, A., 2004. The two mechanisms of intercostal muscle action on the lung. J. Appl. Physiol. 96, 483–488. doi:10.1152/japplphysiol.00553.2003

Wilson, T.A., Legrand, A., Gevenois, P.A., De Troyer, A., 2001. Respiratory effects of the external and internal intercostal muscles in humans. J. Physiol. (Lond.) 530, 319–330.

Wilson, T.A., Rehder, K., Krayer, S., Hoffman, E.A., Whitney, C.G., Rodarte, J.R., 1987. Geometry and respiratory displacement of human ribs. J. Appl. Physiol. 62, 1872–1877.

Wu, G., Cavanagh, P.R., 1995. ISB recommendations for standardization in the reporting of kinematic data. J Biomech 28, 1257–1261.

Wu, G., Siegler, S., Allard, P., Kirtley, C., Leardini, A., Rosenbaum, D., Whittle, M., D'Lima, D.D., Cristofolini, L., Witte, H., Schmid, O., Stokes, I., 2002. ISB recommendation on definitions of joint coordinate system of various joints for the reporting of human joint motion--part I: ankle, hip, and spine. International Society of Biomechanics. J Biomech 35, 543–548.

Next steps

The previous chapter described the relation between rib kinematics and lung volumes obtained from functional pulmonary measurements. Results quantitatively described kinematic parameters for each single respiratory ribs 1 to 10. It has been demonstrated that lung volume and rib level had a significant influence on ranges of rib motion. The laterality had significant influence neither on ROMs nor on MHA orientation whatever the rib level considered

At this stage, one could consider that rib kinematics description in asymptomatic human breathing is achieved. However, a question remains: does a pathological condition alter kinematic parameters in breathing? The next chapter is dedicated to answer this question.

Chapter 5:

In vivo 3D modelling of costovertebral joint kinematics in breathing: comparison between asymptomatic subjects and patients with cystic fibrosis.

Submitted in Clinical Biomechanics

Benoît Beyer[1,2,4;*], Serge Van Sint Jan[1], Laurence Chèze[4], Victor Sholukha[1,3], Véronique Feipel[2]

1: Laboratory of Anatomy, Biomechanics and Organogenesis (L.A.B.O), Université Libre de Bruxelles, Brussels, Belgium.
2: Laboratory of Functional Anatomy, Université Libre de Bruxelles, Brussels, Belgium.
3: Department of Applied Mathematics, St. Petersburg Polytechnic University (SPbPU), Russia.
4: Université de Lyon, F-69622, Lyon, France; Université Claude Bernard Lyon 1, F- 69 622, Villeurbanne ; IFSTTAR, UMR_T9406, LBMC Laboratoire de Biomécanique et Mécanique des Chocs, F-69675, Bron
***: Corresponding author. bbeyer@ulb.ac.be; L.A.B.O, Lennik Street 808; CP 619; 1070 Brussel; Belgium**

Abstract

*Background: T*horax kinematics in various breathing conditions has been intensively studied considering global shape but the literature concerning the costovertebral joints is really scarce in both normal and pathologic breathing conditions. Recent studies analyzed costovertebral joint physiology at different lung volumes in normal subjects. This paper presents results from comparison of in vivo costovertebral joints kinematics between asymptomatic subjects and patients with cystic fibrosis.

Methods: Retrospective spiral computed tomography data from samples of 12 asymptomatic subjects and 12 patients with cystic fibrosis were processed following a previously described method. These CT were obtained at three different lung volumes allowing computing 3D kinematics at each costovertebral joints of the ten first rib pairs. A fusion method was used to quantify and visualize 3D ranges of motion and helical axes parameters between each breathing poses.

Findings: A significant decrease in rib ranges of motion was demonstrated in patients with cystic fibrosis at upper rib levels. The interaction between rib level and lung volume had also a significant influence on RoMs. However, the orientation of the axes of rib rotation was not altered in patients with cystic fibrosis.

Interpretation: The results highlight for the first time the effect of a pathological condition such as cystic fibrosis on the costovertebral joint physiology during breathing. However, the decrease in RoMs should not be attributed to cystic fibrosis itself but rather to the lung hyperinflation which is a common symptom in such a pathological condition.

1. Introduction

Rib cage dimensions and chest wall kinematics are demonstrated to be substantially influenced by various factors such as physical activity, stature, age, as well as various lung diseases such as cystic fibrosis (J. F. Bellemare et al., 2001; Cala et al., 1996; Laurin et al., 2012; Wilkens et al., 2010). Hyperinflation is a common symptom in cystic fibrosis (CF), and a previous study reported a sex influence in thoracic adaptation to this phenomenon (Bellemare and Jeanneret, 2007). Nevertheless, high level of inter-individual variability was shown to impact chest wall expansion in both asymptomatic conditions (Hurtado and Fray, 1933) and lung diseases (Cassart et al., 1996; Sharp et al., 1986; Walsh et al., 1992). At joint level, chest wall kinematic variations during breathing were quantified at each costovertebral joint (CVJ) levels in recent studies focusing on asymptomatic subjects (Beyer et al., 2015b; Beyer et al., 2014b, 2013a). The method is based on computed tomography (CT) data obtained at three different lung volumes to reconstruct ribs and vertebrae in 3D models that were subsequently used to quantify CVJ kinematics at rib level 1 to 10 (Beyer et al, submitted). Segmental kinematics was demonstrated to have non uniform relation with different lung volumes at various breathing poses (Beyer et al., 2015a), Beyer et al, submitted). To our best knowledge, the influence of CF on CVJ kinematics has not yet been quantified. Therefore, the first objective of this study was to quantify and analyze CVJ kinematics in a sample of patients with CF, using a previously described methodology (Beyer et al., 2015b; Beyer et al., 2014b). Secondly, we tested the hypothesis that this specific clinical condition has no influence on CVJ kinematic parameters by assessing the comparison of results with asymptomatic subjects (AS).

2. Materials and method

2.1. Data collection

The procedure used in this paper was previously published (Beyer et al., 2015b; Beyer et al., 2014b, 2013a) (Beyer et al, submitted). In summary, the protocol included processing and analysis of retrospective codified medical imaging datasets obtained from the Department of Radiology of the Erasme Academic Hospital. Spiral computed tomography (Siemens SOMATOM, helical mode, slice thickness = 0.5 mm, inter-slice spacing = 1 mm, image data format: DICOM 3.0) performed at 3 lung volumes: total lung capacity (TLC), functional residual capacity (FRC) and middle inspiratory capacity (MIC). In order to relax their respiratory muscles at TLC and FRC plus one-half inspiratory capacity, the subjects should hold their breath and relax against a closed airway while they were connected to a spirometer during CT acquisitions.

2.2. Subjects

Data from a sample of twelve asymptomatic subjects (AS) was previously analysed and the results obtained (Beyer et al, submitted) were used in this study as control group to test the influence of pathological condition on CVJ kinematics. The aim was to determine if CF could alter CVJ 3D

kinematic parameters. Twelve CF patients were included in the second sample (two of them were later excluded due to significant scoliosis found during CT imaging). Finally, the data obtained in 12 asymptomatic subjects and 10 patients with CF showing similar age and morphology were available and analysed (table 1). Note that Kolmogorov-Smirnov test has demonstrated normal distribution; therefore t-test for independent samples was used to estimate differences in anthropometric and respiratory parameters.

	AS (n=12)	CF (n=10)	p
VC	4,57 ±0,99	3,25 ±1,30*	0,013
CI	2,82 ±0,87	2,34 ±0,85	0,216
FRC	3,44 ±0,43	4,13 ±0,80*	0,018
MIC	4,86 ±0,70	5,30 ±0,83	0,191
TLC	6,25 ±1,08	6,47 ±1,04	0,636
RV	1,67 ±0,37	3,21 ±0,97*	<0.001
Age, year	30,5 ±6,30	28,0 ±6,2	0,351
Weigth, Kg	63,1 ±12,63	58,5 ±8,7	0,344
Heigth, m	1,71 ±0,08	1,73 ±0,06	0,543

Table 1: Physical and pulmonary function characteristics of subjects. Values are mean ± SD; p: values obtained T-Test for indepedendant samples, * for p<0.05

2.3. Kinematics computation

Virtual palpation of anatomical landmarks (ALs, see Figure) was performed on each of the above-mentioned reconstructed 3D models for the 3 available lung volumes (Beyer et al., 2015b; Beyer et al., 2014b). Least square procedures were then applied on each AL cloud to determine the rigid transformation matrices (Söderkvist and Wedin, 1993) between the TLC, MIC and FRC poses. The matrices were then used to define the kinematics of each rib relative to the vertebra of same level as previously described (Beyer et al., 2014b). Rotation angles were further described using angular displacement around the helical axis (Beyer et al., 2015b) to represent rib rotation as a single component. Full details for kinematics computation are given in previous studies (Beyer et al., 2015b; Beyer et al., 2014b). Finite helical axis (i.e. axis of rib rotation between two consecutive poses) were computed and orientation of the mean (i.e. mean from FHAs) helical axis (MHA) (de Lange et al., 1990) was determined as well from direction cosines expressed in the global thorax coordinate system, x-axis pointing to the front, y-axis vertically from Th12 to Th1 and z-axis pointing laterally to the right (see Figure). To avoid sign errors, orientation results were mirrored and expressed as same side (Meskers et al., 1998). As proposed in previous work (Beyer et al., 2015b), the dispersion angle of MHAs (i.e. the angle between different MHAs) was also calculated to indicate the variation of MHA between subjects at a specific CVJ level.

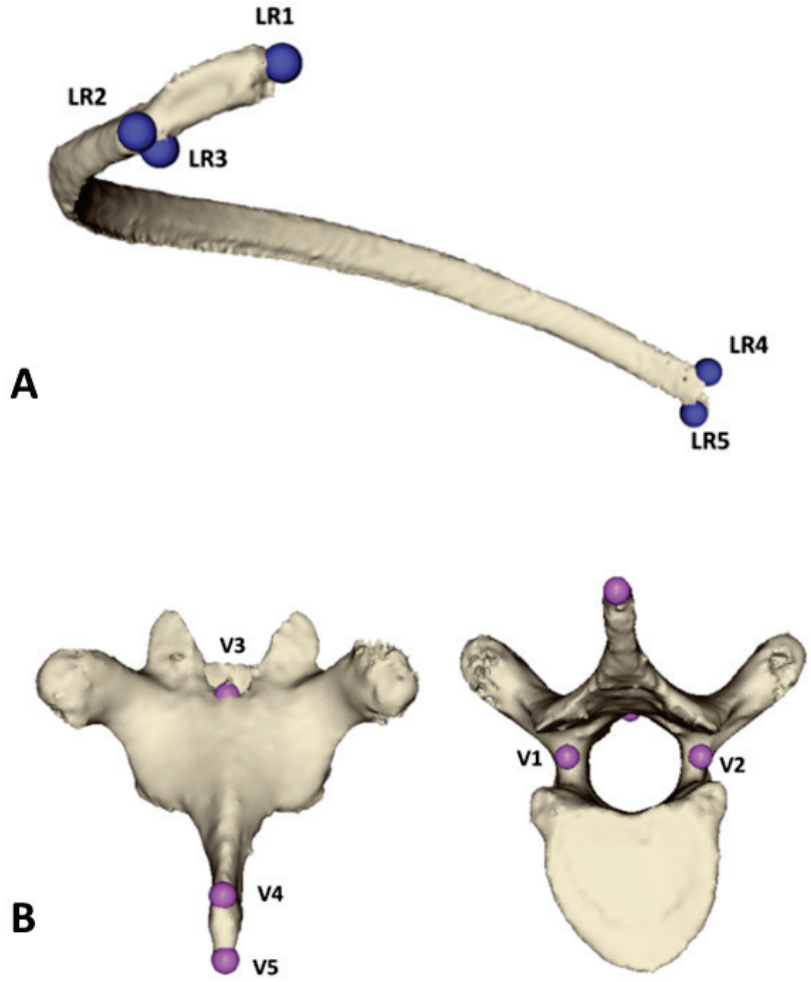

Figure 1: Anatomical landmarks (ALs) used for ribs and vertebrae. In this figure, rib laterality is indicated with the prefix L for left side. A) Rib landmraks: R1: Posterior apex of tuberosity; R2: Anterior apex of inter-articular crest of costo-corporeal joint; R3: Inferior point of tuberosity; R4: Superior apex of costo-chondral surface; R5: Inferior apex of costo chondral surface; B) Vertebra landmarks: V1: Centre of inferior border of left pedicle; V2: Centre of inferior border of right pedicle; V3: Superior junction of lamina; V4: Posterior and superior apex of spinous process; V5: Posterior and inferior apex of spinous process

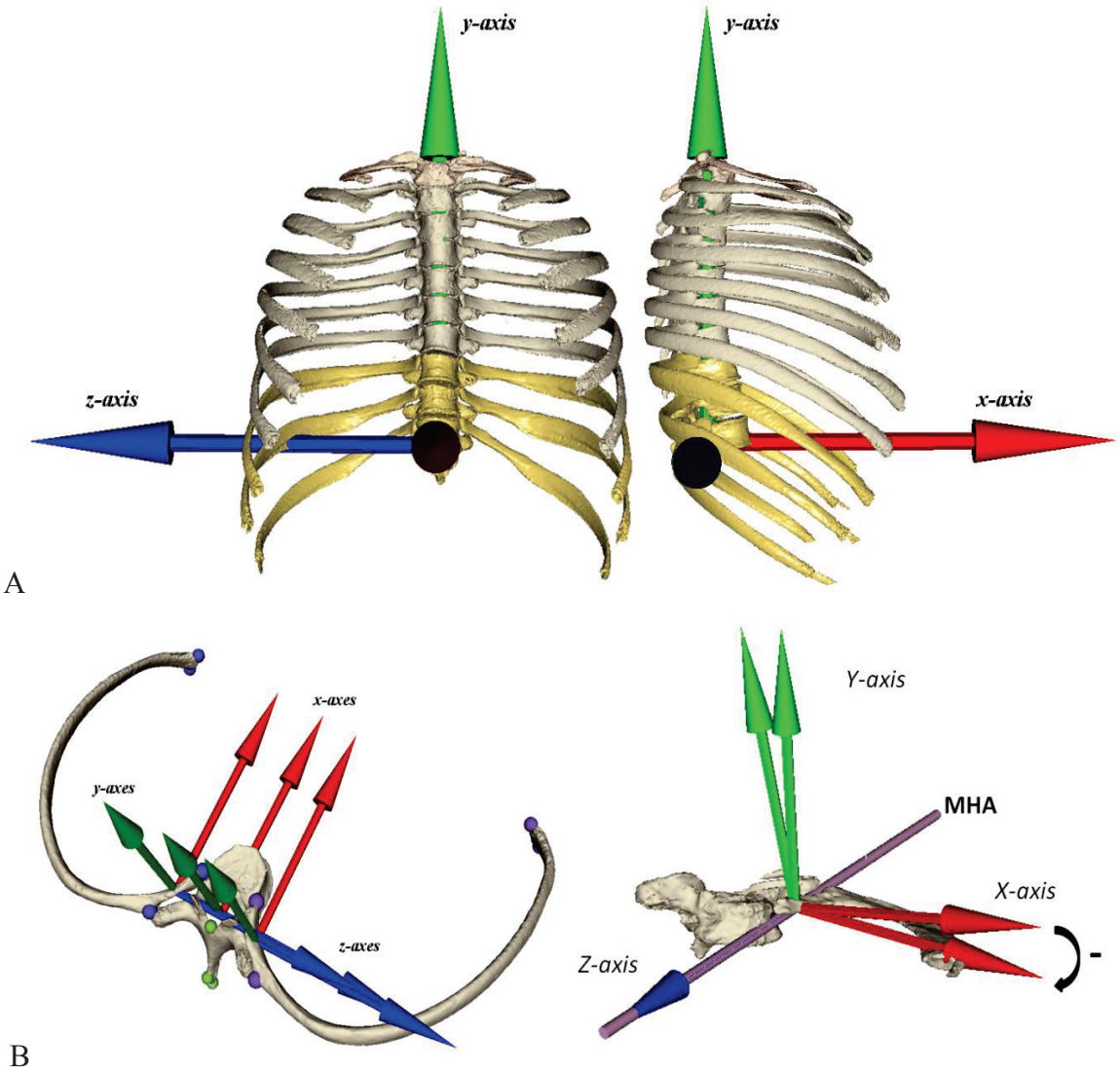

Figure 2: 3D models showing coordinate systems used to express kinematic results. A: global thorax coordinate system on frontal (left) and sagittal (right) view. B: Costovertebral joint complex with vertebra and rib coordinate systems oriented following global thorax axes orientation (Left) and following MHA orientation (Right).

2.4. Data analysis

Analysis of angular displacements was processed using mixed design analysis of variance (ANOVA) for repeated measurements according to 3 within-subjects factors: side (left/right), lung volume (TLC/MIC/FRC) and CVJ_i level (i varying from 1 to 10). Same statistical tests were performed on MHA data according to different factors: side (left/right), CVJ_i level and orientation component (on x-, y- and z-axes). The pathological condition was chosen as between-subject variable. When appropriate, Bonferroni post-hoc tests were performed at a significant level of P=0.05 to detect statistical relationships between groups, lung volumes and CVJ displacements.

3. Results

3.1. Subjects characteristics

The two groups did not differ significantly with respect for age, weight, height, inspiratory capacity (IC). Note that the residual volume (RV) and vital capacity (VC) differed significantly between AS and CF groups which highlights lung hyperinflation. (see Table).

3.2. CVJ angular displacements

Firstly, results of ANOVA for repeated measurements showed that laterality had no significant influence on CVJ ranges-of-motion (ROM) (P=0.401). The interaction between side and pathology did not have a significant effect (P=0.464). This reflects the symmetrical aspect of CVJ ranges of motion at any level. Averages between left and right RoMs were therefore calculated for each participant to express CVJ as a single value for each CVJ level considered.

Results of angular displacement (around MHA) at each CVJ level 1-10, at each lung volume in both AS and CF groups are given in figure 3.

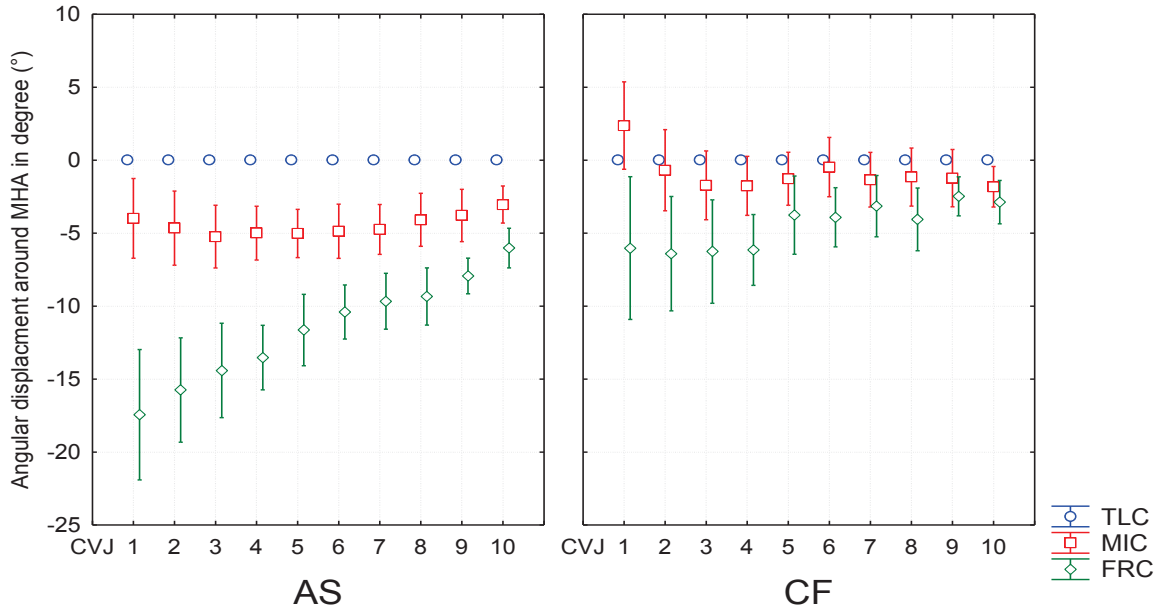

Figure 3: Angular displacements around MHA in degree (°) at each CVJ_i level for each lung volume (TLC, MIC and FRC) in both AS and CF groups.

For the AS sample, mean range of angular displacements decreased inversely with the CVJ level: from 17.4° (CVJ1) to 6.0° (CVJ10). In CF patients, displacements ranged from 6.4° (CVJ2) to 2.5° (CVJ9). In the latter sample similar values were obtained between CVJ1 and CVJ4 and decrease with increasing CVJ level. Note that range at CVJ1 (6.0°) was inferior to CVJ2, while range at CVJ10 (2.9°) was superior to CVJ9. At MIC in CF patients, mean angular displacement at almost all CVJ levels showed some positive values, i.e. a cephalic rotation between TLC and MIC ranging from 1.6° to 7.1°.

Results also indicated that CF significantly influenced CVJ RoMs (P<0.001). In addition the interaction between lung volume and pathology had a significant influence on RoMs (P=0.005) (see figure 4). Bonferonni post-hoc test indicated significant RoM differences between AS and CF only at below MIC (P<0.001), while such differences were not significant at high lung volume (i.e., above MIC, P=0.069). Note that in each group, RoMs were significantly influenced by lung volumes (see figure 4) (AS: P<0.001 and CF: P=0.002).

CVJ level had also a significant influence (P<0.001) on RoMs. At MIC, Bonferroni test could not show any significant differences of CVJ RoM at most CVJ levels between AS and CF groups. Only CVJ1 showed a significant difference between groups. (See figure 5 upper part). At FRC, differences between CF and AS were significant for CVJ1 to CVJ5 (P <0.05), but not significant between CVJ6 and CVJ10 (see figure 5 lower part).

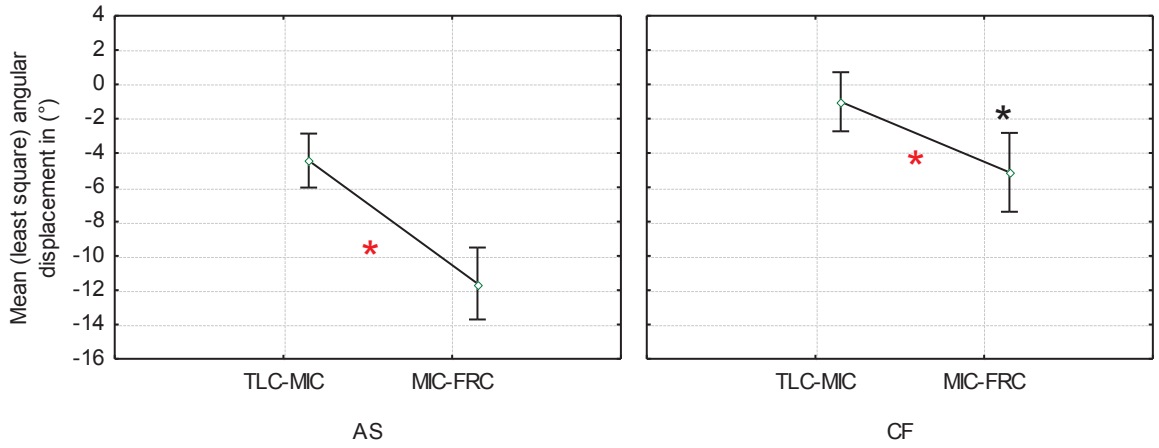

Figure 4: Average of angular displacements (between CVJ levels) as a function of the two studied populations (i.e., AS and CF) and three lung volumes (TLC, MIC and FRC). Red stars denote significant difference between lung volumes. Black stars denote significant difference between AS and CF group for a specific lung volume.

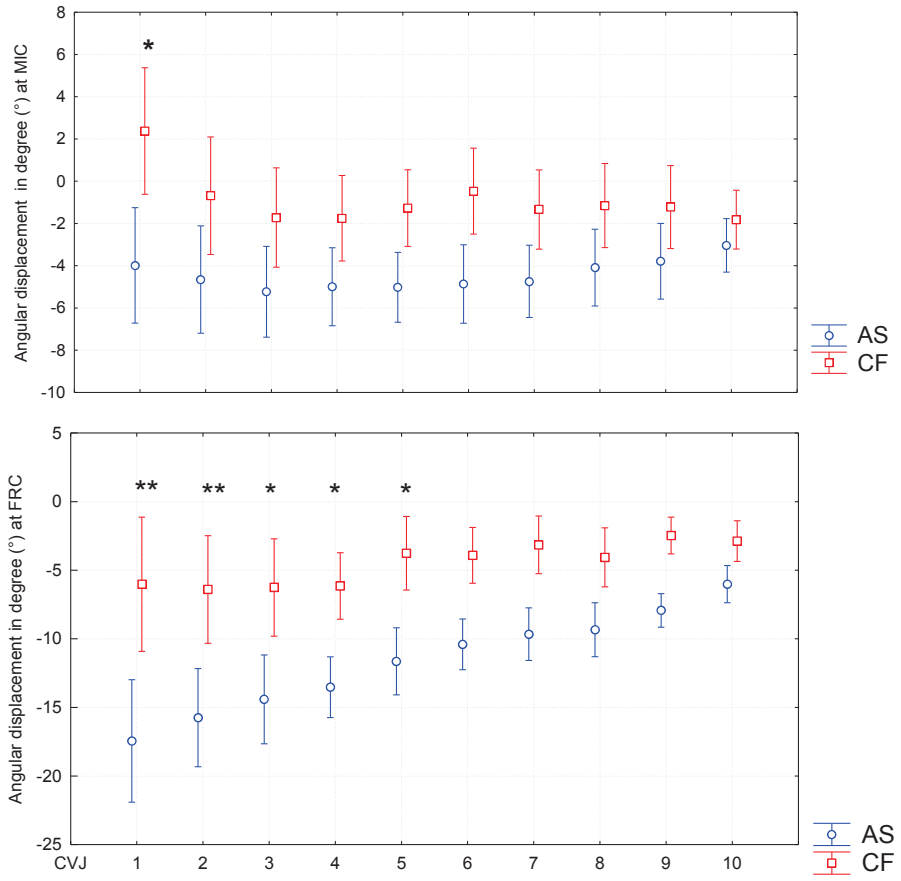

Figure 5: Angular displacement at MIC (upper part) and FRC (lower part) in both AS (blue) and CF (red) groups according to each CVJ_i level. Black stars demonstrate significant difference between the AS and CF groups at each specific CVJ_i level. Vertical bars denote 0.95 confidence intervals.

Maximal RoMs (figure 6) showed significant differences between groups (P <0.001) and between CVJ_i level (P =0.012). Bonferroni tests further indicated significant differences between groups for the first four CVJ levels (CVJ1 to CVJ4). For lower CVJ levels differences in maximal RoMs between groups did not reach significance but remained lower in CF group.

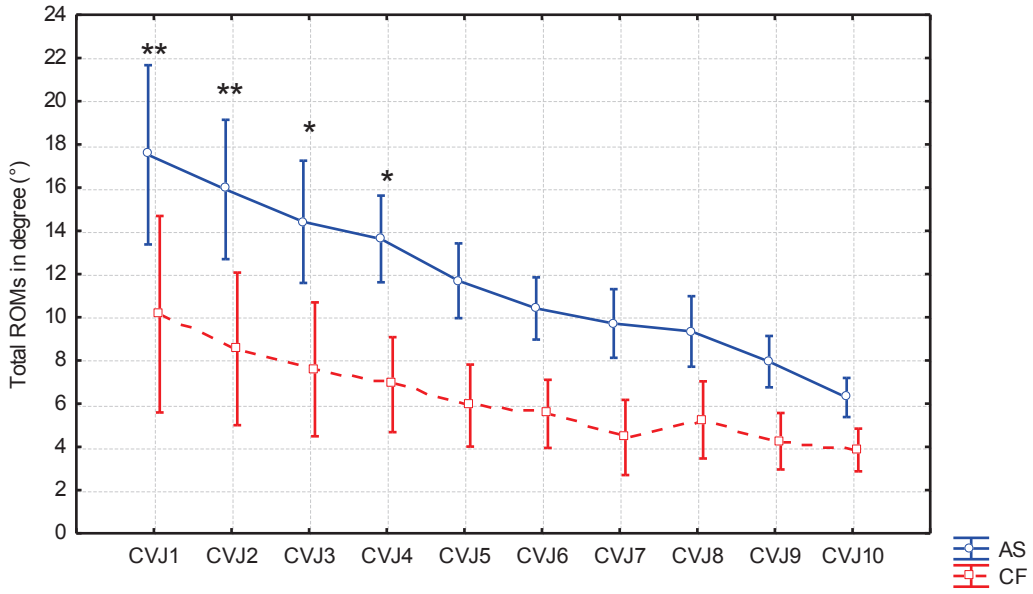

Figure 6: RoMs at CVJ_i in both AS and CF group. Double stars indicated a highly significant difference ($P < 0.01$), single stars show significant difference between groups ($P < 0.05$). Vertical bars denote 0.95 confidence intervals. Note the RoM decrease with increasing rib number in both groups. RoMs tended to be smaller in CF group at all CVJ levels, while significant differences were found from CVJ1 to CVJ4 only.

3.3. Mean helical axis orientation at each CVJ level

The orientation of MHA is presented using its direction cosines expressed in the global thorax coordinate system at TLC reference position (figure 7). No difference was found for laterality (P=0.437) and between the two groups (P=0.818). Therefore, as for RoMs, averages between sides were calculated and are presented in the below-section.

The interaction between pathological condition and CVJ level was shown to impact MHA orientation (P<0.001). However, Bonferonni test indicated a significant difference between AS and CF for CVJ9 only. In the AS group, the level did not have any impact on MHA orientation while a significant difference was present between CVJ level 9 and 10 (P<0.001) in CF group.

An interaction between pathological condition and MHA orientation component was demonstrated (P<0.001). Note that this difference was observed only on z-axis component (P<0.001) that was smaller in CF group. In addition the interaction between pathology, CVJ level and MHA components did not show significant effect (P=0.641).

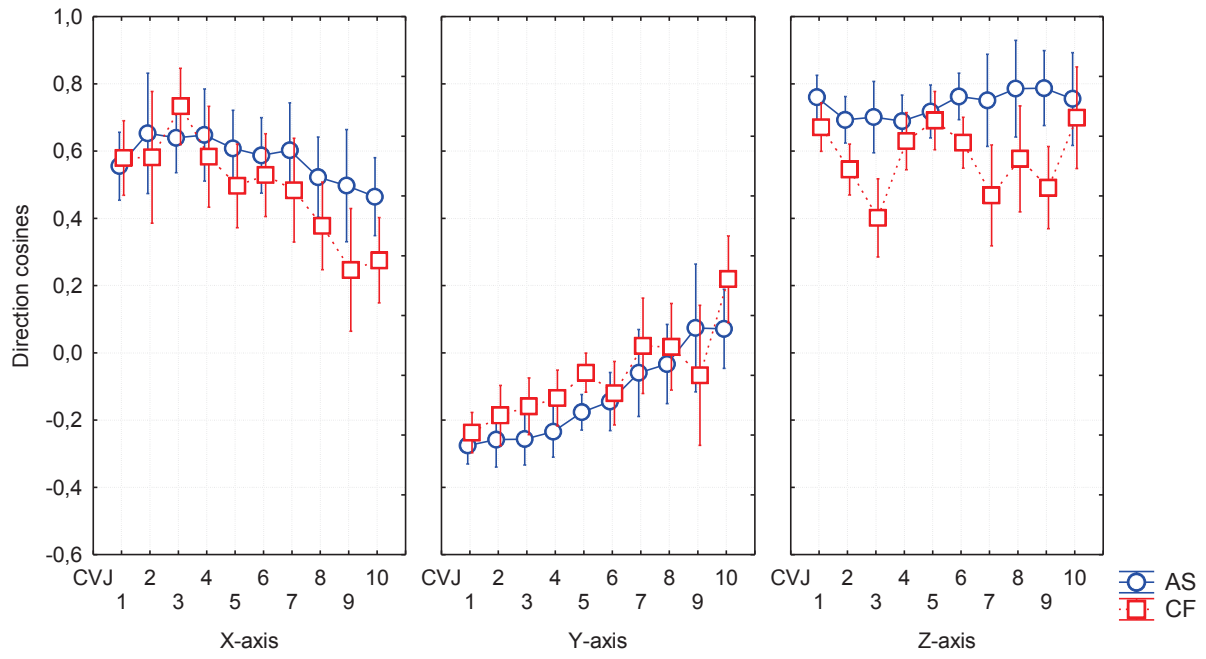

Figure 7: MHA direction cosines according to each axis of vertebra coordinate system in both AS (blue circles) and CF (red squares) group. Vertical bars denote 0.95 confidence intervals.

The dispersion angle of MHA is ranging between 9.3° to 24.9° in AS and from 20.7° to 44.5° in CF patients. The dispersion was similar between CVJ1 and CVJ6 in both groups, and then increased for other lower CVJ levels. This increase is greater in CF group. Also the ratio between CF and AS shows that MHA dispersion is about two times greater in CF than in AS.

Dispersion angle (°)	AS	CF
CVJ1	10,9	20,7
CVJ2	9,3	24,2
CVJ3	10,0	24,6
CVJ4	12,3	25,6
CVJ5	16,0	25,0
CVJ6	12,8	29,6
CVJ7	15,0	38,9
CVJ8	18,1	38,6
CVJ9	20,0	44,5
CVJ10	24,9	30,1

Table 3 : Dispersion angle of MHA in degree (°) at each CVJ level in both AS and CF group.

4. Discussion

The principal findings of this study could be summarized as follows: 1- CF patients showed smaller and altered CVJ RoMs compared to AS. 2- The cystic fibrosis pathological process did not alter the orientation of MHA.

To the best of the authors' knowledge, this paper reports the first study that demonstrates the influence of a pathological condition such as cystic fibrosis on CVJ kinematic parameters. A previous report (Beyer et al., 2015a) presented preliminary results related to CVJ displacements along anatomical planes and indicated significant RoMs differences between CF and AS groups at upper CVJi levels for both "bucket-handle" and "pump-handle" components of rib motion. However, these previous results were difficult to interpret further due to the motion decomposition into 3 components (i.e., the 3 anatomical planes). MHA representation (6) used in the present works enables description of rib displacements relative to vertebra and allows to analyze both CVJ RoM and MHA simultaneously. Spatial MHA orientation found in this paper confirmed previously-published results reporting that rib kinematics during breathing would alter the thorax shape in both anteroposterior and lateral planes simultaneously (Beyer et al., 2014b; Cassart et al., 1996) due to similar global x- and z-axis components at all CVJ levels in both groups. Note that the principal orientation of MHA close to the global lateral axis suggests a principal shape modification in anteroposterior diameter as previously described in both AS and chronic obstructive pulmonary disease (COPD) patients (Beyer et al., 2014b; Cassart et al., 1996; Groote et al., 1997; Walsh et al., 1992).

Interestingly MHA orientation did not globally differ between AS and CF which demonstrates that modifications of thoracic shape associated to patients with CF or hyperinflation (Bellemare and Jeanneret, 2007; Botton et al., 2003; Wilkens et al., 2010) does not alter the mean orientation of CVJ axes. Note that the MHA medio-lateral component (i.e. along z-axis) was smaller in CF group which could lead to an increase in lateral diameter variations. However, the dispersion angle of MHA between the 10 analyzed CVJ_i levels was approximately twice as large in CF as in AS. This dispersion could be attributed to the smaller RoMs in patients with CF, that could lead to MHA ill-determination (Chèze et al., 1998; Woltring et al., 1985). Another explanation could be the possible structural modifications of CVJ but this was not previously described in the literature (Laurin et al., 2012). Furthermore, this paper was limited to the processing of data obtained in discrete positions and thorax shape behavior in patients with CF could be altered during an active continuous breathing cycle, however, it does not appear that CVJ kinematics analysis during continuous breathing is possible with today available technologies.

The influence of pathological condition on thorax dimension was previously described in COPD (J. F. Bellemare et al., 2001; Cassart et al., 1996; Sharp et al., 1986; Walsh et al., 1992) and patients with CF (Bellemare and Jeanneret, 2007; J. F. Bellemare et al., 2001). Considering the rib angular displacements, previous studies assessed rib angles (RA) from lateral radiographs (Sharp et al., 1986; Walsh et al., 1992) at CVJ4 to CVJ7. RA was demonstrated to be similar in COPD and normal subjects at TLC, FRC and residual volume (RV). Decreased in RA differences (i.e., more similar to rib RoMs) was demonstrated in both groups (Walsh et al., 1992). These results of decreasing RoMs with increasing rib number could be confirmed by the present study and previous work in AS (Beyer et al., 2015b; Beyer et al., 2014b; Wilson et al., 2001, 1987). However, this was not observed in the present study at high volume level between TLC and MIC, where RoMs were similar for all CVJ_i in both groups. Note that in patients with CF, no significant differences were observed between CVJ_i levels. In CF, the effect of hyperinflation on RA was not significantly different but AS values were greater indicating more horizontal ribs (Sharp et al., 1986; Walsh et al., 1992). This could be correlated to a possible modification of rib interdependence due to diaphragm muscle contraction altering upper ribs displacement (De Troyer, 2012). This phenomenon was previously demonstrated in AS: neighboring ribs, grouped by 4 to 5 ribs, showed no significant differences in range of angular displacements (Beyer et al, submitted). Therefore, the alteration of diaphragmatic surface and area in hyperinflated patients with CF (Cassart et al., 1997; Pettiaux et al., 1997) could lead to this alteration of rib interdependence (De Troyer and Leduc, 2004).

As reported in the literature, patients with cystic fibrosis frequently display back pain in the thoracic region (Rose J et al., 1987; Tattersall and Walshaw, 2003). In our opinion, the present work opens perspectives to consider costovertebral joints physiology as a possible cause of thoracic back pain. In addition, the fact that limitations occurred specifically at upper rib levels should be of interest for further studies concerning the effect of manual therapy/physiotherapy techniques that could be evaluated using the present protocol.

Respiratory muscles contraction during the breathing old procedure against closed airway could also contribute to the differences observed in angular displacements in patients with CF. Indeed, even if the subjects were encouraged to relax against closed airway during the CT procedure, the discomfort in patients with CF could have led to involuntary muscles activation as it was highlighted in previous study using the same CT acquisition protocol (Cassart et al., 1996). Note that respiratory muscles impairments were also demonstrated in patients with CF (Dassios et al., 2013; Pinet et al., 2003). This could explain the “paradoxical” motion demonstrated in the present results of patients with CF at MIC of various CVJ levels, and more especially the upper ones 1-2. A second alternative is that respiratory muscles activity could be altered in patients with CF at different lung volumes. Supplementary material gives the opportunity to visualize the synchronized breathing motion of one AS with one CF patient.

Today respiratory medicine is mainly based on lung-centered approach, and rib behavior as described in this paper is not of major interest for most clinicians. However, many other clinical fields use joint physiology to objectivize secondary clinical signs related to a primary lesion of some organs (for example, limb gait analysis in Cerebral Palsy patients with brain lesions). This work represents a first step into this direction, i.e. to find the link between rib behaviors (i.e., the secondary clinical sign) with a primary disorder (e.g., cystic fibrosis). Further research, including clinical validation, should demonstrate the real interest of this paradigm in clinical practice.

5. Conclusion

To the authors' knowledge, the present study is the first to assess 3D kinematics of the costovertebral joints during breathing in a group of patients with CF compared to AS. The influence of pathological condition on rib kinematics is demonstrated and gives relevant information that could be taken into account during physical examination and/or treatment by physical and/or manual therapies for CF patients. The alteration of both rib interdependence and RoMs highlighted in the present study is of importance to understand the effect of hyperinflation on breathing kinematic parameters. Further analysis in various non respiratory clinical conditions such as musculo-skeletal or neurologic conditions could lead to a better understanding of joints respiratory mechanics of the thorax.

6. Acknowledgements

The authors thank the Radiology department of Erasme Academic Hospital and Dr Dufresne. We are also most grateful to Pr. Leduc and Pr De Troyer for helpful discussions. Finally, we also thank the students implied in the CT-scan segmentation procedure: Rochas D., Djoko Mbopda A., Volet P., Robert. C.

7. References

Bellemare, F., Jeanneret, A., 2007. Sex differences in thoracic adaptation to pulmonary hyperinflation in cystic fibrosis. Eur. Respir. J. 29, 98–107. doi:10.1183/09031936.00045606

Bellemare, J.F., Cordeau, M.P., Leblanc, P., Bellemare, F., 2001. Thoracic dimensions at maximum lung inflation in normal subjects and in patients with obstructive and restrictive lung diseases. Chest 119, 376–386.

Beyer, B., Feipel, V., Coupier, J., Snoeck, O., Dugailly, P.M., Van Sint Jan, S., Rooze, M., 2013. Thorax 3D modelling from costovertebral joint complex kinematics: preliminary results. Presented at the XXIV Congress of the International Society of Biomechanics, Natal, Brazil, p. 185.

Beyer, B., Feipel, V., Sholukha, V., Chèze, L., Van Sint Jan, S., 2015a. Relation between rib kinematics and lung volumes: comparison between normal subjects and cystic fibrosis patients, in: Abstract Book. Presented at the XXV congress of the International society of biomechanics, Glasgow, pp. 1164–1165.

Beyer, B., Sholukha, V., Dugailly, P.M., Rooze, M., Moiseev, F., Feipel, V., Van Sint Jan, S., 2014. In vivo thorax 3D modelling from costovertebral joint complex kinematics. Clin Biomech (Bristol, Avon) 29, 434–438. doi:10.1016/j.clinbiomech.2014.01.007

Beyer, B., Sholukha, V., Salvia, P., Rooze, M., Feipel, V., Van Sint Jan, S., 2015b. Effect of anatomical landmark perturbation on mean helical axis parameters of in vivo upper costovertebral joints. J Biomech 48, 534–538. doi:10.1016/j.jbiomech.2014.12.035

Botton, E., Saraux, A., Laselve, H., Jousse, S., Le Goff, P., 2003. Musculoskeletal manifestations in cystic fibrosis. Joint Bone Spine 70, 327–335.

Cala, S.J., Kenyon, C.M., Ferrigno, G., Carnevali, P., Aliverti, A., Pedotti, A., Macklem, P.T., Rochester, D.F., 1996. Chest wall and lung volume estimation by optical reflectance motion analysis. J. Appl. Physiol. 81, 2680–2689.

Cassart, M., Gevenois, P.A., Estenne, M., 1996. Rib cage dimensions in hyperinflated patients with severe chronic obstructive pulmonary disease. Am. J. Respir. Crit. Care Med. 154, 800–805. doi:10.1164/ajrccm.154.3.8810622

Cassart, M., Pettiaux, N., Gevenois, P.A., Paiva, M., Estenne, M., 1997. Effect of chronic hyperinflation on diaphragm length and surface area. Am. J. Respir. Crit. Care Med. 156, 504–508.

Chèze, L., Fregly, B.J., Dimnet, J., 1998. Determination of joint functional axes from noisy marker data using the finite helical axis. Human Movement Science 17, 1–15. doi:10.1016/S0167-9457(97)00018-3

Dassios, T., Katelari, A., Doudounakis, S., Mantagos, S., Dimitriou, G., 2013. Respiratory muscle function in patients with cystic fibrosis. Pediatr. Pulmonol. 48, 865–873. doi:10.1002/ppul.22709

de Lange, A., Huiskes, R., Kauer, J.M., 1990. Effects of data smoothing on the reconstruction of helical axis parameters in human joint kinematics. J Biomech Eng 112, 107–113.

De Troyer, A., 2012. Respiratory effect of the lower rib displacement produced by the diaphragm. J. Appl. Physiol. 112, 529–534. doi:10.1152/japplphysiol.01067.2011

De Troyer, A., Leduc, D., 2004. Effects of inflation on the coupling between the ribs and the lung in dogs. J. Physiol. (Lond.) 555, 481–488. doi:10.1113/jphysiol.2003.057026

Groote, A.D., Wantier, M., Cheron, G., Estenne, M., Paiva, M., 1997. Chest wall motion during tidal breathing. Journal of Applied Physiology 83, 1531–1537.

Hurtado, A., Fray, W.W., 1933. Studies of total pulmonary capacity and its sub-divisions. II. Correlation with physical and radiological measurements. J Clin Invest 12, 807–823.

Laurin, L.-P., Jobin, V., Bellemare, F., 2012. Sternum length and rib cage dimensions compared with bodily proportions in adults with cystic fibrosis. Can. Respir. J. 19, 196–200.

Meskers, C.G., van der Helm, F.C., Rozendaal, L.A., Rozing, P.M., 1998. In vivo estimation of the glenohumeral joint rotation center from scapular bony landmarks by linear regression. J Biomech 31, 93–96.

Pettiaux, N., Cassart, M., Paiva, M., Estenne, M., 1997. Three-dimensional reconstruction of human diaphragm with the use of spiral computed tomography. J. Appl. Physiol. 82, 998–1002.

Pinet, C., Cassart, M., Scillia, P., Lamotte, M., Knoop, C., Casimir, G., Mélot, C., Estenne, M., 2003. Function and Bulk of Respiratory and Limb Muscles in Patients with Cystic Fibrosis. Am J Respir Crit Care Med 168, 989–994. doi:10.1164/rccm.200303-398OC

Rose J, Gamble J, Schultz A, Lewiston N, 1987. BAck pain and spinal deformity in cystic fibrosis. Am J Dis Child 141, 1313–1316. doi:10.1001/archpedi.1987.04460120079039

Sharp, J.T., Beard, G.A., Sunga, M., Kim, T.W., Modh, A., Lind, J., Walsh, J., 1986. The rib cage in normal and emphysematous subjects: a roentgenographic approach. J. Appl. Physiol. 61, 2050–2059.

Söderkvist, I., Wedin, P.A., 1993. Determining the movements of the skeleton using well-configured markers. J Biomech 26, 1473–1477.

Tattersall, R., Walshaw, M.J., 2003. Posture and cystic fibrosis. J R Soc Med 96, 18–22.

Walsh, J.M., Webber, C.L., Fahey, P.J., Sharp, J.T., 1992. Structural change of the thorax in chronic obstructive pulmonary disease. J. Appl. Physiol. 72, 1270–1278.

Wilkens, H., Weingard, B., Lo Mauro, A., Schena, E., Pedotti, A., Sybrecht, G.W., Aliverti, A., 2010. Breathing pattern and chest wall volumes during exercise in patients with cystic fibrosis, pulmonary fibrosis and COPD before and after lung transplantation. Thorax 65, 808–814. doi:10.1136/thx.2009.131409

Wilson, T.A., Legrand, A., Gevenois, P.A., De Troyer, A., 2001. Respiratory effects of the external and internal intercostal muscles in humans. J. Physiol. (Lond.) 530, 319–330.

Wilson, T.A., Rehder, K., Krayer, S., Hoffman, E.A., Whitney, C.G., Rodarte, J.R., 1987. Geometry and respiratory displacement of human ribs. J. Appl. Physiol. 62, 1872–1877.

Woltring, H.J., Huiskes, R., de Lange, A., Veldpaus, F.E., 1985. Finite centroid and helical axis estimation from noisy landmark measurements in the study of human joint kinematics. J Biomech 18, 379–389.

Next steps

Chapter 5 described rib kinematics in a sample of patients with cystic fibrosis and compared them to a control group. Results have shown a significant influence of pathological condition on rib ROMs while no significant difference was established for mean helical axes orientation. These results demonstrate that a pathological condition is able to alter rib kinematic parameters in breathing, although not significantly modifying CVJ kinematics. This could seem at first view contradictory. However, the description of the CVJ kinematics mainly describes the posterior joints of each rib, and did not consider the anterior joints of the thorax (i.e. sternocostal arches); this could explain the above paradox. In order to fine-tune the overall rib behaviour during breathing closed kinematic chains should be considered. Therefore, the next chapter focuses on applying the developed methodology on analysing sternum and sternocostal kinematics during breathing starting from the same database, and considering closed kinematic chains to describe rib behaviour related to the corresponding vertebrae posteriorly and the sternum anteriorly.

Chapter 6:

In vivo analysis of sternal angle, sternal and sterno-costal kinematics in supine humans at various lung volumes.

Submitted in Journal of Biomechanics

[1,2,*] Benoît Beyer, [1,2] Véronique Feipel, [1,3] Victor Sholukha, Laurence Chèze[4], [1] Serge Van Sint Jan.
[1] Laboratory of Anatomy, Biomechanics and Organogenesis (LABO), Université Libre de Bruxelles, Brussels, Belgium
[2] Laboratory of functional anatomy (LAF), Université Libre de Bruxelles, Brussels, Belgium
[3] Department of Applied Mathematics, Peter the Great St.Petersburg Polytechnic University (SPbPU), Russia
[4] Univ Lyon, Université Claude Bernard Lyon 1, Ifsttar, UMR_T9406, LBMC, F69622, Lyon, France

Abstract

This paper investigates for the first time in supine humans the combination of sternum displacement, sternal angle variations and sternocostal joints (SCJ) kinematic of the seven fist rib pairs over the inspiratory capacity (IC). Retrospective codified spiral-CT data obtained at total lung capacity (TLC), middle of inspiratory capacity (MIC) and at functional residual capacity (FRC) were used to compute kinematic parameters of the bones and joints of interest in a sample of 12 asymptomatic subjects. 3D models of rib, thoracic vertebra, manubrium and sternum were processed to determined anatomical landmarks (ALs) on each bone. These ALs were used to create local coordinate system and compute spatial transformation of ribs and manubrium relative to sternum, and sternum relative to thoracic vertebra. The rib angular displacements and associated orientation of rotation axes and joint pivot(JPP), the sternal angle variations and the associated displacement of the sternum relative to vertebra were computed between each breathing pose at the three lung volumes. Results can be summarized as following: 1) sternum cephalic displacement ranged between 17.8 and 19.2mm over the IC; 2) the sternal angle showed a mean variation of 4.4° ± 2.7° over the IC; 3) ranges of rib rotation relative to sternum decrease gradually with increasing rib level; 4) axes of rotation are similarly oriented at each SCJ; 5) JPP spatial displacements showed less variations at first SCJ compared levels underneath; 6) linear relation is demonstrated between SCJ ROMs and sternum cephalic displacement over the IC.

1. Introduction

The sternum was demonstrated to participate to rib cage stability (Watkins et al., 2005) and to be related to rib motion during breathing (De Troyer and Decramer, 1985; De Troyer and Wilson, 1993). Sternocostal junctions (SCJ) include two joint components, i.e., the costo-chondral joint and the chondro-sternal joint, that are involved into thorax shape alterations and motion transmission from ribs towards the sternum. The 3D geometry of the ribs, their decreasing ranges-of-motion (ROMs) at costovertebral joints with increasing rib number (Beyer et al., 2015b; Beyer et al., 2014b; Wilson et al., 2001, 1987), and the shape and size differences in costal cartilages seem to have an influence on the coupling between the ribs and sternum during breathing. Thus, the nature of each joint is specific to different region of the thorax. Indeed, all chondro-sternal joints, but the first one, are synovial joints. The first chondro-sternal joint and all costo-chondral joints show an anatomical and functional continuity between bone and cartilage (i.e., so called synchondrosis joints) (Osmond, 1995). Furthermore, the manubrio-sternal joint (MSJ) is recognized to allow slight variation of the sternal angle (or angle of Louis) as a secondary cartilaginous pliable hinge joint, enabling thorax deformation during deep breathing (Kaneko and Horie, 2012; Osmond, 1995). Previous works have analyzed the mechanical coupling between the ribs and sternum in dog (De Troyer and Decramer, 1985; De Troyer and Wilson, 1993), and concluded that the upper rib cage is tightly linked to the sternum (De Troyer and Decramer, 1985; De Troyer and Wilson, 1993). Similar relation was then observed in 2 high tetraplegic patients (De Troyer et al., 1986a). While the relationships between sternum and rib motions are widely recognized, no quantitative data are available in literature, neither on asymptomatic human subjects nor in pathological conditions. Therefore, the aim of the present study was to obtain quantitative analysis of sternal angle variations and the relation between the “true ribs” rotation (i.e., ribs 1 to 7 articulating anteriorly with the sternum) and sternum displacements as a function of lung volume over the inspiratory capacity.

The following hypotheses were tested: - 1) the sternal angle is altered with increasing lung volume - 2) the rib rotation relative to sternum decreases with increasing rib number following costo-vertebral joints pattern (rib rotation relative to vertebrae was previously reported to decrease inversely with rib number (Beyer et al., 2015b; Beyer et al., 2014b; Wilson et al., 2001) - 3) the position and orientation of the axes of rib rotation relative to sternum differ between rib level.

2. Materials and method

2.1.Sample and data collection

The protocol included processing and analysis of retrospective codified medical imaging datasets obtained from the Department of Radiology of the Erasme Academic Hospital. Spiral computed tomography (Siemens SOMATOM, helical mode, slice thickness = 0.5 mm, inter-slice spacing = 1 mm, image data format: DICOM 3.0) performed at 3 lung volumes: total lung capacity

(TLC), functional residual capacity (FRC) and middle of inspiratory capacity (MIC) which corresponds to FRC + 50% of the inspiratory capacity (Cassart et al., 1997; Pettiaux et al., 1997). CT images were sequentially performed while the subjects were connected to a spirometer and instructed to maintain inflation at each lung volume of interest while relaxing their respiratory muscle against closed airway (Cassart et al., 1997). A sample of 12 datasets from asymptomatic adults (mean age 31± 6 years old) was analysed. Details of anthropometric characteristics of the subjects are given in Annex 1.

2.2. 3D models, anatomical landmarks and local coordinate systems

From the available CT data, 3D models of ribs, vertebrae, manubrium and sternal body with xiphoid process were obtained using a dedicated data segmentation software (Amira 4.0, San Diego, CA, USA) as previously detailed (Beyer et al., 2014b). Models were then imported within a custom-made software called lhpFusionBox (Van Sint Jan et al., 2013) to obtain the spatial coordinates of anatomical landmarks (ALs) located at the surface of the models following previously published recommendations for ribs, vertebrae and sternum (Beyer et al., 2014b; Van Sint Jan, 2007). Note that all details concerning the ALs are given in Figure 1A.

ALs were then virtually grouped into so-called "AL clouds" that were subsequently used to build anatomical frames (AFs) on each bone of interest. Ribs and vertebrae coordinate systems were obtained as explained in previous analysis of costovertebral joints (Beyer et al., 2015b; Beyer et al., 2014b). Manubrium and sternum AFs are detailed in Figure B.

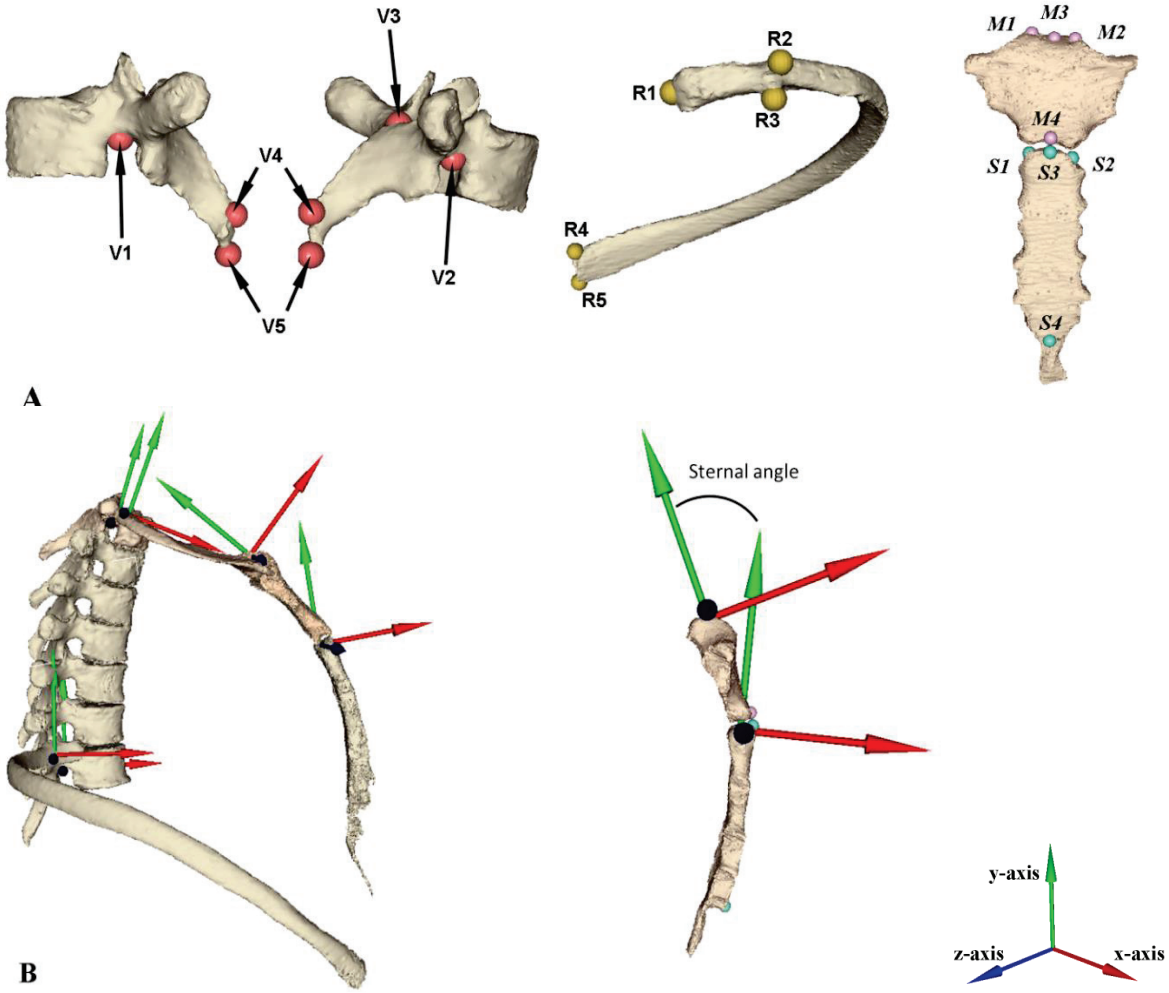

Figure 1: A: Anatomical landmarks (ALs) located on vertebrae, ribs, manubrium and sternum. For ribs and vertebrae: see Beyer et al, 2015, 2016; For manubrium: M1: uppermost point of the right clavicular surface, M2: uppermost point of the left clavicular surface, M3: central point of the jugular notch, M4: at the center of manubriosternal edge on the manubrium, For sternum body: S1: on the right top of the 2nd chondro-sternal surface, S2: on the left top of the 2nd chondro-sternal surface, S3: at the center of manubriosternal edge on the sternum (mirror of M4), S4: at the center of the lowermost extremity of the sternum at xyphisternal joint.

B: Anatomical coordinate systems used to describe displacements. For manubrium: y-axis (cephalo-caudal, in green) was computed between M4 and M3 (along the body of the manubrium), z-axis (lateral to the right, in blue) between M2 and M1, and x-axis (dorso-ventral, in red) normal to others and pointing forward. For sternum: y-axis was computed between S4 and S3 along the sternum body, z-axis between S2 and S1 normal to y-axis, and x-axis normal to others pointing forward. The sternal angle (angle of Louis) was calculated as the angle between manubrium and sternum y-axes within the sagittal plane. For ribs and vertebrae: see Beyer et al, 2015, 2016

2.3.3D kinematic parameters computation

Note that all rib landmarks clouds were registered in Th7 coordinate system at FRC position chosen as reference position. The displacement of the sternum was computed in both Th1 and Th7 coordinate systems using change in the position vector of the sternum body relative to the origin of the vertebra coordinate system of interest (i.e. at the midpoint between V1 and V2 in Figure). In addition, the sternal angle (also called angle of Louis) is usually described at MSJ level as the angle in the anatomical sagittal plane between the manubrium and the sternal body (Kaneko and Horie, 2012; Osmond, 1995). Therefore, this sternal angle was computed as the angle between the y-axes of the manubrium and sternum coordinate systems (see Figure 1B) at each breathing pose.

The kinematics of ribs AL clouds relative to sternum were computed using rigid body transformation (Söderkvist and Wedin, 1993) and determination of finite helical axis (FHA) including joint pivot point (JPP) (Beyer et al., 2015b; Beyer et al., 2014b; de Lange et al., 1990; Ehrig et al., 2007). The rotation around FHA was used to express rib rotation relative to sternum as a single rotation component. Dispersion of FHA orientation and position were also computed following previous recommendations (Beyer et al., 2015b). Rib position dispersion was determined from the JPP displacements as following. Firstly, the range of the JPP spatial coordinates along each axis was determined to create a "bounding box" including all successive JPPs. The norm of the vector that represents the "bounding box" was then calculated.

Finally, the mean helical axes (MHA) at each rib level were computed as the optimal direction vector with the smallest angle between FHA (Stokdijk et al., 1999; Woltring, 1990). Details of the procedure to define spatial position and orientation of MHA in local coordinate systems were previously published (Beyer et al., 2015b; Beyer et al., 2014b). MHA direction cosines in sternum coordinate system were then used to report axes orientation. The location of the mean rotation center (i.e. the mean pivot point (MPP), see (Beyer et al., 2015b; Woltring et al., 1985)) was also determined in the sternum coordinate system.

2.4.Statistical analysis

Analysis of variance (ANOVA) for repeated measurements was used to evaluate the influence of the side, rib level and breathing pose on rib kinematics. A one-way ANOVA test was used to analyse the influence of breathing pose on sternal angle. The relation between rib kinematics and sternal displacements was tested using Pearson correlation coefficient (r). Values of $p<0.05$ were considered statistically significant. When ANOVA indicated significant difference for specific factor, Bonferroni post-hoc tests were used to determine the significant comparisons at $p<0.05$. A linear regression was conducted to elucidate the relation between sternum axial displacement and SCJ ROMs. Statistical analysis was performed using Statistica software (Statistica 8.0© StatSoft. Inc., Tulsa, USA).

3. Results

All results are given as mean ± standard errors.

3.1.Sternum displacement in thoracic vertebra coordinate system

The displacement of the sternum relative to vertbera Th1 and Th7 are presented in Figure . Note that displacement along dorso-ventral axis (i.e. x-axis) significantly differed when expressed in Th1 or Th7 coordinate system. In both Th1 and Th7, the displacement occurred mainly on the cephalo-caudal axis (i.e. y-axis). The mean displacements were 9.6 mm ± 7.1, 17.8 ± 5.9 and 0.8 ± 2.3 along x- , y- and z-axis respectively. In Th1, the mean displacements were 3.8 mm ± 4.2, 19.2 ± 8.4 and 1.0 ± 2.7 along x-, y- and z-axis respectively.

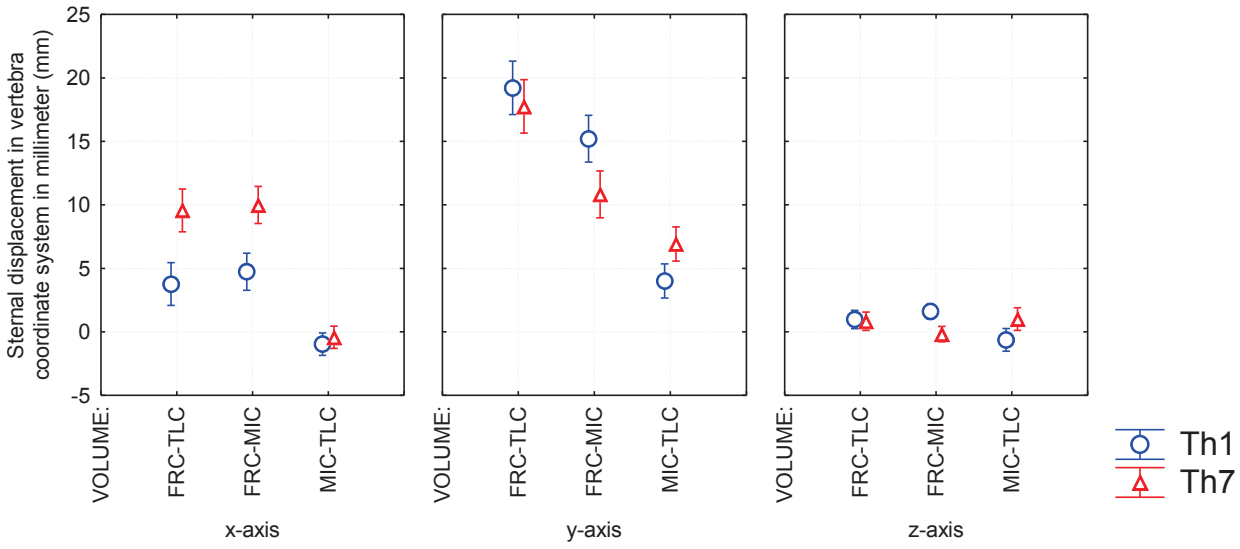

Figure 2: Sternal displacement relative to Th1 and Th7 coordinate systems. Results are presented according to each axis of the coordinate systems in millimeters +/- standard errors.

3.2.Sternal angle variations

The mean sternal angle was significantly decreasing from 16.7° ± 5.5° at TLC to 14.9° ± 5.2° at MIC (p=0.016) and to 12.4° ± 4.9° (p=0.0011) at FRC. The average ROM around the sternal angle was 4.4° ± 2.7° similarly distributed above and below MIC with respectively 1.9° ± 1.2° and 2.5° ± 2.1°.

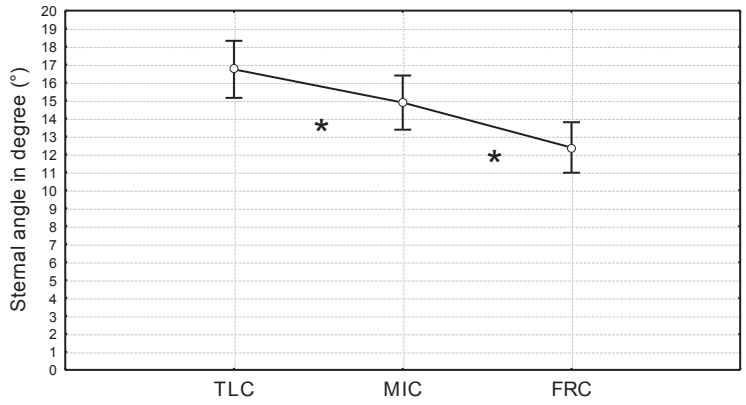

Figure 3: Sternal angle variations between each available lung volume in degree (°). Black stars represent significant difference (p<0.05) between lung volumes. Vertical bars denote +/- standard errors.

3.3.Rib angular displacement relative to sternum

Rib1 to Rib7 angular displacements were then all expressed in sternum coordinate system to facilitate comparison and interpretation (see Figure 4). ROMs were significantly influenced by lung volume ($p<0.001$) and rib level ($p<0.001$). The interaction between the lung volume and the rib level also had a significant influence ($p<0.001$) on ROMs. The total ROMs gradually decreased from 15.5° ± 1.7° at Rib1 to 7.6 ± 0.8° at Rib7. Note that Bonferroni post hoc tests demonstrated no significant differences between two to four adjacent rib levels.

Above MIC, the ROMs ranged from 4.7° ± 0.9° at Rib1 to 3.9 ± 0.7° at Rib7 without any significant difference between rib levels. Below MIC, ROMs were gradually decreasing from 10.9° ± 1.8° at Rib1 to 3.7° ± 0.9° at Rib7. Note that as between TLC and FRC, no significant ROMs difference was demonstrated between adjacent rib levels (similarly as below MIC). Furthermore, from Rib1 to Rib3, ROMs significantly differs between above and below MIC while other lower rib levels (i.e. Rib4 to Rib7) were not altered by lung volume above or below MIC.

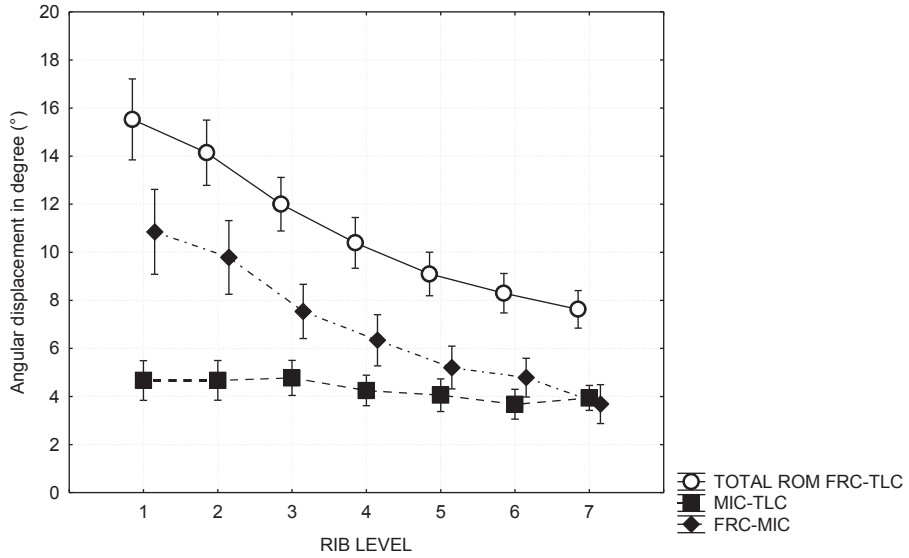

Figure 4: Rib1 to Rib7 ROMs between each available lung volume. Results are presented in degree (°) in the sternum coordinate system. Vertical bars denote +/- standard errors.

3.4 Dispersion of the FHAs and joint pivot points (JPP)

Results are presented in figure 5. The dispersion angle between FHAs was not altered by rib level ($p>0.05$) and ranged between 14.7° ± 1.3° and 18.5° ± 1.5°. The displacement of the JPP increased significantly with increasing rib number ($p<0.001$). Note that significant difference ($p<0.01$) was observed for all rib levels but the first one when compared to the one at Rib2. The mean dispersion of JPP ranged between 28.9 ± 3.8mm at Rib2 to 151.3 ± 10.6mm at Rib7. Supplementary material gives opportunity to visualize the displacement of each FHA.

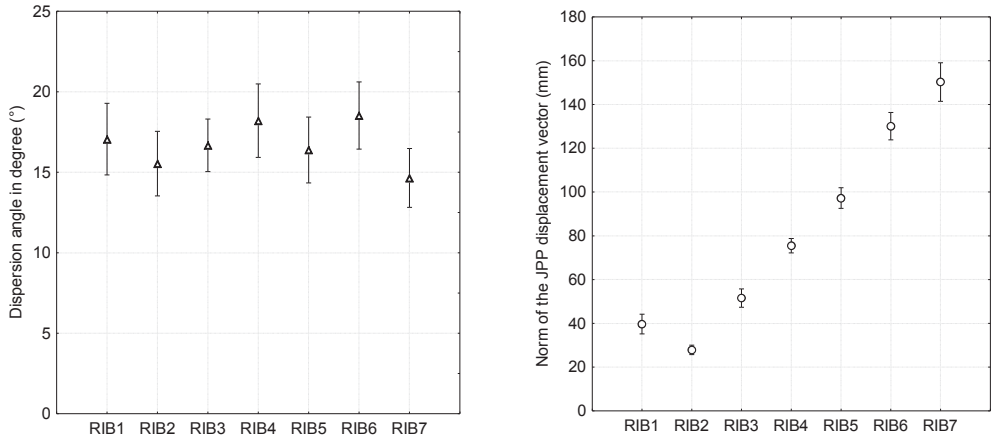

A B

Figure 5: A: Dispersion of FHAs in degree at each rib level regardless of the side. Results are expressed in degree (°), vertical bars denote +/- standard errors.
B: Displacement of JPP. Results correspond to the norm of the vector that represents the "bounding box" in millimeter. Vertical bars denote +/- standard errors.

3.5 Mean helical axes orientation and centers of rotation

All direction cosines for the left bones were mirrored and expressed as right sided to enable comparison between sides. The side had no significant influence on the orientation of MHAs (p=0.864) (see Figure 6).

MHA mean direction cosines ranged between -0.52 and -0.31 on x-axis; between 0.49 and 0.53 on y-axis and between 0.35 and 0.56 on z-axis. In other words, the axes were oriented obliquely caudally, ventrally and medially at all rib levels considered (i.e. Rib1 to Rib7). No significant difference were observed between rib level (p=0.587). The interaction between level and component did not show any significant influence (p=0.06). An example of the 3D visualization obtained is presented in Figure 8 where the left sides MHAs are pointing obliquely caudally, ventrally and medially at each rib level.

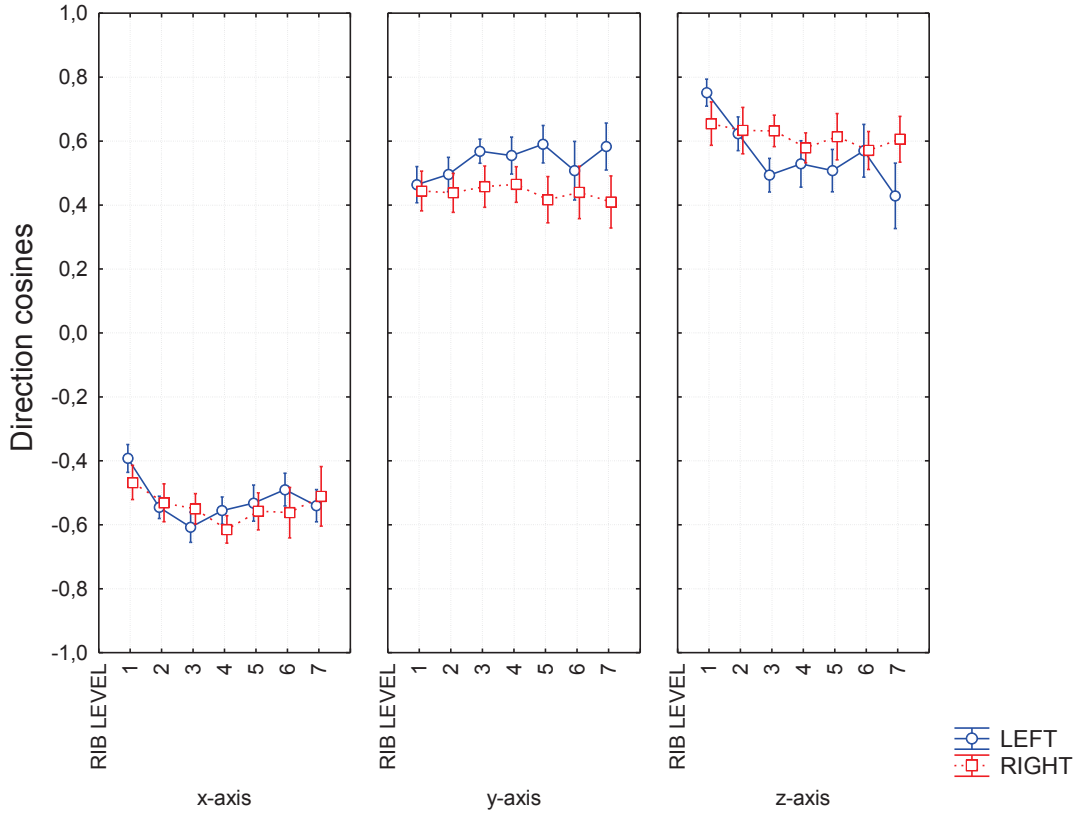

Figure 6: A: MHA direction cosines according sternal coordinate system. Note that direction cosines of left ribs were mirrored and expressed as right ribs. Results are presented as mean direction cosines; vertical bars denote +/- standard errors.

The side had no influence on the position of the mean pivot point (p=0.701) while significant differences were observed between rib levels (p<0.001). The position of the MPP was close to 0 mm on dorso-ventral axis (x-axis), in other words close to the sternum frontal plane, laterally to the sternal body and gradually caudally regarding each rib level. See Figure 7.

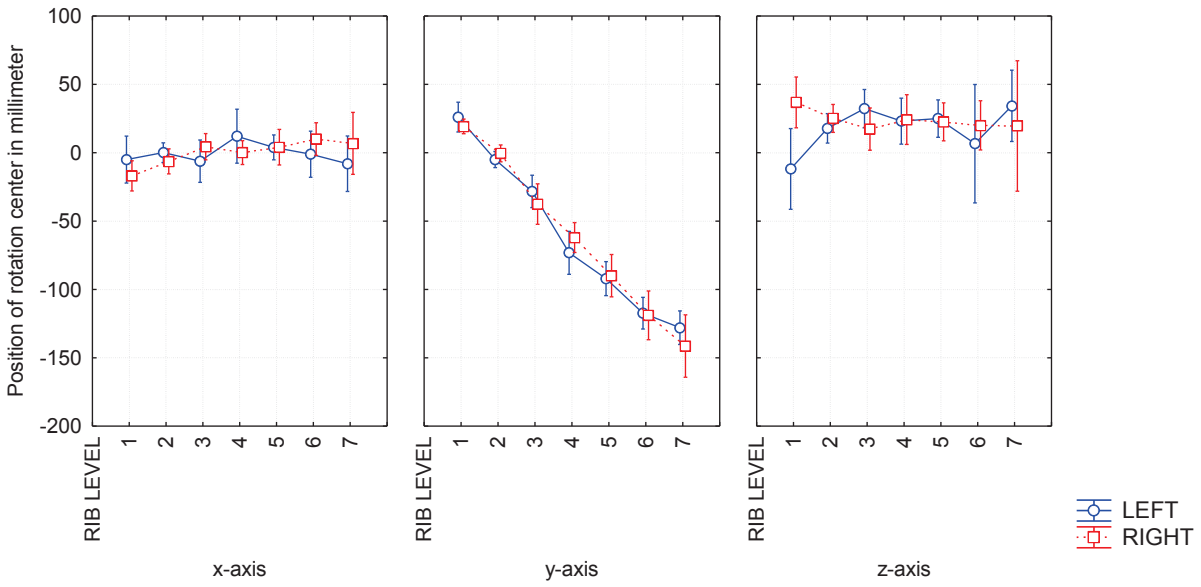

Figure 7: Position of the mean pivot point in sternum coordinate system. Data are presented in millimeter +/- 0.95 confidence intervals along each axis of the sternal frame. Note that left sided rotation centers were mirrored to right side to allow comparison.

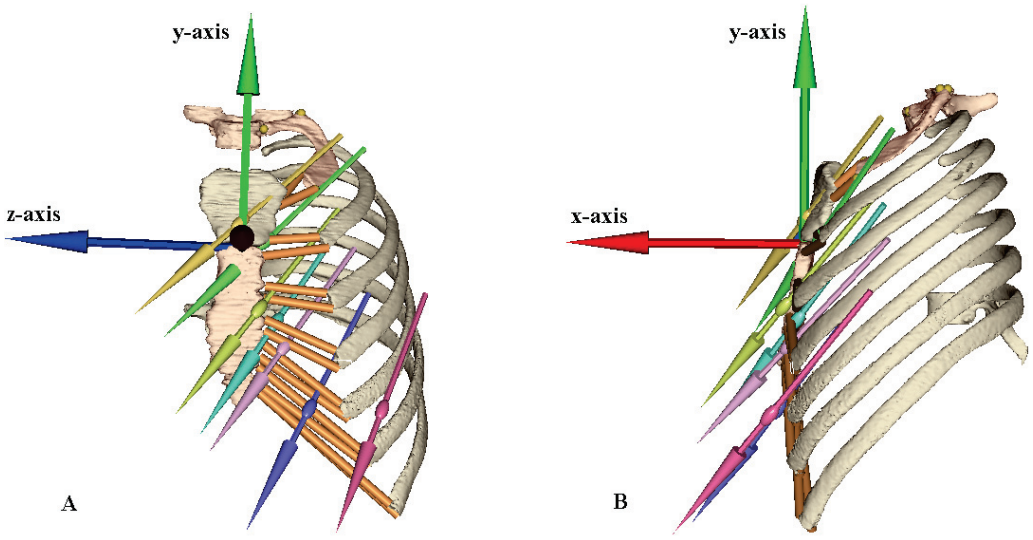

Figure 8: 3D representation of mean helical axes (MHAs), anatomical frames and bones of interest observed in this study. Because they were not clearly visible in the original CT datasets used for this study, costal cartilages were approximated as straight lines between the anterior extremity of the rib and the insertion site on the sternum body or manubrium. The mean pivot point is displayed as a ball on each MHA. A: Frontal plane B: Sagittal plane. 3D visualization of finite helical axes during breathing motion is available in supplementary material.

3.6. Relation between rib and sternum displacement

The range of cephalo-caudal displacement of the sternum was related to the ROMs at SCJ 1 (r=0.92 , p<0.001) and SCJ7 (r=0.74, p =0.006). Linear regressions were determined at these 2 levels of interest (see Figure 9). In addition, ROMs obtained in previous study at costovertebral joints (Beyer et al., 2015b) were used to test the correlation and linear regression between costovertebral kinematics and cephalic displacement of the sternum. A significant correlation was demonstrated between costovertebral ranges of motion and sternum displacement at rib1 (r=0.95, p<0.001) and rib7 (r=0.81, p<0.01).

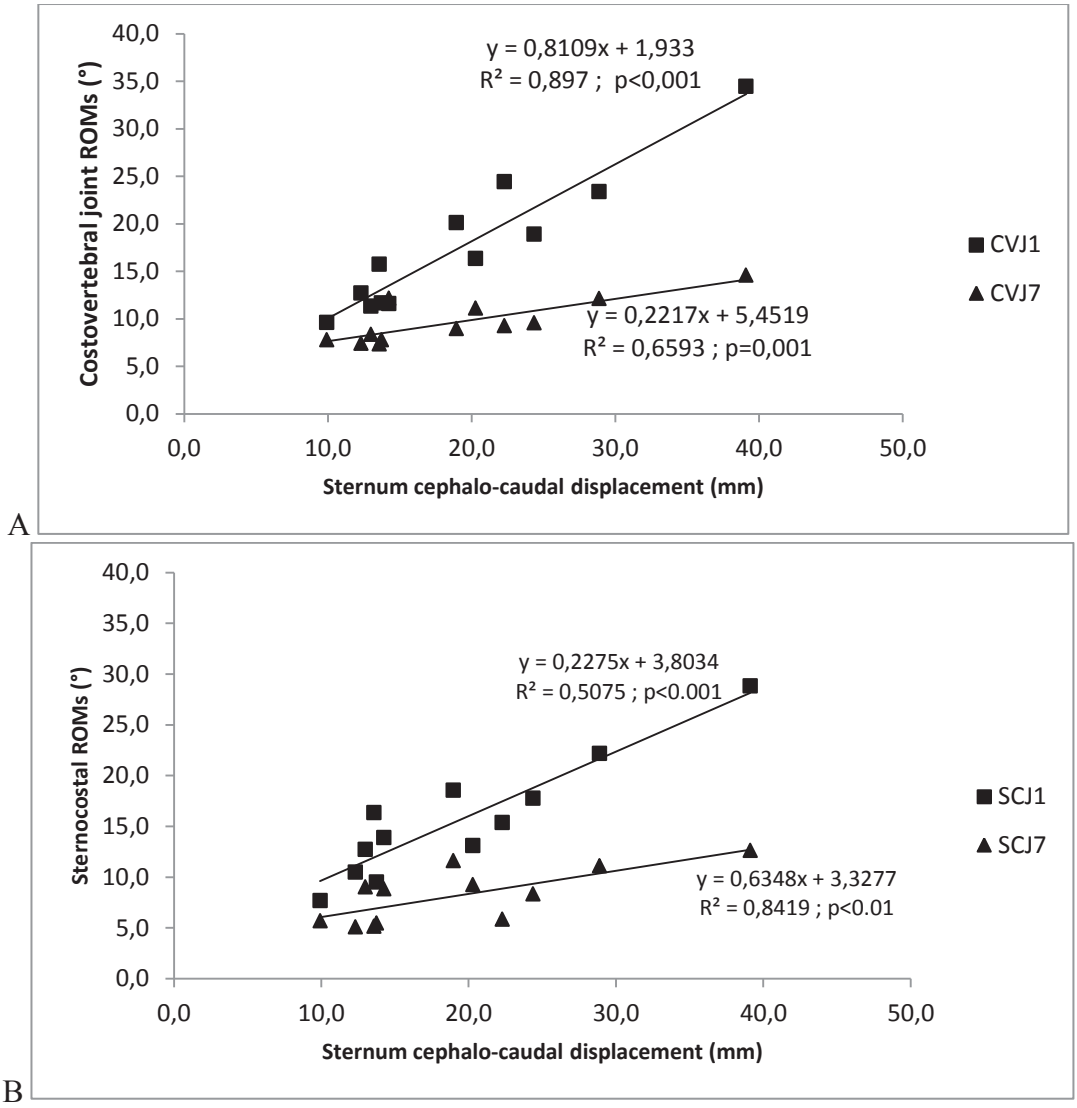

Figure 9: Rib angular displacement as a function of cephalo-caudal displacement of the sternum at costovertebral joint (A) and sternocostal joint (B). Results are given for each of the 12 subjects, at uppermost rib1 and lowermost rib7. Ranges of motions are expressed in degree and sternum displacement in millimeter.

4. Discussion

The present study describes the sternal displacement, sternal angle variations and sternocostal kinematics between different positions obtained at three different lung volumes on a sample of 12 supine human adults. To the author's best knowledge, this is the first study reporting detailed in-vivo quantification of these specific joints of the human thorax in breathing conditions. The functional role of costal cartilages was previously analyzed in dogs using experimental approach (Fick, 1911) and during recent in-vitro experimentation (De Troyer and Decramer, 1985; De Troyer and Wilson, 1993). The linkage between sternal displacement and ribs was also described in 2 tetraplegic patients (De Troyer et al., 1986a). Mechanical properties of the costal cartilages and the influence of growth on cartilage geometry were reported in the literature (Andriacchi et al., 1974; Sandoz et al., 2013). However, the present study enabled for the first time to describe quantitative in-vivo human data related to rib and sternum kinematic behavior (i.e. ROM and axes of rotation).

The first major finding concerns averaged variation of 4.4° observed at the sternal angle. Since the sternal angle increases between each lung volume (see Figure 3), MSJ could act as a torsion spring able to store energy during lung inflation and restore it to facilitate thoracic cage deflation. This is supported by the fact that exhalation is recognized to be a mainly passive mechanism resulting from elastic recoil of mainly the lungs (i.e. pulmonary alveoli) with contribution of chest wall above 75% of the TLC (Agostoni et al., 1965; Agostoni and Hyatt, 2011; Osmond, 1995). Note that aging seems to be responsible of altering the torsion elastic modulus of cartilaginous joint leading to a decrease in rib cage compliance (Estenne et al., 1985; Sharma and Goodwin, 2006). The increase in sternal angle with increasing lung volume could have been related to the differences in rib length. Indeed, during cephalic displacement of the sternum, the shortest ribs (i.e. rib1 and 2) should lead to a backward shift of the cephalic extremity of the sternum (i.e. manubrium), and by consequence to an increase of the sternal angle.

Another result obtained in this study concerns the gradual decrease of sternocostal ROMs occurring inversely to the analyzed rib level (i.e., the larger the rib level, the smaller the related ROM). As previously underlined (De Troyer and Decramer, 1985), if the rib cage behaved as a rigid entity, all ribs should display equal motions relative to the sternum. However, it was not the case in dogs for which the upper portion of the rib cage was demonstrated to behave more as a unit than the lower ribs (De Troyer and Decramer, 1985; De Troyer and Wilson, 1993). The present study seems to indicate similar behavior in human, and that the rib cage does not move as a rigid entity.

The mechanical linkage between ribs and sternum is highlighted by the variability of both FHAs orientation and position of the JPP during breathing motion. From a mechanical aspect, when a joint mechanism is more constrained, the dispersion of the FHAs and the position of the JPP should be more stable. The present result showed that the dispersion of FHAs orientation was similar at all SCJ levels; however, the displacement of the JPP increased significantly and gradually from Rib1 to Rib7.

In other words, the constraint is higher at Rib1 and decreases gradually at the rib levels underneath. The supplementary material enables to visualize this finding.

Results of the present study indicates that the conclusion of De Troyer & Decramer (1985) obtained in dogs largely apply to humans. Note that the decrease in sternocostal ROMs is similar to costovertebral joint motion behavior in breathing (Beyer et al., 2015b; Beyer et al., 2014b; Wilson et al., 1987) . Furthermore, the sample used in the present analysis was the same as in previously-reported costovertebral joint (CVJ) analysis (Beyer et al., 2015b; Beyer et al., 2014b). Comparing the CVJ and SCJ ROMs, it appears that ROMs were systematically smaller at SCJ than at CVJ levels. This difference in ROMs could be attributed to the difference in MHA orientation at CVJ and SCJ (i.e. which are not parallel) and moreover the small rotation obtained at each intervertebral joint (Beyer et al., 2014b).

In addition, the significant influence of lung volume and rib level on SCJ ROMs amplitude is a behavior that was already observed at CVJ levels (Beyer et al., 2016). Similar to CVJs, SCJ ROMs decreased above MIC. Besides, this observation was not true for all rib levels. Indeed, only Rib1 to Rib3 showed larger SCJ ROMs below MIC, while Rib4 to Rib7 showed similar ROM above or below MIC. Previous CVJ analysis (Beyer et al., 2015b) reported similar ROM decrease above MIC at rib level 1 to 7. These observations are in agreement with the change in rib cage compliance with increasing lung volume (Agostoni and Hyatt, 2011).

Finally, to the author's knowledge, the orientation of SCJ axes of rotation (i.e., MHAs) was never previously described. MHAs observed in the present study were orientated obliquely, ventrally, downward and inward, and were not influenced by rib level. The computation of rib transformation relative to manubrium gives insight about the cartilages structures in-between. The costal cartilages were positioned close to the sternal frontal plane and gradually oriented downward from the second to the seventh level (Osmond, 1995). The orientation of the first costal cartilage was almost parallel to the 3D oblique orientation of the first MHA. At lower rib levels (Rib2 to Rib7) the MHAs were clearly intersecting the plane of the costal cartilage. Note that the position of the MPP followed the position of the costal cartilage, (see figure 7 along y-axis). Mechanically, MHA orientation variations indicate different costal cartilage behavior during breathing. From a mechanical point-of-view, when the axis of rotation is following the natural longitudinal axis of a costal cartilage (like for the first costal cartilage), one might assume that such costal cartilage is working as a one degree-of-freedom torsion bar (or spring) with a torque generated perpendicular to the axis of the bar. However, for lower rib levels (i.e., with MHAs intersecting the cartilage) the torque generated during inflation should be considered around multiple degrees-of-freedom. These considerations are in agreement with the fact that the first rib is more rigidly attached to the first costal cartilage and to the sternum. Thus, it could be considered that the first SCJ is driving the rib cage displacement, and is not able to deform as much as the SCJ underneath.

5. Conclusion

To the authors' best knowledge, the present study is the first to describe sternocostal joint behavior quantitatively in breathing humans. Reported results are of interest to improve our current understanding related to normal thorax joints physiology and present data should be useful for modelling of respiratory mechanics. Moreover, 3D representation of results enables both qualitative and quantitative kinematics visualization that can be used for pedagogical purposes. Further research will focus on the effect of pathological conditions on MSJ and SJC kinematics.

6. Acknowledgement

The authors thank the Radiology department of Erasme Academic Hospital and Dr Dufresne. The authors are most grateful to Pr. De Troyer for helpful discussions. The authors also thank Mr. L. Campestrini for his help during his Master thesis related to the present paper.

7. References

Agostoni E, Hyatt RE. Static Behavior of the Respiratory System [Online]. In: Comprehensive Physiology. John Wiley & Sons, Inc. http://dx.doi.org/10.1002/cphy.cp030309.

Agostoni E, Mognoni P, Torri G, Agostoni AF. Static features of the passive rib cage and abdomen-diaphragm. Journal of Applied Physiology 20: 1187–1193, 1965.

Andriacchi T, Schultz A, Belytschko T, Galante J. A model for studies of mechanical interactions between the human spine and rib cage. J Biomech 7: 497–507, 1974.

Beyer B, Sholukha V, Dugailly PM, Rooze M, Moiseev F, Feipel V, Van Sint Jan S. In vivo thorax 3D modelling from costovertebral joint complex kinematics. Clin Biomech (Bristol, Avon) 29: 434–438, 2014.

Beyer B, Sholukha V, Salvia P, Rooze M, Feipel V, Van Sint Jan S. Effect of anatomical landmark perturbation on mean helical axis parameters of in vivo upper costovertebral joints. J Biomech 48: 534–538, 2015.

Beyer B, Van Sint Jan S, Chèze L, Sholukha V, Feipel V. Relationship between costovertebral joint kinematics and lung volume in supine humans. Respir Physiol Neurobiol 232: 57–65, 2016.

Cassart M, Pettiaux N, Gevenois PA, Paiva M, Estenne M. Effect of chronic hyperinflation on diaphragm length and surface area. Am J Respir Crit Care Med 156: 504–508, 1997.

De Troyer A, Decramer M. Mechanical coupling between the ribs and sternum in the dog. Respiration Physiology 59: 27–34, 1985.

De Troyer A, Estenne M, Vincken W. Rib cage motion and muscle use in high tetraplegics. Am Rev Respir Dis 133: 1115–1119, 1986.

De Troyer A, Wilson TA. Sternum dependence of rib displacement during breathing. Journal of applied physiology 75: 334–340, 1993.

Ehrig RM, Taylor WR, Duda GN, Heller MO. A survey of formal methods for determining functional joint axes. J Biomech 40: 2150–2157, 2007.

Estenne M, Yernault JC, Troyer AD. Rib cage and diaphragm-abdomen compliance in humans: effects of age and posture. Journal of Applied Physiology 59: 1842–1848, 1985.

Fick R. Handbuch der Anatomie und Mechanik der Gelenke T. 3. T. 3. Jena: Fischer, 1911.

Kaneko H, Horie J. Breathing Movements of the Chest and Abdominal Wall in Healthy Subjects. Respir Care 57: 1442–1451, 2012.

de Lange A, Huiskes R, Kauer JM. Effects of data smoothing on the reconstruction of helical axis parameters in human joint kinematics. J Biomech Eng 112: 107–113, 1990.

Osmond DG. Functionnal anatomy of the chest wall. In: The Thorax: Part A, 2nd ed. New York: Roussos C., 1995, p. 413–444.

Pettiaux N, Cassart M, Paiva M, Estenne M. Three-dimensional reconstruction of human diaphragm with the use of spiral computed tomography. J Appl Physiol 82: 998–1002, 1997.

Sandoz B, Badina A, Laporte S, Lambot K, Mitton D, Skalli W. Quantitative geometric analysis of rib, costal cartilage and sternum from childhood to teenagehood. Med Biol Eng Comput 51: 971–979, 2013.

Sharma G, Goodwin J. Effect of aging on respiratory system physiology and immunology. Clin Interv Aging 1: 253–260, 2006.

Söderkvist I, Wedin PA. Determining the movements of the skeleton using well-configured markers. J Biomech 26: 1473–1477, 1993.

Stokdijk M, Meskers CG, Veeger HE, de Boer YA, Rozing PM. Determination of the optimal elbow axis for evaluation of placement of prostheses. Clin Biomech (Bristol, Avon) 14: 177–184, 1999.

Van Sint Jan. Color atlas of skeletal landmark definitions: guidelines for reproducible manual and virtual palpations. Edinburgh ; New York: Churchill Livingstone/Elsevier, 2007.

Van Sint Jan S, Wermenbol V, Van Bogaert P, Desloovere K, Degelaen M, Dan B, Salvia P, Ortibus E, Bonnechère B, Le Borgne Y-A, Bontempi G, Vansummeren S, Sholukha V, Moiseev F, Rooze M. A technological platform for cerebral palsy - The ICT4Rehab project. Médecine/Sciences 29: 529–536, 2013.

Watkins R 4th, Watkins R 3rd, Williams L, Ahlbrand S, Garcia R, Karamanian A, Sharp L, Vo C, Hedman T. Stability provided by the sternum and rib cage in the thoracic spine. Spine 30: 1283–1286, 2005.

Wilson TA, Legrand A, Gevenois PA, De Troyer A. Respiratory effects of the external and internal intercostal muscles in humans. J Physiol (Lond) 530: 319–330, 2001.

Wilson TA, Rehder K, Krayer S, Hoffman EA, Whitney CG, Rodarte JR. Geometry and respiratory displacement of human ribs. J Appl Physiol 62: 1872–1877, 1987.

Woltring HJ. Biomechanics of Human Movement, Applications in Rehabilitation, Sport and Ergonomics; Biomechanics of Human Movement, Applications in Rehabilitation, Sport and Ergonomics. .

Woltring HJ, Huiskes R, de Lange A, Veldpaus FE. Finite centroid and helical axis estimation from noisy landmark measurements in the study of human joint kinematics. J Biomech 18: 379–389, 1985.

Chapter 7:

General discussion and conclusions

The aim of this doctoral thesis was to investigate the human thorax joint physiology in breathing conditions, trying to obtain both qualitative and quantitative results using 3D infographics techniques. 3D modelling is an interesting tool that gives the opportunity to visualize complex mechanisms such as specific joint kinematics. Based on the processing of medical imaging datasets, the 3D models obtained from CT-scan images lead to accurate geometry of the joint surfaces compared to geometry estimated from "direct modelling" using geometrical primitives. The present methodology combines simultaneous 3D anatomically realistic reconstruction, motion visualization and analysis. The use of custom-made software called "lhp-FusionBox" (Van Sint Jan et al., 2013) gives the opportunity to combine anatomical landmarks spatial coordinate definition, anatomical frame construction, kinematic parameters estimation from various formally published methods (i.e. Grood & Suntay; Eular angles, helical axes parameters….) and moreover fusion and visualization of kinematic parameters with 3D bone models of interests.

The major topic of the present thesis was therefore to develop a full methodology that allows 3D modelling visualization and kinematic quantification of the thorax joints involved in breathing mechanism. A second objective was then to test the influence of a pathological condition on the kinematic parameters obtained. Finally, to describe the closed kinematic chains that link the vertebrae to the sternum, we applied the methods to the anterior sternocostal joints.

The current general discussion will provide a short summary of each chapter focusing on major findings. Then, various aspects of the developed method and associated findings will be criticized. Finally, clinical considerations and research perspectives will be discussed.

1. Summary and methodological considerations

The first part of the present work (**Chapter 2**) focused on the development of a methodology to enable *in vivo* 3D modelling of the costovertebral joint complexes at different lung volumes starting from currently available CT-scan acquisition techniques. The methods focused on the true ribs and proposed the use of mean helical axis orientation and ranges of motion obtained in anatomical planes. Note that as noticed in the introduction, joint kinematics was computed considering ribs as rigid bodies in breathing movement following previous recommendation (Saumarez, 1986). However, to assess the validity of the "rigid ribs" assumption, a registration procedure using iterative closest point algorithm was performed between each lung volume on few rib reconstructions. The root mean square distance obtained from these registrations were inferior to 0.5mm and allows considering the "rigid rib" assumption valid. The kinematic results obtained confirmed and complemented previously published results concerning rib motion (Wilson et al., 2001, 1987) and added the intervertebral displacement as a part of breathing motion over the entire inspiratory capacity. Eventually, this study led to preliminary results considering only total ranges of motion of costovertebral joint and

representation of the mean helical axis computed from only 3 available discrete poses. The reproducibility of anatomical palpation was assessed and showed accurate palpation (MSD=1.4mm inter session, and ± 1mm inter examiner) however the propagation of palpation error on kinematic parameters was not assessed. The results of the propagation are presented in Figure 1 below along each anatomical axis.

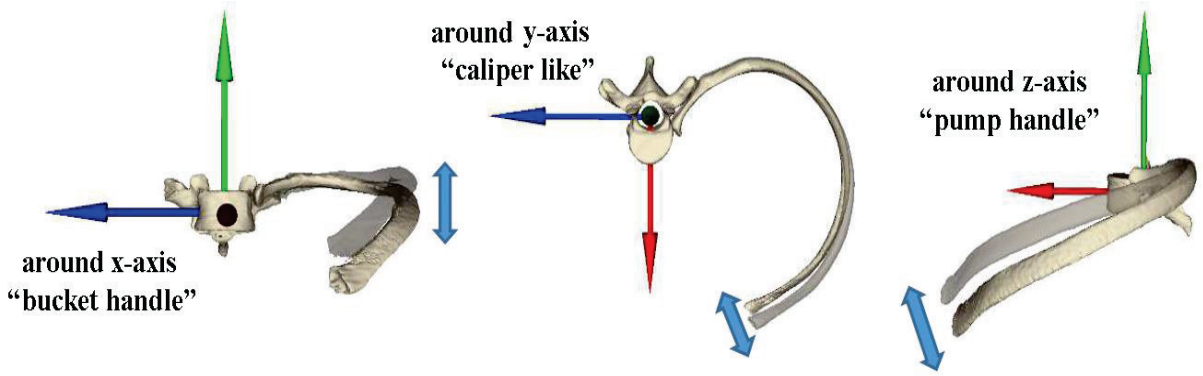

	x-axis	y-axis	z-axis
MSD	2°	1°	2°
MAX	4°	2°	5°

Figure 1: Mean standard deviation of ranges of motion obtained from 3 palpations performed by 2 observers. Results are expressed in degree (°) on each component of the anatomical frame. Note that MSD was obtained from averaging results of all rib levels considered (i.e. rib1 to rib7)

These results highlight that small dispersion in ALs palpation could lead to important alteration of the ROMs obtained in anatomical planes, (Max=5° on a total ROM of ±15°).

In addition, the mean helical axes obtained showed important dispersion in orientation, with high standard deviations (Max SD=0.7637) of the direction cosines. This demonstrated a directrelationship between AL palpation error and discrepancy in the results related to the mean helical axes. Furthermore, the use of only 3 discrete poses, or the magnitude of the step between each successive pose used to compute MHA could have been a second factor for altering MHA orientation and position. Figure illustrates the alteration of MHA orientation and position from the use of various ALs palpation trials. In this case (A: 4 different ALs palpations on a single CVJ level), while MHA orientation was moderately altered, position discrepancies for the MPP is clearly noticeable.

Note that the procedure to test reproducibility and propagation was time consuming and therefore improvement was needed for both reiteration of the procedure and computation of all the kinematic parameters at all CVJ levels on a larger sample.

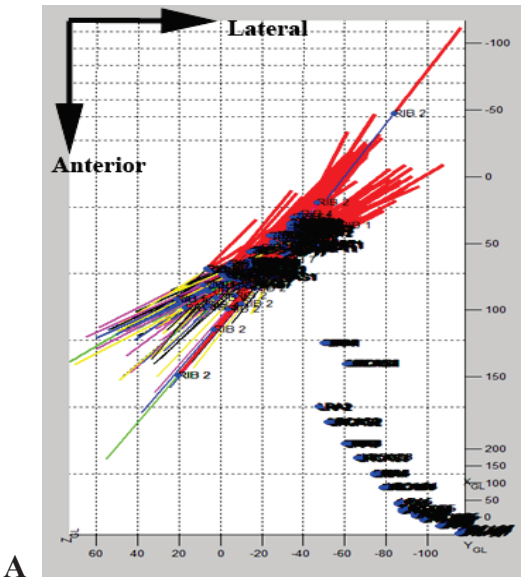

A

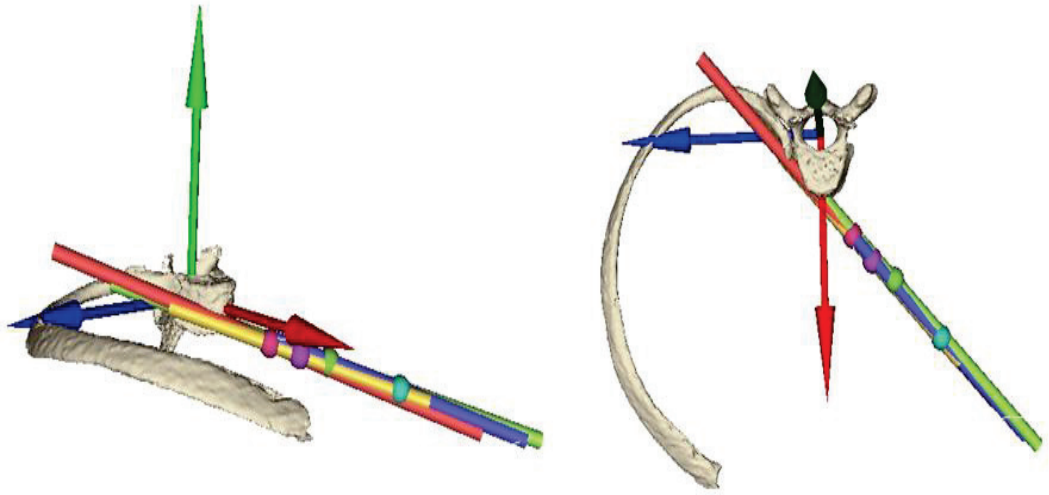

B

Figure 2: Representation of MHA and MPP for different ALs palpation. A: Superior view (transverse plane) of series of MHAs obtained at left CVJ1 to CVJ 7 following simulations of ALs dispersion. B: 3D representation of MHAs obtained at right CVJ7 with 4 iterations of AL displacements. The ball represent the "mean pivot point" (MPP) of each MHA obtained (4 iterations are displayed).

The second part of the present work (**Chapter 3**) especially focused on improving/optimizing the computational method. The aim was to develop an automated procedure that would give the opportunity to simulate dispersion of the AL spatial coordinate and to compute kinematic parameters automatically at each CVJ level. Different parameters that could alter kinematic results were tested (i.e., interpolation, range step for FHA determination, range AL perturbation) in order to obtain an optimal procedure. The effect of AL perturbation on MHA parameters was therefore tested. In addition, the use of interpolation to increase the number of discrete poses, and consequently the number of FHA available for computation of MHA was tested. Finally the procedure demonstrated satisfactory results with dispersion of MHA ranging between 7.5° and 13.6°.

The MATLAB procedure developed enables to process all kinematic parameters in about 1s, i.e. all rigid body transformation parameters, for both left and right ribs and intervertebral segments. Results were stored in a standard file format usually used in the field of motion analysis (i.e., C3D files). The parameters obtained (i.e. AL trajectories, transformation matrices, position and orientation vectors) are then directly observable in open-source software such as MOKKA® that are commonly used in movement analysis laboratories. The final step was then the possibility to fuse trajectories of each AL cloud with the 3D bone models from a single C3D file. This was achieved thanks to lhpfusionBox software (Van Sint Jan et al., 2013). Note that this particular step is of interest since it allows direct visualization of bone motion, to detect visually any typical modelling problem such as bone positioning errors (i.e. collision or dislocation) (Schwartz et al., 2013).

The computation of the dispersion of the MHA was obtained following previously developed methods (de Lange et al., 1990; Woltring et al., 1985). The use of interpolation is still questionable since it may still differ partly from results obtained during continuous motion processing. However, only one method was previously developed to obtain costovertebral kinematic parameters from external measurements (Jordanoglou and Smith, 1970). Jordanoglou started from geometrical parameters (Jordanoglou, 1970) to develop their jig, which corresponds to a linear displacement transducer applied externally to the extremity of the ribs. Geometrical parameters were then used to obtain rib rotation around a "plausible" axis of motion. However, the real position of the axis of rotation was not known. Further development should use similar methods, which integrate regression models of both geometrical and kinematic parameters of the spine and chest wall to obtain anatomically relevant results. Finally, chapters 2 and 3 focused on the development of the methodology with attention on accuracy and repeatability of preliminary results. The obtained protocol had to be expanded to lower ribs and further analysis was needed to describe the relation between rib kinematics and lung volumes on the respiratory ribs 1 to 10.

Consequently, in **chapter 4**, data from respiratory ribs were processed from a larger sample (n=12) and the hypothesis that laterality, lung volume and rib level should alter rib kinematics was tested. These questions were assessed to establish a link between joint mechanics and lung physiology. Statistical analysis was performed to estimate the influence and correlations of the above mentioned factors on the ranges of motion and MHA parameters. Results showed that rib displacements were altered by lung volume, i.e. above MIC, the ribs displayed similar ROMs, while below MIC, ROMs were gradually decreasing with increasing rib number. Results also demonstrated the symmetry between left and right ribs that one could have expected. Finally considering total ROMs, results showed that ribs rotate as small groups of adjacent ribs (3 or 4 ribs). By analogy, the interdependence of rib motion could be described in the manner of an accordion bellows (Figure 3). The first upper ribs are driving the rib underneath. We hypothesized that this linkage is obtained through the force

transmission of intercostal muscles, which is in agreement with previous work (De Troyer et al., 1986, 2005b; Wilson et al., 2001; Wilson and De Troyer, 2004).

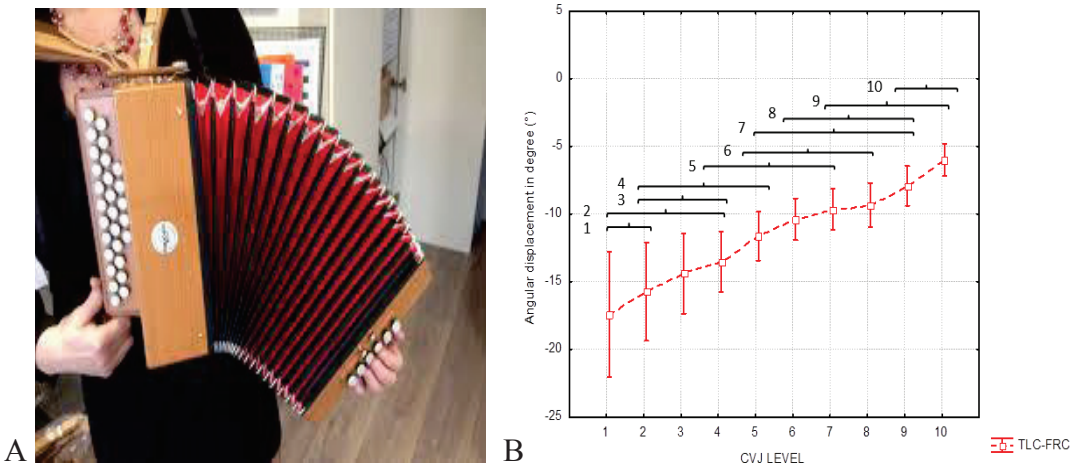

Figure 3: A: Movement of an accordion. B: Relation between ROMs obtained at each CVJ1 to CVJ10 (Beyer et al., 2016).

The laterality had no significant influence, (which was expected) however, many local differences were observed in the results of MHA orientation. One explanatory hypothesis concerned the anatomic variability of the costovertebral joint facets as it was similarly demonstrated on facets of the thoracolumbar (Masharawi et al., 2004, 2004) and cervical vertebra (Laville et al., 2009; Pal et al., 2001). Note that no previous study on CVJ facet geometry was found in literature. Finally, the analysis of the orientation of joint facet showed interesting geometrical asymmetry as presented in the figure below:

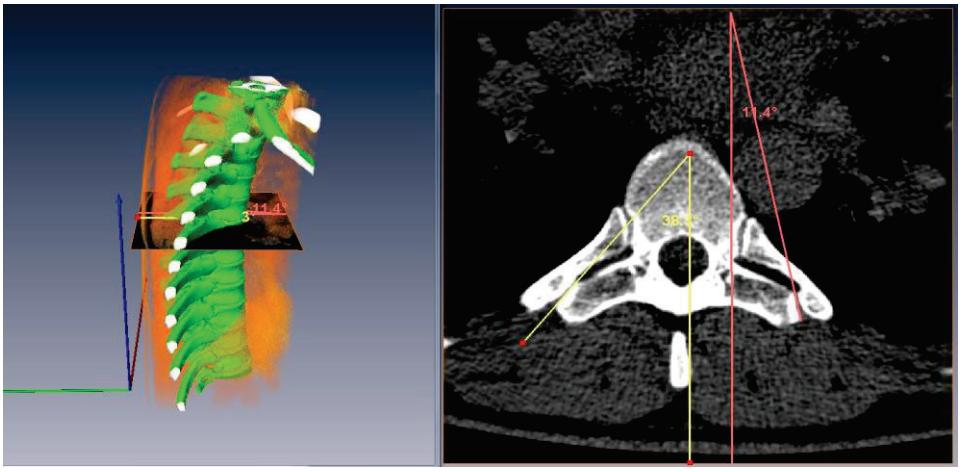

Figure 4: Left: 3D representation of a thoracic spine from CTscan images. Reconstruction is focused on thoracic vertebra and rib heads only. Right: CT image reconstruction in transverse plane at Th6. Firstly, a line was fitted to the joint surface of the transverse process, and then the angle between this line and the antero-posterior axis was estimated. The difference between left (red lines) and right (yellow lines) orientations is obvious.

At this step, we considered that relevant results concerning CVJ kinematics and their relation with lung volume in asymptomatic conditions were achieved. However, one question remained unclear: has a pathologic condition the ability to alter CVJ kinematics?

The **chapter 5** focused on answering the latter question by applying the entire methodology in a sample of patients with cystic fibrosis (CF). This pathology is associated with respiratory symptoms such as chronic dynamic lung hyperinflation. Results showed that patients with CF had a significant decrease of CVJ ROMs. The influence of the pathology was mainly observed at upper rib levels. To the authors' knowledge, this is the first study that demonstrates quantitatively the influence of a pathological condition on the CVJ kinematics at a segmental level. The reduced rib excursion associated with hyperinflation was expected, however the present work enables to demonstrate it quantitatively and moreover allows segmental analysis. Results concerning the effect of CF could be criticized. Indeed, the reduced rib excursion has to be related to lung hyperinflation rather than to cystic fibrosis itself. However, results from this work lead to an interesting hypothesis that CVJ limitations could be part of the cause of back pain, which is a common symptom in such a pathological condition (Rose J et al., 1987; Tattersall and Walshaw, 2003).

The previous chapters focused on determining rib kinematics at costovertebral joints in asymptomatic and pathological conditions. However, the true ribs connect vertebrae to the sternum through the costal cartilages. These anatomical structures are organized as a series of closed kinematic chains, therefore, it seemed necessary to investigate the relation between rib and sternum displacement at sternocostal joints.

The **Chapter 6** focused on applying the above mentioned methodology to sternocostal joints. Note that no previous quantitative results in humans were found in literature. Results demonstrated that the axes of rib motion relative to the sternum were similar at Rib 1 to Rib 7. Furthermore, SCJ ranges of motion gradually decreased with increasing rib level such as at CVJ. The significant correlation between rib and sternum displacement allowed estimating a regression function that gives opportunity to estimate CVJ or SCJ displacement from the vertical displacement of the sternum. This regression is promising since it allows estimating joint kinematics from external measurements obtained at the sternum for example using optoelectronic stereo-photogrammetry. Further research should try to validate the present proposal. Note that the SCJ kinematics were computed as a rotation of the ribs relative to the sternum since the segmentation of costal cartilage remains a challenge. A few anatomical landmarks should be added to the sternum in order to compute the orientation of the costal cartilages during the respiratory motion. However, such a simplistic straight line representation remains of limited realism, especially for the lower half of the costal cartilages.

2. Main limitations of the research

- Position of the subject

The CT data used in the present research were obtained from patients lying in supine position. As it was previously demonstrated, the change in posture leads to a significant alteration of chest wall kinematics (Lee et al., 2010; Romei et al., 2010; Sharp et al., 1975). As an example, Lee et al, 2010 have demonstrated that single plane changes in sitting posture are leading to a three-dimensional alteration of both ribcage configuration and chest wall kinematics during breathing, while respiratory function remains constant. In addition, the contact at the posterior part of the thorax could lead to some limitations of the rib displacement since a load (weight of the thorax) is applied to the posterior part of the ribs. Another parameter that was not "strictly" controlled is the position of the thoracic spine. The inter-individual variability of thoracic spine curvature could also lead to an alteration of rib kinematics. As a consequence, further studies should investigate rib kinematics in standing /sitting position with specific concern on the thoracic spine curvature.

- Age and gender influence

The data set analyzed in this study covers a small age range (i.e. mean age < 40 years old) while aging was demonstrated to influence the morphology of ribs and thorax morphology (Kent et al., 2005; Gayzik et al., 2008; Weaver et al., 2014). Therefore, further analysis of the present samples should estimate the influence of gender on rib kinematics since gender was shown to possibly influence both rib geometry (Bellemare et al., 2003, 2006) or thoracic shape (Bellemare et al., 2003; Bellemare and Jeanneret, 2007).

- Respiratory disease?

In the present research, the effect of a pathological condition on rib kinematics was assessed in a sample of patient with cystic fibrosis. The variability in clinical conditions of such patients is wide. However, the patients included in the present protocol seemed to have been selected when they were stable. Due to their respiratory impairments, it could have been difficult for them to maintain apnea at different lung volume.

Further research should focus on estimating rib kinematics parameters in patients with diseases that affect especially the joint structures such as ankylosing spondylitis or kyphoscoliosis.

- Discrete kinematics

The present results are obtained from discrete poses, and further interpolation between static positions was used to optimize the computation of the helical axes parameters. It remains questionable whether these artificial positions really imitate a continuous motion. Therefore, further investigation should estimate segmental kinematic parameters from a continuous measurement. Note that to our best knowledge, such a method is actually not available.

- **Lung volumes**

In the present research, thorax joint kinematics analysis was obtained from three lung volumes above the functional residual capacity. However, to estimate the full displacement of the ribs over the vital capacity, another position should have been added at residual volume (end of the forced exhalation).

3. Clinical considerations

3.1. Applications to physical and manual therapies?

A previous study analyzed CVJ in rabbits and cats using microscopy aiming to verify the existence of mechano-receptors in such a joint and trying to characterize their responses to rib movement. They concluded that alike many other arthrodial joints, costovertebral joints contain mechano-receptors, and moreover, their response are influenced by two main factors: rib position and rib movement (Godwin-Austen, 1969). The discharge response was demonstrated to increase with faster movements compared to slower ones. In addition, the same increase in discharge frequency was demonstrated for movement in caudal direction compared to cephalic.

In humans, a comparable analysis was performed to determine if costovertebral joints are able to produce pain (Erwin et al., 2000). The authors analyzed the presence of nociceptive-capable neurons to verify if these joints had the anatomic capabilities to cause pain. They concluded that similarly to spinal facet joints, the costovertebral joints contain specific nociceptive neurons that can cause pain (Erwin et al., 2000). Literature reports also that costovertebral joints could be the origin of misdiagnose chest pain (Arroyo et al., 1992), and could be sometimes related to rheumatologic disorders (Pascual et al., 1992; Sales et al., 2007), in which treatment consists partly in physical and manual therapies in order to reduce pain and improve joints mobility.

The new insights on costovertebral and sternocostal joints kinematics during breathing movement are of interest in understanding the evaluation of symmetry and ranges of motion during manual testing and manual therapeutic procedures. Indeed, thorax displacement evaluation is commonly used in the examination of the thorax in patients with back pain or with respiratory diseases (Tuteur, 1990; White et al., 2013). At a regional or local level, rib evaluation in breathing is based on the feeling of displacement restriction. As an example, some authors report to evaluate rib cage following a “triad of asymmetry, altered range of motion, and tissue texture abnormality” (DeStefano, 2011; Lee, 2015).

The present doctoral thesis adds quantification parameters that could lead to a better understanding and estimation of this specific respiratory motion. Since one of the goal in manual therapies is to estimate joint limitation, and to use various manual approaches (stretching, trigger points, joint mobilization with or without high velocity thrusts, figure 5) to restore “normal” joint mechanics, it seemed important to answer a simple question: What is the “normal” range of rib motion in breathing manoeuver? The present kinematic results enable for the first time to describe both qualitatively and

quantitatively the CVJs. Further work should investigate the relation between a loss of mobility (global, regional or at a single rib level) perceived by the practitioner and the quantitative estimation of such a limitation to validate clinical testing.

Symmetry evaluation in breathing:

The laterality had significant influence neither on ROMs nor on MHA orientations, whatever the rib level considered. However, as mentioned in the discussion, small orientation variations could have been related to anatomical variations of the joint facets. Therefore, this has to be considered when evaluating symmetry at a specific rib level. One could not estimate whether the asymmetry should be considered as "normal" or as a "restriction" when only considering movement orientation.
When rib motion is evaluated relative to the laterality (e.g. 7^{th} right rib relative to 7^{th} left rib), one should keep in mind the axes of motion as presented in figure 6.

Figure 5: Example of various techniques used in manual therapies. Left: Diaphragmatic release technic; Middle: rib mobilization in supine position; Right: Costovertebral joint mobilization or manipulation.

Rib displacement evaluation in breathing:

Considering ROMs, the displacement of the ribs occurred mainly below the middle of inspiratory capacity; therefore, ballistic displacement could be estimated without asking a full deep inspiration. When considering the orientation of the axes of rib rotation relative to the vertebra of same level (i.e. MHAs in our studies), one should consider that rib excursion will be maximized at the rib part further away from the rotation axis, due to rib shape. While the axes were oriented obliquely between the frontal and sagittal planes, the greatest rib excursion should be perceived between the mid-clavicular and the anterior axillary lines.

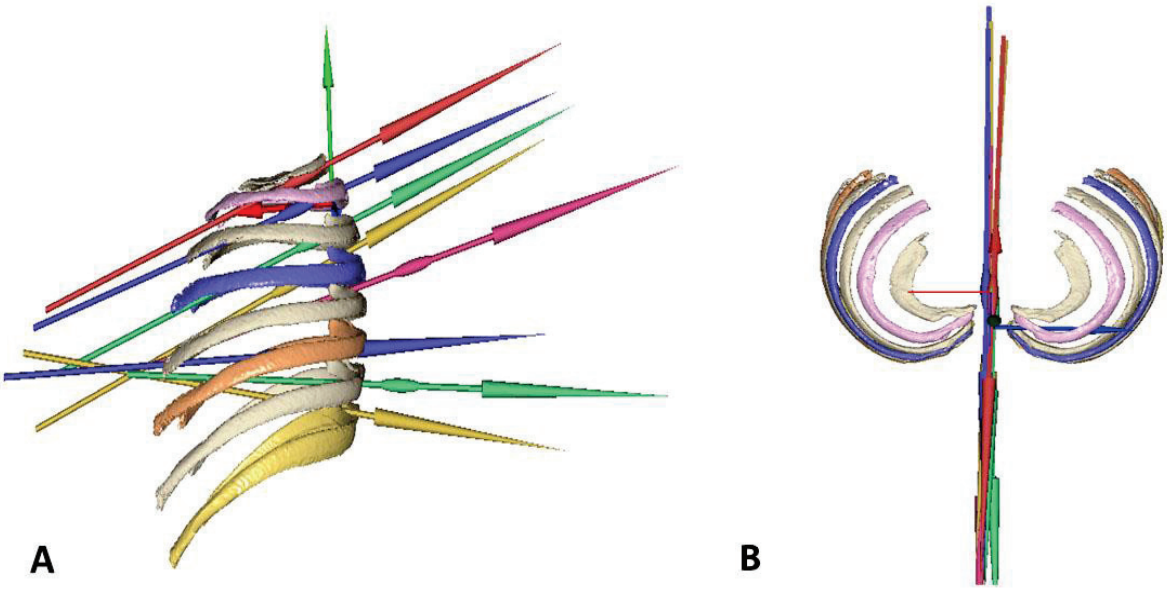

Figure 6: Mean helical axes estimated from the motion of right ribs relative to the left ones at levels 1 to 8 in sagittal (A) and transverse (B) planes. Note that MHAs orientation in sagittal plane (A) are following the orientation of vertebral endplates and thoracic kyphosis. The uppermost axis is pointing obliquely forward and downward and this orientation becomes gradually closer to the horizontal in lower levels.

Orientation of the axes of motion: relevant for reappraising manual techniques?

Manual approaches request from therapists to apply forces usually through their hands on some regions of the patient anatomy in order to obtain some therapeutical effects (see figure 5 for examples of manual approaches of the rib cage). The knowledge of the underlying joint mechanism is of importance to understand the real intra-articular effect of the applied force.

The findings concerning MHA orientation can be useful for a reappraisal of manual techniques applied to the ribs. Indeed, for example, when a force is applied on a rib for mobilizing a CVJ in rotation, the farther from the MHA the force is applied by the practitioner, the larger will be the lever arm (i.e. the orthogonal distance between the MHA and the line of action of the force generated by the practitioner's hand). Depending on the goal reached by the therapist and the patient's symptoms, the knowledge of these axes of motion is of interest to better adapt manual techniques. As an example, for a given force applied by the therapist, positioning the hand close to the anterior end of the rib (at costochondral junction) will exert an important torque at CVJ when, on the other hand, force applied close to the rib posterior tubercle in direction of the rib head would produce a smaller torque since the force vector will tend to be aligned and close to the CVJ axis of motion.

Example related to "muscle energy techniques" and stretching:

Another manual approach frequently used to relieve pain in various anatomical regions is called "muscle energy techniques" (Mitchell and Mitchell, 2001; Selkow et al., 2009) in which the concept is to mobilize a joint by use of muscle contraction and an imposed fixed segment of the joint. The knowledge of the axis of rib motion in breathing enables to consider the effect of respiratory movement on various muscles lever arm.

To emphasize this aspect, a trial was done on the datasets of one subject in whom an entire cervical spine was scaled and registered to fit with the first thoracic vertebra. Anatomical landmarks were placed on the 3D models at the insertion sites of the anterior scalenus muscle (on the anterior tubercles of the transverse process of the cervical vertebrae C2 to C4; on the tubercle of the first rib). Then, moment arms were computed as the shortest distance from the muscle action lines to the MHA obtained at the first CVJ. The 3D model and moment arm variations during breathing are shown in figure 7.

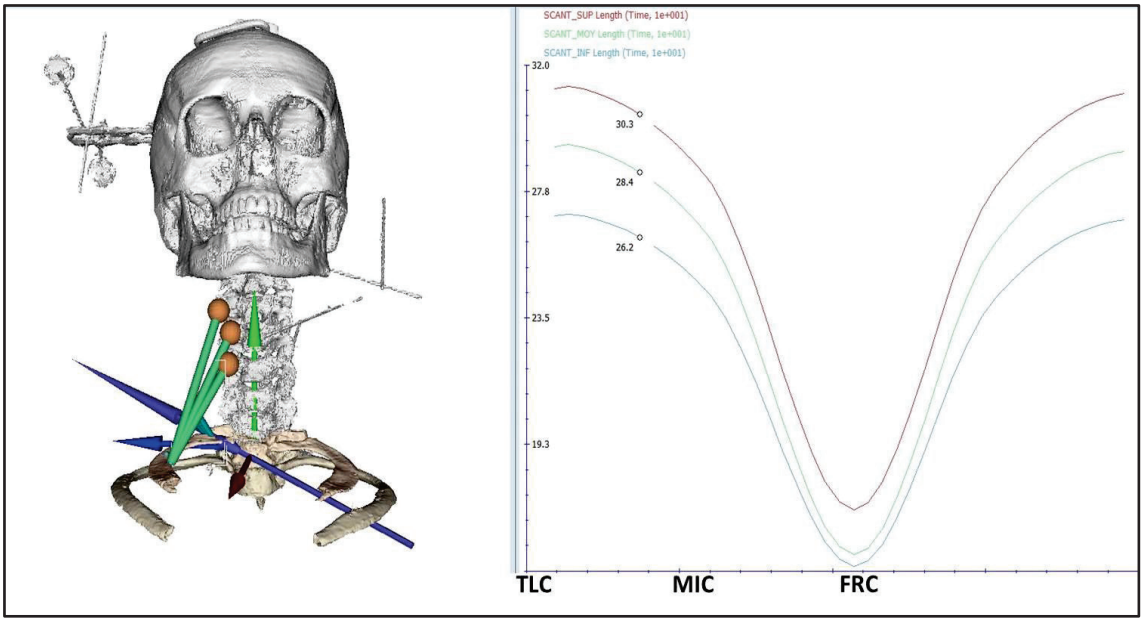

Figure 7: Left: 3D model of a « generic » cervical spine and the first two costovertebral joints. The MHA of the right first CVJ is displayed in blue and was used to compute lever arms of the anterior scalenus muscle. Right: lever arm obtained for each fascicle of the anterior scalenus muscle

The moment arm decreases with the lung volume (see right part of figure 7); and in the same time muscle length increases. If the goal is to stretch the muscle, then exhalation is to be recommended since muscle length is maximal at FRC. If the goal is to mobilize the first rib at CVJ1 through the action of the anterior scalenus muscle, both length and moment arm should be taken into account to maximize force and torque generated at the CVJ. Therefore, further work should determine the length/moment arm ratio as a function of lung volume.

4. Perspectives

Beside the above-mentioned clinical applications, results of this thesis may lead to various new research tracks. Some of these topics have been already prospected and are presented in this section. It shows that the thesis results are relevant for the futur and that more effort should be invested to improve further our knowledge on the thorax kinematics.

4.1. Modelling

The kinematic results obtained at each joint of the thorax could be useful to improve modelling of the breathing thorax that could integrate joint kinematics, dynamics, and muscle activity, in both normal and pathological conditions. It represents also sustantial data to create or validate models of the thorax.

Starting from the kinematic results obtained during the present work, we developed a simplistic kinematic model as following.

Three assumptions were considered, although they are known to simplify the physiologic reality: the symmetry between right and left sides; non-deformability of the sternum; non-deformability of the costal cartilage. The objective of this model is to allow simplified representation of the thorax movement in breathing, and to estimate the impact of various parameters alteration (such as orientation of the MHA, ranges of motion, rib geometry) on the global kinematics of the thorax. Furthermore, the model gives the opportunity to verify that thorax movement in breathing (in the context of the previous assumptions) could have been determined from only one degree of freedom.

Firstly, the origin of a referential system was defined at the intersection between MHA of the right and left seventh ribs, close to the vertebral body of Th7. The axes of this thorax coordinate system were oriented as follows, X_0-axis to the front, Y_0-axis vertically to the top and Z_0-axis laterally to the right (see figure 8).

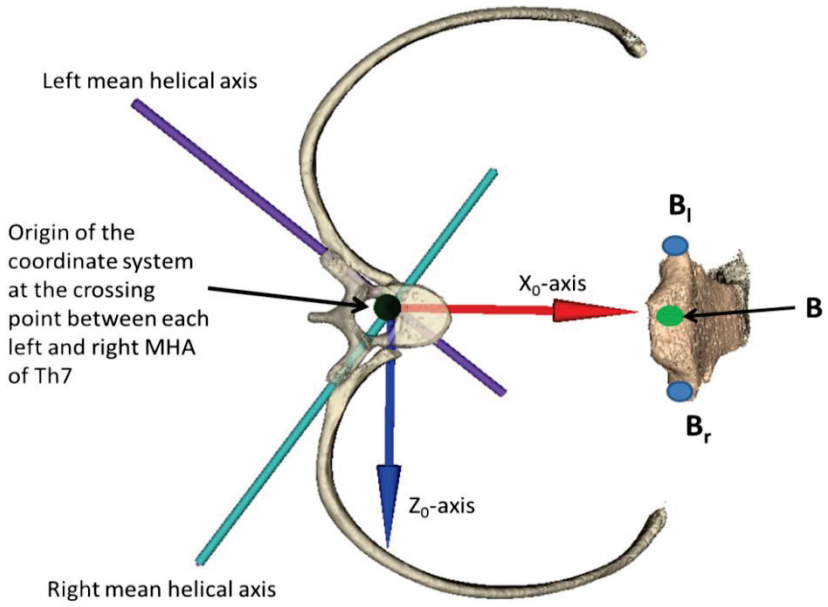

Figure 8: Illustration of the referential coordinate system defined for the kinematic model. Axes in blue and purple correspond to the MHA of the right and left 7th CVJ respectively. B corresponds to midpoint between B_r and B_l. B_r and B_l correspond to sternal attachment of the 7th costal cartilage considered as the rib anterior extremity.

The spine was also considered rigid as a first attempt but could be later considered with an additional degree of freedom. Each costovertebral joint was defined as a Cardan joint (i.e. two hinges oriented at 90° to each other), with the possibility to define the orientation of the first axis as a constant parameter (i.e. α in figure 9A). To be consistent with a unique rotation about the MHA, the angular parameter around this first axis of the cardan, β, is dependent on the angular parameter around the second axis θ. The relation between both parameters is computed from an analytical equation expressing the symmetry of the mechanism, i.e. the velocity of point B is assumed null on the Zo axis. Note that the anterior extremity of the rib is considered rigidly attached to the sternum through the non-deformable costal cartilage as a single spherical joint (in Br).

To test the model, the orientation of Z-axis of the ribs (Zr, coinciding with the MHA direction) were defined from data measured on one subject of the present thesis. Only the right rib is described thereafter (see figure 9A) since geometry is considered following right/left symmetry.

Geometrical parameters of the ribs (ar, dr and Xr) are defined, on the same subject, through the anterior extremity of the rib at the point B considered at sternal attachment (B_r for right rib in figure 8). As it is a first attempt, only 2 levels were implemented, Th1 and Th7.

Then, using an optimization algorithm to consider the non-deformability of the sternum (i.e. fixed distances between the four points Br, Br', Bl and Bl'), it is possible to compute the value of Θ_7 as a function of Θ_1 at each instant of time.

As an example, when parametrizing the model from data of one subject of the present thesis, (i.e. with $\alpha 1 = \alpha 7 = -10°$; initial values of $\beta 1 = \beta 7 = -3°$ since the orientation of MHA was demonstrated to be similar between each rib level; and initial values of $\Theta_1 = 34°$ and $\Theta_2 = 14°$) the model obtained a vertical displacement of the sternum (i.e. along Y_o-axis) of 25.6 mm. The measured sternum displacement in Th7 (reported in Chapter 6) for this specific subject was equal to 28.5 mm which is close to the predicted one.

As mentioned above, note that this result should be only considered as an interesting starting point to further develop a more sophisticated model. This model could be further modified, for example without following the assumption of symmetry. Then, it could lead to estimate the impact of asymmetry of motion at a single rib level on the behavior of the entire thorax during breathing. In medicine and manual therapies, the examination of the thorax contains the evaluation of symmetry of motion; furthermore, in manual therapies, joint kinematics is a basis knowledge for evaluating ranges of motion, stiffness, symmetry that could be related to specific pathological conditions.

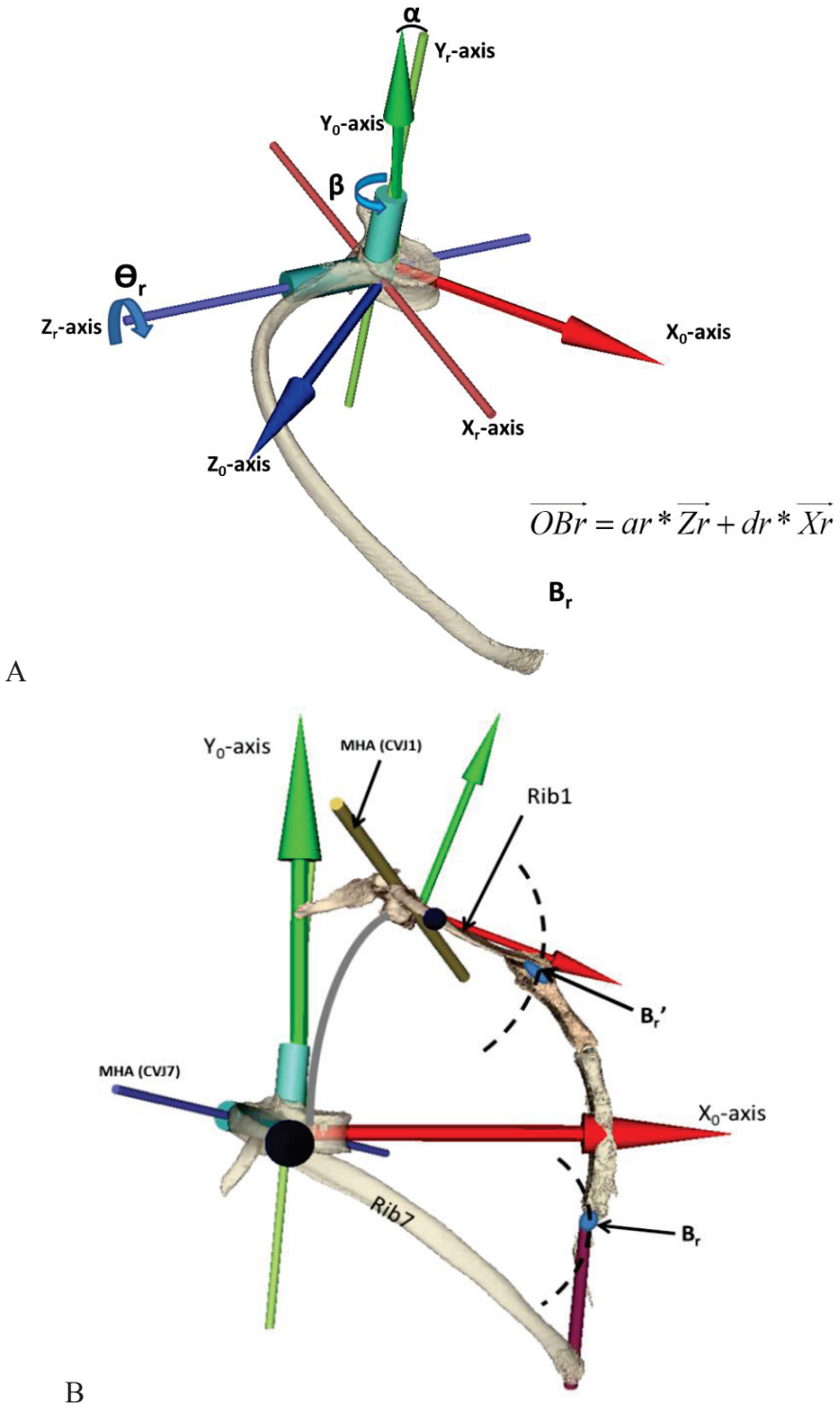

Figure 9: A: Illustration of the cardan joint defined from the Mean helical axis obtained at the CVJ of the right 7th rib.
B: Model containing Th7, Th1, rib1, rib7 and sternum. The spine is considered rigid (grey line between th1 and Th7). B_r and B'_r represent the anterior extremity of the rib (respectively 7 and 1) connected to the sternum.

4.2. Influence of other pathological conditions and surgical procedures on thorax joint kinematics

The present work focused on the influence of a respiratory condition; further analysis should concentrate on the influence of musculoskeletal or neurologic disorder on kinematic parameters. The present methodology could be proposed to evaluate these questions. The development of imaging techniques should maybe give the future opportunity to reduce dramatically irradiation dose. In addition, many 4D imaging techniques are presently under development such as 4D computed tomography, or dynamic radiography to estimate thorax respiratory displacement (Brandner et al., 2006; Rit et al., 2005; Saadé et al., 2012; Tanaka et al., 2015). The present computational method that processes segmental kinematics from a set of 5 ALs on each structure of interest could be implemented in a protocol of discrete pose imaging. This could lead to obtain quantitative data in many other clinical conditions and moreover to study the effect of therapeutic procedures, such as rib mobilization, or spinal manipulation on kinematic parameters.

In addition, the influence of various surgical procedures on the breathing kinematics of the thorax could be estimated using the present protocol. Rib cage mechanics was shown to be altered after media sternotomy, leading to a post-op restrictive ventilatory defect (Locke et al., 1990). It was also reported that pulmonary complications after thoracotomy are frequent and that risk level should be estimated before surgery. In scoliosis, various surgical procedures are described depending on the severity of the curvature misalignment. The severity of the curve will depend on different variables such as type and location of the defect, number of malformed/healthy vertebra or potential growth of the patient (Piantoni et al., 2015), as will the therapeutic decision. The methods developed in our work could serve as a basis for the design of surgical planning and follow-up methods that could improve patient care.

4.3. Relation between CVJ kinematics, rib geometry and thorax shape

The present thesis focuses on analyzing thorax joint kinematics however the relation between joint kinematics and thorax shape was not reported. Many studies focused on external measurements of the thorax in breathing conditions (Causey, 1953; Konno and Mead, 1967; White et al., 2013). Also the influence of posture on thoracic shape is well documented (Estenne et al., 1985; Lee et al., 2010; Romei et al., 2010; Verschakelen and Demedts, 1995). However, the relation between thoracic shape measurement and joint kinematics was never assessed. From the present CT database, we developed a protocol to obtain anteroposterior and lateral diameters of the thorax (Beyer et al., 2015b). Further analysis is currently running.

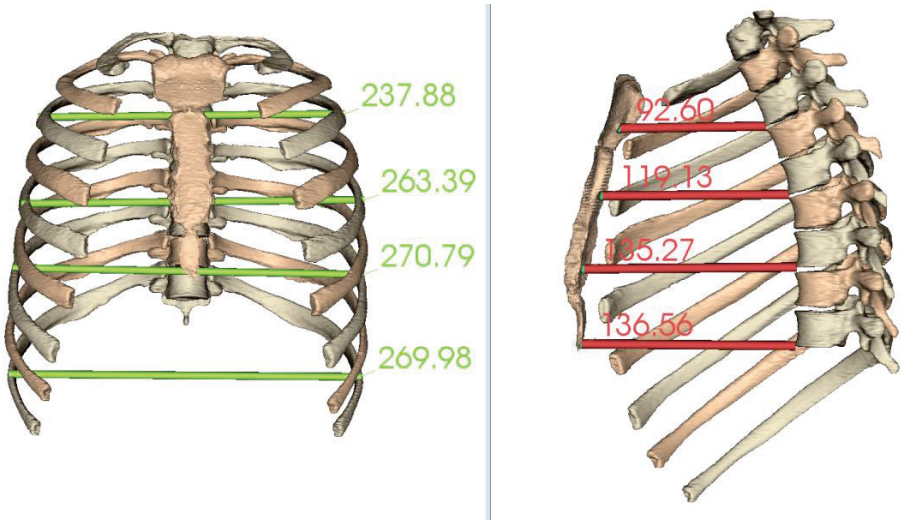

Figure 10: Thorax models obtained to compute anteroposterior and lateral diameters at four different thoracic levels. (See supplementary material CHAP_7_1)

In addition, it was anticipated that rib shape could have been related to regional changes in thoracic shape that contribute to level specific lung volume displacements. Therefore, a method was developed to determine rib geometrical parameters from rib 3D reconstructions. Various geometrical parameters (such as arc length, chord length, rib width, rib bending, torsion, etc.) were computed (see figure 11) following a previously published method (Dansereau and Stokes, 1988; Kindig and Kent, 2013). Results were obtained (Beyer et al., 2015a) but still have to be related to kinematic results. An interesting issue will be to quantify regional volume change of the thoracic cage according to specific rib geometry combined with kinematic parameters. Note that results obtained using this method were used in paleoanthropology to compare ribs of Neanderthals to those of modern human adults. (Chapman & Beyer et al, submitted, 2016).

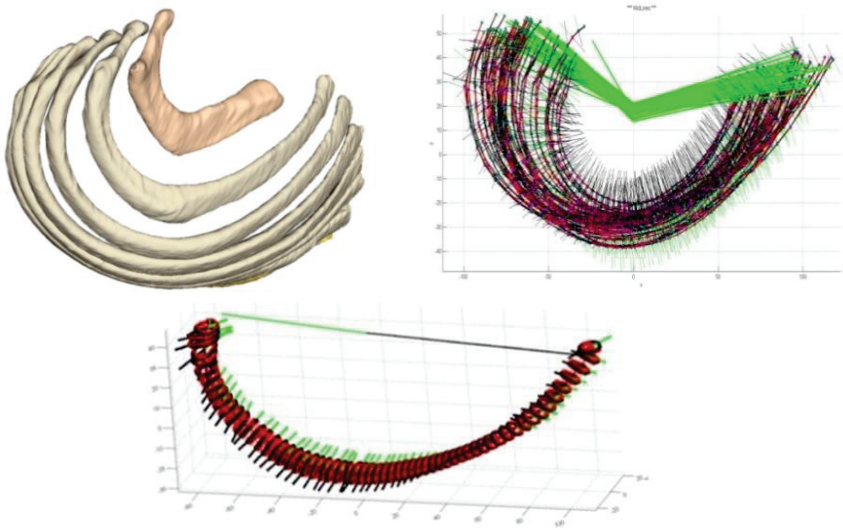

Figure 11: Top: 3D model of the ribs (left) and representation of the "rib-midlines" (right) obtained from the centroid of each rib section. The green line represents the bending angle along the body of the ribs. Bottom: Representation of each rib "slice" and their ellipse long semi-axes.

It must be emphasized that rib and thoracic shape could have been influenced by sex in both normal subjects (Bellemare et al., 2003) and patients with chronic lung hyperinflation (Bellemare and Jeanneret, 2007). Due to the size of the sample, this parameter was not tested and will be estimated in future work. As an example, see in Figure 12 the possible differences in thoracic shape of two males and two females.

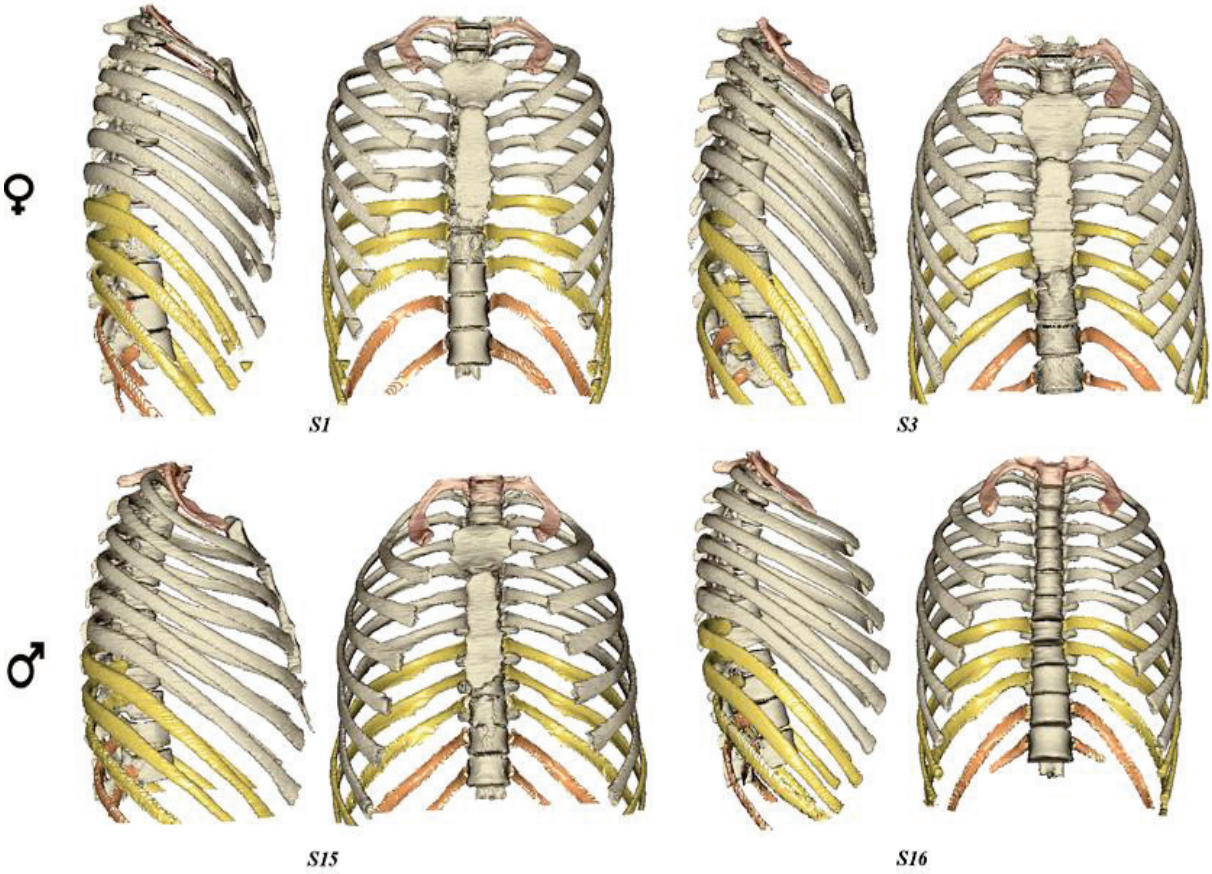

Figure 12: Examples of thoracic shape in 2 males and 2 females. Reconstructions are displayed in both sagittal and frontal plane for 2 males and 2 females at functional residual capacity.

4.4. Integration of muscle parameters in the thorax model

The present thesis focused on joint kinematics; however, the breathing mechanism is obtained from a combination of joint displacement exerted by muscle activation and contraction. As the diaphragm is considered as the main respiratory muscle, we are currently working on the same imaging dataset in order to quantify the displacement and shape change of the diaphragmatic domes in relation with the lung volume variations. A quick overview of the method is presented in figure 13.

A series of anatomical landmarks were set on the inferior aspect of the reconstructed lungs at each breathing pose. Then, Delaunay triangulation is computed for right and left diaphragmatic domes (RDD and LDD respectively in figure 13). From the 3D surfaces obtained, it is possible to compute the volume contained between 2 successive surfaces. As results, the kinematics and the volume displaced by the diaphragmatic domes can be obtained and further related to rib kinematics. (See supplementary material CHAP_7_2).

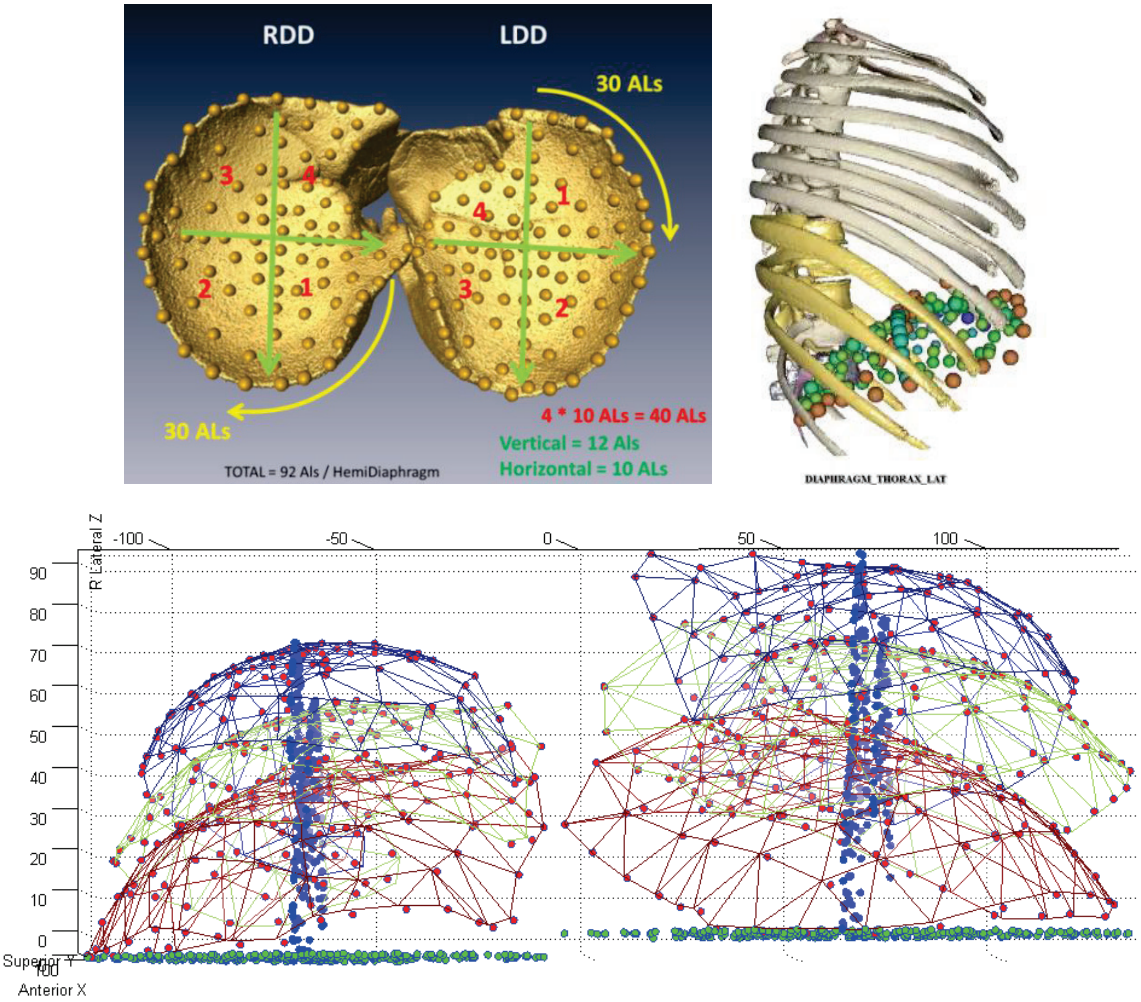

Figure 13: Top: Representation of the anatomical landmarks (Left) placed on the inferior part of the reconstructed lungs.3D model from the entire thorax and the anatomical landmarks of the diaphragmatic domes (Right). Bottom: Representation of the Delaunay's surfaces obtained from the diaphragmatic domes anatomical landmarks at each breathing pose (red: total lung capacity; green middle of the inspiratory capacity; blue: functional residual capacity).

Note that the relation between rib and diaphragm kinematics is of clinical interest and was largely studied from radiographic images (Bellemare et al., 2001), CT (Gauthier et al., 1994; Ladjal et al., 2013; Pettiaux et al., 1997; Saadé et al., 2012) or MRI (Cluzel et al., 2000) imaging techniques. While physiological aspects are to date deeply analyzed (Breslin et al., 1990; De Troyer, 2012; De Troyer et al., 2005a; Hodges and Gandevia, 2000), literature concerning the influence of manual approaches on diaphragm and thorax kinematics is still scarce especially considering physical and manual therapeutic procedures applied in patients with lung or neurologic disorders. As an example, a recent study describes the effect of a "diaphragmatic release technique" on inspiratory capacity and diaphragmatic dome displacement in patients with COPD (Rocha et al., 2015).

4.5. Integration into multiscale modelling of the respiratory system

A modern perspective related to modelling of the human physiology appeared in the last decade with emerging new technologies. The Virtual physiological human project (Viceconti et al., 2008) has for objective to elaborate multi-scales models to answer the need of integration of various field related to health (i.e. physiology, anatomy, systems biology, biomedical informatics etc…) (Hunter et al., 2010). This project has for perspective to develop integrated models across dimension scales, e.g. from the cells, to tissues, to the organs, and to clinical applications. The present work focuses on musculo-skeletal aspects of the respiratory mechanics, however various teams have already developed models such as for lung parenchyma (Denny and Schroter, 2006), circulatory flow in the pulmonary capillaries (Burrowes et al., 2004; Burrowes and Tawhai, 2006; Nabors et al., 2003). All these development could be integrated together to reach the goal of a multi-scale, multi-physics modelling of the entire respiratory system (Burrowes et al., 2008).

5. Conclusion

The present doctoral thesis contributes to the quantitative and qualitative description of costovertebral and sternocostal joints during breathing movement. The determination of ranges of motion and axes of rib rotation in breathing conditions was achieved as well as their relation with lung volume. In addition, the possible alteration of such kinematic parameters was demonstrated from the analysis of the results obtained in patients with cystic fibrosis. The 3D modelling approach developed along the present work allows subject specific and anatomical representation, and could be useful for pedagogical use in various health disciplines. Results obtained in the present work represent a substantial basis for modelling the breathing thorax from various approaches. Further work will concentrate on establishing relation between thorax kinematics and respiratory muscle parameters (e.g. shape, kinematics, activation …).

6. References

Arroyo, J.F., Jolliet, P., Junod, A.F., 1992. Costovertebral joint dysfunction: another misdiagnosed cause of atypical chest pain. Postgrad Med J 68, 655–659.

Bellemare, F., Couture, J., Cordeau, M.P., Leblanc, P., Lafontaine, E., 2001. Anatomic landmarks to estimate the length of the diaphragm from chest radiographs: effects of emphysema and lung volume reduction surgery. Chest 120, 444–452.

Bellemare, F., Fuamba, T., Bourgeault, A., 2006. Sexual dimorphism of human ribs. Respir Physiol Neurobiol 150, 233–239. doi:10.1016/j.resp.2005.04.002

Bellemare, F., Jeanneret, A., 2007. Sex differences in thoracic adaptation to pulmonary hyperinflation in cystic fibrosis. Eur. Respir. J. 29, 98–107. doi:10.1183/09031936.00045606

Bellemare, F., Jeanneret, A., Couture, J., 2003. Sex differences in thoracic dimensions and configuration. Am. J. Respir. Crit. Care Med. 168, 305–312. doi:10.1164/rccm.200208-876OC

Beyer, B., Chapman, T., Sholukha, V., Semal, P., Feipel, V., Louryan, S., Van Sint Jan, S., 2015a. Géométrie et morphométrie des côtes : de Kebara 2 à l'humain moderne. Morphologie, 97e Congrès de l'Association des morphologistes, Bruxelles 29-31 janvier 2015 99, 96. doi:10.1016/j.morpho.2015.07.062

Beyer, B., Feipel, V., Sholukha, V., Salvia, P., Rooze, M., Van Sint Jan, S., 2015b. Modélisation 3D du thorax durant le mouvement respiratoire : analyse cinématique et géométrique. Morphologie, 97e Congrès de l'Association des morphologistes, Bruxelles 29-31 janvier 2015 99, 83. doi:10.1016/j.morpho.2015.07.030

Beyer, B., Van Sint Jan, S., Chèze, L., Sholukha, V., Feipel, V., 2016. Relationship between costovertebral joint kinematics and lung volume in supine humans. Respir Physiol Neurobiol 232, 57–65. doi:10.1016/j.resp.2016.07.003

Brandner, E.D., Wu, A., Chen, H., Heron, D., Kalnicki, S., Komanduri, K., Gerszten, K., Burton, S., Ahmed, I., Shou, Z., 2006. Abdominal organ motion measured using 4D CT. Int. J. Radiat. Oncol. Biol. Phys. 65, 554–560. doi:10.1016/j.ijrobp.2005.12.042

Breslin, E.H., Garoutte, B.C., Kohlman-Carrieri, V., Celli, B.R., 1990. COrrelations between dyspnea, diaphragm and sternomastoid recruitment during inspiratory resistance breathing in normal subjects. Chest 98, 298–302. doi:10.1378/chest.98.2.298

Burrowes, K.S., Swan, A.J., Warren, N.J., Tawhai, M.H., 2008. Towards a virtual lung: multi-scale, multi-physics modelling of the pulmonary system. Philos Trans A Math Phys Eng Sci 366, 3247–3263. doi:10.1098/rsta.2008.0073

Burrowes, K.S., Tawhai, M.H., 2006. Computational predictions of pulmonary blood flow gradients: gravity versus structure. Respir Physiol Neurobiol 154, 515–523. doi:10.1016/j.resp.2005.11.007

Burrowes, K.S., Tawhai, M.H., Hunter, P.J., 2004. Modeling RBC and neutrophil distribution through an anatomically based pulmonary capillary network. Ann Biomed Eng 32, 585–595.

Causey, G., 1953. The Anatomy of the Thorax in Relation to the Flow of Tidal Air. Ann R Coll Surg Engl 13, 127–135.

Cluzel, P., Similowski, T., Chartrand-Lefebvre, C., Zelter, M., Derenne, J.-P., Grenier, P.A., 2000. Diaphragm and Chest Wall: Assessment of the Inspiratory Pump with MR Imaging—Preliminary Observations1. Radiology 215, 574–583.

Dansereau, J., Stokes, I.A., 1988. Measurements of the three-dimensional shape of the rib cage. J Biomech 21, 893–901.

de Lange, A., Huiskes, R., Kauer, J.M., 1990. Effects of data smoothing on the reconstruction of helical axis parameters in human joint kinematics. J Biomech Eng 112, 107–113.

De Troyer, A., 2012. Respiratory effect of the lower rib displacement produced by the diaphragm. J. Appl. Physiol. 112, 529–534. doi:10.1152/japplphysiol.01067.2011

De Troyer, A., Cappello, M., Scillia, P., 2005a. Effect of inflation on the interaction between the left and right hemidiaphragms. J Appl Physiol 99, 1301–1307. doi:10.1152/japplphysiol.00192.2005

De Troyer, A., Estenne, M., Vincken, W., 1986. Rib cage motion and muscle use in high tetraplegics. Am. Rev. Respir. Dis. 133, 1115–1119.

De Troyer, A., Kirkwood, P.A., Wilson, T.A., 2005b. Respiratory Action of the Intercostal Muscles. Physiological Reviews 85, 717–756. doi:10.1152/physrev.00007.2004

Denny, E., Schroter, R.C., 2006. A model of non-uniform lung parenchyma distortion. J Biomech 39, 652–663. doi:10.1016/j.jbiomech.2005.01.010

DeStefano, L.A., 2011. Greenman's Principles of Manual Medicine. Lippincott Williams & Wilkins.

Erwin, W.M., Jackson, P.C., Homonko, D.A., 2000. Innervation of the human costovertebral joint: implications for clinical back pain syndromes. J Manipulative Physiol Ther 23, 395–403. doi:10.1067/mmt.2000.108144

Estenne, M., Yernault, J.C., De Troyer, A., 1985. Rib cage and diaphragm-abdomen compliance in humans: effects of age and posture. J. Appl. Physiol. 59, 1842–1848.

Gauthier, A.P., Verbanck, S., Estenne, M., Segebarth, C., Macklem, P.T., Paiva, M., 1994. Three-dimensional reconstruction of the in vivo human diaphragm shape at different lung volumes. J. Appl. Physiol. 76, 495–506.

Gayzik, F.S., Yu, M.M., Danelson, K.A., Slice, D.E., Stitzel, J.D., 2008. Quantification of age-related shape change of the human rib cage through geometric morphometrics. Journal of Biomechanics 41, 1545–1554. doi:10.1016/j.jbiomech.2008.02.006

Godwin-Austen, R.B., 1969. The mechanoreceptors of the costo-vertebral joints. J. Physiol. (Lond.) 202, 737–753.

Hodges, P.W., Gandevia, S.C., 2000. Activation of the human diaphragm during a repetitive postural task. J Physiol 522, 165–175. doi:10.1111/j.1469-7793.2000.t01-1-00165.xm

Hunter, P., Coveney, P.V., de Bono, B., Diaz, V., Fenner, J., Frangi, A.F., Harris, P., Hose, R., Kohl, P., Lawford, P., McCormack, K., Mendes, M., Omholt, S., Quarteroni, A., Skår, J., Tegner, J., Randall Thomas, S., Tollis, I., Tsamardinos, I., van Beek, J.H.G.M., Viceconti, M., 2010. A vision and strategy for the virtual physiological human in 2010 and beyond. Philos Trans A Math Phys Eng Sci 368, 2595–2614. doi:10.1098/rsta.2010.0048

Jordanoglou, J., 1970. Vector analysis of rib movement. Respir Physiol 10, 109–120.

Jordanoglou, J., Smith, L., 1970. A new instrument for measuring rib movement. J Appl Physiol 28, 501–504.

Kent, R., Lee, S.-H., Darvish, K., Wang, S., Poster, C.S., Lange, A.W., Brede, C., Lange, D., Matsuoka, F., 2005. Structural and material changes in the aging thorax and their role in crash protection for older occupants. Stapp Car Crash J 49, 231–249.

Kindig, M.W., Kent, R.W., 2013. Characterization of the Centroidal Geometry of Human Ribs. J Biomech Eng 135, 111007–111007. doi:10.1115/1.4025329

Konno, K., Mead, J., 1967. Measurement of the separate volume changes of rib cage and abdomen during breathing. J Appl Physiol 22, 407–422.

Ladjal, H., Saade, J., Beuve, M., Azencot, J., Moreau, J.-M., Shariat, B., 2013. 3D Biomechanical Modeling of the Human Diaphragm Based on CT Scan Images, in: Long, M. (Ed.), World Congress on Medical Physics and Biomedical Engineering May 26-31, 2012, Beijing, China, IFMBE Proceedings. Springer Berlin Heidelberg, pp. 2188–2191.

Laville, A., Laporte, S., Skalli, W., 2009. Parametric and subject-specific finite element modelling of the lower cervical spine. Influence of geometrical parameters on the motion patterns. Journal of Biomechanics 42, 1409–1415. doi:10.1016/j.jbiomech.2009.04.007

Lee, D.G., 2015. Biomechanics of the thorax – research evidence and clinical expertise. J Man Manip Ther 23, 128–138.

Lee, L.-J., Chang, A.T., Coppieters, M.W., Hodges, P.W., 2010. Changes in sitting posture induce multiplanar changes in chest wall shape and motion with breathing. Respiratory Physiology & Neurobiology 170, 236–245. doi:10.1016/j.resp.2010.01.001

Locke, T.J., Griffiths, T.L., Mould, H., Gibson, G.J., 1990. Rib cage mechanics after median sternotomy. Thorax 45, 465–468.

Masharawi, Y., Rothschild, B., Dar, G., Peleg, S., Robinson, D., Been, E., Hershkovitz, I., 2004. Facet orientation in the thoracolumbar spine: three-dimensional anatomic and biomechanical analysis. Spine 29, 1755–1763.

Mitchell, F.L., Mitchell, P.K.G., 2001. The Muscle Energy Manual. MET Press.

Nabors, L.K., Baumgartner, W.A., Janke, S.J., Rose, J.R., Wagner, W.W., Capen, R.L., 2003. Red blood cell orientation in pulmonary capillaries and its effect on gas diffusion. J. Appl. Physiol. 94, 1634–1640. doi:10.1152/japplphysiol.01021.2001

Pal, G.P., Routal, R.V., Saggu, S.K., 2001. The orientation of the articular facets of the zygapophyseal joints at the cervical and upper thoracic region. J Anat 198, 431–441. doi:10.1046/j.1469-7580.2001.19840431.x

Pascual, E., Castellano, J.A., López, E., 1992. Costovertebral joint changes in ankylosing spondylitis with thoracic pain. Br. J. Rheumatol. 31, 413–415.

Pettiaux, N., Cassart, M., Paiva, M., Estenne, M., 1997. Three-dimensional reconstruction of human diaphragm with the use of spiral computed tomography. J. Appl. Physiol. 82, 998–1002.

Piantoni, L., Francheri Wilson, I.A., Tello, C.A., Noel, M.A., Galaretto, E., Remondino, R.G., Bersusky, E.S., 2015. Hemivertebra Resection With Instrumented Fusion by Posterior Approach in Children. Spine Deformity 3, 541–548. doi:10.1016/j.jspd.2015.04.008

Rit, S., Sarrut, D., Ginestet, C., 2005. Respiratory Signal Extraction for 4D CT Imaging of the Thorax from Cone-Beam CT Projections, in: Duncan, J.S., Gerig, G. (Eds.), Medical Image Computing and Computer-Assisted Intervention – MICCAI 2005, Lecture Notes in Computer Science. Springer Berlin Heidelberg, pp. 556–563. doi:10.1007/11566465_69

Rocha, T., Souza, H., Brandão, D.C., Rattes, C., Ribeiro, L., Campos, S.L., Aliverti, A., de Andrade, A.D., 2015. The Manual Diaphragm Release Technique improves diaphragmatic mobility, inspiratory capacity and exercise capacity in people with chronic obstructive pulmonary disease: a randomised trial. J Physiother 61, 182–189. doi:10.1016/j.jphys.2015.08.009

Romei, M., Mauro, A.L., D'Angelo, M.G., Turconi, A.C., Bresolin, N., Pedotti, A., Aliverti, A., 2010. Effects of gender and posture on thoraco-abdominal kinematics during quiet breathing in healthy adults. Respiratory Physiology & Neurobiology 172, 184–191. doi:10.1016/j.resp.2010.05.018

Rose J, Gamble J, Schultz A, Lewiston N, 1987. BAck pain and spinal deformity in cystic fibrosis. Am J Dis Child 141, 1313–1316. doi:10.1001/archpedi.1987.04460120079039

Saadé, J., Ladjal, H., Behzad, S., Beuve, M., Azencot, J., 2012. Modélisation biomécanique du diaphragme humain : du CT-4D au modèle du mouvement, in: Actes de La Conférence RFIA 2012. Presented at the RFIA 2012 (Reconnaissance des Formes et Intelligence Artificielle).

Sales, J.R., Beals, R.K., Hart, R.A., 2007. Osteoarthritis of the costovertebral joints: the results of resection arthroplasty. J Bone Joint Surg Br 89–B, 1336–1339. doi:10.1302/0301-620X.89B10.19721

Saumarez, R.C., 1986. An analysis of possible movements of human upper rib cage. J Appl Physiol 60, 678–689.

Schwartz, C., Leboeuf, F., Rémy-Néris, O., Brochard, S., Lempereur, M., Burdin, V., 2013. Detection of incoherent joint state due to inaccurate bone motion estimation. Computer Methods in Biomechanics and Biomedical Engineering 16, 165–174. doi:10.1080/10255842.2011.613379

Selkow, N.M., Grindstaff, T.L., Cross, K.M., Pugh, K., Hertel, J., Saliba, S., 2009. Short-Term Effect of Muscle Energy Technique on Pain in Individuals with Non-Specific Lumbopelvic Pain: A Pilot Study. J Man Manip Ther 17, E14–E18.

Tanaka, R., Sanada, S., Sakuta, K., Kawashima, H., 2015. Quantitative analysis of rib kinematics based on dynamic chest bone images: preliminary results. J Med Imaging (Bellingham) 2, 024002. doi:10.1117/1.JMI.2.2.024002

Tattersall, R., Walshaw, M.J., 2003. Posture and cystic fibrosis. J R Soc Med 96, 18–22.

Tuteur, P.G., 1990. Chest Examination, in: Walker, H.K., Hall, W.D., Hurst, J.W. (Eds.), Clinical Methods: The History, Physical, and Laboratory Examinations. Butterworths, Boston.

Van Sint Jan, S., Wermenbol, V., Van Bogaert, P., Desloovere, K., Degelaen, M., Dan, B., Salvia, P., Ortibus, E., Bonnechère, B., Le Borgne, Y.-A., Bontempi, G., Vansummeren, S., Sholukha, V., Moiseev, F., Rooze, M., 2013. A technological platform for cerebral palsy - The ICT4Rehab project. Médecine/Sciences 29, 529–536. doi:10.1051/medsci/2013295017

Verschakelen, J.A., Demedts, M.G., 1995. Normal thoracoabdominal motions. Influence of sex, age, posture, and breath size. Am J Respir Crit Care Med 151, 399–405. doi:10.1164/ajrccm.151.2.7842198

Viceconti, M., Clapworthy, G., Van Sint Jan, S., 2008. The Virtual Physiological Human - a European initiative for in silico human modelling -. J Physiol Sci 58, 441–446. doi:10.2170/physiolsci.RP009908

Weaver, A.A., Schoell, S.L., Stitzel, J.D., 2014. Morphometric analysis of variation in the ribs with age and sex. J. Anat. 225, 246–261. doi:10.1111/joa.12203

White, B.M., Zhao, T., Lamb, J., Bradley, J.D., Low, D.A., 2013. Quantification of the thorax-to-abdomen breathing ratio for breathing motion modeling. Med Phys 40, 063502. doi:10.1118/1.4805099

Wilson, T.A., De Troyer, A., 2004. The two mechanisms of intercostal muscle action on the lung. J. Appl. Physiol. 96, 483–488. doi:10.1152/japplphysiol.00553.2003

Wilson, T.A., Legrand, A., Gevenois, P.A., De Troyer, A., 2001. Respiratory effects of the external and internal intercostal muscles in humans. J. Physiol. (Lond.) 530, 319–330.

Wilson, T.A., Rehder, K., Krayer, S., Hoffman, E.A., Whitney, C.G., Rodarte, J.R., 1987. Geometry and respiratory displacement of human ribs. J. Appl. Physiol. 62, 1872–1877.

Woltring, H.J., Huiskes, R., de Lange, A., Veldpaus, F.E., 1985. Finite centroid and helical axis estimation from noisy landmark measurements in the study of human joint kinematics. J Biomech 18, 379–389.

General bibliography

Agostoni, E., Hyatt, R.E., 2011. Static Behavior of the Respiratory System, in: Comprehensive Physiology. John Wiley & Sons, Inc.

Agostoni, E., Mognoni, P., Torri, G., Agostoni, A.F., 1965. Static features of the passive rib cage and abdomen-diaphragm. Journal of Applied Physiology 20, 1187–1193.

Aliverti, A., Pedotti, A. (Eds.), 2014. Mechanics of Breathing. Springer Milan, Milano.

Andriacchi, T., Schultz, A., Belytschko, T., Galante, J., 1974. A model for studies of mechanical interactions between the human spine and rib cage. J Biomech 7, 497–507.

Arroyo, J.F., Jolliet, P., Junod, A.F., 1992. Costovertebral joint dysfunction: another misdiagnosed cause of atypical chest pain. Postgrad Med J 68, 655–659.

Bellemare, F., Couture, J., Cordeau, M.P., Leblanc, P., Lafontaine, E., 2001. Anatomic landmarks to estimate the length of the diaphragm from chest radiographs: effects of emphysema and lung volume reduction surgery. Chest 120, 444–452.

Bellemare, F., Fuamba, T., Bourgeault, A., 2006. Sexual dimorphism of human ribs. Respir Physiol Neurobiol 150, 233–239. doi:10.1016/j.resp.2005.04.002

Bellemare, F., Jeanneret, A., 2007. Sex differences in thoracic adaptation to pulmonary hyperinflation in cystic fibrosis. Eur. Respir. J. 29, 98–107. doi:10.1183/09031936.00045606

Bellemare, F., Jeanneret, A., Couture, J., 2003. Sex differences in thoracic dimensions and configuration. Am. J. Respir. Crit. Care Med. 168, 305–312. doi:10.1164/rccm.200208-876OC

Bellemare, J.F., Cordeau, M.P., Leblanc, P., Bellemare, F., 2001. Thoracic dimensions at maximum lung inflation in normal subjects and in patients with obstructive and restrictive lung diseases. Chest 119, 376–386.

Besier, T.F., Sturnieks, D.L., Alderson, J.A., Lloyd, D.G., 2003. Repeatability of gait data using a functional hip joint centre and a mean helical knee axis. J Biomech 36, 1159–1168.

Beyer, B., Chapman, T., Sholukha, V., Semal, P., Feipel, V., Louryan, S., Van Sint Jan, S., 2015a. Géométrie et morphométrie des côtes : de Kebara 2 à l'humain moderne. Morphologie, 97e Congrès de l'Association des morphologistes, Bruxelles 29-31 janvier 2015 99, 96. doi:10.1016/j.morpho.2015.07.062

Beyer, B., Dugailly, P.M., Moiseev, F., Van Sint Jan, S., Sobczak, S., Feipel, V., Salvia, P., Rooze, M., 2011. Kinematics analysis of the costovertebral joint complex. Presented at the XXIIIrd congress of the International Society of Biomechanics, Bruxelles, p. 119.

Beyer, B., Feipel, V., Coupier, J., Snoeck, O., Dugailly, P.M., Van Sint Jan, S., Rooze, M., 2013a. Thorax 3D modelling from costovertebral joint complex kinematics: preliminary results. Presented at the XXIV Congress of the International Society of Biomechanics, Natal, Brazil, p. 185.

Beyer, B., Feipel, V., Rooze, M., Van Sint Jan, S., Dugailly, P.-M., 2013b. In Vivo spinal and costo-spinal kinematics in the respiratory mechanism: A preliminary study on Helical Axis and dynamic 3D anatomical Model. La Revue de l'ostéopathie 10, 29–35.

Beyer, B., Feipel, V., Sholukha, V., Chèze, L., Van Sint Jan, S., 2015a. Relation between rib kinematics and lung volumes: comparison between normal subjects and cystic fibrosis patients, in: Abstract Book. Presented at the XXV congress of the International society of biomechanics, Glasgow, pp. 1164–1165.

Beyer, B., Feipel, V., Sholukha, V., Salvia, P., Rooze, M., Van Sint Jan, S., 2015b. Modélisation 3D du thorax durant le mouvement respiratoire : analyse cinématique et géométrique. Morphologie, 97e Congrès de l'Association des morphologistes, Bruxelles 29-31 janvier 2015 99, 83. doi:10.1016/j.morpho.2015.07.030

Beyer, B., Sholukha, V., Dugailly, P.M., Rooze, M., Moiseev, F., Feipel, V., Van Sint Jan, S., 2014a. In vivo thorax 3D modelling from costovertebral joint complex kinematics. Clin Biomech (Bristol, Avon). doi:10.1016/j.clinbiomech.2014.01.007

Beyer, B., Sholukha, V., Dugailly, P.M., Rooze, M., Moiseev, F., Feipel, V., Van Sint Jan, S., 2014b. In vivo thorax 3D modelling from costovertebral joint complex kinematics. Clin Biomech (Bristol, Avon) 29, 434–438. doi:10.1016/j.clinbiomech.2014.01.007

Beyer, B., Sholukha, V., Salvia, P., Rooze, M., Feipel, V., Van Sint Jan, S., 2015b. Effect of anatomical landmark perturbation on mean helical axis parameters of in vivo upper costovertebral joints. J Biomech 48, 534–538. doi:10.1016/j.jbiomech.2014.12.035

Beyer, B., Van Sint Jan, S., Chèze, L., Sholukha, V., Feipel, V., 2016. Relationship between costovertebral joint kinematics and lung volume in supine humans. Respir Physiol Neurobiol 232, 57–65. doi:10.1016/j.resp.2016.07.003

Bir, C., Viano, D., King, A., 2004. Development of biomechanical response corridors of the thorax to blunt ballistic impacts. J Biomech 37, 73–79.

Botton, E., Saraux, A., Laselve, H., Jousse, S., Le Goff, P., 2003. Musculoskeletal manifestations in cystic fibrosis. Joint Bone Spine 70, 327–335.

Brandner, E.D., Wu, A., Chen, H., Heron, D., Kalnicki, S., Komanduri, K., Gerszten, K., Burton, S., Ahmed, I., Shou, Z., 2006. Abdominal organ motion measured using 4D CT. Int. J. Radiat. Oncol. Biol. Phys. 65, 554–560. doi:10.1016/j.ijrobp.2005.12.042

Breslin, E.H., Garoutte, B.C., Kohlman-Carrieri, V., Celli, B.R., 1990. COrrelations between dyspnea, diaphragm and sternomastoid recruitment during inspiratory resistance breathing in normal subjects. Chest 98, 298–302. doi:10.1378/chest.98.2.298

Bruni, G.I., Gigliotti, F., Scano, G., 2011. Optoelectronic Plethysmography for Measuring Rib Cage Distortion. INTECH Open Access Publisher.

Burrowes, K.S., Swan, A.J., Warren, N.J., Tawhai, M.H., 2008. Towards a virtual lung: multi-scale, multi-physics modelling of the pulmonary system. Philos Trans A Math Phys Eng Sci 366, 3247–3263. doi:10.1098/rsta.2008.0073

Burrowes, K.S., Tawhai, M.H., 2006. Computational predictions of pulmonary blood flow gradients: gravity versus structure. Respir Physiol Neurobiol 154, 515–523. doi:10.1016/j.resp.2005.11.007

Burrowes, K.S., Tawhai, M.H., Hunter, P.J., 2004. Modeling RBC and neutrophil distribution through an anatomically based pulmonary capillary network. Ann Biomed Eng 32, 585–595.

Cala, S.J., Kenyon, C.M., Ferrigno, G., Carnevali, P., Aliverti, A., Pedotti, A., Macklem, P.T., Rochester, D.F., 1996. Chest wall and lung volume estimation by optical reflectance motion analysis. J. Appl. Physiol. 81, 2680–2689.

Cappello, M., De Troyer, A., 2002. On the respiratory function of the ribs. J Appl Physiol 92, 1642–1646. doi:10.1152/japplphysiol.01053.2001

Cappozzo, A., Catani, F., Croce, U.D., Leardini, A., 1995. Position and orientation in space of bones during movement: anatomical frame definition and determination. Clin Biomech (Bristol, Avon) 10, 171–178.

Cassart, M., Gevenois, P.A., Estenne, M., 1996. Rib cage dimensions in hyperinflated patients with severe chronic obstructive pulmonary disease. Am. J. Respir. Crit. Care Med. 154, 800–805. doi:10.1164/ajrccm.154.3.8810622

Cassart, M., Pettiaux, N., Gevenois, P.A., Paiva, M., Estenne, M., 1997. Effect of chronic hyperinflation on diaphragm length and surface area. Am. J. Respir. Crit. Care Med. 156, 504–508.

Cattrysse, E., Cescon, C., Clijsen, R., Barbero, M., 2013. Finite Helical Axis Behavior In Cervical Kinematics. Presented at the XXIV Congress of the International Society of Biomechanics, Natal, Rio Grande do Norte - Brazil.

Causey, G., 1953. The Anatomy of the Thorax in Relation to the Flow of Tidal Air. Ann R Coll Surg Engl 13, 127–135.

Cescon, C., Cattrysse, E., Barbero, M., 2014. Methodological analysis of finite helical axis behavior in cervical kinematics. J Electromyogr Kinesiol 24, 628–635. doi:10.1016/j.jelekin.2014.05.004

Chen, P.H., 1978. Finite element dynamic structural model of the human thorax for chest impact response and injury studies. Aviat Space Environ Med 49, 143–149.

Chèze, L., Fregly, B.J., Dimnet, J., 1998. Determination of joint functional axes from noisy marker data using the finite helical axis. Human Movement Science 17, 1–15. doi:10.1016/S0167-9457(97)00018-3

Chèze, L., Fregly, B.J., Dimnet, J., 1995. A solidification procedure to facilitate kinematic analyses based on video system data. J Biomech 28, 879–884.

Closkey, R.F., Schultz, A.B., Luchies, C.W., 1992. A model for studies of the deformable rib cage. J Biomech 25, 529–539.

Cluzel, P., Similowski, T., Chartrand-Lefebvre, C., Zelter, M., Derenne, J.-P., Grenier, P.A., 2000a. Diaphragm and Chest Wall: Assessment of the Inspiratory Pump with MR Imaging—Preliminary Observations1. Radiology 215, 574–583.

Cluzel, P., Similowski, T., Chartrand-Lefebvre, C., Zelter, M., Derenne, J.-P., Grenier, P.A., 2000b. Diaphragm and Chest Wall: Assessment of the Inspiratory Pump with MR Imaging—Preliminary Observations1. Radiology 215, 574–583.

Cohen, M.J., Ezekiel, J., Persellin, R.H., 1978. Costovertebral and costotransverse joint involvement in rheumatoid arthritis. Ann Rheum Dis 37, 473–475.

Dansereau, J., Stokes, I.A., 1988. Measurements of the three-dimensional shape of the rib cage. J Biomech 21, 893–901.

Dassios, T., Katelari, A., Doudounakis, S., Mantagos, S., Dimitriou, G., 2013. Respiratory muscle function in patients with cystic fibrosis. Pediatr. Pulmonol. 48, 865–873. doi:10.1002/ppul.22709

de Lange, A., Huiskes, R., Kauer, J.M., 1990. Effects of data smoothing on the reconstruction of helical axis parameters in human joint kinematics. J Biomech Eng 112, 107–113.

De Troyer, A., 2012. Respiratory effect of the lower rib displacement produced by the diaphragm. J. Appl. Physiol. 112, 529–534. doi:10.1152/japplphysiol.01067.2011

De Troyer, A., Cappello, M., Scillia, P., 2005a. Effect of inflation on the interaction between the left and right hemidiaphragms. J Appl Physiol 99, 1301–1307. doi:10.1152/japplphysiol.00192.2005

De Troyer, A., Decramer, M., 1985. Mechanical coupling between the ribs and sternum in the dog. Respiration Physiology 59, 27–34. doi:doi/10.1016/0034-5687(85)90015-5

De Troyer, A., Estenne, M., Vincken, W., 1986a. Rib cage motion and muscle use in high tetraplegics. Am. Rev. Respir. Dis. 133, 1115–1119.

De Troyer, A., Estenne, M., Vincken, W., 1986b. Rib cage motion and muscle use in high tetraplegics. Am. Rev. Respir. Dis. 133, 1115–1119.

De Troyer, A., Kirkwood, P.A., Wilson, T.A., 2005b. Respiratory Action of the Intercostal Muscles. Physiological Reviews 85, 717–756. doi:10.1152/physrev.00007.2004

De Troyer, A., Leduc, D., 2004. Effects of inflation on the coupling between the ribs and the lung in dogs. J. Physiol. (Lond.) 555, 481–488. doi:10.1113/jphysiol.2003.057026

De Troyer, A., Wilson, T.A., 2002. Coupling between the ribs and the lung in dogs. The Journal of Physiology 540, 231–236. doi:10.1113/jphysiol.2001.013319

De Troyer, A., Wilson, T.A., 1993. Sternum dependence of rib displacement during breathing. Journal of applied physiology 75, 334–340.

Denny, E., Schroter, R.C., 2006. A model of non-uniform lung parenchyma distortion. J Biomech 39, 652–663. doi:10.1016/j.jbiomech.2005.01.010

DeStefano, L.A., 2011. Greenman's Principles of Manual Medicine. Lippincott Williams & Wilkins.

Didier, A.-L., Villard, P., Bayle, J.-Y., Beuve, M., Shariat, B., 2007. Breathing Thorax Simulation based on Pleura Physiology and Rib Kinematics, in: International Conference on Medical Information Visualisation - BioMedical Visualisation, 2007. MediVis 2007. Presented at the International Conference on Medical Information Visualisation - BioMedical Visualisation, 2007. MediVis 2007, pp. 35–42. doi:10.1109/MEDIVIS.2007.8

Drake, R.L., Vogl, W., Mitchell, A.W.M., Gray, H., Gray, H., 2010. Gray's anatomy for students. Churchill Livingstone/Elsevier, Philadelphia, PA.

Dufresne, V., Knoop, C., Van Muylem, A., Malfroot, A., Lamotte, M., Opdekamp, C., Deboeck, G., Cassart, M., Stallenberg, B., Casimir, G., Duchateau, J., Estenne, M., 2009. Effect of Systemic Inflammation on Inspiratory and Limb Muscle Strength and Bulk in Cystic Fibrosis. Am J Respir Crit Care Med 180, 153–158. doi:10.1164/rccm.200802-232OC

Dugailly, P.-M., Beyer, B., Sobczak, S., Salvia, P., Rooze, M., Feipel, V., 2014. Kinematics of the upper cervical spine during high velocity-low amplitude manipulation. Analysis of intra- and inter-operator reliability for pre-manipulation positioning and impulse displacements. Journal of Electromyography and Kinesiology 24, 621–627. doi:10.1016/j.jelekin.2014.05.001

Dugailly, P.-M., Sobczak, S., Lubansu, A., Rooze, M., Jan, S.S., Feipel, V., 2013. Validation protocol for assessing the upper cervical spine kinematics and helical axis: An in vivo preliminary analysis for axial rotation, modeling, and motion representation. J Craniovertebr Junction Spine 4, 10–15. doi:10.4103/0974-8237.121617

Dugailly, P.-M., Sobczak, S., Sholukha, V., Jan, S.V.S., Salvia, P., Feipel, V., Rooze, M., 2010. In vitro 3D-kinematics of the upper cervical spine: helical axis and simulation for axial rotation and flexion extension. Surg Radiol Anat 32, 141–151. doi:10.1007/s00276-009-0556-1

Duprey, S., Subit, D., Guillemot, H., Kent, R.W., 2010. Biomechanical properties of the costovertebral joint. Med Eng Phys 32, 222–227. doi:10.1016/j.medengphy.2009.12.001

Eckert, M., 2001. Comportement des articulations costo-vertébrales lors du chargement frontal quasi-statique de la cage thoraxique.

Eckert, M., Fayet, M., Cheze, L., Bouquet, R., Voiglio, E., Verriest, J.P., 2000. Costovertebral joint behaviour during frontal loading of the thoracic cage. Presented at the Proceedings of the 2000 International IRCOBI conference on the biomechanics of impact , September 20-22, 2000, Montpelier, France.

Ehrig, R.M., Taylor, W.R., Duda, G.N., Heller, M.O., 2007. A survey of formal methods for determining functional joint axes. J Biomech 40, 2150–2157. doi:10.1016/j.jbiomech.2006.10.026

Erwin, W.M., Jackson, P.C., Homonko, D.A., 2000. Innervation of the human costovertebral joint: implications for clinical back pain syndromes. J Manipulative Physiol Ther 23, 395–403. doi:10.1067/mmt.2000.108144

Estenne, M., Yernault, J.C., De Troyer, A., 1985. Rib cage and diaphragm-abdomen compliance in humans: effects of age and posture. J. Appl. Physiol. 59, 1842–1848.

Estenne, M., Yernault, J.C., Troyer, A.D., 1985. Rib cage and diaphragm-abdomen compliance in humans: effects of age and posture. Journal of Applied Physiology 59, 1842–1848.

Felix, W., 1928. Topographische Anatomie des Brustkorbes der Lungen und der Lungenfelle. [S.l.].

Fick, R., 1911. Handbuch der Anatomie und Mechanik der Gelenke T. 3. T. 3. Fischer, Jena.

Finucane, K.E., Singh, B., 2009. Human diaphragm efficiency estimated as power output relative to activation increases with hypercapnic hyperpnea. J. Appl. Physiol. 107, 1397–1405. doi:10.1152/japplphysiol.91465.2008

French, R.K., 1978. The thorax in history 1. From ancient times to Aristotle. Thorax 33, 10–18.

Gauthier, A.P., Verbanck, S., Estenne, M., Segebarth, C., Macklem, P.T., Paiva, M., 1994a. Three-dimensional reconstruction of the in vivo human diaphragm shape at different lung volumes. J. Appl. Physiol. 76, 495–506.

Gauthier, A.P., Verbanck, S., Estenne, M., Segebarth, C., Macklem, P.T., Paiva, M., 1994b. Three-dimensional reconstruction of the in vivo human diaphragm shape at different lung volumes. J. Appl. Physiol. 76, 495–506.

Gayzik, F.S., Yu, M.M., Danelson, K.A., Slice, D.E., Stitzel, J.D., 2008. Quantification of age-related shape change of the human rib cage through geometric morphometrics. Journal of Biomechanics 41, 1545–1554. doi:10.1016/j.jbiomech.2008.02.006

Gilmartin, J.J., Gibson, G.J., 1986. Mechanisms of paradoxical rib cage motion in patients with chronic obstructive pulmonary disease. Am. Rev. Respir. Dis. 134, 683–687.

Godwin-Austen, R.B., 1969. The mechanoreceptors of the costo-vertebral joints. J. Physiol. (Lond.) 202, 737–753.

Graeber, G.M., Nazim, M., 2007. The anatomy of the ribs and the sternum and their relationship to chest wall structure and function. Thorac Surg Clin 17, 473–489, vi. doi:10.1016/j.thorsurg.2006.12.010

Groote, A.D., Wantier, M., Cheron, G., Estenne, M., Paiva, M., 1997. Chest wall motion during tidal breathing. Journal of Applied Physiology 83, 1531–1537.

Hayek, H. von, 1953. Die menschliche Lunge. Springer, Berlin; Göttingen; Heidelberg.

Hayek, H. von, 1960. The human lung. Hafner Pub. Co.

Hodges, P.W., Gandevia, S.C., 2000. Activation of the human diaphragm during a repetitive postural task. J Physiol 522, 165–175. doi:10.1111/j.1469-7793.2000.t01-1-00165.xm

Hunter, P., Coveney, P.V., de Bono, B., Diaz, V., Fenner, J., Frangi, A.F., Harris, P., Hose, R., Kohl, P., Lawford, P., McCormack, K., Mendes, M., Omholt, S., Quarteroni, A., Skår, J., Tegner, J., Randall Thomas, S., Tollis, I., Tsamardinos, I., van Beek, J.H.G.M., Viceconti, M., 2010. A vision and strategy for the virtual physiological human in 2010 and beyond. Philos Trans A Math Phys Eng Sci 368, 2595–2614. doi:10.1098/rsta.2010.0048

Hurtado, A., Fray, W.W., 1933. Studies of total pulmonary capacity and its sub-divisions. II. Correlation with physical and radiological measurements. J Clin Invest 12, 807–823.

Jordanoglou, J., 1970. Vector analysis of rib movement. Respir Physiol 10, 109–120.

Jordanoglou, J., 1969. Rib movement in health, kyphoscoliosis, and ankylosing spondylitis. Thorax 24, 407–414.

Jordanoglou, J., Kontos, J., Gardikas, C., 1972. Relative position of the rib within the chest and its determination on living subjects with the aid of a computer program. Respir Physiol 16, 41–50.

Jordanoglou, J., Smith, L., 1970. A new instrument for measuring rib movement. J Appl Physiol 28, 501–504.

Kaneko, H., Horie, J., 2012. Breathing Movements of the Chest and Abdominal Wall in Healthy Subjects. Respir Care 57, 1442–1451. doi:10.4187/respcare.01655

Kapandji, I.A., 1964. Illustrated physiology of joints. Med Biol Illus 14, 72–81.

Kent, R., Lee, S.-H., Darvish, K., Wang, S., Poster, C.S., Lange, A.W., Brede, C., Lange, D., Matsuoka, F., 2005. Structural and material changes in the aging thorax and their role in crash protection for older occupants. Stapp Car Crash J 49, 231–249.

Kenyon, C.M., Pedley, T.J., Higenbottam, T.W., 1991. Adaptive modeling of the human rib cage in median sternotomy. Journal of Applied Physiology 70, 2287–2302.

Kindig, M.W., Kent, R.W., 2013. Characterization of the Centroidal Geometry of Human Ribs. J Biomech Eng 135, 111007–111007. doi:10.1115/1.4025329

Konno, K., Mead, J., 1967. Measurement of the separate volume changes of rib cage and abdomen during breathing. J Appl Physiol 22, 407–422.

Ladjal, H., Saade, J., Beuve, M., Azencot, J., Moreau, J.-M., Shariat, B., 2013a. 3D Biomechanical Modeling of the Human Diaphragm Based on CT Scan Images, in: Long, M. (Ed.), World Congress on Medical Physics and Biomedical Engineering May 26-31, 2012, Beijing, China, IFMBE Proceedings. Springer Berlin Heidelberg, pp. 2188–2191.

Ladjal, H., Shariat, B., Azencot, J., Beuve, M., 2013b. Appropriate biomechanics and kinematics modeling of the respiratory system: Human diaphragm and thorax, in: 2013 IEEE/RSJ International Conference on Intelligent Robots and Systems. Presented at the 2013 IEEE/RSJ International Conference on Intelligent Robots and Systems, pp. 2004–2009. doi:10.1109/IROS.2013.6696623

Laghi, F., Tobin, M.J., 2003. Disorders of the Respiratory Muscles. Am J Respir Crit Care Med 168, 10–48. doi:10.1164/rccm.2206020

Laurin, L.-P., Jobin, V., Bellemare, F., 2012. Sternum length and rib cage dimensions compared with bodily proportions in adults with cystic fibrosis. Can. Respir. J. 19, 196–200.

Laville, A., Laporte, S., Skalli, W., 2009. Parametric and subject-specific finite element modelling of the lower cervical spine. Influence of geometrical parameters on the motion patterns. Journal of Biomechanics 42, 1409–1415. doi:10.1016/j.jbiomech.2009.04.007

Lee, D.G., 2015. Biomechanics of the thorax – research evidence and clinical expertise. J Man Manip Ther 23, 128–138.

Lee, L.-J., Chang, A.T., Coppieters, M.W., Hodges, P.W., 2010. Changes in sitting posture induce multiplanar changes in chest wall shape and motion with breathing. Respiratory Physiology & Neurobiology 170, 236–245. doi:10.1016/j.resp.2010.01.001

Locke, T.J., Griffiths, T.L., Mould, H., Gibson, G.J., 1990. Rib cage mechanics after median sternotomy. Thorax 45, 465–468.

Loring, S.H., 1986. Structural model of thorax and abdomen for respiratory mechanics. Mathematical Modelling 7, 1083–1098. doi:10.1016/0270-0255(86)90150-8

Macklem, P.T., Macklem, D.M., De Troyer, A., 1983. A model of inspiratory muscle mechanics. J Appl Physiol Respir Environ Exerc Physiol 55, 547–557.

Manchikanti, L., Boswell, M.V., Singh, V., Pampati, V., Damron, K.S., Beyer, C.D., 2004. Prevalence of facet joint pain in chronic spinal pain of cervical, thoracic, and lumbar regions. BMC Musculoskelet Disord 5, 15. doi:10.1186/1471-2474-5-15

Mannel, H., Marin, F., Claes, L., Dürselen, L., 2004. Establishment of a knee-joint coordinate system from helical axes analysis--a kinematic approach without anatomical referencing. IEEE Trans Biomed Eng 51, 1341–1347. doi:10.1109/TBME.2004.828051

Marshall, B., Miller, K., Wittek, A., Nielsen, P.M.F., 2015. Computational Biomechanics for Medicine: New Approaches and New Applications. Springer.

Masharawi, Y., Rothschild, B., Dar, G., Peleg, S., Robinson, D., Been, E., Hershkovitz, I., 2004. Facet orientation in the thoracolumbar spine: three-dimensional anatomic and biomechanical analysis. Spine 29, 1755–1763.

Mead, J., Loring, S.H., 1982. Analysis of volume displacement and length changes of the diaphragm during breathing. Journal of Applied Physiology 53, 750–755.

Meessen, N.E.L., van der Grinten, C.P.M., Folgering, H.T.M., Luijendijk, S.C.M., 1993. Tonic activity in inspiratory muscles during continuous negative airway pressure. Respiration Physiology 92, 151–166. doi:10.1016/0034-5687(93)90035-9

Meskers, C.G., van der Helm, F.C., Rozendaal, L.A., Rozing, P.M., 1998. In vivo estimation of the glenohumeral joint rotation center from scapular bony landmarks by linear regression. J Biomech 31, 93–96.

Mitchell, F.L., Mitchell, P.K.G., 2001. The Muscle Energy Manual. MET Press.

Mueller, G., Perret, C., Michel, F., Berger, M., Hopman, M.T.E., 2012. Reproducibility of assessing rib cage mobility from computed tomography images. Clin Physiol Funct Imaging 32, 282–287. doi:10.1111/j.1475-097X.2012.01123.x

Muller, N., Bryan, A.C., Zamel, N., 1981. Tonic inspiratory muscle activity as a cause of hyperinflation in asthma. J Appl Physiol Respir Environ Exerc Physiol 50, 279–282.

Nabors, L.K., Baumgartner, W.A., Janke, S.J., Rose, J.R., Wagner, W.W., Capen, R.L., 2003. Red blood cell orientation in pulmonary capillaries and its effect on gas diffusion. J. Appl. Physiol. 94, 1634–1640. doi:10.1152/japplphysiol.01021.2001

Oda, I., Abumi, K., Cunningham, B.W., Kaneda, K., McAfee, P.C., 2002. An in vitro human cadaveric study investigating the biomechanical properties of the thoracic spine. Spine 27, E64-70.

Oda, I., Abumi, K., Lü, D., Shono, Y., Kaneda, K., 1996. Biomechanical role of the posterior elements, costovertebral joints, and rib cage in the stability of the thoracic spine. Spine 21, 1423–1429.

Osmond, D.G., 1995. Functionnal anatomy of the chest wall, in: The Thorax: Part A, 2nd Ed. Roussos C., New York, pp. 413–444.

Pal, G.P., Routal, R.V., Saggu, S.K., 2001. The orientation of the articular facets of the zygapophyseal joints at the cervical and upper thoracic region. J Anat 198, 431–441. doi:10.1046/j.1469-7580.2001.19840431.x

Parreira, V.F., Vieira, D.S.R., Myrrha, M.A.C., Pessoa, I.M.B.S., Lage, S.M., Britto, R.R., 2012. Optoelectronic plethysmography: a review of the literature. Rev Bras Fisioter 16, 439–453.

Pascual, E., Castellano, J.A., López, E., 1992. Costovertebral joint changes in ankylosing spondylitis with thoracic pain. Br. J. Rheumatol. 31, 413–415.

Pelosi, P., Aliverti, A., Dellaca, R., 1998. Chest Wall Mechanics: Methods of Measurement and Physiopathologic Insights, in: Vincent, P.J.-L. (Ed.), Yearbook of Intensive Care and Emergency Medicine 1998, Yearbook of Intensive Care and Emergency Medicine. Springer Berlin Heidelberg, pp. 361–376. doi:10.1007/978-3-642-72038-3_32

Perz, R., Toczyski, J., Subit, D., 2015. Variation in the human ribs geometrical properties and mechanical response based on X-ray computed tomography images resolution. J Mech Behav Biomed Mater 41, 292–301. doi:10.1016/j.jmbbm.2014.07.036

Pettiaux, N., Cassart, M., Paiva, M., Estenne, M., 1997. Three-dimensional reconstruction of human diaphragm with the use of spiral computed tomography. J. Appl. Physiol. 82, 998–1002.

Piantoni, L., Francheri Wilson, I.A., Tello, C.A., Noel, M.A., Galaretto, E., Remondino, R.G., Bersusky, E.S., 2015. Hemivertebra Resection With Instrumented Fusion by Posterior Approach in Children. Spine Deformity 3, 541–548. doi:10.1016/j.jspd.2015.04.008

Piazza, S.J., Cavanagh, P.R., 2000. Measurement of the screw-home motion of the knee is sensitive to errors in axis alignment. J Biomech 33, 1029–1034.

Pinet, C., Cassart, M., Scillia, P., Lamotte, M., Knoop, C., Casimir, G., Mélot, C., Estenne, M., 2003. Function and Bulk of Respiratory and Limb Muscles in Patients with Cystic Fibrosis. Am J Respir Crit Care Med 168, 989–994. doi:10.1164/rccm.200303-398OC

Portney, L.G., Watkins, M.P., 2015. Foundations of clinical research: applications to practice.

Proulx, A.M., Zryd, T.W., 2009. Costochondritis: diagnosis and treatment. Am Fam Physician 80, 617–620.

Rit, S., Sarrut, D., Ginestet, C., 2005. Respiratory Signal Extraction for 4D CT Imaging of the Thorax from Cone-Beam CT Projections, in: Duncan, J.S., Gerig, G. (Eds.), Medical Image Computing and Computer-Assisted Intervention – MICCAI 2005, Lecture Notes in Computer Science. Springer Berlin Heidelberg, pp. 556–563. doi:10.1007/11566465_69

Roberts, S.B., Chen, P.H., 1972. Global geometric characteristics of typical human ribs. Journal of Biomechanics 5, 191–201. doi:10.1016/0021-9290(72)90055-3

Roberts, S.B., Chen, P.H., 1970. Elastostatic analysis of the human thoracic skeleton. Journal of Biomechanics 3, 527–545. doi:10.1016/0021-9290(70)90037-0

Rocha, T., Souza, H., Brandão, D.C., Rattes, C., Ribeiro, L., Campos, S.L., Aliverti, A., de Andrade, A.D., 2015. The Manual Diaphragm Release Technique improves diaphragmatic mobility, inspiratory capacity and exercise capacity in people with chronic obstructive pulmonary disease: a randomised trial. J Physiother 61, 182–189. doi:10.1016/j.jphys.2015.08.009

Romei, M., Mauro, A.L., D'Angelo, M.G., Turconi, A.C., Bresolin, N., Pedotti, A., Aliverti, A., 2010. Effects of gender and posture on thoraco-abdominal kinematics during quiet breathing in healthy adults. Respiratory Physiology & Neurobiology 172, 184–191. doi:10.1016/j.resp.2010.05.018

Rose J, Gamble J, Schultz A, Lewiston N, 1987. BAck pain and spinal deformity in cystic fibrosis. Am J Dis Child 141, 1313–1316. doi:10.1001/archpedi.1987.04460120079039

Roussos, C., 1995. The Thorax -- Part A: Physiology (In Three Parts), Second Edition. CRC Press.

Saadé, J., Ladjal, H., Behzad, S., Beuve, M., Azencot, J., 2012. Modélisation biomécanique du diaphragme humain : du CT-4D au modèle du mouvement, in: Actes de La Conférence RFIA 2012. Presented at the RFIA 2012 (Reconnaissance des Formes et Intelligence Artificielle).

Sales, J.R., Beals, R.K., Hart, R.A., 2007. Osteoarthritis of the costovertebral joints: the results of resection arthroplasty. J Bone Joint Surg Br 89–B, 1336–1339. doi:10.1302/0301-620X.89B10.19721

Salvia, P., Woestyn, L., David, J.H., Feipel, V., Van, S., Jan, S., Klein, P., Rooze, M., 2000. Analysis of helical axes, pivot and envelope in active wrist circumduction. Clin Biomech (Bristol, Avon) 15, 103–111.

Sandoz, B., Badina, A., Laporte, S., Lambot, K., Mitton, D., Skalli, W., 2013. Quantitative geometric analysis of rib, costal cartilage and sternum from childhood to teenagehood. Med Biol Eng Comput 51, 971–979. doi:10.1007/s11517-013-1070-5

Saumarez, R.C., 1986. An analysis of possible movements of human upper rib cage. J Appl Physiol 60, 678–689.

Schultz, A.B., Benson, D.R., Hirsch, C., 1974a. Force-deformation properties of human costo-sternal and costo-vertebral articulations. J Biomech 7, 311–318.

Schultz, A.B., Benson, D.R., Hirsch, C., 1974b. Force-deformation properties of human ribs. J Biomech 7, 303–309.

Schwartz, C., Leboeuf, F., Rémy-Néris, O., Brochard, S., Lempereur, M., Burdin, V., 2013. Detection of incoherent joint state due to inaccurate bone motion estimation. Computer Methods in Biomechanics and Biomedical Engineering 16, 165–174. doi:10.1080/10255842.2011.613379

Selkow, N.M., Grindstaff, T.L., Cross, K.M., Pugh, K., Hertel, J., Saliba, S., 2009. Short-Term Effect of Muscle Energy Technique on Pain in Individuals with Non-Specific Lumbopelvic Pain: A Pilot Study. J Man Manip Ther 17, E14–E18.

Sharma, G., Goodwin, J., 2006. Effect of aging on respiratory system physiology and immunology. Clin Interv Aging 1, 253–260.

Sharp, J.T., Beard, G.A., Sunga, M., Kim, T.W., Modh, A., Lind, J., Walsh, J., 1986. The rib cage in normal and emphysematous subjects: a roentgenographic approach. J. Appl. Physiol. 61, 2050–2059.

Sharp, J.T., Goldberg, N.B., Druz, W.S., Danon, J., 1975. Relative contributions of rib cage and abdomen to breathing in normal subjects. J Appl Physiol 39, 608–618.

Singh, B., Panizza, J.A., Finucane, K.E., 2003. Breath-by-breath measurement of the volume displaced by diaphragm motion. J. Appl. Physiol. 94, 1084–1091. doi:10.1152/japplphysiol.00256.2002

Söderkvist, I., Wedin, P.A., 1993. Determining the movements of the skeleton using well-configured markers. J Biomech 26, 1473–1477.

Stokdijk, M., Meskers, C.G., Veeger, H.E., de Boer, Y.A., Rozing, P.M., 1999. Determination of the optimal elbow axis for evaluation of placement of prostheses. Clin Biomech (Bristol, Avon) 14, 177–184.

Takeuchi, T., Abumi, K., Shono, Y., Oda, I., Kaneda, K., 1999. Biomechanical role of the intervertebral disc and costovertebral joint in stability of the thoracic spine. A canine model study. Spine 24, 1414–1420.

Tanaka, R., Sanada, S., Sakuta, K., Kawashima, H., 2015. Quantitative analysis of rib kinematics based on dynamic chest bone images: preliminary results. J Med Imaging (Bellingham) 2, 024002. doi:10.1117/1.JMI.2.2.024002

Tattersall, R., Walshaw, M.J., 2003. Posture and cystic fibrosis. J R Soc Med 96, 18–22.

Tobin, M.J., Chadha, T.S., Jenouri, G., Birch, S.J., Gazeroglu, H.B., Sackner, M.A., 1983. Breathing patterns. 1. Normal subjects. Chest 84, 202–205.

Tuteur, P.G., 1990. Chest Examination, in: Walker, H.K., Hall, W.D., Hurst, J.W. (Eds.), Clinical Methods: The History, Physical, and Laboratory Examinations. Butterworths, Boston.

Van Sint Jan, 2007. Color atlas of skeletal landmark definitions: guidelines for reproducible manual and virtual palpations. Churchill Livingstone/Elsevier, Edinburgh ; New York.

Van Sint Jan, S., Della Croce, U., 2005. Accurate palpation of skeletal landmark locations: Why standardized definitions are necessary. A proposal. Clinical biomechanics 20, 659–660.

Van Sint Jan, S., Giurintano, D.J., Thompson, D.E., Rooze, M., 1997. Joint kinematics simulation from medical imaging data. IEEE Trans Biomed Eng 44, 1175–1184. doi:10.1109/10.649989

Van Sint Jan, S., Salvia, P., Feipel, V., Sobzack, S., Rooze, M., Sholukha, V., 2006a. In vivo registration of both electrogoniometry and medical imaging: development and application on the ankle joint complex. IEEE Trans Biomed Eng 53, 759–762. doi:10.1109/TBME.2006.870208

Van Sint Jan, S., Sobzack, S., Dugailly, P.-M., Feipel, V., Lefèvre, P., Lufimpadio, J.-L., Salvia, P., Viceconti, M., Rooze, M., 2006b. Low-dose computed tomography: A solution for in vivo medical imaging and accurate patient-specific 3D bone modeling? Clinical Biomechanics 21, 992–998. doi:10.1016/j.clinbiomech.2006.05.007

Van Sint Jan, S., Wermenbol, V., Van Bogaert, P., Desloovere, K., Degelaen, M., Dan, B., Salvia, P., Ortibus, E., Bonnechère, B., Le Borgne, Y.-A., Bontempi, G., Vansummeren, S., Sholukha, V., Moiseev, F., Rooze, M., 2013. A technological platform for cerebral palsy - The ICT4Rehab project. Médecine/Sciences 29, 529–536. doi:10.1051/medsci/2013295017

Verschakelen, J.A., Demedts, M.G., 1995. Normal thoracoabdominal motions. Influence of sex, age, posture, and breath size. Am J Respir Crit Care Med 151, 399–405. doi:10.1164/ajrccm.151.2.7842198

Vezin, P., Berthet, F., 2009. Structural characterization of human rib cage behavior under dynamic loading. Stapp Car Crash J 53, 93–125.

Vezin, P., Verriest, J.P., 2005. Development of a Set of Numerical Human Models for Safety. Presented at the 19th International Technical Conference on the Enhanced Safety of Vehicles (ESV).

Viano, D.C., 1978. Evaluation of biomechanical response and potential injury from thoracic impact. Aviat Space Environ Med 49, 125–135.

Viceconti, M., Clapworthy, G., Van Sint Jan, S., 2008. The Virtual Physiological Human - a European initiative for in silico human modelling -. J Physiol Sci 58, 441–446. doi:10.2170/physiolsci.RP009908

Viceconti, M., Zannoni, C., Testi, D., Petrone, M., Perticoni, S., Quadrani, P., Taddei, F., Imboden, S., Clapworthy, G., 2007. The multimod application framework: a rapid application development tool for computer aided medicine. Comput Methods Programs Biomed 85, 138–151. doi:10.1016/j.cmpb.2006.09.010

Von Hayek, H., 1970. Die Menschliche Lunge. Springer.

Walsh, J.M., Webber, C.L., Fahey, P.J., Sharp, J.T., 1992. Structural change of the thorax in chronic obstructive pulmonary disease. J. Appl. Physiol. 72, 1270–1278.

Ward, M.E., Macklem, P.T., 1995. Kinematics of the chest wall, in: The Thorax: Part A, 2nd Ed. Roussos C., New York, pp. 515–533.

Ward, M.E., Ward, J.W., Macklem, P.T., 1992. Analysis of human chest wall motion using a two-compartment rib cage model. J. Appl. Physiol. 72, 1338–1347.

Watkins, R., 4th, Watkins, R., 3rd, Williams, L., Ahlbrand, S., Garcia, R., Karamanian, A., Sharp, L., Vo, C., Hedman, T., 2005. Stability provided by the sternum and rib cage in the thoracic spine. Spine 30, 1283–1286.

Weaver, A.A., Schoell, S.L., Stitzel, J.D., 2014. Morphometric analysis of variation in the ribs with age and sex. J. Anat. 225, 246–261. doi:10.1111/joa.12203

Weber, B., Smith, J.P., Briscoe, W.A., Friedman, S.A., King, T.K., 1975. Pulmonary function in asymptomatic adolescents with idiopathic scoliosis. Am. Rev. Respir. Dis. 111, 389–397. doi:10.1164/arrd.1975.111.4.389

West, J.B., 2012. Respiratory Physiology: The Essentials. Lippincott Williams & Wilkins.

White, B.M., Zhao, T., Lamb, J., Bradley, J.D., Low, D.A., 2013. Quantification of the thorax-to-abdomen breathing ratio for breathing motion modeling. Med Phys 40, 063502. doi:10.1118/1.4805099

Wilkens, H., Weingard, B., Lo Mauro, A., Schena, E., Pedotti, A., Sybrecht, G.W., Aliverti, A., 2010. Breathing pattern and chest wall volumes during exercise in patients with cystic fibrosis, pulmonary fibrosis and COPD before and after lung transplantation. Thorax 65, 808–814. doi:10.1136/thx.2009.131409

Wilson, T.A., De Troyer, A., 2004. The two mechanisms of intercostal muscle action on the lung. J. Appl. Physiol. 96, 483–488. doi:10.1152/japplphysiol.00553.2003

Wilson, T.A., Legrand, A., Gevenois, P.A., De Troyer, A., 2001. Respiratory effects of the external and internal intercostal muscles in humans. J. Physiol. (Lond.) 530, 319–330.

Wilson, T.A., Rehder, K., Krayer, S., Hoffman, E.A., Whitney, C.G., Rodarte, J.R., 1987. Geometry and respiratory displacement of human ribs. J. Appl. Physiol. 62, 1872–1877.

Woltring, H.J., 1990. Biomechanics of Human Movement, Applications in Rehabilitation, Sport and Ergonomics; Biomechanics of Human Movement, Applications in Rehabilitation, Sport and Ergonomics 203–237.

Woltring, H.J., Huiskes, R., de Lange, A., Veldpaus, F.E., 1985. Finite centroid and helical axis estimation from noisy landmark measurements in the study of human joint kinematics. J Biomech 18, 379–389.

Wu, G., Cavanagh, P.R., 1995. ISB recommendations for standardization in the reporting of kinematic data. J Biomech 28, 1257–1261.

Wu, G., Siegler, S., Allard, P., Kirtley, C., Leardini, A., Rosenbaum, D., Whittle, M., D'Lima, D.D., Cristofolini, L., Witte, H., Schmid, O., Stokes, I., 2002. ISB recommendation on definitions of joint coordinate system of various joints for the reporting of human joint motion--part I: ankle, hip, and spine. International Society of Biomechanics. J Biomech 35, 543–548.

Zhu, Y., Fang, Y., Bermond, F., Bruyère-Garnier, K., Ellouz, R., Rongieras, F., Mitton, D., 2013. Relationship between human rib mechanical properties and cortical bone density measured by high-resolution quantitative computed tomography. Comput Methods Biomech Biomed Engin 16 Suppl 1, 191–192. doi:10.1080/10255842.2013.815888